9

MARTIN MARIETTA ENERGY SYSTEMS LIBRARIES
3 4456 0049749 7

CENTRAL RESEARCH LIBRARY
DOCUMENT COLLECTION

ORNL-2493
Reactors—Power
TID-4500 (13th ed., Rev.)
February 15, 1958

cy. 9

HOMOGENEOUS REACTOR PROJECT

QUARTERLY PROGRESS REPORT

FOR PERIOD ENDING JANUARY 31, 1958

OAK RIDGE NATIONAL LABORATORY
operated by
UNION CARBIDE CORPORATION
for the
U.S. ATOMIC ENERGY COMMISSION

OAK RIDGE NATIONAL LABORATORY
CENTRAL RESEARCH LIBRARY
CIRCULATION SECTION
4500N ROOM 175
LIBRARY LOAN COPY
DO NOT TRANSFER TO ANOTHER PERSON
If you wish someone else to see this report, send in name with report and the library will arrange a loan.
UCN-7969 (3 9-77)

Printed in USA. Price $3.50 cents. Available from the

Office of Technical Services
U. S. Department of Commerce
Washington 25, D. C.

LEGAL NOTICE

This report was prepared as an account of Government sponsored work. Neither the United States, nor the Commission, nor any person acting on behalf of the Commission:

A. Makes any warranty or representation, express or implied, with respect to the accuracy, completeness, or usefulness of the information contained in this report, or that the use of any information, apparatus, method, or process disclosed in this report may not infringe privately owned rights; or

B. Assumes any liabilities with respect to the use of, or for damages resulting from the use of any information, apparatus, method, or process disclosed in this report.

As used in the above, "person acting on behalf of the Commission" includes any employee or contractor of the Commission to the extent that such employee or contractor prepares, handles or distributes, or provides access to, any information pursuant to his employment or contract with the Commission.

ORNL-2493
Reactors–Power
TID-4500 (13th ed., Rev.)
February 15, 1958

Contract No. W-7405-eng-26

HOMOGENEOUS REACTOR PROJECT

QUARTERLY PROGRESS REPORT

For Period Ending January 31, 1958

Project Director – R. B. Briggs
Associate Director – C. E. Winters

Homogeneous Reactor Test – S. E. Beall
Reactor Design, Research, and Analysis – R. N. Lyon
Engineering Development – R. N. Lyon
Reactor Materials Research – E. G. Bohlmann
Chemical Engineering Development – D. E. Ferguson
Supporting Chemical Research – E. H. Taylor
Analytical Chemistry – M. T. Kelley

DATE ISSUED JUL 15 1958

OAK RIDGE NATIONAL LABORATORY
Oak Ridge, Tennessee
operated by
UNION CARBIDE CORPORATION
for the
U. S. ATOMIC ENERGY COMMISSION

MARTIN MARIETTA ENERGY SYSTEMS LIBRARIES
3 4456 0049749 7

HRP QUARTERLY PROGRESS REPORT

SUMMARY

PART I. HOMOGENEOUS REACTOR TEST

1. HRT Operations

Following the HRT tests with light water and depleted uranium, the piping was leak-tested by pressurizing to 500 psig with nitrogen containing 40 curies of Kr^{85}. The roof of the shield was sealed with a plastic cover, and the pressurized system was allowed to stand for five days. Daily samples of the confined shield volume were checked for Kr^{85} activity. As a further leak test, the pressure was partially relieved and helium was injected to yield a 60% helium mixture in the system at 512 psia. After an additional five-day period, the cell volume and auxiliary piping were checked for helium content. The reactor was found to be leaktight to within 0.2 std cc/day.

The adsorption capacity of two charcoal beds was tested and found satisfactory, completing the experiments on the off-gas system. After checking was complete on the beds and the reactor piping, the reactor shield was reopened to allow final insulating of the piping, inspection and repairs to thermocouples and conduit, and reinstallation of the fuel recombiner. The latter vessel now contains silver-coated stainless steel Yorkmesh in the iodine-removal section, replacing the silver-impregnated alumina pellets; these were found to release sodium ions into the low-pressure system when leached.

The shield was resealed, and 5879 lb of heavy water was charged to the reactor. A precritical inspection run at 1700 psi and 280°C, started on December 14, was temporarily interrupted the next day, to remove an obstruction from the inlet to the purge pump of the fuel circulating pump. The run was continued until December 20, for a total of 82 hr of operation. The reactor was cooled to 25°C in preparation for the initial critical test.

The HRT was charged with U^{235} beginning December 24, and was brought to criticality at a temperature of 29°C on December 27. Following shutdown, a trial installation and removal of the core corrosion specimens was made, using dry, direct maintenance techniques. Repairs to the reactor-shield containment vessel reduced inleakage from 25 to $\frac{1}{4}$ cfm, with the cell evacuated to 7.5 psia. The rest of the low-power criticality experiments, seven in all, were run from January 8 to January 11, to establish the temperature coefficient of reactivity.

The remainder of the month was spent in leak-testing the containment vessel; the helium leak detector was used to scan the surface, and mercaptan was used for a final odor test. After repairing all the leaks which could be located, the total leakage was measured as 4.5 liters/min with the cell at 30 psia. The normal operating pressure is 7.5 psia.

Preparations for the initial critical test of the HRT were completed on December 23. The two installed fission chambers were supplemented by a third chamber in the blanket thimble; the antimony-beryllium source was suspended in the core thimble at the center of the core.

After the reactor was filled with D_2O and pressurized, 100 to 400 g of U^{235} increments of concentrated fuel were added to the D_2O in the dump tanks and pumped into the high-pressure system, which circulated continuously at 400 gpm. Fuel injection began on December 24; in the afternoon of December 27, the reactor began chain-reacting at 29°C with a mass of 2060 g. With the source completely removed, the fission rate rose with a period of about 17 min, indicating a core temperature about 0.06°C below the critical temperature.

Seven subsequent experiments were conducted with the fuel thimble removed and with the source in the blanket thimble. The first of these was conducted with the same fuel concentration as that used in the initial critical test; removal of the poisoning effect from the core thimble, however, caused the reactor to attain criticality at 65°C. This temperature was approached by cooling the reactor with water circulated through the heat exchanger shells. The reactor temperature coefficient was measured at seven temperatures between 25°C and 280°C by supplying steam to the shells of the steam generators.

Samples taken during the experiments show critical concentrations averaging 6% below the calculated values. The reason for this discrepancy is not yet established; however, further analyses by the isotopic dilution method are in progress.

The observed critical concentrations agree well with the predictions of Edlund and Wood, which were based upon a harmonics calculation.

The carbon-steel transition strips between the galvanized-iron roof seal pans and the containment cell walls were replaced by type 347 stainless steel transition strips. After the pans were ground to remove zinc from the edges, they were edge-welded to the stainless steel strips. The reactor cells were pressurized with air; many leaks were found, several of which proved difficult to repair. Macroexamination of sections removed from the leaking joint revealed cracks located primarily in the stainless steel base metal. The cracks appeared to be the result of rapid intergranular diffusion of zinc from the galvanized iron into the stainless steel.

2. HRT Design

The design of facilities for the removal and replacement of the core and blanket corrosion-sample holders and the pressure-balancing-system rupture-disk assembly was completed.

Recent tests in the flange test facility confirm that a mismatch of as much as 0.010 in. between the pitch diameters of ring-joint gaskets and flange grooves is permissible for flanged joints in the HRT.

3. HRT Component Development

The 400A-1 Westinghouse pump was used to circulate 0.04 *m* UO_2SO_4 solution, saturated with gas, for 1585 hr. Localized pitting of stainless steel parts in areas of high turbulence was observed and was attributed to erosion by bubbles. Shaft-seal mixing rates were determined for the 400A-2 Westinghouse pump in which the motor coolant was routed as in the 200A slurry pump, which uses the lower radial bearing as a secondary shaft seal. The measured mixing flow was 0.001 liter/hr at a purge flow of 7.3 liters/hr; the flow for the best previous configuration was 0.003 liter/hr. However, the lower bearing was severely damaged by overheating when the pump circulated 0.04 *m* UO_2SO_4 solution at 250°C. The HRT mockup 300A pump, which had circulated 0.04 *m* UO_2SO_4 for 5040 hr, was dismantled and found to be in good condition.

Two failures in feed-pump components occurred during the quarter. An old-style head, containing a 0.019-in.-thick diaphragm protected by a 40-mesh screen, suffered a diaphragm failure after 8997 hr of operation. A fatigue failure of a butt weld in one of the test-loop intermediate lines after 26×10^6 pressure cycles was attributed to a notch caused by overpenetration of the weld bead.

Seven feed-pump heads continue to operate satisfactorily on fuel solution; one has been operating for 7389 hr, and two latest-style heads have each been in service for 6520 hr.

Various surface treatments have had no significant effect on the endurance limit of type 347 stainless steel exposed to uranyl sulfate solution as compared with the performance of sheet given a standard ASTM No. 9 finish. Titanium was found to have a very high endurance limit, which may permit greatly increased capacity in a diaphragm pump.

Testing of the secondary gasket to be used when removing light water from a flanged-joint during underwater reassembly showed that 90% of the light water was removed by a 2-liter heavy water flush.

The HRT mockup completed a 2210-hr run at 1700 psi and 280°C with a 0.042 *m* UO_2SO_4 solution containing 0.021 *m* H_2SO_4 and 0.005 *m* $CuSO_4$. The generalized corrosion rate was 1.3 mpy.

A second silver-plated wire-mesh bed, having a density of 29 lb/ft^3, was tested for iodine removal efficiency, which was found to be 99.8% at 120°C. A 650-hr stability test of another bed loaded with 20 g of iodine showed a loss of only one part in 4000 of the silver from the bed.

A small bypass stream was heated to 300°C in a ½-in. stainless steel line for 1500 hr to test scale buildup. A 0.03-in. deposit of a rusty red scale formed.

The generalized corrosion rates of stressed specimens exposed to stagnant solution for 2210 hr were low, varying from 0.1 to 0.5 mpy with temperatures from 50 to 280°C.

Fuel solution containing an excess of uranium and a deficiency of free acid, due probably to the presence of sodium and potassium from the iodine removal tests, precipitated uranium and copper when the pressurizer purge rate was high (about

13 gph), but the precipitate redissolved when the purge flow rate was lowered.

4. HRT Controls and Instrumentation

Electric-signal differential-pressure transmitters were tested and were installed in the leak-detection system.

Spurious radiation signals were eliminated from two fission-chamber channels, whose chambers are in water-filled thimbles, by running the coaxial signal cables in a plastic tube and by grounding the amplifier rack directly to the thimbles.

Design was completed and construction was begun on instrument panels to be used in conjunction with tests of the radiation resistance of pump-stator-winding insulation.

A control-valve-stem position transmitter was installed on the HRT mockup letdown valve to observe performance. This transmitter was designed to withstand reactor-cell environmental conditions.

A remote disconnect for metal-clad mineral-insulated electrical cable was constructed.

The differential-expansion type of valve used to meter oxygen into the reactor high-pressure system was redesigned to utilize a tantalum plug (instead of zirconium), thus eliminating the possibility of an ignition reaction between the hot metal and the oxygen gas.

A core-positioning device for differential transformers was fabricated to permit ready testing, for sensitivity and range, of instruments utilizing this type of motion-sensing element.

A television camera with associated control and monitoring equipment was received and will be used to aid reactor maintenance operations. A camera small enough to go through a 2-in.-dia opening was ordered for this system.

5. HRT Processing Plant

Leak rates from the piping system of the processing plant were acceptably low after one leak in an instrument pressure tap had been repaired. Operation of all equipment in the hydroclone loop was normal during the D_2O run prior to the critical experiments.

The cell closure was completed with the welding of seal pans between the top roof plugs. Preliminary measurements of leakage through service-line penetrations were made in preparation for the over-all cell leak test.

The times required for Kr^{85} tracer activity to break through the charcoal beds were determined. Individual beds varied slightly, but all should provide sufficient holdup to maintain acceptable activity levels in the reactor off-gas streams at oxygen flows several times the design rate.

The design of the loading-pit facility and carrier for transferring waste solution to the Thorex Pilot Plant was completed.

PART II. REACTOR DESIGN, RESEARCH, AND ANALYSIS

6. HRE-3 Design

The blanket low-pressure system and the tabulation of preliminary HRE-3 design data have been revised. Proposed process designs of the core and blanket dump systems, the letdown system, the reactor pressurization system, and the iodine removal system have been completed.

7. Research and Analysis

The effect of the value of η^{23} in the resonance region upon the breeding ratio in thorium breeder reactors was studied by means of multigroup calculations. It was found that resonance fissions contribute about 10 to 40% of the total fission in reactors containing from 0 to 300 g of Th per liter in the core region. If η^{23} in the resonance region were 0.9 of its value in the thermal region, the breeding ratio in solution-core reactors would be about 0.02 lower than if η^{23} were independent of energy and equal to its thermal value.

Time-dependent studies of slurry-core, slurry-blanket thorium breeder reactors generating about 60 thermal megawatts indicate that the core poison fraction is the major variable affecting the breeding ratio. With a core thorium concentration of 100 g/liter, a period of 700 days following startup is required before the core poison fraction reaches 7%, while the corresponding time is 1360 days when the core thorium concentration is 200 g/liter. A period of about 800 days is required before the U^{233} concentration in the blanket reaches 3 g/liter.

Revised calculations were performed to determine the heat generation rates in the HRE-3 core vessel. Values obtained with a core power of 50 Mw were about 10.5, 9.4, and 9.0 w/cc, respectively, for the cases of a D_2O blanket and blankets containing 500 and 1000 g of Th per liter.

Digestion of freshly precipitated thorium oxalate before filtration and firing resulted in thorium oxide particles which were resistant to degradation. The cake resuspension index of thoria prepared from digested precipitates was lower than that of thoria prepared similarly but without digestion. The addition of sodium aluminate to a flocculated slurry reduced the yield stress significantly. The effect of the sodium aluminate was not altered by autoclaving at 280°C.

Laminar heat transfer measurements with aqueous thorium oxide slurries indicate that the corresponding heat transfer coefficients are greater than the conventional Newtonian-fluid coefficients by a factor of

$$\left[1 + \left(g_c \tau_y D/24\eta V\right)\right]^{1/3} .$$

It was demonstrated that a hydroclone can be used to effect a size classification of thoria particles. After the second pass, 98 wt % of the material contained in the overflow from the hydroclone was less than 2 μ in diameter, whereas 65 wt % of the original material was less than 2 μ in diameter.

8. HRE-3 Instrumentation and Controls System Design

A conceptual one-line diagram of the HRE-3 plant power distribution system was made, and the proposed bus loads were tabulated. The plant distribution voltage was indicated, and proposed d-c emergency and control power supplies were shown.

A layout of the electrical equipment in a special room was made in order to indicate the building space that would be necessary if all the equipment were to be grouped.

Proposed layouts of the main control room to house the reactor operating controls and instruments and of an auxiliary instrument room for data-collecting instruments, transducers, amplifiers, etc., were also made.

PART III. ENGINEERING DEVELOPMENT

9. Development of Fuel-System Components

The reconstructed high-pressure recombiner loop was operated for 500 hr at 600 psi and temperatures up to 500°C before failure of welds in the boiler necessitated termination. Specimens of crystal-bar zirconium disintegrated in the superheated vapor, while Zircaloy-2 was not attacked.

The 20-cfm blower, after 428 hr of operation with 2-g/liter ThO_2 slurry as bearing fluid, suffered no measurable bearing wear.

It was determined from tests conducted on the 4000-gpm Byron Jackson pump that the external heat exchanger is necessary to prevent motor overheating. It was also found that purge rates of 60 to 150 liters/hr are adequate for maintaining an acceptably low mixing flow between motor fluid and pump fluid.

Preliminary hydraulic and electrical design of the Reliance 6000-gpm pump was completed. Three small test stators which simulate the insulating systems in the HRT pumps and in the Reliance pump were received for radiation testing.

An order was placed for a three-stage high-pressure oxygen compressor rated at 2-scfm delivery.

Excessive wear in the Stellite-piston pump resulted in its being eliminated from further consideration. A diaphragm head containing 20-μ Poroloy screens has operated satisfactorily for 476 hr. A double-diaphragm feed pump was built and operated for 500 hr.

Palladium, tungsten carbide flame-coated on type 347 stainless steel, Allegheny Ludlum AM-355 stainless steel, and gold dump-valve trims were tested. Only the gold trim, which maintained its integrity after 2000 dumps, was satisfactory.

Test pieces of titanium-lined 3½-in. and 20-in. carbon-steel pipe suffered weld failures during hydrostatic testing. A second length of extruded 3½-in. A-110AT titanium pipe has been completed, except for boring the interior. One cap for this pipe has been fabricated.

An all-titanium letdown heat exchanger was constructed for the HRT mockup and was installed by use of titanium–stainless steel ring-joint transition flanges.

Testing of the titanium-to-stainless-steel transition joint and of type 347 stainless steel ring-joint flanges revealed that leakage is not affected by elimination of the bolt ferrules.

Several austenitic materials are being investigated for use as bolting materials in fuel solutions.

The thermal-cycle facility was operated, with a large autoclave being used as a test piece. The experimental cycles fall within the specified limits of the cycle proposed for the HRT spare heat exchanger.

Two tube bundles were examined after 2700 hr of thermal cycling in 200°C boiler water containing 50 ppm Cl^- and 10–25 ppm O_2 and showed no evidence of cracking.

Contract negotiations for the fabrication of heat exchangers for the heat exchanger test facility are nearing completion. Delivery is expected in the fall of 1958.

Boiling HRT fuel solution has had no deleterious effects on a titanium container after 1200 hr at 1500 psi and 313°C.

Testing of a jet eductor as a contactor indicated an efficiency of 60% at design flow, with the efficiency falling rapidly as the flow was decreased.

Preliminary measurement of the heat transfer rate between the core wall and the circulating fluid in a 4-ft-dia core indicated a forced convection heat transfer coefficient in excess of 2000 Btu/hr/ft^2/°F at a flow of 6000 gpm.

The 300A slurry loop is nearing completion. A full-scale glass model of the loop demonstrated that no undesirable vortices or stagnant regions will exist in the pressurizer if a net downward flow is maintained. Downward flows greater than 0.13 fps resulted in gas bubbles being carried into the main loop stream.

A slurry feed-pump head is being constructed with a recessed chamber on the slurry side into which the diaphragm will never bottom. Another system employing remotely located check valves connected to a standard diaphragm head by a vertical leg is being constructed. A facility which will supply well-agitated, constant-concentration slurry to the suctions of test feed pumps has been designed.

Check-valve seats of type 347 stainless steel and Stellite No. 1 and balls of Stellite Star J failed quickly in 200 g of Th per liter, 1600°C-fired slurry. Kennametal K501 appears to be the best material for balls and seats tested to date.

A sintered stainless steel filter, a settling tank device, and a continuous centrifuge are under investigation as means of providing purge water for slurry systems.

Design and fabrication of a 30-in. model of the HRE-3 blanket was initiated. The model will incorporate an internal jet eductor to increase the apparent throughput.

A slurry dump-tank–evaporator model is being constructed. It will contain a steam coil surrounded by a perforated draft tube to provide slurry agitation. Foaming and dehydration of slurry will be investigated.

10. Development of Reactor Slurry Systems

Slurry and water were circulated in the 100- and 200-gpm loops for more than 4103 hr during the quarter. Run 200A-14, to determine the degradation characteristics of 1600°C-fired oxide, was terminated after 3787 hr at 300°C and 2000 psig. The mean particle size decreased during the run from 2.5 μ to 1.8 μ. However, the nitrogen adsorption surface area remained constant at 1.6 m^2/g, and the generalized corrosion rate stayed at 1.2 mpy. The slurry was easily removed, and no cakes or films were found. The pump scroll liner was heavily eroded near the seal rings, but the other parts of the pump showed surprisingly little wear.

A thrust bearing designed for the Westinghouse 100A pump operated satisfactorily on water but failed during a test with 1200°C-fired spheres of thoria. After modification of operating techniques, a 384-hr test with slurry was successful.

Seven runs were made in the 100-gpm loops to determine the effect of additives on the caking and sphere-forming tendencies of 800°C-fired oxide. Apparently the presence of ½ wt % of uranium (as $UO_3 \cdot H_2O$), 1.16 mole % MoO_3, or 2500 ppm sulfate [as $Th(SO_4)_2$], singly or combined, is sufficient to prevent the formation of spheres or cakes in a slurry which has been observed to form cakes and spheres without additives.

Blanket run SM-4 was terminated on schedule after 2400 hr of operation. The pump was operated at various frequencies from 42 to 60 cycles, and the system contained a charged concentration of up to 720 g of Th per kg of H_2O at 200°C. Only once was the circulating concentration as high as the charged concentration, and generally it was 30 to 80 kg lower at 60 cycles. At the lower frequencies the discrepancy was much greater.

At charged concentrations above 500 g of Th per kg of H_2O, pressure control became difficult owing to accumulation of dense thoria masses in the pressurizer.

Two uranium additions were made in order to trace the interchange of slurry between the circulating stream and the blanket contents. These additions confirmed previous indications that stagnant thoria existed in the bottom of the blanket, on top of the core vessel, and in the pressurizer.

Steam spargers were used to keep the thoria in suspension during dumping, and nearly all the thoria flowed out of the blanket into the dump tanks. The remainder was easily washed out by successive water rinses.

The vessel interior showed a few badly eroded areas in regions of high free-stream velocities and flow separation. The stainless steel weld pads laid down in front of the inlet nozzles were not appreciably attacked.

The pump was found to be in generally good condition. The titanium impeller showed only slight attack at flow-separation regions. A wear ring (or sleeve) of uniform inside diameter, rather than a labyrinth, was installed for this run, and this design appears to be advantageous.

The conclusions reached during run SM-4 are as follows:

1. Completely uniform thoria suspension was probably not achieved under any conditions, and there were stagnant regions within the vessel.
2. At concentrations above about 500 g of Th per kg of H_2O, there was a tendency for massive thoria to accumulate in the pressurizer.
3. At comparable conditions of flow and temperature, the suspension achieved with the $1\frac{1}{2}$-in. inlet nozzles appeared to be better than that achieved with the 2-in. HRT nozzles.
4. Steam or gas sparging is required to maintain the slurry in suspension during dumping operations.

11. Instrument and Valve Development

Two test bobbins were wound with 30-gage anodized aluminum wire, thus simulating the windings used in differential transformers for sensing primary-element motions. These were exposed to 6×10^{17} fast neutrons per square centimeter and 1×10^8 r of gamma radiation in the ORNL Graphite Reactor without insulation failure.

A long-lived silicon-junction rectifier was tested satisfactorily as a replacement for a thermionic vacuum-tube type of rectifier utilized in an instrument much used in HRP systems.

An alarm-scanner for process-variable instruments, which is capable of continuously scanning 14 variables, one per second, was placed in checkout service on simulated signals.

Two airborne-alpha-contamination monitors of the automatic sample-taking type were constructed and have proved reliable in operation.

Operation of the valve test loop was transferred to the Component Development Section after 4776 hr of operation. The most satisfactory plugs found during this operation were Armco 17-4 PH and gold-gasketed type 347 stainless steel.

A prototype pneumatic actuator for large valves was built; it utilizes two pneumatically powered bellows in a tandem yoke with opposing springs. Each bellows has an effective area of 123 in.^{2} and a pressure rating of 100 psi.

Gold plating to increase the corrosion resistance of the stainless steel bellows used for control-valve stem seals was not satisfactory.

A 2-in. valve especially constructed for slurry use, incorporating a long-radius-bend body configuration, a Colmonoy hard-faced stem, and tungsten carbide trim, was received for installation in a slurry loop.

Stellite No. 6 plugs and Armco 17-4 PH seats were severely eroded, one after intermittent usage totaling 31 hr in slurry sampling, the other after intermittent usage totaling 10 hr in slurry sampling and feeding.

PART IV. REACTOR MATERIALS RESEARCH

12. Solution Corrosion

The corrosion rate of carbon steel in boiler water containing various concentrations of oxygen has been determined. Average corrosion rates of 4, 12, and 22 mpy were observed during 200-hr tests at 300°C with oxygen concentrations of <0.1, 2, and 10 ppm, respectively. In addition, pitting was observed; so the rate of penetration at some localized areas was greater than the values shown.

The corrosion resistance of a number of alloys was determined in 0.17 *m* UO_2SO_4 at temperatures of 200, 250, and 295°C. Types 430, 431, 446, AM-350, and Croloy 16-1 stainless steels; Incoloy; Carpenter alloys 10, 20, and 20Cb; CD4MCu; Hastelloy R-235; Multimet; and Timken 16-25-6 showed corrosion resistance comparable with that of type 347 stainless steel. Nionel, types 414 and 1515 N stainless steel, Hastelloys B, C, and X, and Haynes 25 showed lower corrosion resistance than type 347 stainless steel.

Dynamic loop tests showed that increasing the copper to 0.03 *m* or decreasing the uranium concentration to 0.02 *m* in the HRT core solution (0.04 *m* UO_2SO_4, 0.02 *m* H_2SO_4, and 0.005 *m* $CuSO_4$) had no measurable effect on the stability or corrosiveness of the solution.

Additional loop runs with UO_3-Li_2CO_3-CO_2 solution have confirmed previous data with regard to its nonaggressive nature to carbon steel. However, tests in the temperature range of 250 to 300°C have demonstrated the low solubility of uranium at the higher temperatures. For example, at temperatures between 265 and 280°C less than 1 g of uranium per liter remained in the solution.

It was demonstrated that protective films formed in 0.04 *m* UO_2SO_4–0.04 *m* $BeSO_4$–0.005 *m* $CuSO_4$ solutions at 200 to 250°C and that the solution was stable. The same solution was not completely stable at 300°C. Copper and uranium did not appear to be lost from solution, but beryllium was. However, on lowering the loop temperature to 200°C, the beryllium redissolved.

During an attempt to force a piece of Teflon from a titanium loop with 175 psig oxygen, a fire developed and a portion of the titanium nipple in which the Teflon was lodged was consumed.

Stress-corrosion cracking tests in boiling HRT core solution containing chloride ions have shown that the uranyl ion is the most important ion (except chloride) in making the solution an effective stress corrodent. Other tests have shown that if the stress specimens are exposed for periods as short as 50 hr in the chloride-free HRT solution (100°C) and then exposed to the same solution containing chloride ions, cracking will not occur during times in which cracking occurs in the absence of the pretreatment.

Stress-corrosion specimens tested in boiling water containing 25 to 500 ppm chloride have not shown evidence of cracking after 3000 hr. However, when the same test was carried out in an autoclave pressurized with 150 psi oxygen, seven of eight specimens developed cracks during 400 hr. Other tests in chloride-containing water at 300°C have shown that films formed by pretreatment are of little, if any, value in reducing cracking under the conditions of test.

All the austenitic stainless steels tested, except 309 SCb, developed cracks in chloride-containing water in less than 300 hr at 300°C. Only in one case did Incoloy develop a crack, and in no case did Nionel or Croloy 16-1 crack.

Static corrosion tests have shown that carbon steel plated with nickel by a nonelectrolytic process has good corrosion resistance to water under various pH conditions at 300°C.

In static uranyl sulfate solutions Incoloy has shown a general corrosion resistance similar to that of type 347 stainless steel and a lesser susceptibility to cracking in the presence of chloride. Type AM-350 stainless steel showed good corrosion resistance to uranyl sulfate solutions at 100 and 300°C, but its corrosion resistance was poorer at 200°C. Type 202 stainless steel in the annealed condition was as corrosion resistant as type 347 stainless steel in all tests to which it was subjected. However, in the sensitized condition it was seriously attacked by boiling HRT core solution.

Stellites 1 and 3 and Rexalloy 33 corroded at rates between 0.5 and 1.3 mpy in boiling (100°C) HRT core solution. Under the same conditions Stellite 98M2 corroded at a rate of 5 mpy.

13. Slurry Corrosion

The extenuation of the erosive characteristics of thoria as a result of the removal of large particles by sedimentation classification has been demonstrated in loop experiments. In tests at 200°C and with approximately 500 g of Th per kg of H_2O, 1600°C-calcined thoria prepared by jet precipitation or batch precipitation at 25°C was circulated. These tests resulted in high erosive attack, attributed to large-diameter particles (sinters), which did not degrade appreciably during circulation. The jet-precipitated, 1600°C-calcined thoria was classified by sedimentation to remove the large particles. In a subsequent test at 280°C at a concentration of 323 g of Th per kg of H_2O, the corrosion-erosion rates were low and the slurry handling properties were satisfactory.

Type 347 stainless steel, Zircaloy-3A, and titanium 75A exhibited moderate attack rates in tests with oxygenated slurries of 1600- and 1800°C-fired thoria prepared from jet-precipitated thorium oxalate at a concentration of 1000 g of Th per kg of H_2O; however, the 1800°C-calcined thoria was markedly degraded during 300 hr of circulation.

In toroid tests made to study the effect of operating temperature, atmosphere, and thoria calcination temperature on the corrosion-erosion attack by circulating slurries, generally higher attack rates of selected alloys occurred with hydrogenated slurries than with oxygenated slurries. In hydrogenated tests the attack on type 347 stainless steel increased with increased circulation temperature.

Titanium and zirconium alloys displayed higher corrosion rates in hydrogenated slurries at 150°C than at 100 or 200°C. Postrun properties of some slurries were changed as a result of varying operating temperatures.

In toroid tests, experimental preparations of arc-fired and flame-fired thoria produced high metal attack rates and were degraded during circulation at 250 and 280°C at slurry concentrations of 1000 g of Th per kg of H_2O. Similarly, ThO_2-CaO mixed oxides fired at 1700 and 1800°C were readily degraded during circulation at 250°C with attendant high metal attack rates.

Generally, low attack rates were observed with oxygenated slurries of experimental preparations of silica-coated thoria at 280°C. After circulation the slurries were well dispersed and fluid.

In the first of a series of in-pile rocking-autoclave slurry corrosion experiments, a thoria slurry containing 1000 g of Th per kg of D_2O was irradiated for 261 hr in the LITR HB-6 rocking-autoclave facility at 280°C under 800 psi oxygen in a Zircaloy-2 autoclave. A parallel out-of-pile experiment lasting 480 hr was made. Both experiments exhibited the same initial corrosion rate of approximately 1 mpy as estimated from pressure measurements. The out-of-pile experiment exhibited a slower rate in the latter part of the run.

Development work on an in-pile toroid rotator continued. A new single-arm model was designed and fabricated for test evaluation as a result of excessive wear in the universal joint of the double-arm model previously tested. Work on the in-pile toroid rotator was curtailed during this quarter because of increased effort on the HRT core and blanket corrosion specimen assemblies.

During the past quarter, development work was resumed on a 5-gpm in-pile slurry loop. An experimental loop has accumulated 680 hr of operating time circulating a thorium oxide slurry at a concentration of 500 g of Th per kg of H_2O at 250°C. The improved operation of the loop over that experienced in previous tests, last reported in the quarterly progress report for the period ending October 31, 1956, is attributed in large part to the improved handling properties of the recently available thorium oxide of small particle size calcined at 1600°C.

A standard ORNL 5-gpm in-pile-type pump such as is used in the loop described above has been under test, pumping a thorium oxide slurry without the use of a water purge to the pump bearing region. The pump is equipped with aluminum oxide bearings and journal bushings. No radial-bearing wear or operating difficulty was noted after 550 hr of operation at 40°C circulating a thorium oxide slurry of 0.7 μ mean particle diameter, calcined at 1600°C, at a concentration of 500 g of Th per kg of H_2O. There was some thrust-bearing wear.

14. Radiation Corrosion

During an out-of-pile test, the pump in loop L-4-21 (now designated L-2-21) was damaged by a coupon which became dislodged from the core holder. The loop, which was initially scheduled for insertion in beam hole HB-4, was modified and reassembled with a new pump and is now ready for operation at the higher flux installation in beam hole HB-2 at the LITR.

With the exception of metallographic examination, stainless steel loop experiment L-2-17 has been completed. This experiment employed a light-water solution, which was 0.04 m UO_2SO_4 (enriched), 0.025 m H_2SO_4, and 0.005 m $CuSO_4$. The main-stream and pressurizer temperatures were 300 and 315°C, respectively. No evidence of solution instability during the experiment was observed. The over-all corrosion rate of stainless steel based on oxygen consumption was 0.8 mpy.

A material balance of Fe, Cr, Ni, and Zr was attempted, with the results of analyses of scale from low-power-density regions being used together with the results of oxygen, nickel, and weight measurements in this experiment. The results indicate that nearly all the zirconium which was oxidized in the core was transported to portions of the loop outside the core.

The corrosion rate of Zircaloy-2 at a given solution power density in L-2-17 appears to be in approximate agreement with that observed in the 280°C experiment, L-2-10. In both experiments the corrosion rates of the core annulus specimens were higher than those at the same solution power density in the high-velocity core channels. Analyses of a channel and an annulus Zircaloy-2 specimen from the L-2-17 core revealed the presence of uranium sorbed on the surfaces in amounts which are considered significant. The amount of uranium per unit area found on the core annulus specimen was about the same as the amount in a 30-μ layer

of solution adjacent to the specimen. Calculations indicate that, in this case, about 80% of the fission-fragment recoil energy reaching the specimen surface originated in the sorbed surface uranium. Analysis of the specimen from the high-velocity core channel showed an amount of sorbed uranium which is a factor of 4 lower than that found on the annulus specimen. These results are consistent with the interpretation that uranium sorbed on the surface is responsible for an appreciable fraction of the total corrosion attack of a Zircaloy-2 specimen under irradiation.

The corrosion rate of type 347 stainless steel in L-2-17 was higher than that observed in experiment L-2-10 at a given power density.

Three autoclave experiments were assembled and operated in the HB-5 facility of the LITR during the past quarter. On the basis of these three experiments it appears that the galling and wear of the fixed-plug-hole liner have been eliminated by the installation of Oilite bronze bearings and a nose bearing. No solution autoclaves were operated in the HB-6 facility of the LITR during the past quarter; the HB-6 equipment is now being used for radiation-corrosion studies with thorium oxide slurries.

Values reported previously for the neutron flux in the LITR facility HB-5 have been revised. In one experiment, thermal-flux values determined from the induced activity in zirconium are about 30% greater than those determined from cobalt monitors.

Six experiments have included zirconium–15% niobium or zirconium–15% niobium–1.5% tin alloy specimens. The scale on niobium-alloy specimens contains about an order of magnitude less uranium than the scale on Zircaloy-2. Addition of Li_2SO_4 to uranyl sulfate solutions did not substantially alter the corrosion rate of niobium-alloy specimens. Pure niobium has been exposed twice. In both cases niobium scale contained about an order of magnitude more uranium than scales on Zircaloy-2, and the niobium corrosion rate was little affected by Li_2SO_4.

Zircaloy-2 corrosion data from seven autoclaves are reported. Data from two experiments which included Li_2SO_4 are included. Corrosion inhibition by Li_2SO_4 in 0.17 *m* UO_2SO_4 at 280°C was verified. However, the Li_2SO_4 addition appears to have little effect on the corrosion rate at 250°C. The degree of inhibition by Li_2SO_4 in a 0.04 *m* UO_2SO_4 solution at 280°C is uncertain, but appears to be less than that in the 0.17 *m* UO_2SO_4. The scale from the 0.04 *m* UO_2SO_4 experiment contained less uranium than would be expected without the Li_2SO_4 additive. The scale from the 0.17 *m* UO_2SO_4 experiment contained about the amount of uranium that would be expected without the Li_2SO_4.

Stainless steel specimens were irradiated for 45 hr with Van de Graaff electrons. The specimens were contained in a thermal siphon loop and exposed to a uranyl sulfate solution at 280°C. No significant effect of the irradiation on the corrosion of the steel was observed.

Test-specimen assemblies to be used in obtaining radiation-corrosion and mechanical-property information during operation of the HRT were fabricated, and one assembly, containing 24 specimens, was installed in the HRT blanket region. The other assembly will be installed in the core region.

15. Metallurgy

The quench-and-reheat transformation data obtained on the ternary Zr-Nb-*X* alloys and on the binary Zr-Nb alloys over the range of compositions and temperatures of interest to the alloy development program have shown that future investigations should be concentrated on the ternary alloys Zr-15Nb-*X* and Zr-20Nb-*X*, with *X* = 2% Mo, 5% Mo, 2% Pd, and 5% Pd, because of their transformation, oxidation, and corrosion characteristics. Small-scale investigations of the Zr-Pd and Zr-Pt systems will be continued because of their apparent corrosion resistance to the fuel solutions in-pile.

Oxidation data, in air at 600 and 700°C, have been obtained on most of the binary and ternary alloys investigated in the alloy development program. The ternary alloys Zr-15Nb-5Pd, Zr-15Nb-½Cu, and Zr-15Nb-5Mo had oxidation resistance better than Zircaloy-2 at both 600 and 700°C but not so good as that of iodide zirconium. All the other alloys tested had poorer oxidation resistance to air than Zircaloy-2.

Metallographic experiments have been performed to examine and identify the hydride layer formed on the surface of Zircaloy-2 specimens hydrided to 100 and 500 ppm H_2 at 400°C. Identification was successful for the 500 ppm H_2 specimen but was doubtful for the 100 ppm H_2 specimen. Development of procedures for the preservation of the edge of mounted specimens is continuing.

With high-purity unalloyed titanium, a trough occurs in the impact curve in the temperature region of 250°C. It has been shown that this reduction is not caused by a simple aging phenomenon.

With unalloyed titanium, contaminated with hydrogen, a transition from a ductile to a brittle fracture occurs over a relatively narrow temperature range. This range seems to coincide with the range in which the hydrides are going into solution.

Optimistic results are presented on the development of tungsten inert-gas arc-welding methods suitable for air welding of Zircaloy-2 and the alpha titanium alloy A-110AT. Such welds can be made with conventional welding equipment.

Investigations have been started into development of a reliable ultrasonic inspection for stainless steel welds. Progress has been made in eliminating spurious indications from high or irregular cover and root beads.

The fracture path in irradiated impact specimens made of cold-worked iron has been observed to occur on two successive planes 90 deg apart. This unusual behavior is attributed to the joint effect of preferred orientation and radiation embrittlement.

The irradiation-induced transition-temperature shift in subcritically annealed iron was found to be 225°F for an irradiation of less than 10^{19} fast neutrons/cm^2.

PART V. CHEMICAL ENGINEERING DEVELOPMENT

16. Uranyl Sulfate Fuel Processing

Accumulation of solids on type 347 stainless steel pins in contact with agitated slurries of simulated HRT corrosion-product solids at 25–100°C has been generally limited to an equilibrium value of 10 to 50 μg/cm^2. The maximum deposit, 1 mg/cm^2, corresponds to a deposit thickness of 0.05 mil.

Iodine absorbed on silvered Yorkmesh was not removed by various wet and dry thermal-cycling treatments up to 400°C or by heating to 600°C. Diffusion of absorbed iodine into the mass of the silver appeared to limit the rate of iodine absorption, a characteristic not observed with silvered alundum.

17. Gaseous Fission-Product Disposal

Adsorption of iodine from a flowing gas stream by charcoal appeared irreversible, but a very slow movement on a bed of molecular-sieve material was noted. Equilibrium adsorption data for krypton on various molecular-sieve materials did not agree with data obtained in a dynamic system. Xenon is adsorbed 11 to 12 times more strongly than krypton on the adsorbents studied.

18. Uranyl Sulfate Blanket Processing

The results of four runs with plutonium in 1.4 *m* UO_2SO_4 at 250°C under 350–400 psi of oxygen in the P-1 loop were similar to those obtained previously with zirconium. When dissolved plutonyl sulfate was injected into circulating 1.4 *m* UO_2SO_4 at 250°C, most of it stayed in solution until the concentration exceeded 100 mg of Pu per kg of H_2O. At higher concentrations the plutonium was rapidly removed from solution by adsorption on the stainless steel. Less than 1% was removed as solids by the hydroclone. When 850 mg of plutonium as preformed PuO_2 was injected, 20% was removed by the hydroclone, 35% was adsorbed on the stainless steel, and the rest was distributed throughout horizontal sections of the loop as loose solids.

Plutonium adsorption on stainless steel from 1.4 *m* UO_2SO_4 containing plutonium at a concentration of 2 mg per kg of H_2O was about 0.0004 μg/cm^2/hr during a 110-hr run. In a 180-hr run, in which the plutonium concentration was gradually increased from 2 to 75 mg per kg of H_2O, plutonium adsorption on type 347 stainless steel averaged 0.005 μg/cm^2/hr. Adsorption was up to 300 μg/cm^2 when plutonium concentrations were increased to > 100 mg per kg of H_2O, and the amount adsorbed depended on the amount of plutonium added. Total adsorptions of up to 1 mg/cm^2 were obtained. Even preformed PuO_2 was strongly adsorbed.

The hydroclone was apparently effective in removing solids that reached it, but only small amounts of solids actually reached the hydroclone. Less than 1% of the total corrosion products (determined by nickel analysis) was removed as solids by the hydroclone.

Static laboratory tests indicated that the addition of 0.5 *m* H_2SO_4 to the usual 1.4 *m* UO_2SO_4 solution decreased the adsorption of plutonium on

titanium and Zircaloy-2 to 10% of the value for neutral solutions under the same conditions.

19. Thorium Oxide Slurry Development

A slurry of 1600°C-fired thorium oxide in D_2O (~750 g of Th per kg of D_2O) was irradiated for 212 hr in the LITR at 300°C without difficulty. In a slurry (500 g of Th per liter) of Dri-film–coated thorium oxide in diphenyl that was being irradiated at 300°C in the LITR, the autoclave stirrer ceased to operate after four days, presumably as the result of a radiation-induced viscosity increase. The silicate-stabilized Davison thoria sol broke to a slow-settling slurry while under irradiation at 200°C in the LITR. More than 80% of the fission-product and protactinium activities were found in the supernatant of the recovered slurry. Gas production rates and equilibrium pressures in irradiated slurries of thorium-uranium oxide fired at 650 and 900°C showed no effect of firing temperature.

In out-of-pile studies, slurries of a simple mixture of 1600°C-fired thorium oxide and $UO_3 \cdot H_2O$ and of 1600°C-fired thorium-uranium oxide prepared from the coprecipitated oxalates containing MoO_3 at concentrations 0.05 *m* and above both gave gas combination rates far in excess of those required in a TBR blanket.

The effects of the chemical and physical variables of the batch oxalate precipitation step on the production of sized thorium oxide are being evaluated. The average particle size of the oxide products decreased with decreasing precipitation temperature and increasing reagent concentration. Products of more uniform particle size were produced at lower precipitation temperatures. The fraction of oversize particles decreased with increasing stirring rate and reagent addition rate. Well-digested and more uniform materials appeared to give less clinker formation on high firing.

A Tolhurst basket centrifuge was tested on thorium oxide and thorium oxalate and was delivered to the Pilot Plant Section for interim use. Evaluation of alternative precipitation, classification, and centrifugation equipment for use in a pilot plant production facility is continuing. The procedure for flame calcination of thorium oxide in quantities sufficient for loop tests will utilize an alcohol slurry feed to an aspirating nozzle and a product collection system consisting of a spray column and a bag filter.

The thorium oxide production facility was modified to permit preparation of 750 lb/month of thorium oxide of about 1 μ average particle size calcined at 1600°C. A capacity of 1500 lb/month is anticipated. About 550 lb of 1600°C-calcined oxide, classified to less than 5 μ and to about 1 μ average size, was produced.

The effect of length/diameter ratio on the hindered settling rate in vertical cylinders of slurries of 800- and 1600°C-fired thorium oxide in water at thorium concentrations of 200, 400, and 700 g per kg of H_2O was not discernible at *L/D* ratios less than 10. In general, the 1600°C-fired oxide gave more reproducible results than the 800°C-fired oxide.

Oxide products produced by the 650°C firing of a thorium oxalate precipitated in the presence of cellulose were more bulky than the normal products; they had lower surface areas, but similar x-ray crystallite sizes.

A pronounced induction period for thorium oxalate precipitation was obtained in the presence of 5 *M* excess nitric acid (0.1 *M* thorium nitrate, 0.22 *M* oxalic acid). Despite the induction period, oxalate precipitation appeared essentially complete.

Thorium nitrate solution by itself and with H_2SO_4, H_2SiO_3, $Al(NO_3)_3$, $Pb(NO_3)_2$, or $Na_4P_2O_7$ additives (at mole ratios of added oxide to thorium oxide in the final product ranging from 0.005 to 1) was evaporated under a heat lamp and calcined at 650°C. None of the final products appeared to be acceptable slurry materials.

The adsorption potential of carbon dioxide on thoria varied linearly with surface coverage. Two kinds of surface sites were involved below 200°C, but only one above that temperature. Desorption curves indicated a variation of activation energy or adsorption potential with surface coverage.

Studies on the adsorption of sulfuric acid from aqueous solution indicated that for each surface site four hydrogen ions and two sulfate ions disappear from solution. Infrared absorption studies with the recovered solids showed that the adsorbed sulfate can be determined by this means. The data correlated directly with the data from chemical analyses.

Approximately 50 kg of thoria microspheres (1000°C fired) classified into <3 μ, 3–30 μ, and 30–50 μ fractions is being prepared.

20. In-Pile Slurry Loop

The design of the ORR installation for the in-pile slurry loop is approximately 65% complete, based on the original project concept. The major items of design required for installation at the reactor are approximately 90% complete; these items include the five shielded equipment chambers, the special reactor plug, the shield door and shutter, and other miscellaneous equipment. The various shielded carriers and handling tools which do not require installation are approximately 50% complete.

PART VI. SUPPORTING CHEMICAL RESEARCH

21. Aqueous Systems at Elevated Temperatures

The rates of the copper-catalyzed deuterium-oxygen reactions were measured in heavy-water solutions whose compositions were approximately the same as the composition of the HRT fuel solution. Reaction parameters, including the combined effects of intrinsic solution activity and the distribution of deuterium between the vapor and solution phases, were determined at 250, 275, and 300°C. The combined parameters are directly proportional to the copper concentration, and their temperature dependence corresponds to approximately a 24-kcal activation energy.

PART VII. ANALYTICAL CHEMISTRY

22. Analytical Chemistry

A sensitive spectrophotometric method was devised for the determination of titanium in slurries of thorium oxide. A polarographic method was applied to the determination of microgram quantities of uranium in samples of thorium oxide slurry. A gamma-counting procedure was used successfully in determining thorium in fractions of thorium oxide slurries.

A procedure was devised for the flame-photometric determination of microgram quantities of silver in uranyl sulfate solutions. A pyrolytic separation method for the removal of ruthenium from materials containing salts of this element was applied successfully for the removal of milligram quantities of ruthenium metal from stainless steel parts.

CONTENTS

SUMMARY iii

PART I. HOMOGENEOUS REACTOR TEST

1. HRT OPERATIONS 3
   - 1.1 Reactor Operations 3
   - 1.2 Initial Critical Experiment 4
     - 1.2.1 Critical Experiments at Elevated Temperatures 6
     - 1.2.2 Critical Concentrations 7
   - 1.3 Metallurgy Service Work 8
2. HRT DESIGN 9
   - 2.1 Remote Maintenance 9
   - 2.2 Flange Development Program 9
3. HRT COMPONENT DEVELOPMENT 13
   - 3.1 Fuel Circulating Equipment 13
     - 3.1.1 400A-1 Westinghouse Pump and Loop 13
     - 3.1.2 400A-2 Pump and Loop 14
     - 3.1.3 300A-1 Pump 14
   - 3.2 Feed Pumps 14
     - 3.2.1 Feed Pump Endurance Testing 14
     - 3.2.2 Purge Pumps 15
     - 3.2.3 Corrosion Fatigue Tests 15
   - 3.3 HRT Maintenance 15
   - 3.4 HRT Mockup 16
     - 3.4.1 Operation 16
     - 3.4.2 System Changes 16
     - 3.4.3 Iodine Removal Tests 16
     - 3.4.4 Heating of Fuel Solution 16
     - 3.4.5 Corrosion in Stagnant Lines 16
     - 3.4.6 Fuel-Solution Chemistry 17
4. HRT CONTROLS AND INSTRUMENTATION 18
   - 4.1 Component and System Testing 18
     - 4.1.1 Leak-Detection-System Instrumentation 18
     - 4.1.2 Nuclear Instrumentation 18
     - 4.1.3 Pump-Stator-Winding Insulation Tests 18
   - 4.2 Component Development 18
     - 4.2.1 Control-Valve-Stem Position Transmitter 18
     - 4.2.2 Remote Disconnect for Metal-Clad Mineral-Insulated Electrical Cable 18
     - 4.2.3 Oxygen-Injection System 20
   - 4.3 Maintenance 21
     - 4.3.1 Differential-Transformer Testing Device 21
     - 4.3.2 Television System for Use in Reactor Maintenance 22

5. HRT PROCESSING PLANT 23
5.1 Operations 23
5.1.1 Over-All Piping Leak Test 23
5.1.2 Hydroclone-System D_2O Run 23
5.1.3 Off-Gas Chilled-Water System 23
5.2 Construction and Maintenance 23
5.2.1 Cell Closure 23
5.2.2 Damage to Insulation and Wiring by Shield Water 23
5.3 Holdup Tests on HRT Charcoal Adsorber Beds 24
5.4 Design of Waste Carrier and Loading-Pit Facility 25
5.5 Solids Behavior Development Studies 25

PART II. REACTOR DESIGN, RESEARCH, AND ANALYSIS

6. HRE-3 DESIGN 31
6.1 Low-Pressure-System Flowsheet 31
6.2 Preliminary Design Data 31
6.3 Core and Blanket Dump Systems 31
6.4 Letdown from the High-Pressure System 31
6.5 Oxygen Pressurization 33
6.6 Iodine Removal 33

7. RESEARCH AND ANALYSIS 35
7.1 Breeding Ratio in Thorium Breeder Reactors 35
7.2 Time-Dependent Studies of Slurry-Core, Slurry-Blanket Thorium Breeder Reactors 39
7.3 Heat Generation Rates in HRE-3 Core Vessel 41
7.4 Physical Chemistry of Slurries 43
7.4.1 Thorium Oxide Preparation 43
7.4.2 Influence of Surface-Active Agents on Thoria Slurry Properties 43
7.5 Slurry Heat Transfer 44
7.6 Test of a Hydroclone for Partial Size Classification of Thoria Particles 44
7.7 Slurry Rheology 48

8. HRE-3 INSTRUMENTATION AND CONTROLS SYSTEM DESIGN 49
8.1 Plant Power Distribution System 49
8.2 Conceptual Electrical Equipment Layout 49
8.3 Conceptual Control-Room Layouts 49

PART III. ENGINEERING DEVELOPMENT

9. DEVELOPMENT OF FUEL-SYSTEM COMPONENTS 53
9.1 Recombiner Development 53
9.1.1 High-Pressure Recombiner 53
9.1.2 Syracuse Contract 53

9.2 Centrifugal Pumps 53
9.2.1 20-cfm Allis-Chalmers Blower 53
9.2.2 4000-gpm Byron Jackson Pump 53
9.2.3 Reliance 6000-gpm Pump 53
9.3 Oxygen Compressors 54
9.4 Fuel Feed Pumps 55
9.5 Dump-Valve Trim 55
9.6 Titanium Program 55
9.7 Flange Test Program 56
9.7.1 Bolting-Material Program 56
9.8 Thermal-Cycle Facility 57
9.9 Heat Exchangers 58
9.9.1 Tube-Joint Test 58
9.9.2 Heat Exchanger Test Facility 58
9.10 HRE-3 Pressurizer Development 58
9.10.1 Titanium Equipment for Containing Boiling UO_2SO_4 Solutions 58
9.10.2 Heating and Cooling of Steam-Oxygen Mixtures 58
9.10.3 Gas Dissolving Efficiency of Eductor 59
9.11 Heat Transfer from HRE-3 Core Wall to Core Solution 59
9.12 Development of Slurry Components 59
9.12.1 300A Slurry Loop 59
9.12.2 Feed Pumps 59
9.12.3 Slurry Check-Valve Material Test 60
9.12.4 Separation of Water from ThO_2 Slurry 60
9.12.5 30-in. Low-Pressure Model of HRE-3 Blanket 60
9.12.6 Slurry Dump Tanks and Evaporators 60

10. DEVELOPMENT OF REACTOR SLURRY SYSTEMS 62
10.1 Circulating-Slurry Behavior 62
10.1.1 200-gpm-Loop Operation 62
10.1.2 100-gpm-Pump Thrust Bearing 62
10.1.3 100-gpm-Loop Operation 62
10.1.4 Laminar Flow at Elevated Temperatures 65
10.2 HRT Blanket System Development 67
10.2.1 Slurry Distribution Studies 68
10.2.2 Pressurizer Behavior at Concentrations Above 500 Grams of Thorium per Kilogram of Water 72
10.2.3 Dump Operation and Examination of Equipment 73
10.2.4 Conclusions from Run SM-4 75

11. INSTRUMENT AND VALVE DEVELOPMENT 78
11.1 Instrument Development 78
11.1.1 High-Temperature Radiation-Resistant Differential Transformers 78
11.1.2 Solid-State-Component Instrument Systems 78
11.1.3 Instrument Alarm-Scanner 78
11.1.4 Airborne-Alpha-Contamination Monitor 80

11.2 Valve Development 80
11.2.1 Solution-Valve Trim 80
11.2.2 Valve Actuators 83
11.2.3 Stem Sealing Bellows 83
11.2.4 Slurry-Service Valves 83
11.2.5 Slurry-Valve Trim 83

PART IV. REACTOR MATERIALS RESEARCH

12. SOLUTION CORROSION 89
12.1 Dynamic Solution Corrosion 89
12.1.1 Corrosion in Water at 300°C 89
12.1.2 Corrosion Resistance of Several Alloys at 200 to 295°C in 0.17 *m* UO_2SO_4 89
12.1.3 Stability of Dilute Uranyl Sulfate Solutions 91
12.1.4 Circulation of Uranyl Carbonate Solutions at 250 to 300°C 91
12.1.5 Circulation of 0.04 *m* UO_2SO_4 Containing 0.04 *m* $BeSO_4$ 91
12.1.6 Combustion of a Titanium Nipple in Oxygen at Room Temperature 92
12.2 Laboratory Corrosion Studies 92
12.2.1 Stress-Corrosion Cracking in Uranyl Sulfate Solution 92
12.2.2 Stress-Corrosion Cracking in Chloride-Containing Water 94
12.2.3 Corrosion Behavior of Electroless Nickel Plate 96
12.2.4 Miscellaneous Corrosion Tests 96
13. SLURRY CORROSION 99
13.1 100A Pump Loop Tests 99
13.1.1 Introduction 99
13.1.2 Effect of Classification on Corrosion by Slurries of High-Fired Thoria Prepared from Jet-Precipitated Thorium Oxalate 99
13.1.3 Circulation of Slurry of 1600°C-Calcined Thoria Prepared from Thorium Oxalate Precipitated at 25°C 102
13.2 Toroids 103
13.2.1 Introduction 103
13.2.2 Tests with Thorium Oxide Prepared from Jet-Precipitated Thorium Oxalate 103
13.2.3 Effect of Atmosphere, Circulation Temperature, and Thoria Calcination Temperature on Attack by Aqueous Slurries 103
13.2.4 Toroid Tests with Slurries of Arc-Fired and Flame-Fired Thoria 107
13.2.5 Circulation of Slurries of ThO_2-CaO Mixed Oxides 109
13.2.6 Tests with Slurries of Silica-Coated Thoria 110
13.3 In-Pile Autoclave Slurry Tests – LITR 110
13.3.1 Introduction 110
13.3.2 Development, Construction, and Operation 111
13.3.3 Computation of Gas Data 112
13.3.4 Discussion of Results: Pressure Measurements 113
13.4 In-Pile Slurry Toroid 114
13.4.1 Development Engineering 114
13.5 In-Pile Slurry Loop 115
13.5.1 Loop Development 115
13.5.2 Slurry Pump Test 116

14. RADIATION CORROSION 117
14.1 In-Pile Loops 117
14.1.1 Development and Construction 117
14.1.2 General Description of In-Pile Loop Experiment L-2-17 117
14.1.3 Qualitative Results of Inspection and Evaluation of Loop L-2-17 120
14.1.4 Quantitative Inspection, Results, and Discussion of Loop L-2-17 123
14.1.5 In-Pile Loop L-2-19 133
14.2 In-Pile Solution Autoclave Tests – LITR 134
14.2.1 Development, Construction, and Operation 134
14.2.2 HB-5 Experiments 134
14.2.3 HB-6 Experiments 135
14.3 Supporting Research 139
14.4 HRT Corrosion Specimens 139
15. METALLURGY 141
15.1 Physical Metallurgy 141
15.1.1 Zirconium-Alloy Development 141
15.1.2 Zirconium-Hydrogen Study 143
15.2 Mechanical Metallurgy 144
15.2.1 Titanium 144
15.2.2 Zirconium Alloys 145
15.2.3 Mechanical Properties of Irradiated Titanium Alloys 146
15.2.4 Creep Studies 147
15.3 Welding Development 147
15.3.1 Titanium-Alloy Welding 147
15.3.2 Zirconium-Alloy Welding 148
15.4 Nondestructive-Testing Development 148
15.4.1 Weld Inspection 148
15.5 Active-Metal Reactions 149
15.5.1 Titanium 149
15.5.2 Zirconium 151
15.6 Ceramic Developments 151
15.6.1 Calcination of Thorium Oxide at 1600°C 151
15.6.2 Calcining Techniques for Thorium Oxide 151
15.7 Effects of Radiation on Structural Metals and Alloys 151
15.7.1 Equipment and Facilities 151
15.7.2 Steels and Iron 152
15.7.3 Zirconium Alloys 152

PART V. CHEMICAL ENGINEERING DEVELOPMENT

16. URANYL SULFATE FUEL PROCESSING 155
16.1 Solids Behavior 155
16.2 Iodine Chemistry 155
17. GASEOUS FISSION-PRODUCT DISPOSAL 157
17.1 Dynamic Studies 157
17.2 Equilibrium Studies 157

18. URANYL SULFATE BLANKET PROCESSING 162
18.1 Loop P-1 Operation 162
18.2 Plutonium Behavior in the P-1 Loop 163
18.2.1 Plutonium Distribution 163
18.2.2 Solids Removal 163
18.2.3 Plutonium Solubility 164
18.2.4 Plutonium Adsorption on Metals 165
18.3 Plutonium Adsorption on Metals in Static Tests 166
19. THORIUM OXIDE SLURRY DEVELOPMENT 167
19.1 Slurry Irradiation Studies 167
19.1.1 Slurry Irradiations in the LITR 167
19.1.2 Postirradiation Examinations 167
19.1.3 In-Pile Gas Production and Recombination 168
19.2 Gas Recombination Studies 168
19.2.1 Studies with Simple Mixtures 168
19.2.2 Mixed-Oxide Slurries 168
19.3 Thorium Oxide Preparation Development 168
19.3.1 Laboratory Studies 168
19.3.2 Thorium Oxalate and Thorium Oxide Slurry Concentration 171
19.3.3 Flame Preparation Methods 172
19.3.4 Thorium Oxide Classification 172
19.4 Thorium Oxide Production 172
19.5 Hindered-Settling Studies 173
19.6 Special Preparations 173
19.6.1 Cellulose Additions 173
19.6.2 Nitric Acid Addition to the Thorium Oxalate Precipitation Step 174
19.6.3 Oxide from the Direct Calcination of Thorium Nitrate 174
19.7 Surface-Chemistry Studies 174
19.8 Thoria Microsphere Preparation 175
20. IN-PILE SLURRY LOOP 176
20.1 Status of Design 176
20.1.1 Sampling 177

PART VI. SUPPORTING CHEMICAL RESEARCH

21. AQUEOUS SYSTEMS AT ELEVATED TEMPERATURES 181
21.1 Homogeneous Catalysis of the Hydrogen-Oxygen Reaction in Aqueous Solutions 181

PART VII. ANALYTICAL CHEMISTRY

22. ANALYTICAL CHEMISTRY 187
22.1 Analysis of Thorium Oxide 187
22.1.1 Determination of Titanium 187
22.1.2 Polarographic Determination of Uranium 187
22.1.3 Application of Gamma Counting to the Determination of Thorium Oxide 187

22.2 Analysis of Uranyl Sulfate Solutions 188
22.2.1 Flame-Photometric Determination of Silver 188
22.2.2 Pyrolytic Separation of Ruthenium from Metals 188

Part I

HOMOGENEOUS REACTOR TEST

S. E. Beall

1. HRT OPERATIONS

S. E. Beall

H. F. Bauman
N. C. Bradley
N. A. Brown[1]
D. F. Bruley
J. R. Buchanan
J. R. Engel
J. D. Flynn
D. F. Frech
T. H. Gladney[1]
R. H. Guyman
R. J. Harvey
P. N. Haubenreich
J. Hernandez[2]
J. W. Hill, Jr.
S. I. Kaplan
J. O. Kolb
R. M. Pierce[1]
D. M. Richardson
G. W. Rivenbark
J. A. Russell
H. K. Search[3]
A. J. Sharenberger
J. E. Sutherland
W. Terry
K. W. West
R. Van Winkle

1.1 REACTOR OPERATIONS

After successful performance testing of the HRT with light water and natural uranium, the system was thoroughly drained and final leak-testing of the reactor piping was begun. Forty curies of Kr^{85} were injected into the system in small increments while pressurizing to 500 psig with nitrogen. The reactor shield was sealed by inserting the roof plugs and covering them with a plastic sheet. The pressurized assembly then was allowed to stand for five days, with the space-cooler fans running to mix the atmosphere inside the shield. Daily air samples drawn from inside the shield were analyzed for krypton activity, using the method previously proposed;[4] however, difficulties in purification of the samples during their preparation for counting rendered the results inconclusive. Samples were then withdrawn from the volumes under test and compressed into gas cylinders for storage, pending refinement of the analytical method; and a portion of the krypton-bearing gas was bled from the piping and replaced with helium, to provide a 60% helium concentration in the reactor at 512 psia total pressure. The system again was allowed to stand undisturbed for a five-day interval, following which samples were withdrawn from the shield, heat exchanger shells, instrument cubicles, reactor steam system, and each of the auxiliary piping systems which come in contact with the reactor piping. These samples were checked with helium leak detectors capable of sensing 1 ppm helium in air. After each sample check, the detector in use was rechecked against a prepared standard atmosphere containing 5 ppm helium. The results indicated a total gas leakage from the reactor piping of less than 0.2 std cc/day, referred to a Δp across the leak of 1 atm. The permissible leak rate[5] for the HRT under the above conditions is 1 std cc/day. Further confirmation of the leaktightness of the piping was furnished by analysis of the stored krypton samples, using an improved method. These results also indicated a leak rate of less than 0.2 std cc/day.

During the same period, activity-breakthrough tests were completed on the two remaining charcoal adsorption beds (see Sec 17.1).

After the integrity of the reactor piping was established, the cell was opened in mid-November to permit final insulation of reactor piping and auxiliary lines, inspection and repair of thermocouples, and leak-testing of air lines and conduit, in preparation for over-all testing of the containment vessel. During this maintenance period, the new refrigeration system was also installed in the control area.

The iodine removal bed, at the bottom of the fuel recombiner, was cut open to remove the silver-impregnated alumina pellets, because tests showed that sodium ions continued to leach from the pellets even after they were refluxed over water for several hundred hours. The pellets were replaced with silver-coated stainless steel Yorkmesh. The reassembled unit was temporarily installed above the HRT waste evaporator, to undergo steam-pressure-drop measurements and leaching tests. It was found to be acceptable in both

[1]On loan from TVA.

[2]On loan from Puerto Rico Water Resources Authority.

[3]On loan from Pennsylvania Power and Light Co.

[4]S. E. Beall *et al.*, *HRP Quar. Prog. Rep. Oct. 31, 1957*, ORNL-2432, p 4.

[5]S. E. Beall and S. Visner, ORNL-1834, p 42 (Jan. 1, 1955) (classified).

respects and was reinstalled in the reactor during the first week in December.

During the maintenance period, the bulkhead door was installed in the cell, and each half was flooded separately to test the effectiveness of the door seal. Minor leakage was observed, which could be handled adequately by the sump jets. Leak-testing efforts were continued on the service piping within the cell and on the penetrations through the north shield wall.

Before the cell was reclosed the reactor piping was flushed with a small amount of heavy water to remove residual H_2O, after which 5879 lb of heavy water was charged to the system. The shield was then sealed and evacuated to ½ atm absolute, and the HRT was brought to operating temperature and pressure on December 14, for a final, heavy-water shakedown run (No. 11). This run was interrupted on the following day, however, to investigate the lack of flow from the purge pump of the fuel circulating pump. It was discovered that a rubber stopper had been accidentally left in the pump inlet line when the flanges were connected. Following the removal of the stopper run No. 11 recommenced. Performance was judged satisfactory on December 20, after 82 hr of operation at 1700 psig and 280°C, and the reactor was cooled to 25°C to practice temperature-control techniques to be used for the first critical experiment. During the cooling period the amount of D_2O required to maintain the liquid level, as the contents of the core contracted, was measured to check previous volume calibrations of the core and fuel circulating loop. A volume of 475 liters was indicated by the test; this number agrees with a previous determination to within 2%.

Fuel charging began on December 24, and criticality was achieved on December 27, at 6:00 PM. During the next week the source and core thimble were removed, and a successful trial installation and removal of the core corrosion specimens was made, with lead-shielded direct maintenance techniques.

Leak-testing of the reactor cell was then resumed. The special vacuum valve in the 16-in. duct to the stack was found to be the major source of leakage; removing the valve and blanking the open flange cut the in-leakage, at 7.5 psia, from 25 cfm to approximately ½ cfm. Upon pressurizing the cell and flooding the roof plugs with water, it was found that the welded joints between the galvanized-iron roof seal pans and the stainless steel lips along the cell wall constituted a second major source of leakage. This difficulty is discussed in detail in Sec 1.3. To stop numerous small leaks and ensure against future difficulty, a tough thermosetting resin was cast into the seal lips along the entire periphery of the cells and girder boxes. Any galvanized seal pans which are subsequently removed will be replaced with stainless steel pans.

Upon completion of the roof repairs, which cut cell leakage to approximately ¼ cfm, further operational tests were conducted in preparation for further low-power critical tests to determine the temperature coefficient of reactivity. Heat-loss measurements on the low-pressure system, reactor steam system, and complete reactor piping were conducted also.

During the period January 8–11, the reactor was brought to criticality seven times at successively higher temperatures, from 65 to 281°C, as described in Sec 1.2.1.

Shield leak-testing and repairs were resumed after the critical experiments were completed. The shield was sealed and pressurized to 30 psia, and 2.2 liters of 10% ethyl mercaptan solution was blown into the closed volume and mixed by operating the space-cooler fans. The resultant concentration of 40 ppm was approximately 2000 times the minimum detectable level. All accessible penetrations and exposed areas of the shield were checked for escaping vapor over a 24-hr period. Only one significant leak was found, and it was repaired. The residual leakage of approximately 4.5 liters/min apparently discharges into the ground around the shield.

1.2 INITIAL CRITICAL EXPERIMENT

The HRT was made critical the first time with the core and blanket near room temperature and at a pressure of about 800 psig. In order to maintain the low temperature, it was necessary to circulate water through the shell side of the steam generators to remove heat put in by the circulating pumps and pressurizers. Nuclear instrumentation consisted of three fission chambers: the two permanent chambers in the instrument tube and a special chamber in the blanket thimble (see Fig. 1.1). An antimony-beryllium neutron source was suspended in the thimble in the center of the core. The north shield wall was filled with water during

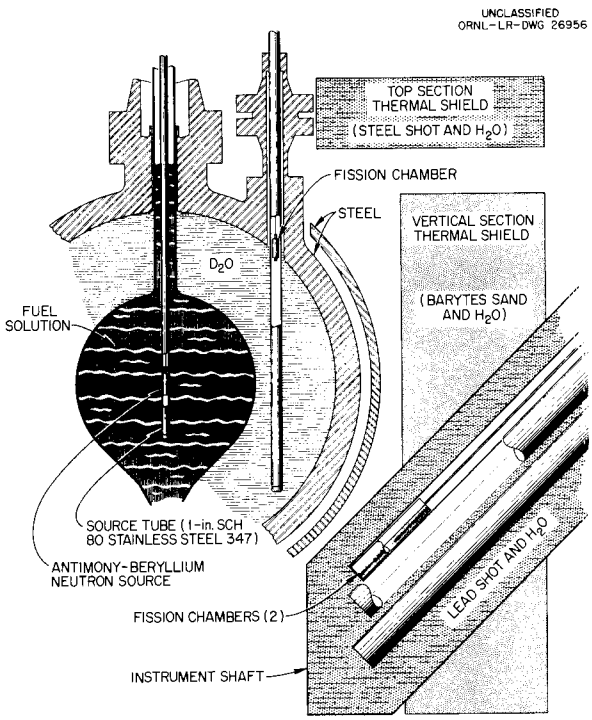

Fig. 1.1. Source and Fission-Chamber Positions During Initial Critical Experiment, Dec. 27, 1957.

the experiment, and the top plug, the cover plates, and access plugs over the core were removed to admit the fission-chamber connections and the source cable. Otherwise, the shield was complete.

The reactor was brought up to the critical condition gradually by the injection of 100- to 400-g increments of U^{235} into the fuel solution. Batches of concentrated fuel solution were added through the sampler to the dump tanks. Fuel-feed and purge pumps were run continuously to provide mixing between the dump tanks and the high-pressure system. Following each addition, the solution concentration in the high-pressure system was allowed to reach steady state, as indicated by a leveling-off of fission count rates. The steady-state count rates were then determined, and a 300-ml sample was taken from the fuel high-pressure system. The inverse of the counting rate was plotted against total uranium in the reactor as a guide for gaging the size of later additions.

A total of 853 g of U^{235} was added on December 24. Additions on December 26 brought the reactor U^{235} inventory to 1709 g. Further additions brought the total U^{235} in the reactor to 2043 g by the afternoon of the next day. At this time it was estimated that another 17 g would make the reactor critical at 25°C, the core temperature up to that time. According to plan, this addition was made only after the core temperature had been raised to 29°C. The intent was to make the reactor critical by slowly lowering the temperature after the uranium concentration had reached steady state; the source was to be withdrawn and replaced a number of times to check on the approach to criticality as the temperature decreased. But the source was withdrawn, in fact, only once. As the source was withdrawn very slowly, count rates on all three fission chambers rose, as shown in Fig. 1.2. With the source out of the reactor, count rates continued to rise, indicating that the reactor had achieved criticality. Apparently the uranium concentration had been brought up so far that multiplication of the source neutrons had raised the flux at the source until the source was absorbing neutrons faster than it was emitting. Then, when the source was removed, the reactor became slightly supercritical. The fission rate rose slowly, with a period of about 17 min. This period corresponds to a positive reactivity, k_{ex}/k_{eff}, of about 6×10^{-5}, or a core temperature about 0.06°C below the critical temperature.

After the power had risen to about 10 w, the core temperature was raised to make the reactor subcritical. This was done by pumping warm water, instead of cool water, into the shell side of the heat exchangers. Almost immediately, at 6:08 PM, the fission rates began to decline, showing that the core temperature had risen above the critical temperature. After a few minutes, cooling was resumed. Judging from the behavior of the fission rates, the core temperature began at about 6:21 PM to decrease, and at about 6:30 PM the critical temperature was reached again.

At 6:50 PM, with the count rates rising very slowly, the source was again inserted. As shown by Fig. 1.2, the count rates rose quickly, then leveled off. The source was then withdrawn with no perceptible effect on count rates. The interpretation is as follows: When the source was inserted, the flux was quite low and the source did not absorb neutrons as fast as it was emitting them. Therefore, the neutron population rose. At the time the source was withdrawn, the core

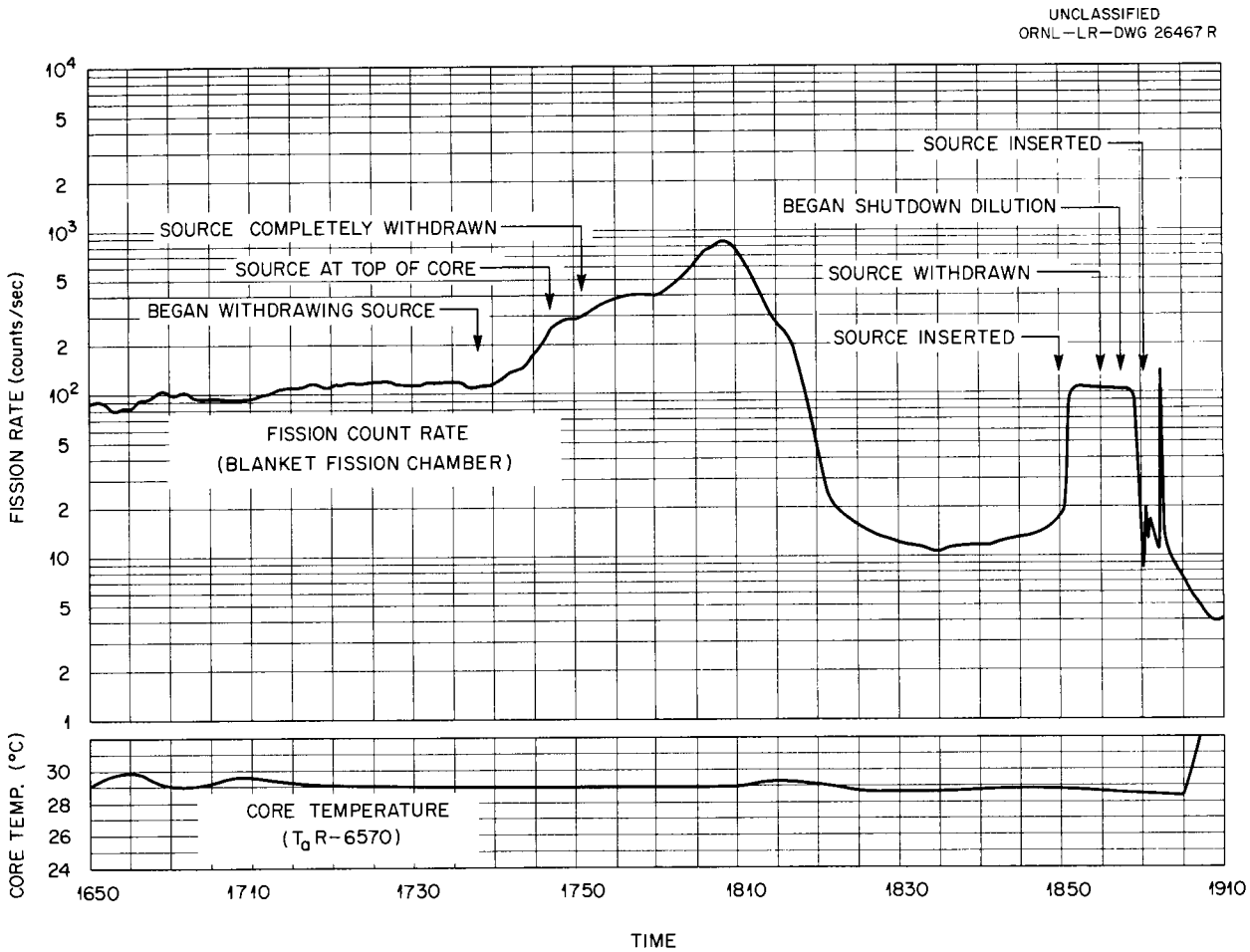

Fig. 1.2. Temperature and Fission Rate During Initial Critical Experiment, Dec. 27, 1957.

concentration and temperature were such that source absorption and emission rates were perfectly balanced. Withdrawal of the source then had no significant effect on the fission rate.

At 6:58 PM the dilute switch was put in the "shutdown" position, and the feed pump began to deliver condensate instead of fuel solution. After a delay of about a minute due to feed-line holdup, the dilution began to take effect and the reactor went subcritical. The sharp peak in the count-rate trace at about 7:03 PM is attributed to an electronic disturbance in the circuitry, rather than a real change in reactor fission rate.

Also shown in Fig. 1.2 is the core temperature recorded by an instrument which averages the readings of thermocouples on the core inlet and outlet. This record was not accurate enough to be useful in the analysis of the small changes in reactivity which were observed during this experiment.

1.2.1 Critical Experiments at Elevated Temperatures

After the initial critical experiment, the source thimble was removed from the core to the blanket thimble, and the reactor was made critical at seven temperatures ranging up to 281°C.

The first point in this series was obtained with a fuel concentration the same as that used in the initial experiment. Because the poison of the core thimble had been removed, the reactor attained criticality at a higher temperature, 65°C. The critical condition was approached by slowly lowering the temperature. For this operation, water was circulated through the shell side of the heat

exchangers to control the core and blanket temperatures. After criticality was reached, the reactor power was allowed to rise briefly to about 1 kw before the reaction was shut off by dilution of the fuel.

In subsequent experiments at higher temperatures, the reactor temperature was maintained by supplying heating steam to the heat exchangers. A typical sequence of operations in going critical was as follows: First, the reactor temperature was raised well above the expected critical temperature. A batch of fuel solution was then injected into the dump tanks. After steady count rates showed that mixing was essentially complete and the core concentration was no longer increasing, the temperature was slowly lowered. Subsequent steps are illustrated by Fig. 1.3, which shows core temperatures and fission-chamber count rates during one experiment. At 1:20 PM, when rising count rates indicated that the critical temperature was being neared, the source was withdrawn; however, the reactor was well below criticality. Count rates dropped rapidly, and the source was reinserted. The next time the source was removed, count rates dropped more slowly, and the core reached the critical temperature before it was necessary to insert the source. The reactor continued to cool and the fission rate rose on an ever-shorter period until a burst of steam to the heat exchangers raised the temperature and made the reactor subcritical. The reactor was held near criticality for about ½ hr before the temperature was raised in preparation for the next experiment.

1.2.2 Critical Concentrations

Figure 1.4 shows the observed critical concentrations at each reactor temperature. With the exception of the 258°C case, every time the

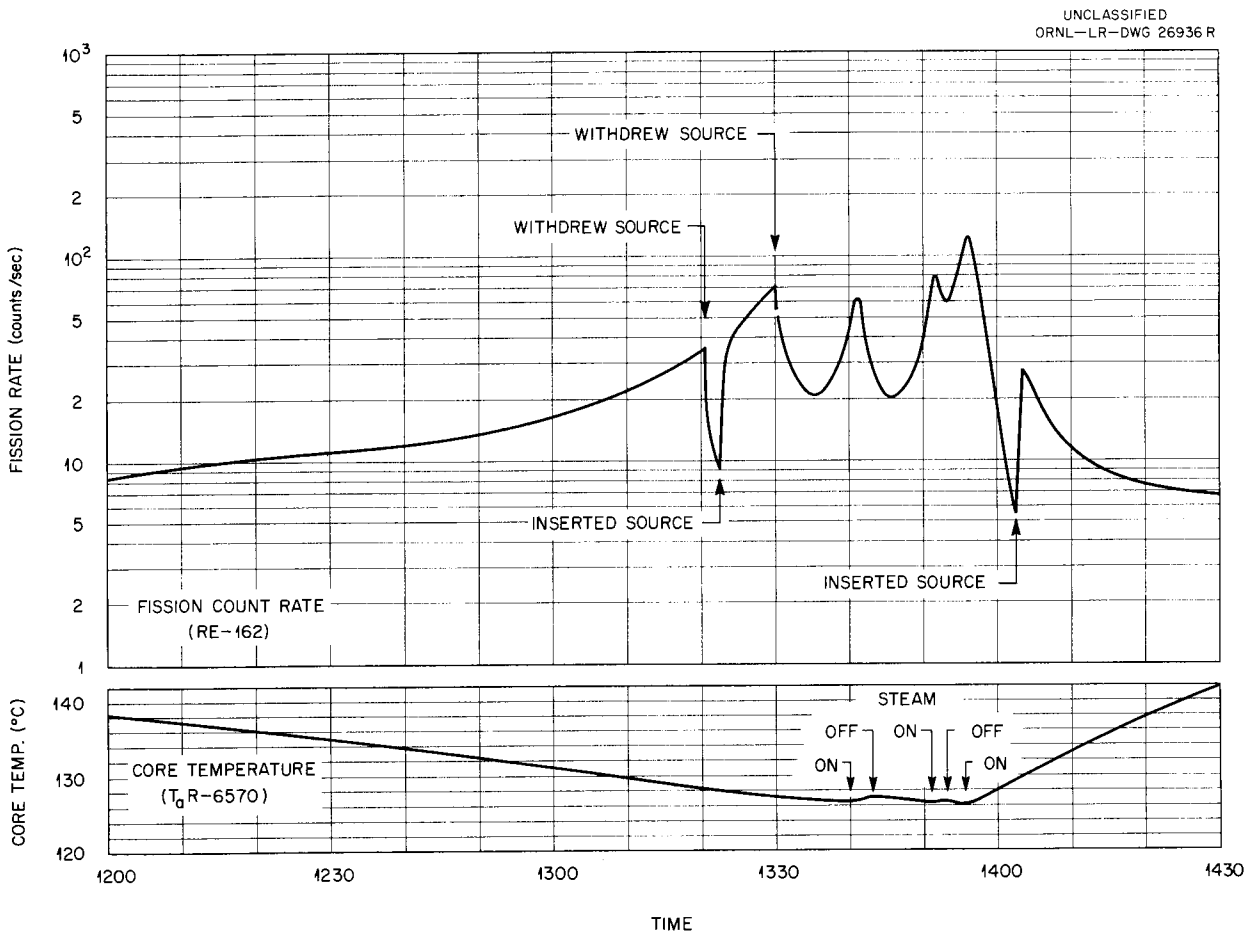

Fig. 1.3. Temperature and Fission Rate During Critical Experiment on Jan. 9, 1958.

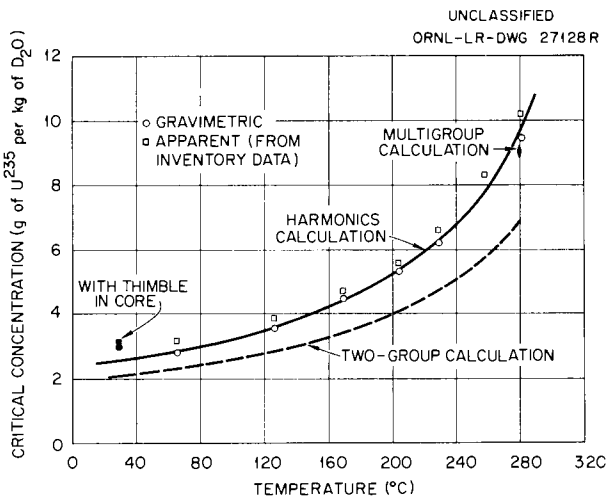

Fig. 1.4. Critical Concentration as a Function of Temperature.

reactor was critical a 300-ml sample was taken from the high-pressure fuel system. The nuclear power was purposely kept low during the experiments so that radioactivity of the samples presented no great problems. The results of gravimetric analyses of the samples are indicated, together with the apparent core concentrations, which were calculated from known system volumes and uranium inventories and the temperatures, pressure, purge and feed rates, and dump-tank weight observed at the time the reactor was critical. The sample results average about 6% lower than the calculated concentrations. The reason for this difference has not yet been established. As a check, the uranium concentration in the samples is presently being determined by an isotopic dilution method.

Results of several critical calculations are shown in Fig. 1.4 for comparison with the experimental points. The harmonics calculation is the one made by Edlund and Wood in 1954 and reported in ORNL-1780.[6] The two-group calculation was made in 1956.[7] The isolated point at 280°C was calculated recently by the Eyewash multigroup, multiregion code.[8]

It can be seen that the two-group calculations predicted critical concentrations about 20% below those observed. This is probably because of inadequate treatment of fast-neutron leakage in the two-group method. The harmonics calculation, which used a convolution of an age and a Yukawa kernel to represent slowing-down in D_2O, gave quite satisfactory results. The multigroup result also was in good agreement with the experimental determination.

1.3 METALLURGY SERVICE WORK[9]

As a safety measure, the containment cells of the HRT are sealed by welded-in pans that are designed to prevent escape of radioactive gases. When the reactor cells were sealed for preliminary testing, the pans, of galvanized iron, were welded to carbon-steel transition strips attached to the cell wall.

During a subsequent maintenance period, the carbon-steel strips were replaced by type 347 stainless steel. After the galvanized-iron pans had been ground in an attempt to remove zinc from the edges, the pans were edge-welded to the stainless steel transition strips by means of a tungsten arc with stainless steel filler metal. The reactor cells were then pressurized with air. Many leaks were found, several of which proved difficult to repair.

Macroexamination of sections removed from the leaking joint revealed cracks located primarily in the stainless steel base metal. Metallographic examination indicated that a typical crack extended into both weld and base metals, with a tendency for greater depth into the stainless steel base metal. Some cracks had apparently formed in the stainless steel base metal below the fusion zone. Only a few large cracks had penetrated the stainless steel to allow leaking under test, although many other cracks were present. The cracks were intergranular and tightly closed.

In the sections examined, no evidence was found of zinc present as an alloy or as inclusions. Results of direct tests for the presence of zinc were negative. It was found, however, that the grinding had not removed all the zinc from the edges to be welded; rapid gas evolution was observed when a few drops of hydrochloric acid were placed on the ground surface.

It is tentatively concluded that rapid intergranular diffusion of zinc from the galvanized iron was responsible for the cracking of the stainless steel.

[6] M. C. Edlund and P. M. Wood, ORNL-1780 (Aug. 27, 1954) (classified).

[7] C. W. Nestor, Jr., *HRT Critical Concentration as a Function of Temperature*, ORNL CF-56-6-123 (June 20, 1956).

[8] P. R. Kasten *et al.*, *HRP Quar. Prog. Rep. Oct. 31, 1957*, ORNL-2432, p 17.

[9] Work performed by G. M. Adamson, C. H. Wodtke, and T. M. Kegley.

2. HRT DESIGN

W. R. Gall M. I. Lundin
F. C. Bowen[1] A. C. Phillips[1]
C. A. Burchsted R. G. Pitkin[1]
R. D. Cheverton C. L. Segaser
C. J. Claffey R. E. Schappel
C. W. Collins D. D. Tarr[1]
E. M. Guglielmo[1] W. L. Wright
F. C. Zapp

2.1 REMOTE MAINTENANCE

The design of facilities for the removal and replacement of the core and blanket corrosion-specimen holders and the pressure-balancing-system rupture-disk assembly was completed.[2] Special lower roof blocks with seal-pan openings (Fig. 2.1) were installed in order to permit access to the corrosion-sample holders and the rupture-disk assembly.[3] Reactor maintenance operations at the cell are performed through the holes in these blocks by use of shielded tools and carriers.

Figure 2.2 shows a typical tool and removable shield assembly in place over the access hole in a lower roof block. After the seal-pan flange has been removed, a drip pan and support ring are placed in position and the access plug is removed. A removable shield assembly is then placed on the support ring, and a replaceable flange plug, consisting of several long-handled tools mounted in a cylindrical shielding plug, is mounted on the removable shield assembly. Accurate location of a given tool is accomplished by rotation of the flange plug and the eccentric plug, which is part of the removable shield assembly, relative to one another. Scales on the plug-flange bearing plate and centering ring, graduated in degrees, permit future duplication of tool position. A television camera and a light can be mounted in the flange plug to permit remote observation of the work area. In general, a given group of tools will remain assembled and will be handled as a unit. The tool extension handles are removable in order to facilitate handling and storage.

The removable shield provides space into which items such as the hold-down flanges or the rupture-disk cartridge assembly may be withdrawn for transportation to or from the storage pool. The drip pan is provided to catch any radioactive liquids or scale which might drop from the part being transported; as an additional safety measure, a cap is placed over the bottom of the transport shield (or other carriers) prior to removal to the storage basin.

Radioactive items from the reactor will be removed to the storage pool located at the east side of the HRT building for storage and/or further processing under water. At one side of the pool is located a decontamination basin, in which will be installed a remotely operated, hydraulic cutting tool, together with appropriate fixtures and storage racks. The cutting facilities will be required only during removal of the corrosion-sample holders, and may be removed when not needed.

A modified hot cell in Building 3029 will be used to reassemble the corrosion-sample holders. Unirradiated specimens will be placed in a new holder manually; then the partially assembled unit will be moved into the hot cell for remote assembly of the irradiated specimens. The completed holder will be placed inside the transport shield and returned to the reactor building for reinstallation.

2.2 FLANGE DEVELOPMENT PROGRAM

Recent experiments in the flange test facility[4-6] indicate that flanges with ring-joint grooves and gaskets machined to a tolerance of ±0.005 in. on

[1]On loan from Vitro Engineering Co.

[2]W. R. Gall *et al.*, *HRP Quar. Prog. Rep. April 30, 1957*, ORNL-2331, p 22–23.

[3]W. R. Gall *et al.*, *HRP Quar. Prog. Rep. Oct. 31, 1956*, ORNL-2222, p 7.

[4]W. R. Gall and M. I. Lundin, *Monthly Report – Design Section – June and July 1957*, ORNL CF-57-8-50.

[5]W. R. Gall and M. I. Lundin, *Monthly Report – Design Section – Aug. 1957*, ORNL CF-57-9-37.

[6]W. R. Gall *et al.*, *HRP Quar. Prog. Rep. Oct. 31, 1957*, ORNL-2432, p 5–6.

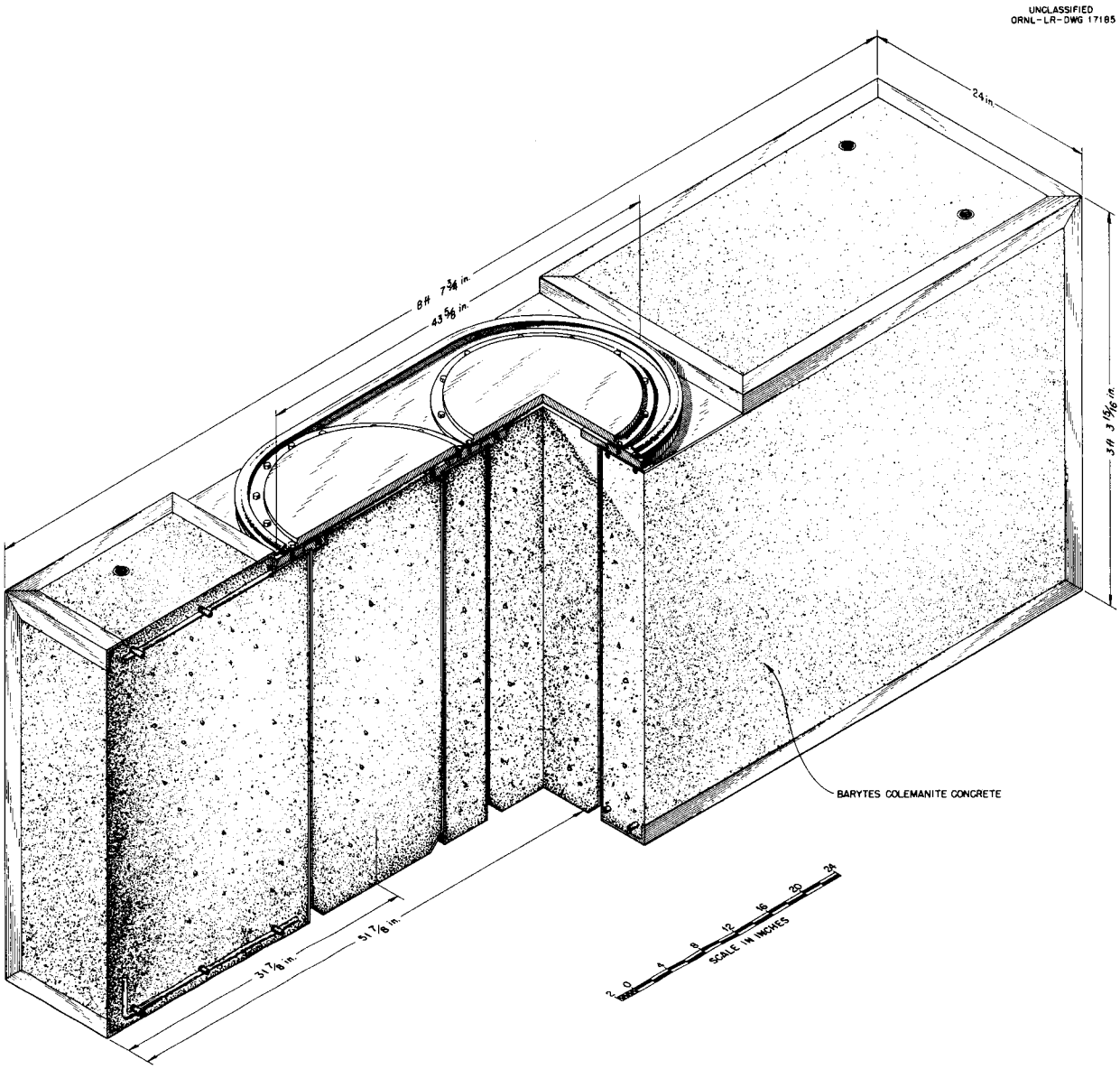

Fig. 2.1. Special Lower Roof Block with Access Hole.

the pitch diameter will be suitable for service in the HRT. It is considered necessary to maintain the fine-finish requirement of 32 μin. rms on the sides of the groove, however, and it is desirable to maintain a finish of 63 μin. rms on the remainder of the face of the flange because that surface is used as a reference plane.[7] The conclusion concerning the pitch-diameter tolerance is valid only under the operating conditions previously stated: that is, flange bolts equipped with ferrules and initially stressed to approximately 45,000 psi; variation of load on all bolts in a given flanged joint less than 20%; pressure-temperature cycling of the system embodying the flanged joint from saturation conditions at 100°C (15 psia) to saturation conditions at 335°C (2000 psia) at a rate not to exceed 55°C/hr; insulation of the joint with 10 layers of aluminum foil or the equivalent.

[7]HRP Specification No. 200a–Modified Type 347 Austenitic Stainless Steel Material, par. 16.4.2.

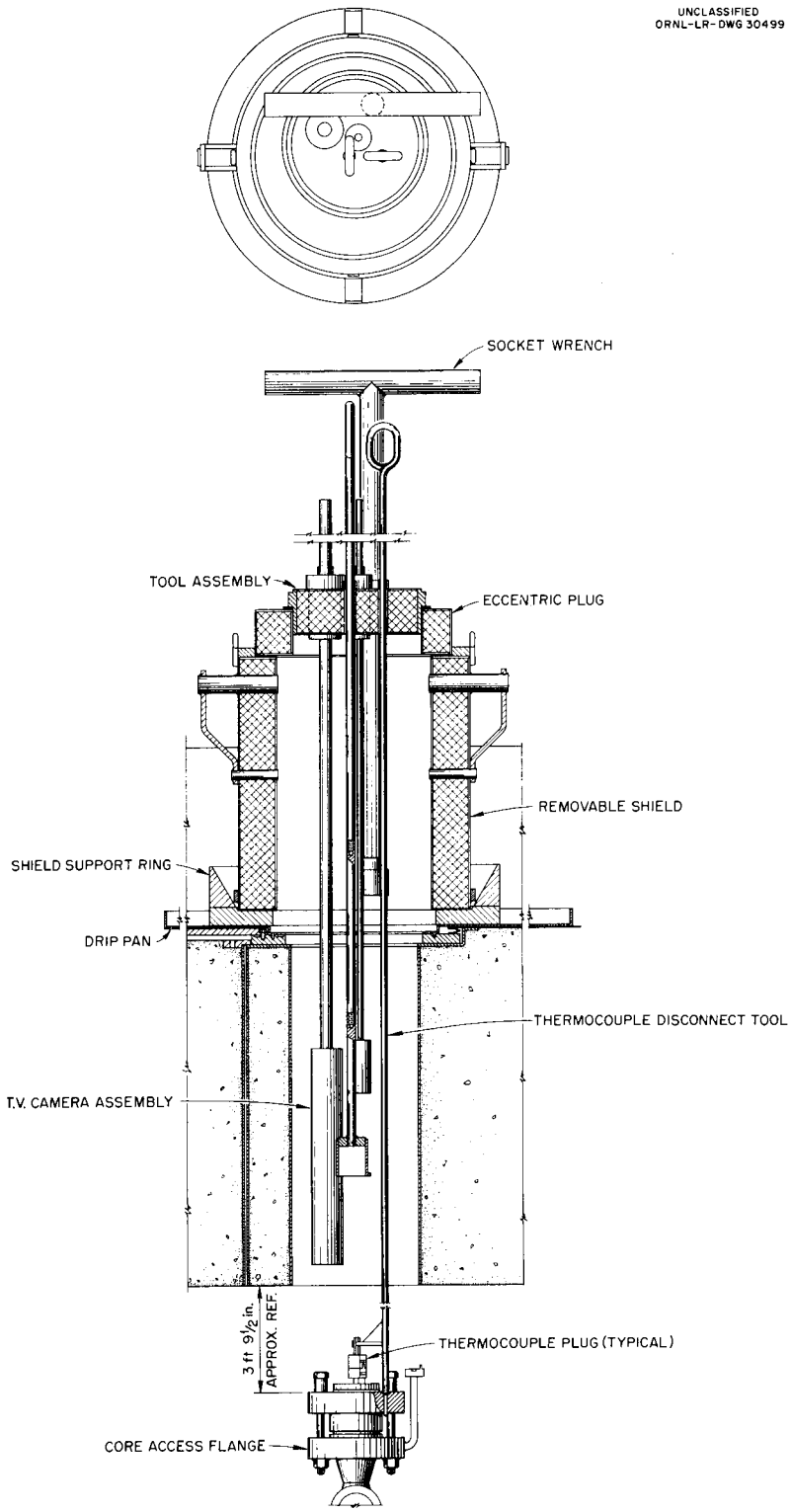

Fig. 2.2. Typical Tool–Transport-Shield Assembly for Remote Maintenance of Sample Holders and Rupture-Disk Assembly.

Contact-surface galling which results from a mismatch of the ring and groove does not appear to depend on size of the flange. However, the amount of bolt stress required for complete seating of the ring with a given degree of mismatch does depend on flange size. The smaller the flange, the greater the required bolt stress. Since the smallest flange tested was a ½-in. 1500-lb flange, the conclusion concerning tolerance of the pitch diameters of ring and groove can be applied to any ring-joint flange with pitch diameter equal to or greater than that of the ½-in. 1500-lb flange.

The standard ASA tolerances[8] are ±0.005 in. on the flange-groove pitch diameter and ±0.007 in. on the ring pitch diameter, permitting a maximum mismatch 20% greater than that imposed in the flange tests. It cannot, therefore, be stated positively that a joint with both ring and groove machined to the ASA tolerance will perform as well as one in which both ring and groove are machined to a tolerance of ±0.005 in. A slight amount of galling was observed on test flanges having a total mismatch of 0.010 in., and it may be assumed that increasing the mismatch to the maximum allowed by the ASA standard would increase the degree of galling of the ring and groove surfaces.

Tests were also made in order to determine the influence of pipe moments on the integrity of a ring-joint type of flanged connection. Joints in the test facility were subjected to moments in excess of those recommended by the Code[9] without an evident increase in leak rates over leak rates found in earlier tests in which the moments were not imposed.

[8] *Ring-Joint Gaskets and Grooves for Steel Pipe Flanges*, ASA B16.20-1956, American Standards Association, New York.

[9] *Code for Pressure Piping*, ASA B31.1-1955, American Standards Association, New York.

3. HRT COMPONENT DEVELOPMENT

I. Spiewak

J. M. Baker
R. Blumberg
J. S. Culver
B. D. Draper
C. H. Gabbard
E. C. Hise
J. C. Moyers
H. R. Payne

3.1 FUEL CIRCULATING EQUIPMENT

3.1.1 400A-1 Westinghouse Pump and Loop

The Westinghouse 400A-1 pump circulated 0.04 *m* UO_2SO_4 solution without incident for 1585 hr. During this run the solution was maintained near saturation with gas by running the gas pressurizer 5°C below the loop temperature of 250°C. This resulted in a gas partial pressure of about 525 psi.

When the pump was examined after the run, several areas of localized attack were noted in stainless steel parts, as illustrated in Figs. 3.1 and 3.2. Pitting had occurred in a number of locations downstream from screws, vane tips, etc., where the turbulence was most pronounced. There was no attack on the titanium impeller. Since the pump had operated previously without pitting for 11,600 hr under similar conditions except for the gas, the corrosive attack is attributed to erosion by bubbles.

Further damage to the pump assembly was noted in the thermal-barrier seal weld and in the Kingsbury thrust bearing. The former had cracked from the motor side in a manner similar to that reported previously[1] for the HRT mockup pump. When the pump was reassembled, the weld design was modified to correspond with the one used successfully in the mockup pump.[2]

Wear of the Stellite thrust shoes had been occurring throughout the entire 13,000-hr life of the bearing assembly, as evidenced by cobalt analyses of the solution. Figure 3.3, a cross section of one of the thrust shoes, shows corroded Stellite-12 overlay as a dark area along the top surface; the attack seems to have started at the stainless steel–Stellite interface. The thrust-shoe leveling links were badly worn, also. The pump was reassembled with new links and with alternatingly disposed shoes of cast Stellite-19 and overlaid Stellite-12 in an effort to solve the Stellite corrosion problems in this application.

[1] I. Spiewak *et al.*, *HRP Quar. Prog. Rep. Jan. 31, 1957*, ORNL-2272, p 28–29.

[2] *Ibid.*, p 29, Fig. 3.2.

UNCLASSIFIED
PHOTO T-14041

Fig. 3.1. Wear Ring Showing Localized Attack.

UNCLASSIFIED
PHOTO T-14040

Fig. 3.2. Diffuser Showing Localized Attack.

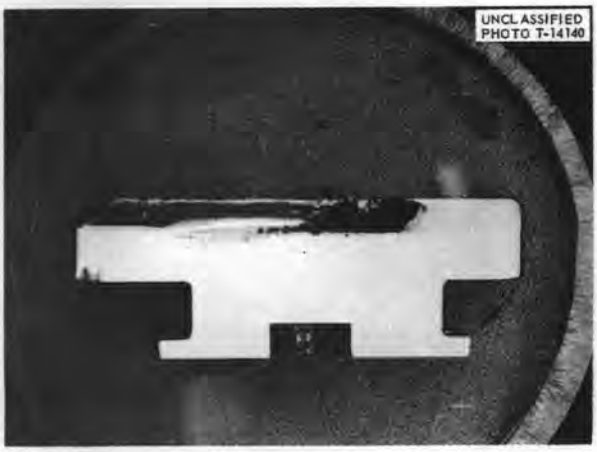

Fig. 3.3. Sectioned Thrust Shoe Showing Corroded Overlay. 2.5X.

This 400A-1 pump has accumulated 13,000 hr of maintenance-free operation with HRT solution. After repairs, the pump was installed in the HRT mockup and will continue to circulate dilute uranyl sulfate solutions.

3.1.2 400A-2 Pump and Loop

Shaft-seal mixing tests[3] were continued with the 400A-2 pump. The internal motor-coolant circulation was routed to conform to that of the 200A slurry pump, which utilizes the lower radial bearing as a secondary shaft seal. The measured mixing rate was 0.001 liter/hr at a purge flow of 7.3 liters/hr; this compares with 0.003 liter/hr for the best previous configuration.

To test the modified seal at operating temperature, the pump circulated 0.04 *m* UO_2SO_4 at 250°C for 1033 hr. Disassembly of the pump revealed severe damage to the lower bearing as a result of overheating. The lower bearing was repaired and the motor-coolant system was modified to conform to the design presently utilized by Westinghouse, which differs from their earlier design in that the shaft cooling passage is eliminated. A run will be made at 250°C to determine whether there is any damage to the lower bearing.

3.1.3 300A-1 Pump

The HRT mockup 300A-1 pump was dismantled after having circulated 0.04 *m* UO_2SO_4 for 5040 hr since the installation of the revised thermal-barrier seal weld.[1] The pump was in good condition; the only wear noted was in an increase in end play of 0.008 in. and in a continuation of the impeller-hub erosion noted previously. The seal weld was machined away and appeared sound throughout. The pump has been rebuilt and will be installed in the 300A slurry loop.

3.2 FEED PUMPS

3.2.1 Feed-Pump Endurance Testing

Two failures were experienced during the quarter in feed-pump components. One involved leakage through a 0.019-in.-thick annealed type 347 stainless steel diaphragm after 8997 hr of operation, of which 8521 hr were in water and 476 hr were in fuel solution. This head was of an old design – a thin diaphragm protected by relatively coarse 40-mesh screen.

An apparently sound butt weld in the $^3/_4$-in. sched-80 intermediate line of feed-pump loop No. 2 failed in fatigue after 26,000,000 pressure cycles from 0 to 2000 psi. This is the first instance on record of a butt-weld fatigue failure in feed-pump service. A photograph of the crack, which originated at the notch formed by the overpenetrated weld bead and the base metal, is shown in Fig. 3.4. Butt welds for fatigue service should be carefully inspected for overpenetration.

Seven feed-pump heads have continued to operate satisfactorily on fuel solution; one has been operating for 7389 hr, and two latest-style heads have each been in service for 6520 hr.

A considerable reduction in noise level was achieved by tapering the slide valve of the Scott &

[3] J. C. Moyers, *Investigation of Effect of Seal Configuration on Mixing Flow and Radiation Damage in HRT-Type Circulating Pumps – Supplement No. 1*, ORNL CF-58-1-77 (Jan. 13, 1958).

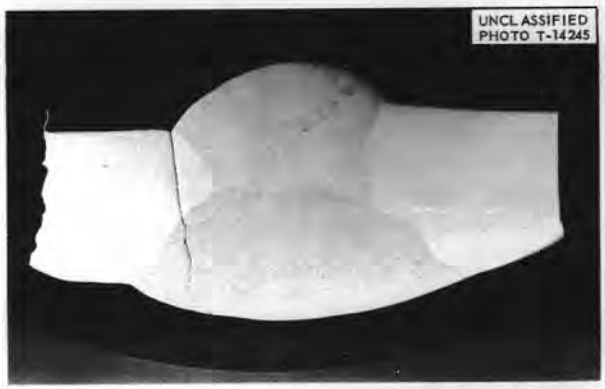

Fig. 3.4. Pipe Butt Weld Showing Fatigue Failure. 8X.

Williams drive in a manner which produces a gradual, instead of a sudden, acceleration of oil at the start of the suction stroke.[4]

3.2.2 Purge Pumps

The operation of purge-pump test loops 1 and 2 was interrupted after 1601 hr by failure of a forging in the Scott & Williams P2 drive unit. Testing was resumed after installation of a replacement part.

The HRT mockup purge pump, which contains 100-mesh screening, has operated satisfactorily for 2844 hr.

3.2.3 Corrosion Fatigue Tests

Ohio State University has investigated the effect of various surface treatments on the endurance limit of type 347 stainless steel sheet in uranyl sulfate solutions. These treatments included liquid blasting, mechanical polishing, scratching, and static aging in fuel solution. None of the treatments affected the endurance limit, as compared with the performance of sheet given a standard ASTM No. 9 finish.

The results of fatigue tests of titanium A-110AT, Allegheny Ludlum AM-350, and CD4M-Cu are given in Table 3.1 along with previous results. The very high endurance limit of titanium (62,500 psi) may permit greatly increased capacity in a diaphragm pump; this possibility will be explored further.

[4]H. R. Payne, *Modification of Oil Control Valve in Scott and Williams P-9 Pulsator Drive*, ORNL CF-58-1-65 (Jan. 14, 1958).

3.3 HRT MAINTENANCE

In a joint effort with the HRT Operations Group, final tests were made on a secondary gasket to be used during the removal of light water from a flange during underwater maintenance. A soft, collapsible copper gasket, with attached hypodermic tubing, was used as a seal ring to permit the alternate addition and discharge of a "heavy water" flush. For test purposes the "heavy water" was a solution of potassium dichromate dissolved in light water with a specific gravity comparable to that of D_2O. The difference in specific gravity

Table 3.1. Results of Corrosion Fatigue Tests

Material	Endurance Limit (psi)			Elongation (%)
	In 0.04 *m* UO_2SO_4 at 60°C	In Water at 60°C	In Air at Room Temperature	
347 SS				
Annealed	34,000	36,000	39,000	42
¼ Hard	30,000	50,000	58,000	14
½ Hard	31,000	57,000	67,000	2.5
¾ Hard	32,000		88,000	2.5
Full Hard	43,000			2.5
316-L SS				
¼ Hard	32,000			14
½ Hard	32,500			10
AM-350 S.B.T.*	39,000	43,000	90,000	11
Titanium A-110AT	62,500	62,500	70,000	10
CD4M-Cu**	42,000			16

*S.B.T. refers to tempering by refrigeration, followed by aging at 650°F.

**CD4M-Cu is a ferritic alloy, developed at Ohio State University, which is hardenable by cold rolling and aging.

of "heavy" and light water was utilized to displace the latter. It was determined that a 2-liter flush of "heavy water" would displace approximately 90% of the light water remaining in the flange above the ice plug.[5]

3.4 HRT MOCKUP

R. B. Korsmeyer

P. H. Harley D. E. Willis

3.4.1 Operation

During the report period the HRT mockup operated 1093 hr to complete a 2210-hr run which started September 3, 1957. The run was made at 1700 psi and 280°C with a 0.042 *m* UO_2SO_4 solution containing 0.021 *m* H_2SO_4 and 0.005 *m* $CuSO_4$ and was terminated on December 8, 1957, for loop modifications. The generalized corrosion rate for the run was 1.3 mpy, based on the increase of nickel in solution.

Near the end of the run the leakage through the letdown valve, which had a type 17-4 PH stainless steel trim, was found to exceed 0.25 gpm at 1700 psi and 50°C. This was not serious while the feed pump was operating; however, the purge-pump flow could not maintain the loop operating level alone. When the letdown valve was checked in the shop after the run, the leakage was only 0.024 gpm.

The electrical relay contacts failed in the pressurizer heater circuit on October 23, 1957, but were replaced without interrupting loop operation.

A feed-pump pulsator housing started leaking on October 4 and was replaced. The leak was in a welded reducer that had cracked and had been patched last May.

3.4.2 System Changes

The 300A Westinghouse circulating pump was replaced by a 400A pump so that the 300A pump could be used on a slurry loop. The 300A pump had been in the mockup for 2½ years and had operated for 13,067 hr, including 4340 hr since the last inspection.

The type 347 stainless steel letdown heat exchanger was replaced by one constructed of A-55 titanium, which was flanged[6] into the system.

A new high-pressure loop heat exchanger was constructed and installed. The failure of the previous heat exchanger was reported previously.[7]

3.4.3 Iodine Removal Tests

The efficiencies (per cent of iodine removed per pass) of three silvered-alundum beds and one silver-plated wire-mesh bed have been reported.[8] The density of the wire-mesh bed was 22 lb/ft^3. A second silver-plated wire-mesh bed, 6 in. dia × 6 in. deep, having a density of 29 lb/ft^3, was tested; the efficiency was 99.8% at 120°C.

A 650-hr stability test was run on a 6-in.-dia × 18-in.-deep silvered wire-mesh bed loaded with 20 g of I_2. At the end of the run 0.136 g of silver was found in solution, which corresponds to c 0.025% loss of the silver from the bed.

3.4.4 Heating of Fuel Solution

A small bypass stream (~1 gpm) of the mockup fuel was heated for 1500 hr at 300°C in a ½-in., sched-80, type 347 stainless steel line. The main-loop temperature was 280°C. The test was run to obtain scale-buildup and corrosion information of use for future pressurizer design.

Upon removal of the pipe, a 0.03-in. deposit of rusty red scale was found to have formed (chemical analyses of the scale have not yet been completed). This is a much heavier scale than that formed while fuel solution was boiled in a titanium pipe.[9] The pipe has been submitted for metallographic examination.

3.4.5 Corrosion in Stagnant Lines

The generalized corrosion rates of the stressed specimens installed in three dead-end ½-in. pipes[9] and exposed to stagnant solution for 2210 hr were low, varying from 0.01 to 0.5 mpy with temperatures from 50 to 280°C. The only circulation was by natural convection. No pits or

[5] B. D. Draper and T. E. Haynes, *Design and Development of a Flange Dewatering Device*, ORNL CF-58-1-42 (Feb. 10, 1958).

[6] B. D. Draper and H. C. Roller, *Design and Development of a 1/2-inch Titanium to Stainless Flange*, ORNL CF-57-11-140 (Nov. 27, 1957); I. Spiewak *et al.*, *HRP Quar. Prog. Rep. Oct. 31, 1957*, ORNL-2432, p 53.

[7] I. Spiewak *et al.*, *HRP Quar. Prog. Rep. July 31, 1957*, ORNL-2379, p 16.

[8] I. Spiewak *et al.*, *HRP Quar. Prog. Rep. Oct. 31, 1957*, ORNL-2432, p 15.

[9] *Ibid.*, p 14.

cracks were noticeable in the defilmed samples, but a metallographic examination will be made.

3.4.6 Fuel-Solution Chemistry

At the end of the last run, the mockup fuel was composed of 0.052 *m* UO_2SO_4, 0.016 *m* H_2SO_4, and 0.005 *m* $CuSO_4$, plus 0.008 *m* SO_4 probably present as sodium and potassium sulfate from the iodine tests. This solution was observed to precipitate uranium and copper when the pressurizer purge rate was high (~13 gph). The precipitated material is believed to have been formed by hydrolysis occurring between the pressurizer and the main loop. The precipitate was redissolved in 24 hr with no pressurizer purge flow (gas-pressurized system) and was redissolved in about 48 hr with a 2 to 3 gph purge to the pressurizer with the system steam-pressurized to 1700 psi. Tests will be made to determine whether a balanced solution (0.042 *m* UO_2SO_4, 0.021 *m* H_2SO_4, and 0.005 *m* $CuSO_4$) reacts in a similar manner.

4. HRT CONTROLS AND INSTRUMENTATION

D. S. Toomb

A. M. Billings
J. R. Brown
R. L. Moore
R. M. Pierce[1]
J. A. Russell
K. W. West

4.1 COMPONENT AND SYSTEM TESTING

4.1.1 Leak-Detection-System Instrumentation

The Swartwout Company electric-signal differential-pressure transmitters purchased for use in the HRT leak-detection system[2] were installed after satisfactory testing. Output of the transmitters is 0 to 0.5 v, 60 cps, for a range of −50 to 0 to +50 in. of water differential. Zero shift was less than 3% for static pressure changes from 0 to 3000 psi, and overranging of the differential to 3000 psi produced less than a 2% zero shift.

4.1.2 Nuclear Instrumentation

During the initial critical experiments the neutron-flux level was detected by three fission chambers, with associated amplifiers, scalers, and rate meter–recorders. Difficulty was encountered with noise in two of the channels whose chambers are in water-filled thimbles. The spurious signals were traced to pulse radiation from solenoid and relay circuits and to improper grounding. These signals were eliminated by running the coaxial signal cables inside a Tygon plastic tube and by grounding the amplifier rack directly to the thimbles.

4.1.3 Pump-Stator-Winding Insulation Tests

Design was completed and construction was begun on the instrument panels to be used to measure the insulation resistance of pump stator windings during exposure to nuclear radiation. Three-phase, 60-cycle power will normally be supplied to the Y-connected winding to maintain the insulation at an operating temperature typical of that experienced in a canned-motor pump. The current will be interrupted periodically while the high-voltage resistance of the insulation is measured. Winding temperature and container pressure will be monitored continuously. One stator is located in the HRT containment tank, and a second will be exposed to gamma radiation in the spent fuel element and storage pool of the ORNL Graphite Reactor.

4.2 COMPONENT DEVELOPMENT

4.2.1 Control-Valve-Stem Position Transmitter

A control-valve position-indicating system utilizing a differential transformer for a transmitting element was installed on the HRT mockup letdown valve for testing. The transmitter, shown mounted on a valve actuator in Fig. 4.1, was designed to withstand the HRT reactor-cell environmental conditions, which include a 140°F ambient temperature, flooding, and radiation levels of 10^5 r/hr. The differential transformer is an Automatic Temperature Control Co. model 6206-K, with a linear range of 0 to ½ in., a linearity of 2%, and an output of 0.1 v for ½-in. core travel with 60-cps primary excitation. The Fiberglas-insulated lead wires leave the waterproof transformer housing in a ¼-in. copper tube.

Similar transmitters will be installed on the HRT letdown valves if operating conditions permit.

4.2.2 Remote Disconnect for Metal-Clad Mineral-Insulated Electrical Cable

Copper-clad electrical cable insulated with magnesium oxide is very desirable for service in extremely radioactive areas because no organic material is used in the insulation. A waterproof disconnect designed to be broken remotely was constructed, as shown in Fig. 4.2, to permit the removal of reactor electrical equipment connected with this type of cable. The electrical connectors are terminated inside the disconnect with a multiple-header ceramic-to-metal seal. The voids are filled with magnesium oxide powder. The outside guides are tapered to simplify remote makeup. Long insulators are used on the connecting terminals to minimize leakage currents after submersion.

---

[1]On loan from TVA.

[2]W. R. Gall *et al.*, *HRP Quar. Prog. Rep. July 31, 1957*, ORNL-2379, p 8.

UNCLASSIFIED
ORNL-LR-DWG 28326

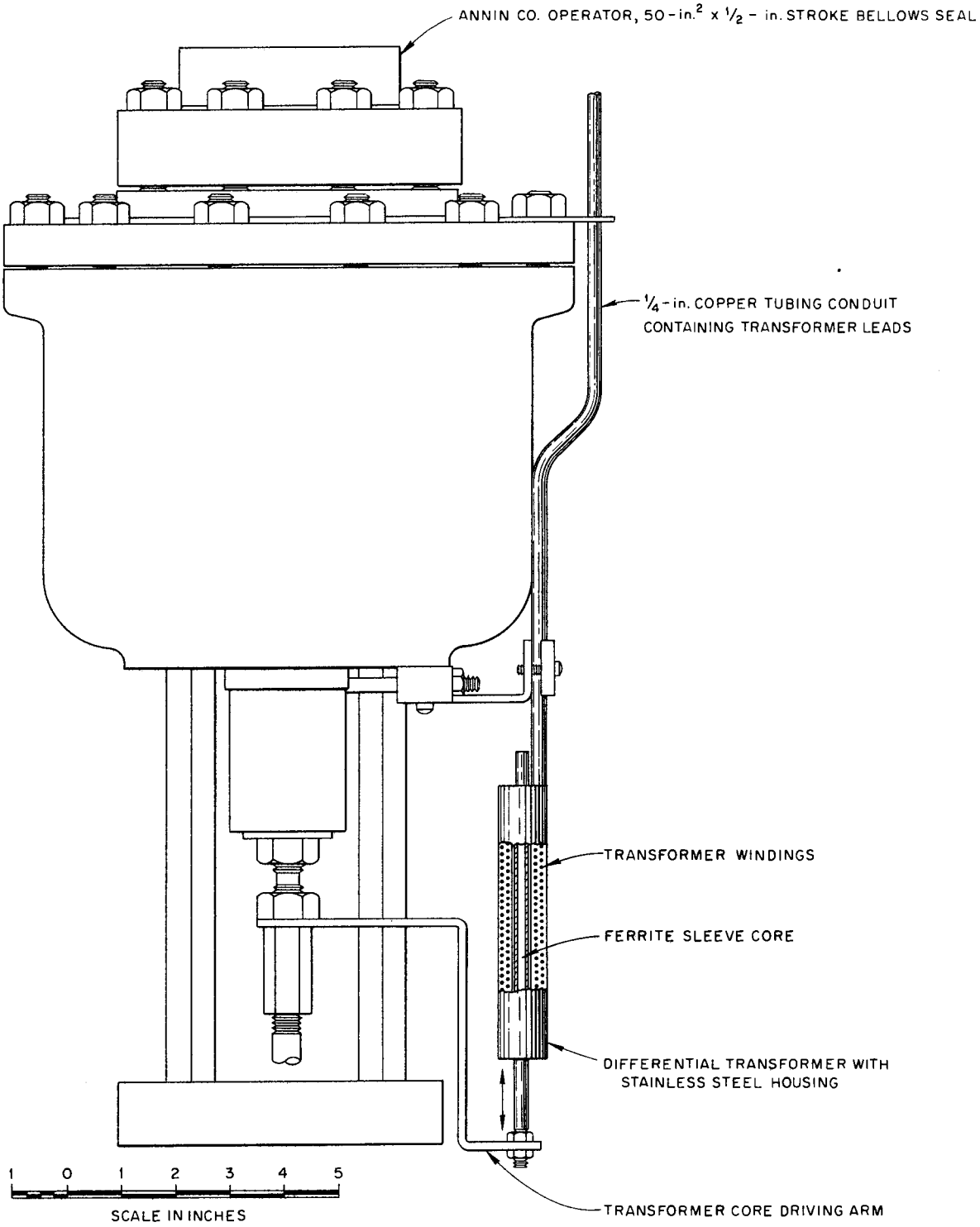

Fig. 4.1. Control-Valve-Stem Position Transmitter. Linear range, 0 to 1/2 in.; linearity, 2%.

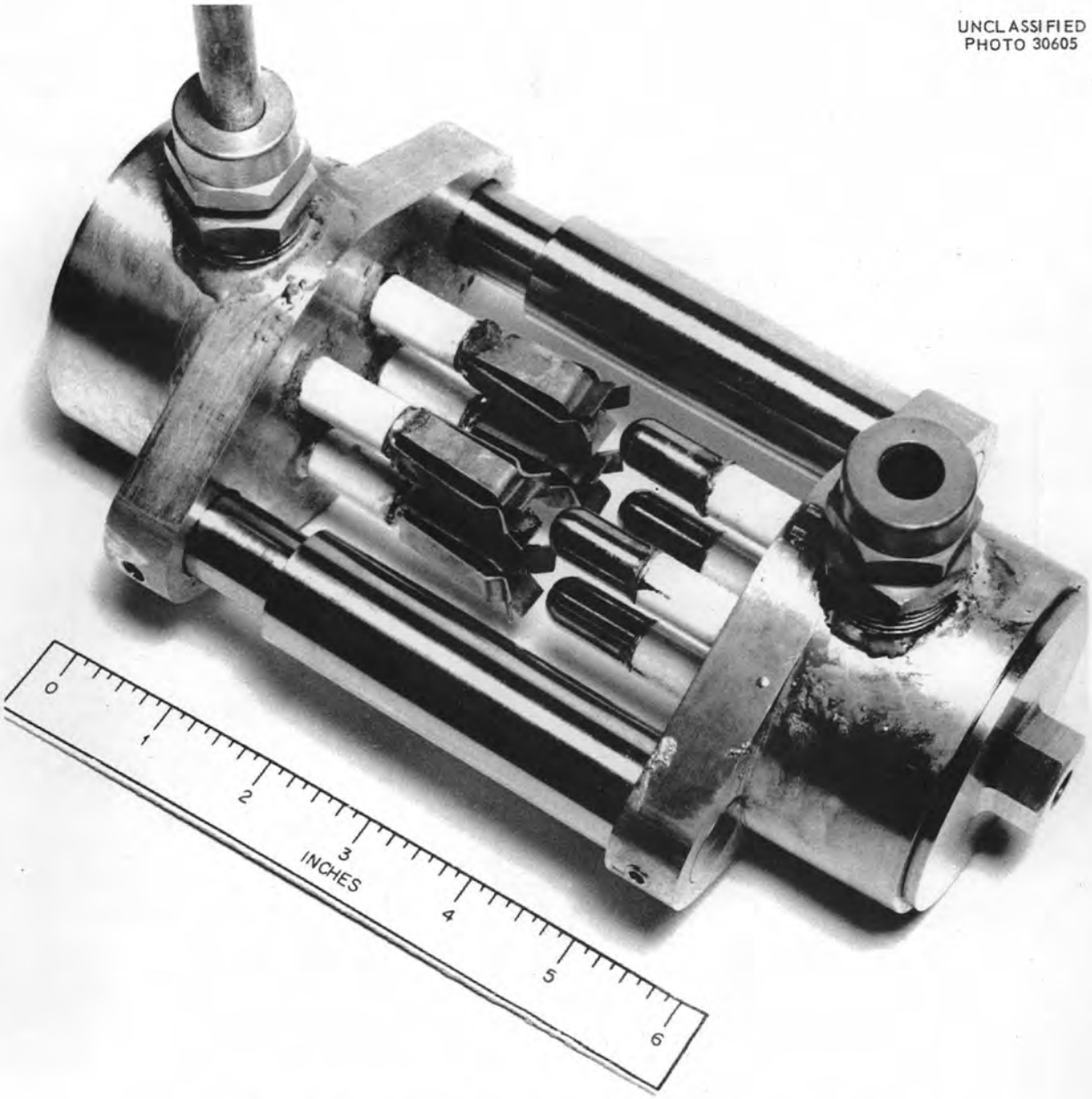

Fig. 4.2. Remote Disconnect for Metal-Clad Mineral-Insulated Cable.

4.2.3 Oxygen-Injection System

The HRT differential-expansion type of metering valve[3] used to regulate the flow of oxygen gas from storage tanks to the reactor high-pressure system was replaced with a similar valve of improved design. The new valve, shown in Fig. 4.3, utilizes a plug of tantalum instead of zirconium and thus eliminates the possibility of an ignition reaction between the oxygen gas and the heated metal plug. The new design also incorporates all-welded construction, eliminating a threaded closure in the previous model. The heating elements and thermocouples are covered with a waterproof protective housing. The resistance heating element and thermocouple are duplicated to ensure continuity of service.

[3]D. S. Toomb *et al.*, *HRP Quar. Prog. Rep. Jan. 31, 1957*, ORNL-2272, p 34.

4.3 MAINTENANCE

4.3.1 Differential-Transformer Testing Device

A core-positioning device for differential transformers was designed and fabricated to test the range and sensitivity of liquid-level transmitters for the pressurizer and outer storage tank. The unit can also be used to bench-test differential transformers and associated recording or indicating instruments.

The tester, shown in Fig. 4.4, simulates the liquid-level-transmitter applications by incorporating a dummy pressure housing; the ferrite core is

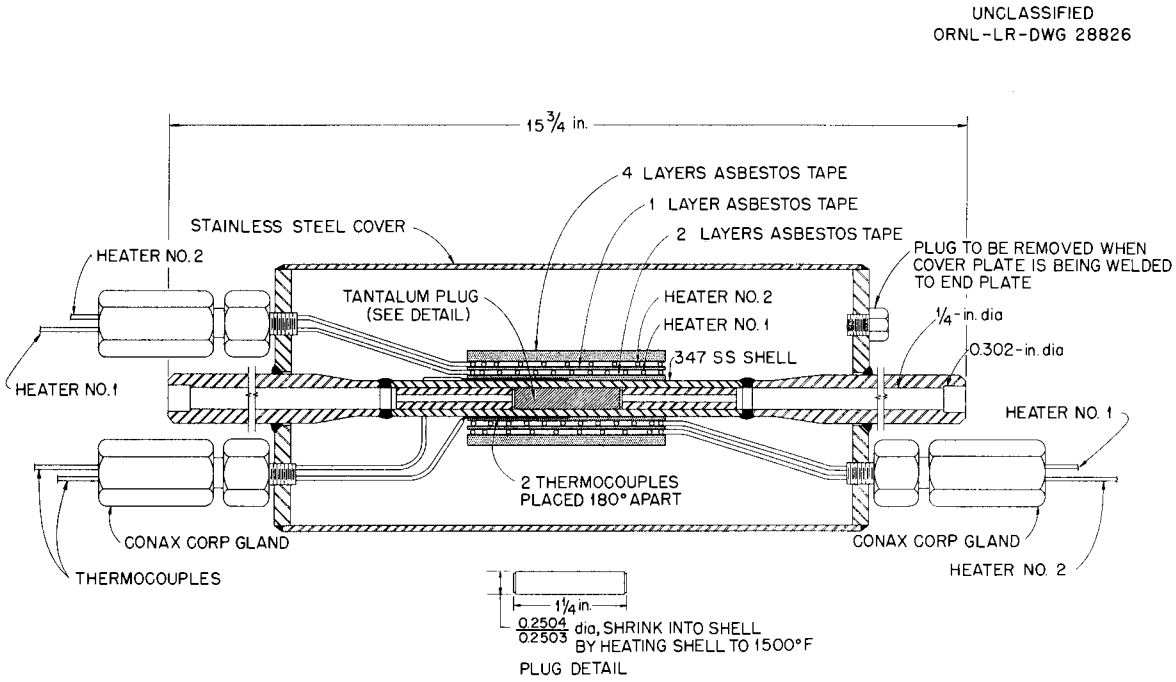

Fig. 4.3. Differential-Expansion Type of Gas Metering Valve.

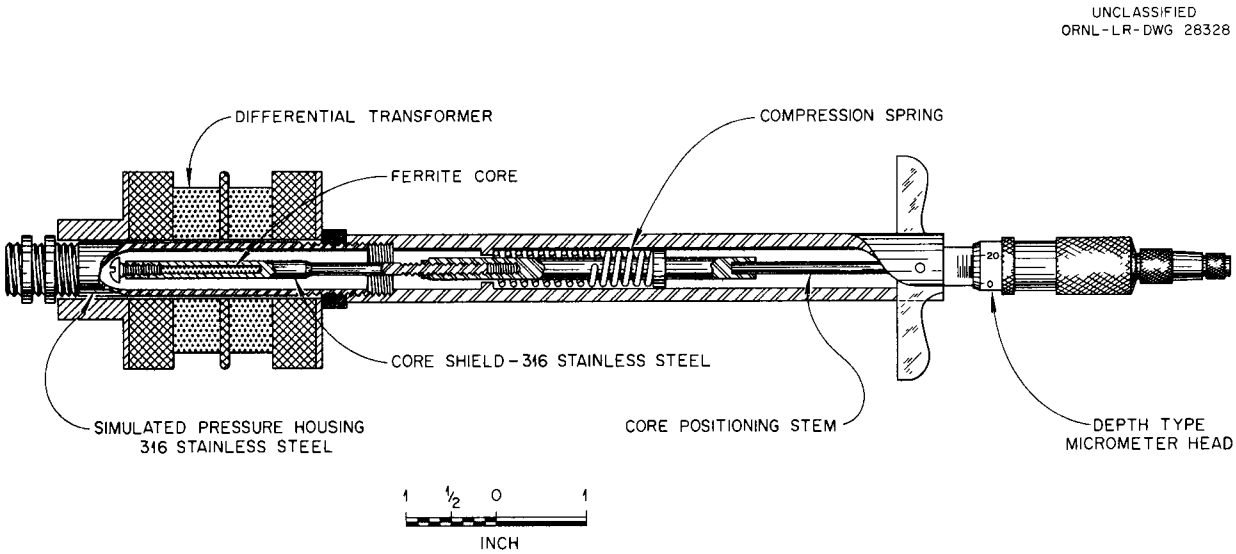

Fig. 4.4. Differential-Transformer Testing Device.

encased in stainless steel to simulate the corrosion-protection housing utilized in the reactor transmitters. Precision core positioning is achieved by the use of a depth-type micrometer head working against a compression spring.

4.3.2 Television System for Use in Reactor Maintenance

A Dage model 112AR television camera with associated control and remote monitors was received. Performance is excellent except for mild horizontal distortion in the top 3 in. of the picture on the 14-in. monitor. A readable picture was obtained with an illumination of only 2 foot-candles.

Specifications were written and a purchase order was placed for a special camera head to be used with this system for remote inspection of the HRT core. The camera head is required to pass through a 2-in.-dia opening and operate in a gamma radiation field of 2×10^5 r/hr. Special design considerations include provision for remote manipulation of the camera and lighting inside the 32-in.-dia core vessel.

5. HRT PROCESSING PLANT

W. D. Burch P. A. Haas W. E. Unger
R. E. Adams W. E. Browning H. O. Weeren
W. L. Albrecht L. H. Chase R. H. Winget
C. S. Lisser

5.1 OPERATIONS

5.1.1 Over-All Piping Leak Test

Initial leak tests of the piping system in the HRT processing plant, performed in conjunction with the reactor leak test (see Sec 1.1), indicated a leak five to ten times the permissible rate of 1 cc of gas per day at a 15-psi differential. By pressurizing the system to 500 psi, the leak rate was increased to 0.5 cc/min; the leak was located in a $\frac{3}{8}$-in.-tubing instrument tap by observing gas bubbles with the cell flooded. Results of a repeat test, following repair of this leak, were erratic but indicated a total leakage no greater than 2 cc/day from both high- and low-pressure systems. Although a 2-cc/day loss from the high-pressure system would be intolerable, it is acceptable for the low-pressure system. By isolating the high-pressure system at 1000 psig, its leak rate was shown to be less than 0.1 cc/day and therefore acceptable.

5.1.2 Hydroclone-System D_2O Run

Operation of the hydroclone system during the final 24 hr of the reactor D_2O run preceding the critical experiments again demonstrated the operability of all components. The processing plant D_2O inventory of 30 liters was charged just prior to the run.

Heat losses in the line from the reactor to the hydroclone were reduced about 25% to approximately 3 kw by the addition of powdered silicon metal to the silica aerogel insulation to reduce radiant heat losses.

5.1.3 Off-Gas Chilled-Water System

Cooling of off-gas from the processing plant is essential to reduce the amount of D_2O vapor discharged in the oxygen stream to the charcoal bed. Cooling to a maximum of 40°F is accomplished with a closed-loop chilled-water system. A small canned-motor pump circulates water through a coil immersed in Freon-11 from the freeze-coil refrigeration system and then through two jacketed-pipe heat exchangers in the off-gas lines. When the system was placed in operation initially, the cooling coil was found to be undersized, but after length of the coil was increased, the system performed satisfactorily.

5.2 CONSTRUCTION AND MAINTENANCE

5.2.1 Cell Closure

Closure of the cell was completed just before the end of January, and leak tests of the cell were in progress. Preliminary leakage tests of lines penetrating the cell walls were completed. The sleeve penetration containing 32 valve-operator air lines was replaced when approximately 10 leaks were found within the sleeve. Approximately one-third of the 25 steam and water service block valves had to be reworked to reduce leakage to an acceptable 1 cc/min at 30 psi.

Repeated efforts to seal leaks at electric-junction-box screwed fittings within the cell by welding, brazing, and soldering were unsuccessful. However, an epoxy-resin cement proved satisfactory in sealing the leaks. Kovar seals were installed to provide positive closures on all power leads outside the cell. Leak rates through the potting-compound plugs on thermocouple conduits outside the cell are acceptable.

5.2.2 Damage to Insulation and Wiring by Shield Water

During the flooding operation to locate piping leaks, water entered two electric level probes and the canned insulation of the refrigeration system. Both systems had been pressurized to 15 psi from outside the cell, but large leaks reduced the pressure below the hydrostatic head near the bottom of the cell.

The insulation was replaced and the shorted level probes were repaired. The leaks were stopped and the air pressurization system on the canned insulation was modified to ensure adequate pressurization.

5.3 HOLDUP TESTS ON HRT CHARCOAL ADSORBER BEDS

The results of tests on charcoal beds 10-C and -D, and the experimental technique used, have been reported previously.[1] Similar tests on beds 10-A and -B have been completed. The data obtained from these tests (see Table 5.1) have been utilized to predict performance at various gas flow rates.

In order to predict the performance of the beds, several assumptions were made. Values for t_b (time for breakthrough of activity) were used in the calculations rather then t_{max} values (time when maximum activity is present in effluent gas stream). The magnitude of the decay heating in the small-diameter charcoal-filled pipes and its effect on the adsorption of the fission gases are not known exactly. Therefore it was assumed that only the charcoal contained in the 6-in.-dia pipe contributes significantly to the holdup of the fission gases. Since the large pipe contains 90% of the charcoal in the bed, the experimental t_b value was reduced by 10% to compensate for the decay heating in the first sections of the bed. Based on laboratory tests, it was assumed that xenon gas is adsorbed 12 times more effectively than krypton gas. These assumptions tend to underestimate the actual delay times in the beds.

The experimental t_b values were normalized to a hypothetical bed containing 500 lb of charcoal, with 1 liter/min oxygen sweep, at 15°C, and then averaged. After the average value was reduced by 10% to compensate for the decay heating in the first section of the bed, a holdup of 180 hr was calculated for krypton. The corresponding holdup value for xenon is therefore 2160 hr. Holdup times are inversely proportional to flow rates.

The expected rates of release of activity from the bed after equilibrium is reached were calculated for each isotope of krypton and xenon. Data from reports by Van Winkle[2] and Kolb[3] on gaseous fission products coming from the reactor core at 10 Mw power and on residence time of the gases in piping and equipment before reaching the beds were used in the calculation. Activity release rates for the various isotopes were combined and plotted in Fig. 5.1 as a function of gas flow rate from the reactor.

Previous conservative calculations[4] have shown that approximately 100 curies can be discharged per day from the 7500 Area stack without hazard. Thus it is evident from Fig. 5.1 that the charcoal beds can handle several times the design oxygen rates without difficulty.

[1] W. D. Burch *et al.*, *HRP Quar. Prog. Rep. Oct. 31, 1957*, ORNL-2432, p 23–24.

[2] R. Van Winkle, *Heating in HRT Cold Traps from Radioactive Fission Product Gases*, ORNL CF-55-7-141 (July 28, 1955).

[3] J. O. Kolb, *Shielding for the HRT Charcoal Pit and Off-Gas Lines*, ORNL CF-56-1-106 (Jan. 20, 1956).

[4] R. F. Myers and J. Z. Holland, U.S. Weather Bureau, Oak Ridge, *Calculations on Dispersion from 7500 Area Stack*, private communication to S. E. Beall.

Table 5.1. Experimental Holdup Tests on HRT Charcoal Beds

Bed	Weight of Charcoal (lb)	Temperature Range (°C)	Average Oxygen Sweep (liters/min)	Experimental t_b (hr)	Experimental t_{max} (hr)	Number of Theoretical Plates	Normalized* t_{max} for Hypothetical Bed (hr)
10-A	520	10–15	1.251	190	227	373	273
10-B	520	10–15	0.896	195	249	148	215
10-C	520	16–19	1.022	186	211	370	232
10-D	360	16–19	0.947	140	170	137	250

*Experimental t_{max} values normalized to hypothetical charcoal bed containing 500 lb charcoal, with 1 liter/min oxygen sweep, at 15°C.

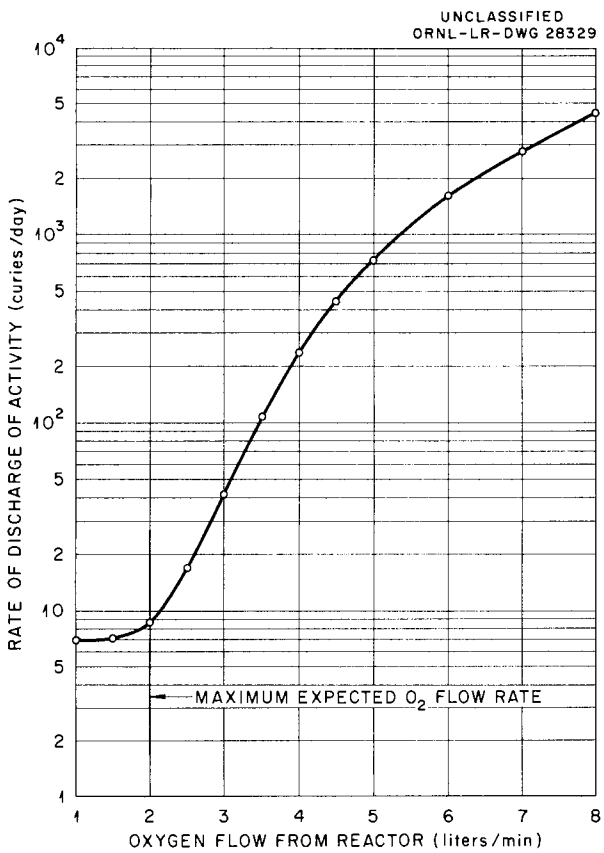

Fig. 5.1. Rate of Discharge of Activity from the HRT Charcoal Bed.

5.4 DESIGN OF WASTE CARRIER AND LOADING-PIT FACILITY

The waste solution from the processing plant will be collected in a carrier in the loading pit outside the building and transported to the Thorex Pilot Plant for recovery and decontamination of the uranium. The design of this carrier and the associated loading-pit equipment was completed.

The carrier has a capacity of 30 gal and weighs 9.3 tons. The 9 in. of lead shielding will reduce surface radiation to about 80 mr/hr. A removable cap over the valves and nozzles on top of the carrier provides additional shielding whenever the carrier is out of the loading pit (see Fig. 5.2).

The waste solution transported in the carrier will have decayed long enough so that there will be little radioactive heat and radiolytic decomposition of water. The estimated temperature rise of 2°F/hr and the pressure rise of 0.6 psi/hr are not high enough to require cooling or recombining during transit.

Waste solution is charged to the carrier with the loading pit flooded to minimize radiation exposure. A trolley-type device positions the carrier beneath the charging nozzles, which can be sprung downward to mate with the carrier nozzles. After bolting the standard ring-joint flanges, the proper valves are adjusted from above with long-handled tools, and the transfer of solution is made. The charging line is then flushed to minimize contamination, the valves are closed, and the charging nozzle connections are broken. The trolley is then cranked back into the original position, the cover lowered into place on the carrier, and the carrier removed from the loading pit. A sketch of the loading pit is shown in Fig. 5.3.

5.5 SOLIDS BEHAVIOR DEVELOPMENT STUDIES

A report has been issued summarizing conclusions for the predicted behavior of insoluble corrosion and fission products in the HRT and in its associated chemical processing plant.[5] In the report, data are presented to support the following conclusions, which are based on observations of the behavior of simulated HRT corrosion- and fission-product solids and of loop corrosion products:

1. A major fraction of the solids resulting from corrosion and from fission-product precipitation will appear in the circulating fuel solution.

2. Significant amounts of the circulating solids will be removed by "separation" owing to centrifugal force or to gravity in areas of low velocity, and by "deposition" in areas which may include those of high velocity. Geometry is an important variable. The complicated HRT geometry and the uncertainty as to the corrosion-product particle size preclude any exact prediction about corrosion-product behavior in the HRT.

3. Hydroclone efficiencies are predictable for known solid and solution characteristics. The simulated corrosion products had smaller particle diameters than those initially predicted for HRT corrosion products. Uncertainty concerning the HRT corrosion-product particle size results in uncertainty concerning the efficiency of the HRT processing plant hydroclone.

---

[5] P. A. Haas *et al.*, *HRP-CP: Conclusions Concerning the Predicted Behavior of Insoluble Corrosion and Fission Products in the HRT*, ORNL CF-58-1-97 (Jan. 23, 1958).

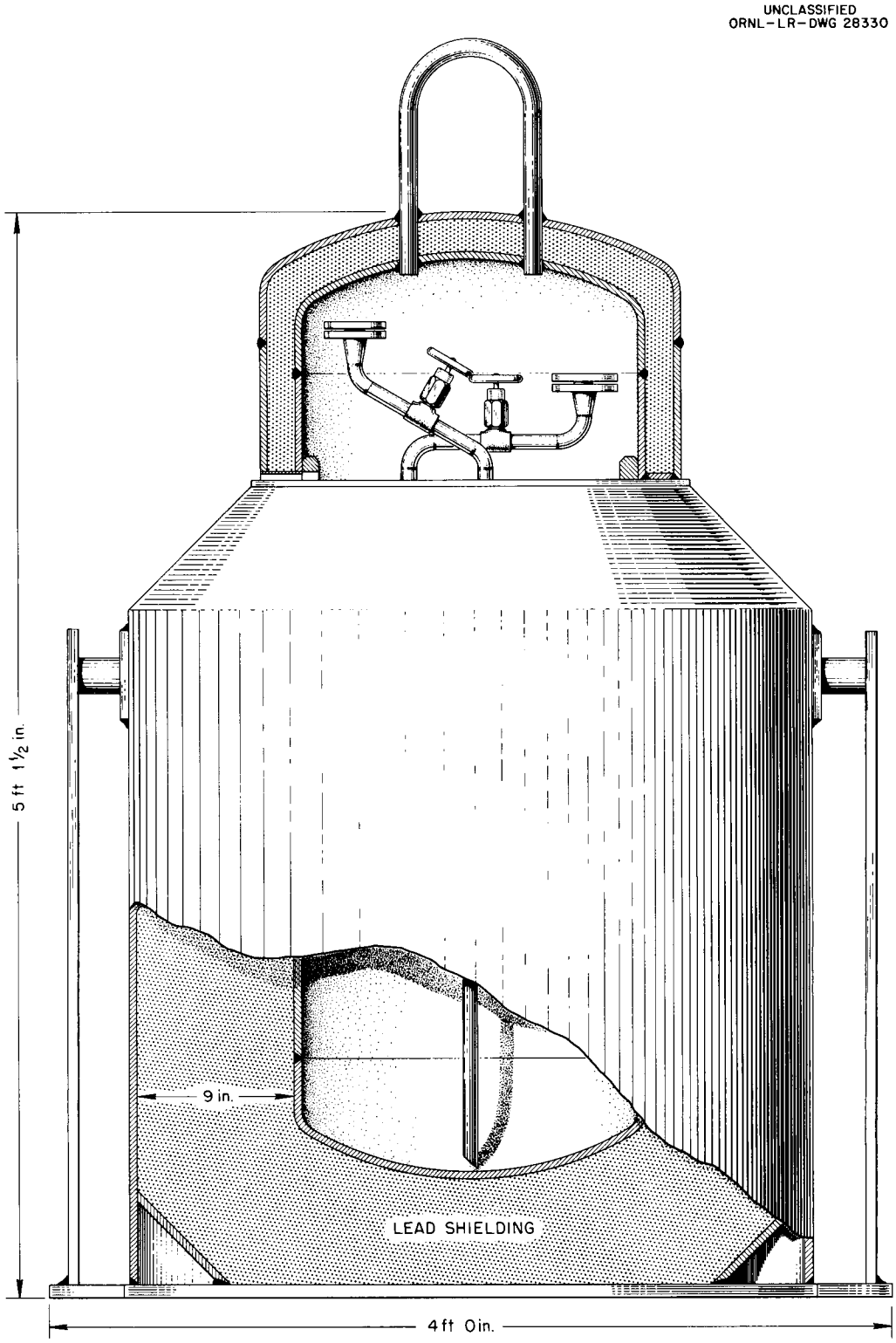

Fig. 5.2. Carrier for Waste Solution from the HRT Processing Plant.

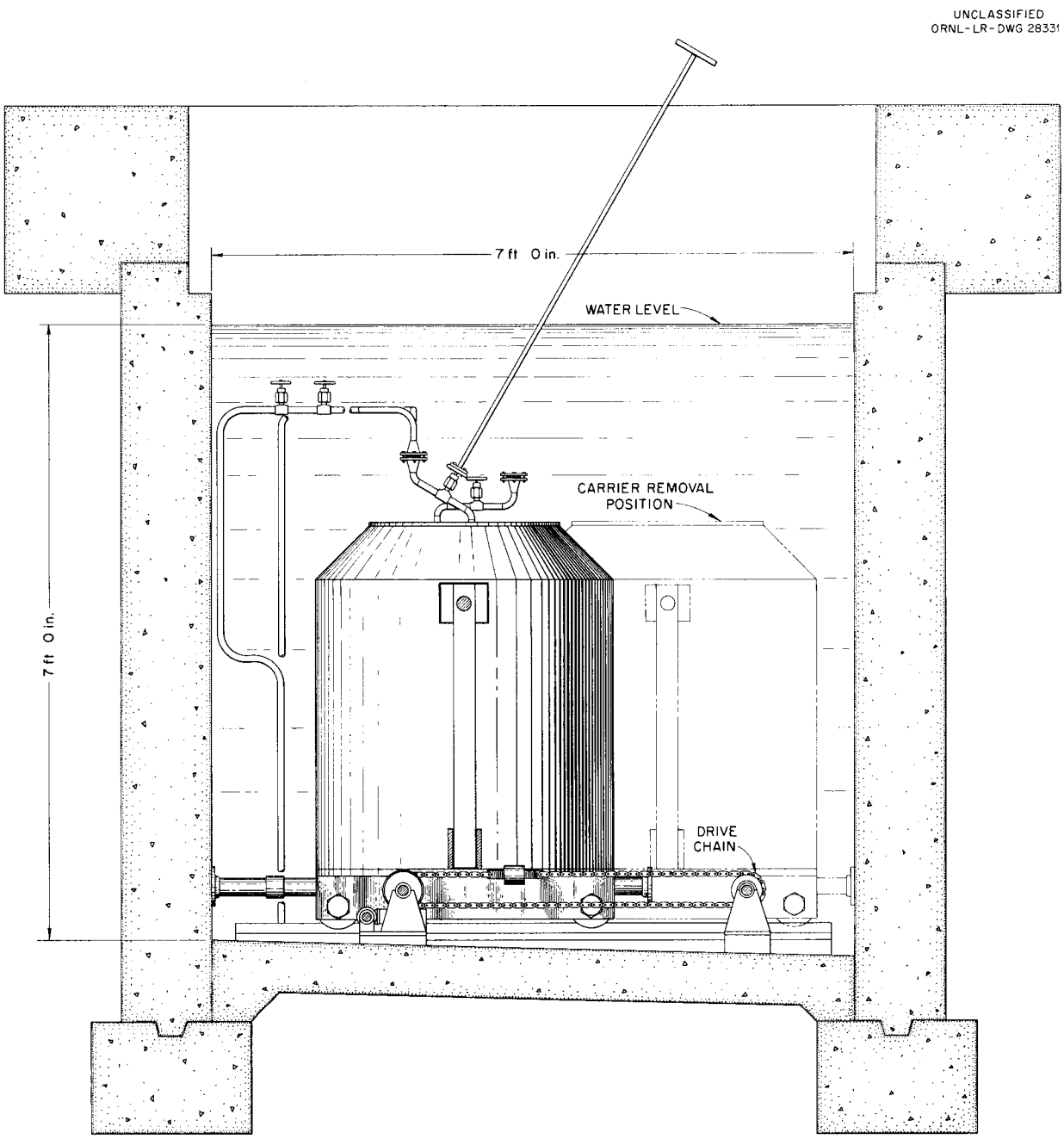

Fig. 5.3. Loading Pit for Waste Carrier.

4. Essentially continuous operation of the HRT processing plant will maintain the circulating solids concentration below 200 ppm, with probable values between 10 and 100 ppm.

5. The effectiveness of a hydroclone system could be increased by increasing the flow through the plant and by designing the reactor system to minimize "separation." Based on this conclusion, the HRT processing plant is starting operation with a 0.56-in.-dia hydroclone instead of the initially designed 0.40-in.-dia hydroclone.

6. The fraction of solids collected by the chemical plant depends on competition of the hydroclone with deposition and/or segregation and is therefore more uncertain than the above factors individually. This fraction should increase from a

zero initial value to a constant average value for periods of steady-state reactor operation. An average value as low as 25% of the corrosion products formed would not be surprising.

7. Fission products present as relatively insoluble sulfate salts will preferentially deposit on hot surfaces. Otherwise, the behavior of insoluble fission products will be obscured or controlled by the corrosion-product behavior, and the same conclusions apply to both.

The quantitative behavior of solids in the reactor system cannot be predicted with confidence from any nonreactor experiments. The number of important variables and their interrelationships invalidate conclusions from a simplified system. Until the HRT and its chemical plant operate, conclusions more definite than those presented above are not justified.

Part II

REACTOR DESIGN, RESEARCH, AND ANALYSIS

R. N. Lyon

6. HRE-3 DESIGN

W. R. Gall
M. I. Lundin
J. C. Bolger
R. H. Chapman
R. D. Cheverton
C. J. Claffey
E. H. Gift
R. O. Maak[1]
R. C. Robertson
J. N. Robinson
W. Robinson
R. E. Schappel
C. L. Segaser
E. H. Volk[2]
D. W. Vroom

6.1 LOW-PRESSURE-SYSTEM FLOWSHEET

The flowsheet for the HRE-3 blanket low-pressure system has been revised as shown in Fig. 6.1. A natural-circulation evaporator and condenser capable of producing about 100 lb/hr of condensate from a slurry feed of 10 gpm has been added; an oxygen gas system is shown for resuspension of the slurry, and the slurry storage tank and reflux condenser have been removed.[3]

6.2 PRELIMINARY DESIGN DATA

Preliminary HRE-3 design data, presented in a previous report,[4] were reissued with minor revisions as a separate memorandum.[5]

6.3 CORE AND BLANKET DUMP SYSTEMS

Rapid cooling of fuel solution and slurry being dumped from the HRE-3 high-pressure system is desirable to minimize pressure buildup in the low-pressure system during a dump. If the core and blanket dump tanks are submerged in water, the fuel solution and slurry can be directly cooled as they flash into their respective tanks.

A possible configuration for the core dump tank consists of ninety, 20-ft-long, 4-in. sched-40 pipes arranged in nine horizontal banks of ten pipes each on 16.5-in. centers. This provides an ever-safe (with regard to criticality) storage volume of 160 ft^3. The heat transfer area is approximately 2130 ft^2. The radiolytic D_2 and O_2 will be recombined in a natural-circulation catalytic recombiner, which is preceded by an iodine removal bed. It is estimated that the D_2 concentration can be maintained at less than 5%.

A tentative design of the blanket dump system (Fig. 6.1) consists of six vertical, conical-bottomed vessels, each 3 ft in inside diameter and approximately 22 ft high. A single large tank will also be considered. The explosion hazard presented by D_2 and O_2 is avoided by natural circulation of the off-gases through an iodine removal bed, a recombiner, and a condenser. An oxygen gas lift is provided for resuspension of the slurry. Steam will also be considered for agitation, but has the disadvantage of requiring either heating of the dump-tank cooling water or insulation of the tanks from the water. Oxygen, on the other hand, requires an oxygen blower, which imposes additional development problems, and appears to cause more severe foaming than does steam. Slurry could be transferred by pressurizing the dump tanks when filling the high-pressure system before startup.

6.4 LETDOWN FROM THE HIGH-PRESSURE SYSTEM

Although the HRE-3 is expected to operate normally without continuous letdown to the low-pressure system, sometimes it will be necessary to operate for short periods on a continuous letdown basis, usually during startup of the reactor, when it is necessary to continuously control liquid levels and the concentrations of slurry and fuel solution. After the reactor has been operating for a period of time, it will occasionally be necessary to regenerate the fuel solution by letting down a portion of the used fuel solution and replacing it with fresh solution from the chemical processing plant. Prior to a scheduled shutdown, operation on a continuous letdown

---

[1] On loan from Foster Wheeler Corp.

[2] On loan from Combustion Engineering, Inc.

[3] W. R. Gall *et al.*, *HRP Quar. Prog. Rep. Oct. 31, 1957*, ORNL-2432, p 29, Fig. 7.2.

[4] *Ibid.*, p 30–37, Table 7.2.

[5] J. C. Bolger *et al.*, *Preliminary HRE-3 Design Data (Revised to Nov. 15, 1957)*, ORNL CF-57-11-74 (Nov. 29, 1957).

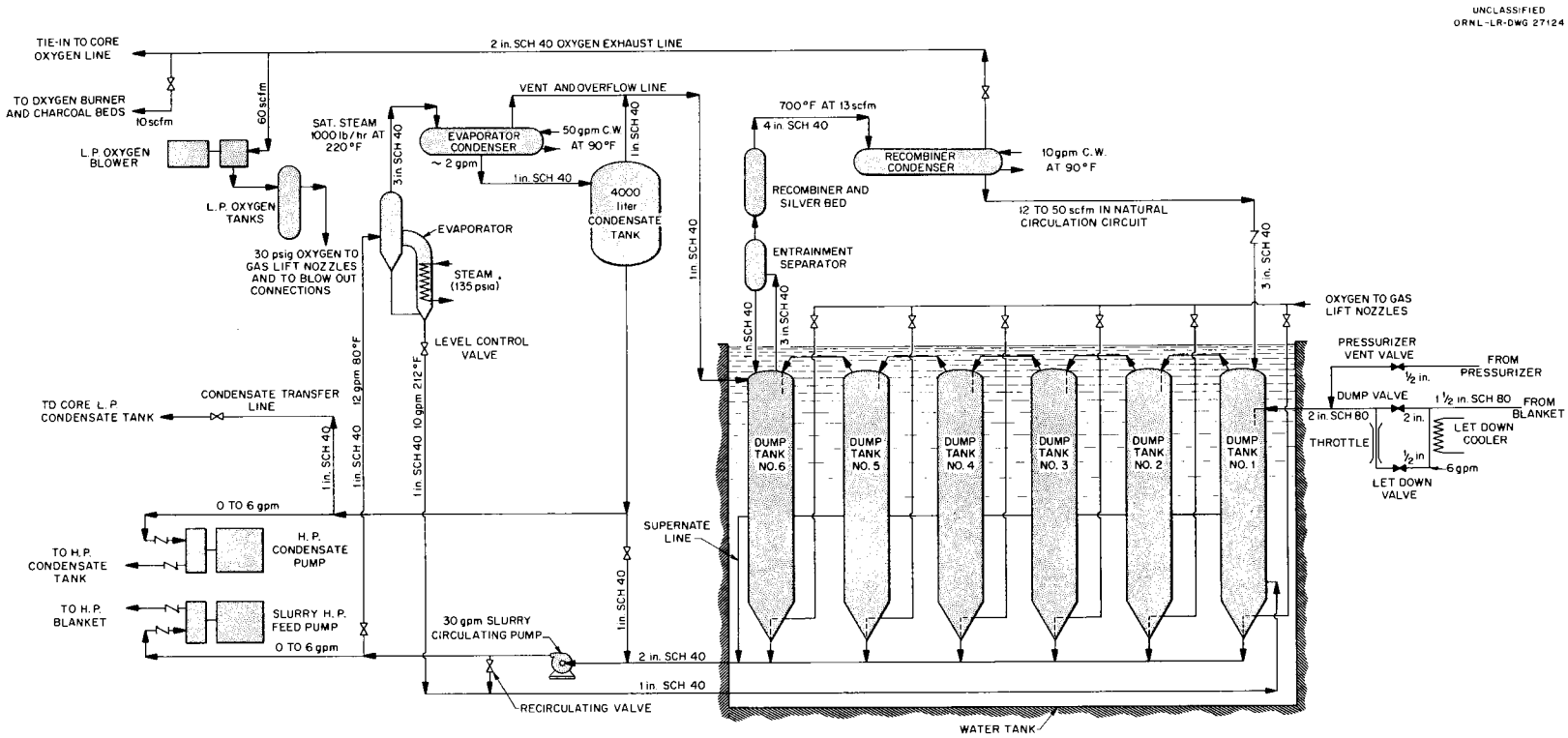

Fig. 6.1. HRE-3 Blanket Low-Pressure System.

cycle would facilitate reduction of the concentrations of the slurry and fuel solution. Operation on a continuous letdown cycle would also permit continued operation of the reactor following failure of the high-pressure condensate pump or failure or plugging of the jet-eductor vapor circuit.

A possible letdown system for the HRE-3 is shown schematically in Fig. 6.2. Control of the letdown rates is by means of restrictor tubes, the letdown valves serving primarily as stop valves. Variable-capacity diaphragm pumps feed condensate (0 to 3 gpm) and fuel solution (0 to 6 gpm) to the high-pressure core system; a diaphragm pump (0 to 6 gpm) or an acid egg feeds slurry to the high-pressure blanket system. The fuel-solution letdown rate is set higher than the estimated actual requirement in order to enhance removal of any heavy-phase fuel solution which might accumulate in the core.

6.5 OXYGEN PRESSURIZATION

Oxygen pressurization, with a jet eductor being used for gas circulation, appears to be the most promising method of pressurizing the HRE-3 if the reactor is to operate without continuous letdown. The jet eductor has a capacity of about 2 cfm, receiving its motive power from the pressure differential across the main circulating pump. The recirculated gas would be humidified by contacting the fuel solution and partially dehumidified in a condenser in order to provide condensate for purging the circulating pumps and for other uses.

Oxygen pressurization introduces the problem of disposal of a large volume of oxygen mixed with the fission-product gases which will be released during a dump. One method of disposal is to burn the waste oxygen in hydrogen, condense the resultant water vapor, and send it to the waste storage system; the uncondensed fission-product gases would be passed through cold traps to charcoal adsorption beds for holdup and decay.

6.6 IODINE REMOVAL

The iodine removal system proposed for the HRE-3 fuel system is based on the fact that iodine is more soluble in D_2O than in fuel solution. Iodine is stripped out of the fuel solution by contact with the recirculated oxygen and is concentrated in the condensate in the pressurizer condenser. This condensate is then passed through a small stripping column in which the iodine is further concentrated in the liquid phase, prior to storage in a waste system.

This system appears less complex than other methods of iodine removal investigated, and does not result in oxygen depletion, bubble formation,

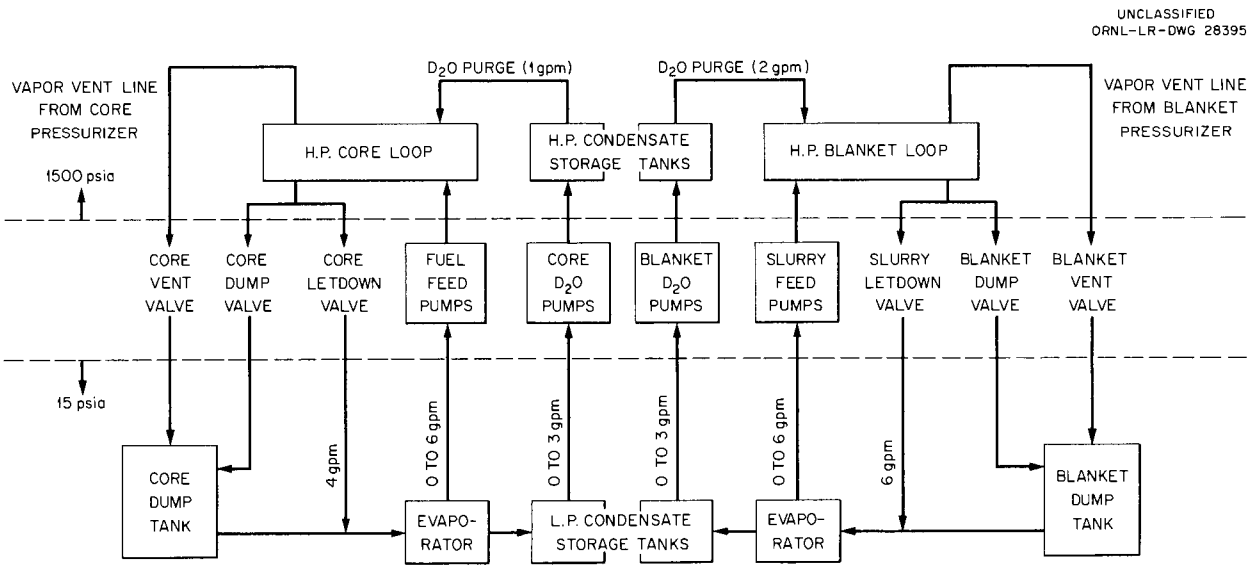

Fig. 6.2. HRE-3 Letdown System, Block Diagram.

or contamination of the fuel solution with fixing agents. Because the letdown of iodine-carrying condensate is estimated to be only about 15 gal/day, pump-up of fresh condensate to the high-pressure system would be required only at relatively long intervals. On the other hand, the electrical requirement for vaporizing water in the stripping column is ~ 120 kw.

Studies indicate that if this stripping-column system is not used some gain in breeding ratio can be obtained by mixing the condensate streams from the core and blanket system pressurizer condensers. Xenon would thus be transferred from the core to the blanket, where the xenon probability of decay is increased with respect to the probability of neutron capture.

7. RESEARCH AND ANALYSIS

P. R. Kasten

L. L. Bennett, H. C. Claiborne, T. B. Fowler, C. S. Morgan, R. H. Nimmo, B. E. Prince, M. W. Rosenthal, D. G. Thomas, M. Tobias

7.1 BREEDING RATIO IN THORIUM BREEDER REACTORS

A study was made of the effect that various values of η^{23} in the resonance energy region would have on the breeding gain and critical concentration of various spherical reactors. The calculations were performed on the UNIVAC, with the Eyewash multigroup-multiregion code.[1] Twenty-seven fast groups, one thermal group, and four space regions (core, Zircaloy-2 core tank, blanket, and pressure vessel) were employed. The reactor was fueled with U^{233} at 280°C, and in all cases it was assumed that no poisons were present. To obtain a comparison with results obtained for a simpler model which does not account for resonance fissions in U^{233}, the same reactor cases were calculated by use of a two-group, two-region code.[2]

An estimate of the value of η for U^{233} as a function of energy was made by fitting a histogram to the cross-section curves in BNL-325,[3] assuming average values for the scattering cross section. It is believed that the resulting values for η^{23} at high energies are lower than the actual values. The value of ν, which is nearly independent of energy in the low and intermediate resonance region, was assumed to be 2.52 neutrons per fission; this was combined with the absorption and fission cross sections to give values for η^{23}. The resulting histogram for η^{23} as a function of energy is given in Fig. 7.1(*a*). These values are more conservative than those derived from cross sections reported by Roberts and Alexander;[4] the latter values are also given in Fig. 7.1(*a*). The importance of the value for η^{23} as a function of energy in influencing breeding ratio is indicated in Figs. 7.1(*b*), (*c*), and (*d*), which give the per cent of total fissions occurring in the various energy groups for three core-thorium concentrations.

Reactors having ThO_2-D_2O slurry blankets were considered, with the core region containing either a fuel solution or a fuel slurry. The specific reactor sizes and fuel concentrations studied are given in Table 7.1.

[1] J. H. Alexander and N. D. Given, *A Machine Multigroup Calculation. The Eyewash Program for Univac*, ORNL-1925 (Sept. 6, 1955).

[2] T. B. Fowler, *Oracle Code for a General Two-Region, Two-Group Spherical Homogeneous Reactor Calculation*, ORNL CF-55-9-133 (Sept. 22, 1955).

[3] D. J. Hughes and J. A. Harvey, *Neutron Cross Sections*, BNL-325 (July 1, 1955).

[4] J. T. Roberts and L. G. Alexander, *Cross Sections for OCUSOL-A Program*, ORNL CF-57-6-5 (July 11, 1957).

Table 7.1. Reactor Sizes and Fuel Concentrations Investigated

Core Inside Diameter (ft)	Pressure-Vessel Inside Diameter (ft)	Blanket U^{233} (g per kg of Th)	Blanket Thorium Concentration (g/liter)	Core Thorium Concentration (g/liter)
4	9	0	250	0
		0	500	0
		0	1000	0
6	10	3.0	1000	0
		3.0	1000	150
		3.0	1000	300

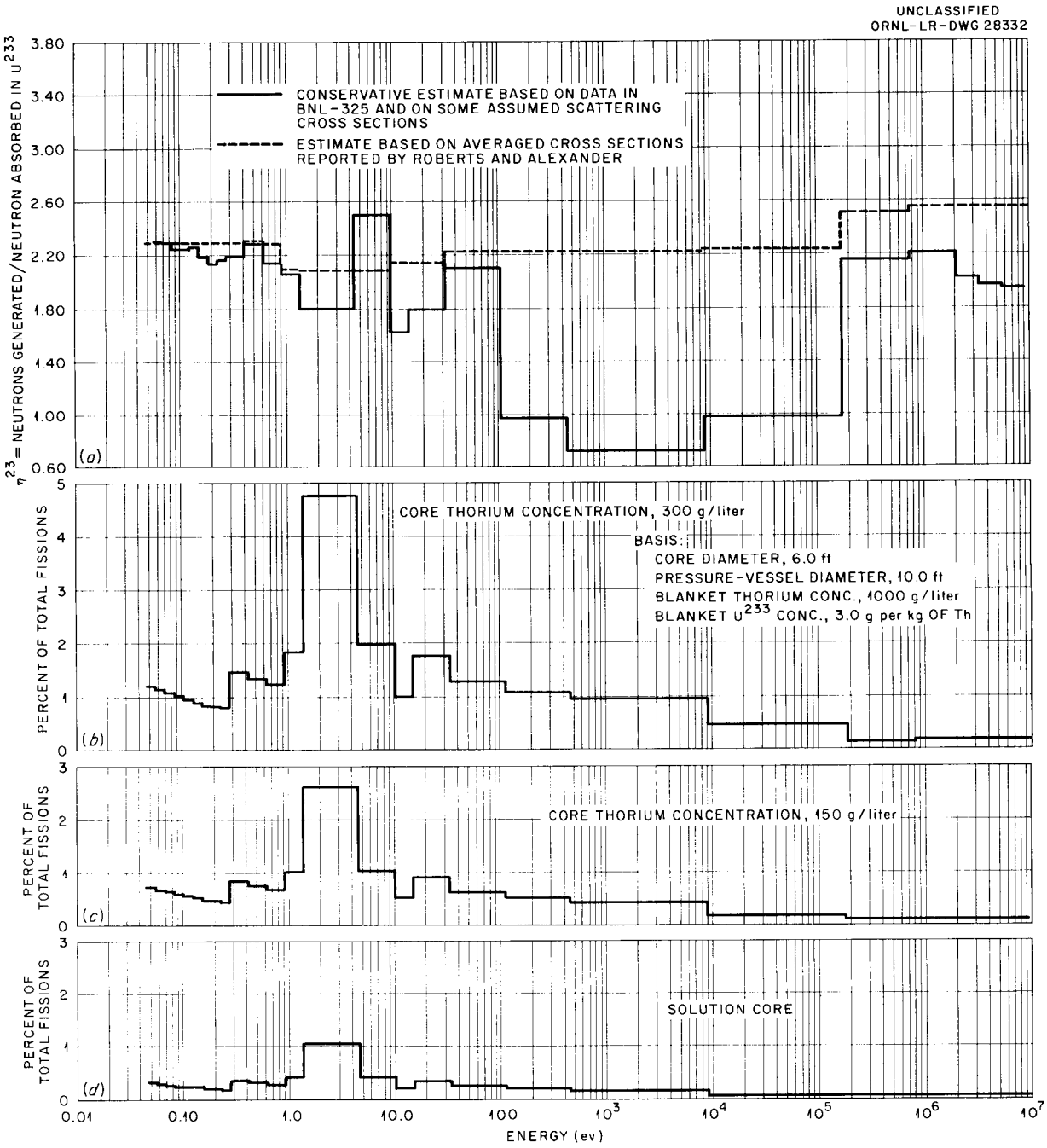

Fig. 7.1. Estimated Value of η^{23} as a Function of Energy and Its Effect on Breeding Ratio. (*a*) Group-averaged values of η^{23} vs neutron energy. (*b*) Relative number of fissions in neutron energy groups. Slurry-core reoctor; core thorium concentration, 300 g/liter. (*c*) Relative number of fissions in neutron energy groups. Slurry-core reoctor; core thorium concentration, 150 g/liter. (*d*) Relative number of fissions in neutron energy groups. Solution-core reactor.

The breeding gain and U^{233} critical concentration obtained from the Eyewash and also from the two-group models are given in Figs. 7.2 and 7.3. From these curves, it may be seen that the breeding ratio is the parameter most sensitive to the value of η^{23}. The loss in breeding ratio, due to a reduced value of η^{23} in the resonance region, is most marked for the slurry-core systems. For these reactors, fissions of U^{233} in the resonance region become more important as the

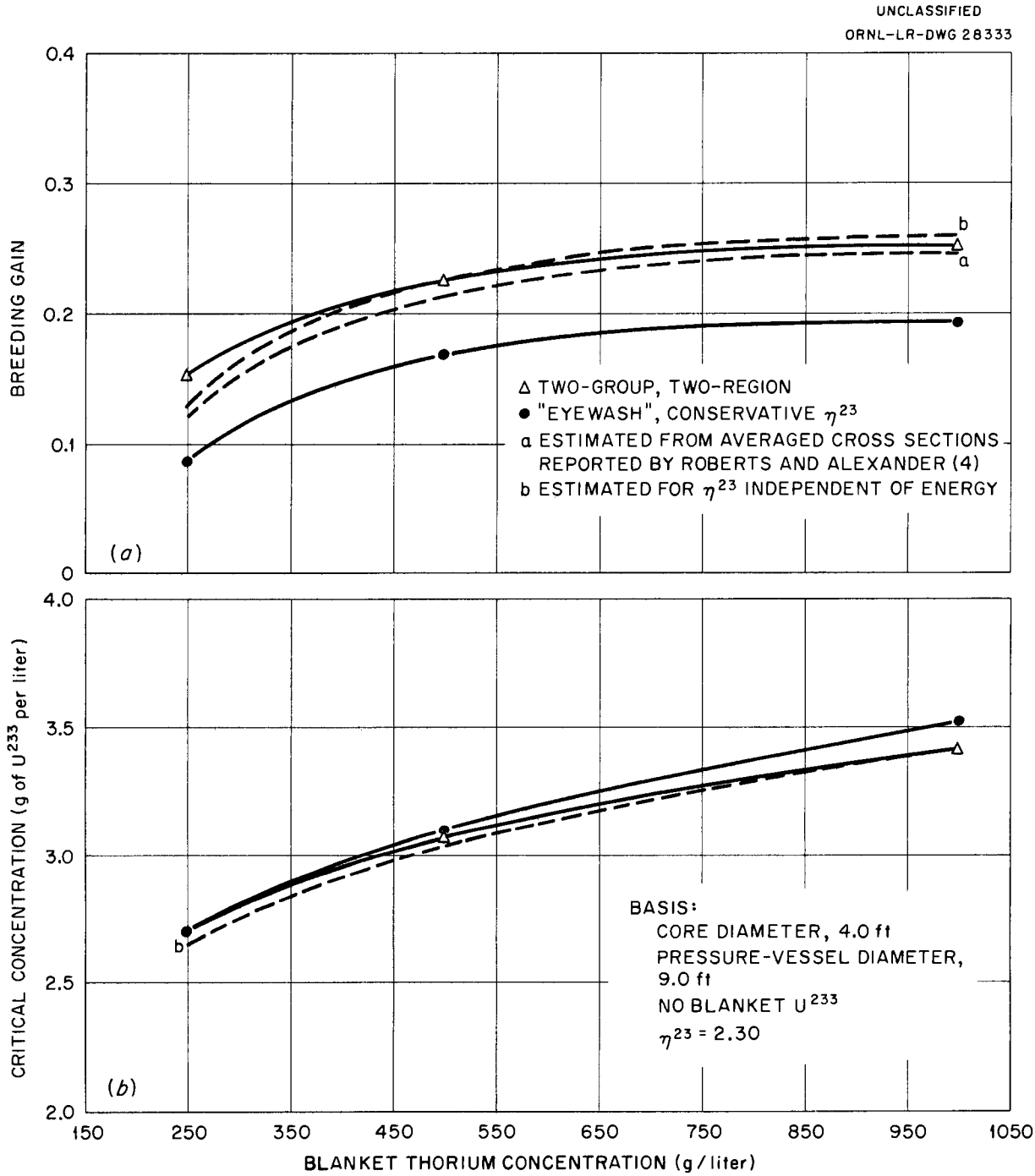

Fig. 7.2. Comparison of Calculations for Solution-Core Reactors. (*a*) Breeding gain vs blanket thorium concentration. (*b*) Critical concentration vs blanket thorium concentration.

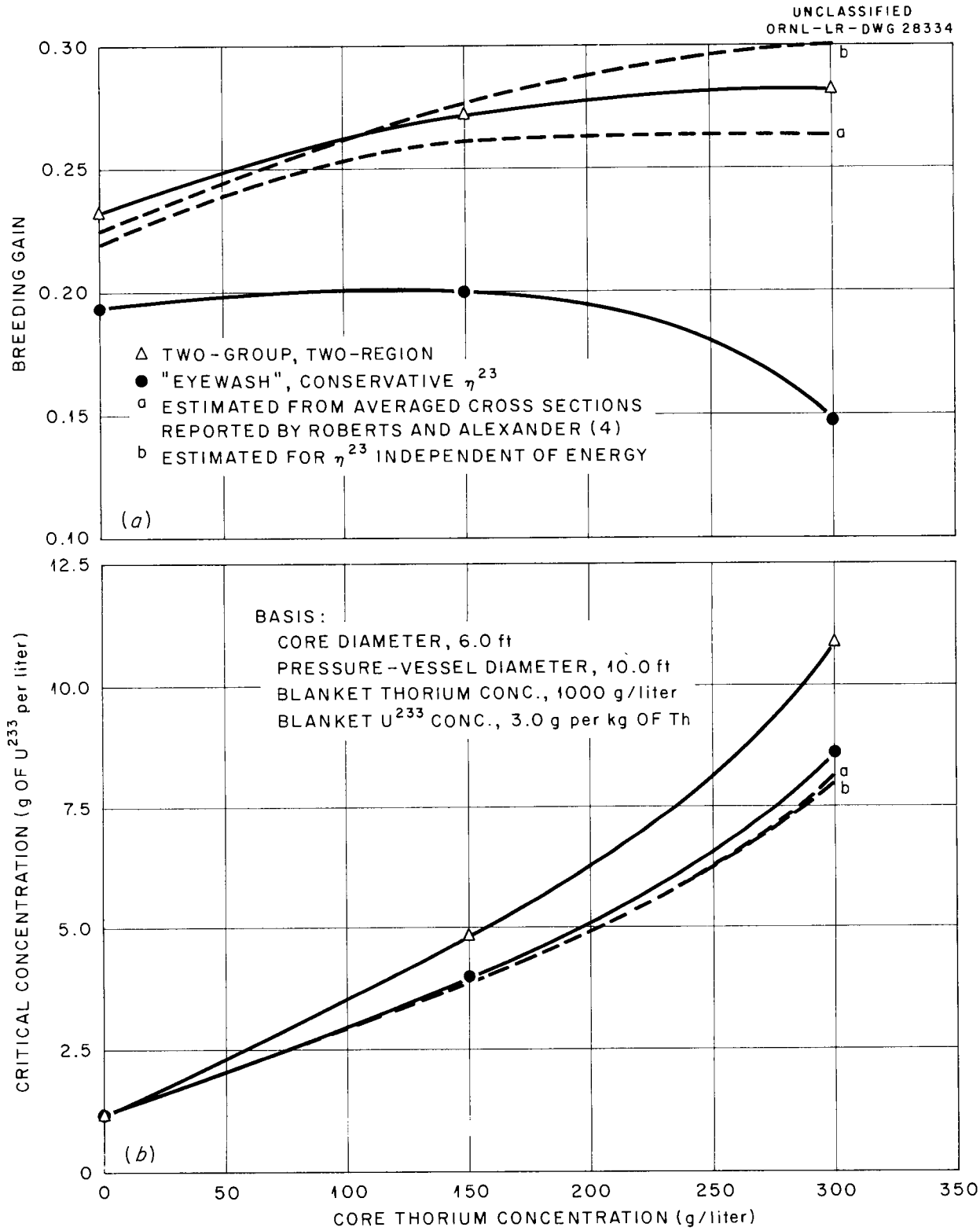

Fig. 7.3. Comparison of Calculations for Slurry-Core Reactors. (*a*) Breeding gain vs core thorium concentration. (*b*) Critical concentration vs core thorium concentration.

core loading is increased. This "hardening" of the spectrum is illustrated by the histograms in Figs. 7.1(*b*), (*c*), and (*d*).

Since the values of η^{23} used in the Eyewash calculation are believed to be low, estimates were made of the breeding ratios using (1) the higher η^{23} values derived from the averaged U^{233} cross sections reported by Roberts and Alexander and (2) η^{23} independent of energy. These latter results, shown in Figs. 7.2 and 7.3, were obtained by a perturbation calculation using the Eyewash fission spectrums. These estimates are close to the values obtained with the two-group model.

In making these calculations it was assumed that the average value of η for U^{233} in the resonance region is nine-tenths of η at thermal energies. Recent experimental data have indicated[5] that η varies rapidly and widely in the region from 1 to 8 ev. Because of the uncertainty in η, the results of this study should be considered only as an indication of the way in which the calculated breeding gain varies with method of calculation and interpretation of the cross-section data.

In general, it was found for a heavily loaded blanket (or core) that the two-group values of total neutron leakage were overestimated relative to the total leakages obtained from the multigroup calculation (the multigroup model allows for competition between fast absorptions in fuel and fast leakage, while the two-group model assumes that fast leakage occurs before any resonance absorption occurs). Conversely, the ratio of thermal to fast leakage was underestimated by the two-group method. Table 7.2 is a comparison of the neutron balances obtained with Eyewash and with the two-group model, for one of the solution-core reactors studied. The "fast" absorptions in the multigroup neutron balance are the sums of the 27 fast groups. The fast effect, ϵ, is defined by the ratio:

$$\epsilon = \frac{\text{Total number of fissions at all energies}}{\text{Number of thermal fissions}}.$$

[5]E. H. Magleby *et al.*, *Energy Dependence of η^{23} for the Region 0.1 to 8.0 ev*, IDO-16366 (Nov. 19, 1956).

Table 7.2. Comparison of Eyewash and Two-Group Neutron Balances for a Solution-Core Reactor*

	Absorptions per 100 Absorptions by U^{233}	
	Eyewash	Two-Group
U^{233}		
Fast, core	15.0	
Thermal, core	85.0	100.0
Thorium		
Fast, blanket	31.8	27.1
Thermal, blanket	87.7	98.1
Zirconium		
Fast	0.3	
Thermal	3.6	3.6
Blanket leakage		
Fast		0.8
Thermal	0.3	0.4
Total	223.7	230.0
Critical U^{233} concentration, g/liter	3.52	3.41
Breeding ratio	1.195	1.252
ϵ	1.14	

*Reactor specifications: core diameter, 4 ft; pressure-vessel diameter, 9 ft; core-tank thickness, ½ in.; pressure-vessel thickness, 6 in.; blanket thorium concentration, 1000 g/liter; no U^{233} in blanket.

7.2 TIME-DEPENDENT STUDIES OF SLURRY-CORE, SLURRY-BLANKET THORIUM BREEDER REACTORS

Previous reports[6] have discussed time-dependent studies of solution-core, two-region breeders operating at 60 Mw. Similar results have also been obtained for two-region breeders having various concentrations of thorium in the core volume. The core diameter was set at 4 ft, the blanket thickness at 2½ ft, and the blanket thorium concentration at 1000 g of Th per liter. The core thorium concentrations studied were 100, 150, and 200 g of Th per liter. As before, the

[6]P. R. Kasten *et al.*, *HRP Quar. Prog. Rep. Oct. 31, 1957*, ORNL-2432, p 42; M. Tobias, M. W. Rosenthal, and T. B. Fowler, *Time-Dependent Studies of the Nuclear Characteristics of HRE-3*, ORNL CF-57-12-1 (Dec. 31, 1957).

moderator was heavy water in both core and blanket volumes, and both regions operated at a mean temperature of 280°C; the Zircaloy-2 core tank was 0.33 in. thick. Calculations were performed in terms of a constant *total* power of 61.5 thermal megawatts. The same chemical processing flowsheet was assumed as before, with the important exception that no hydroclone processing was employed for the slurry-core cases.

Results given in Figs. 7.4 and 7.5 are for a core thorium concentration of 150 g of Th per liter and are typical of all cases studied in their important features. As with solution-core reactors, there is a small but relatively rapid initial drop in breeding ratio during the first 100 days following reactor startup. This is due to the neutron captures in protactinium as its concentration rises and approaches equilibrium conditions. The buildup of protactinium is quite similar to the behavior seen in the solution-core cases. Equilibrium protactinium levels are reached in both the core and the blanket long before chemical processing is started. This period is followed by a more or less linear fall in breeding ratio with time due to core poison-fraction buildup. Initiation of blanket processing produces a relatively minor change in slope of the breeding-ratio–time curve, in contrast to the sharp break caused by the start of core processing. That the buildups of the poison fractions and the higher isotopes are linear with time may also be observed, with U^{234} in the core being the most important higher isotope. As can be seen from Table 7.3, the other isotopes are comparatively minor constituents, even at 1500 days. It is interesting to note that, despite the absence of hydroclone separation, the core poison fraction still takes two or more years to reach a 7% level because of the large fission cross section required by the presence of ThO_2 slurry in the core. Table 7.3 lists results for the various cases considered.

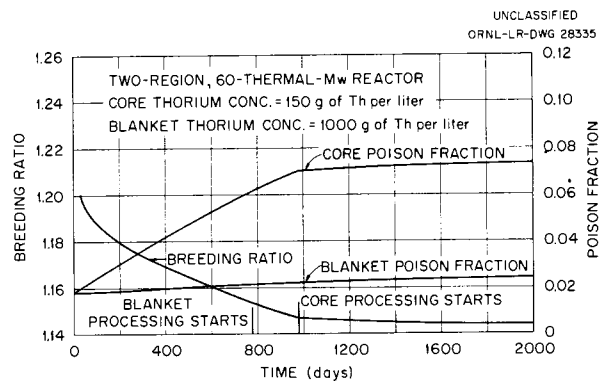

Fig. 7.4. Breeding Ratio, Core Poison Fraction, and Blanket Poison Fraction as Functions of Time for a 60-Mw Thorium Breeder Reactor.

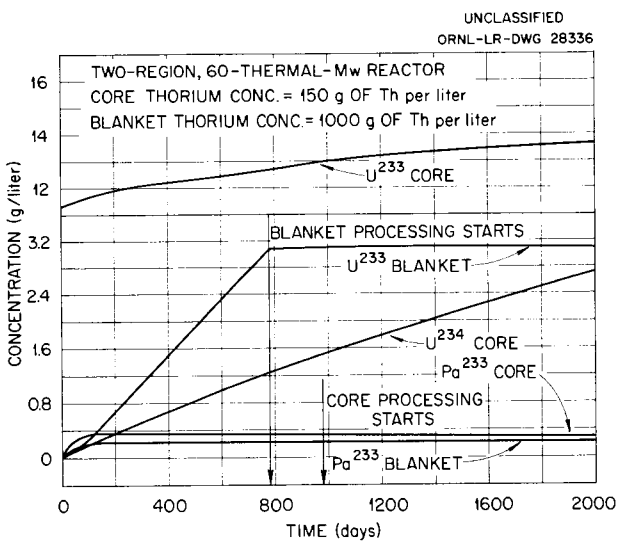

Fig. 7.5. Variation with Time of U^{233}, U^{234}, and Pa^{233} in the Core and of U^{233} and Pa^{233} in the Blanket for a 60-Mw Thorium Breeder Reactor.

In these calculations there was no allowance for the poisoning effect of accumulated corrosion products. The absence of hydroclone processing would result in retention of all corrosion products in the core system, and, for the same corrosion rate, the cross section of corrosion products is about four times[7] as great as in a solution-core system using hydroclones. However, the higher critical concentrations in slurry-core systems compensate for this, and the poison fraction in the core with 200 g of Th per liter could be about the same as in a solution-core reactor.

The critical concentration of U^{233} in the core displays a small but steady rise; this contrasts with solution-core reactors, where the critical core concentration is found to be strikingly constant. Solution-core reactors, because of their longer thermal diffusion length, are more

[7] M. W. Rosenthal and T. B. Fowler, *Nuclear Computations for HRE-3 Design: Equilibrium Results*, ORNL CF-57-7-23 (July 10, 1957).

Table 7.3. Comparison of Breeding Ratios, Poison Fractions, and Isotope Levels in Two-Region Breeder Reactors with Various Concentrations of Thorium in the Core*

Time (days)	Breeding Ratio	Core Poison Fraction	Blanket Poison Fraction	Core Isotopes (g/liter)					Blanket Isotopes (g/liter)				
				U^{233}	U^{234}	U^{235}	U^{236}	Pa^{233}	U^{233}	U^{234}	U^{235}	U^{236}	Pa^{233}
Solution-Core Reactor; Fixed Poison Fraction 3.6%** Blanket processing starts at 490 days; core processing starts at 910 days													
100	1.158	0.041	0.018	3.8	0.2	5×10^{-3}	10^{-4}	0	0.4	2×10^{-3}	5×10^{-6}	10^{-8}	0.25
400	1.143	0.055	0.021	3.8	0.6	0.05	6×10^{-3}	0	2.4	0.03	2×10^{-4}	2×10^{-6}	0.31
490	1.140	0.060	0.022	3.8	0.7	0.06	0.01	0	3.0	0.04	4×10^{-4}	4×10^{-6}	0.32
910	1.124	0.080	0.025	3.9	1.3	0.14	0.04	0	3.1	0.06	10^{-3}	2×10^{-5}	0.29
1200	1.123	0.079	0.026	3.9	1.6	0.18	0.07	0	3.0	0.07	10^{-3}	3×10^{-5}	0.28
Slurry-Core Reactor; 100 g of Th per Liter, in Core as ThO_2 Blanket processing starts at 720 days; core processing starts at 700 days													
120	1.175	0.028	0.018	8.6	0.2	3×10^{-3}	4×10^{-5}	0.28	0.4	2×10^{-3}	2×10^{-6}	2×10^{-9}	0.23
400	1.155	0.050	0.020	9.0	0.7	0.03	10^{-3}	0.28	1.7	0.01	7×10^{-5}	3×10^{-7}	0.24
700	1.140	0.071	0.021	9.3	1.1	0.07	5×10^{-3}	0.27	3.0	0.03	3×10^{-4}	2×10^{-6}	0.24
1000	1.139	0.072	0.023	9.4	1.5	0.11	0.01	0.25	3.1	0.04	5×10^{-4}	5×10^{-6}	0.22
Slurry-Core Reactor; 150 g of Th per Liter, as ThO_2 Blanket processing starts at 780 days; core processing starts at 980 days													
120	1.185	0.026	0.018	11.8	0.2	2×10^{-3}	2×10^{-5}	0.34	0.3	10^{-3}	10^{-6}	10^{-9}	0.21
400	1.169	0.042	0.020	12.2	0.7	0.02	6×10^{-4}	0.34	1.5	0.01	4×10^{-5}	10^{-7}	0.22
780	1.153	0.061	0.021	12.7	1.2	0.07	4×10^{-3}	0.32	3.1	0.03	2×10^{-4}	2×10^{-6}	0.22
1000	1.146	0.070	0.022	13.1	1.5	0.10	7×10^{-3}	0.31	3.1	0.04	4×10^{-4}	3×10^{-6}	0.21
2000	1.144	0.073	0.024	13.6	2.7	0.24	0.04	0.30	3.1	0.05	8×10^{-4}	10^{-5}	0.21
Slurry-Core Reactor; 200 g of Th per Liter, as ThO_2 Blanket processing starts at 820 days; core processing starts at 1360 days													
120	1.192	0.024	0.018	15.6	0.2	2×10^{-3}	10^{-5}	0.38	0.3	10^{-3}	10^{-6}	10^{-9}	0.19
820	1.164	0.052	0.021	16.7	1.3	0.06	3×10^{-3}	0.37	3.1	0.03	2×10^{-4}	10^{-6}	0.21
1500	1.151	0.071	0.023	18.0	2.2	0.15	0.01	0.34	3.1	0.04	5×10^{-4}	6×10^{-6}	0.20
2000	1.149	0.072	0.024	18.4	2.9	0.22	0.02	0.34	3.1	0.05	7×10^{-4}	10^{-5}	0.20

*Core diameter, 4 ft; blanket thickness, 2½ ft; reactor temperature, 280°C; fixed poison fraction, 1.8% (except in the solution-core case); blanket thorium concentration, 1000 g of Th per liter, as ThO_2; core Thorex processing started at 7% poison fraction (except in the solution-core case); blanket Thorex processing started at U^{233} blanket concentration of 3 g/liter.

**Xenon, 1%; Sm group, 0.8%; Cu, 0.8%; fixed poison fraction associated with the solubility product of the precipitable fission products, 1%.

sensitive to the growth of fuel in the blanket than slurry-core machines. The latter have less thermal neutron leakage from core to blanket, and core-poison and higher-isotope growth are less well compensated by the rise of fuel level in the blanket.

It should be noted that the nuclear computations in this study were performed by use of a two-group model which makes no provision for absorption in fuel at neutron energies above thermal. The breeding-ratio values therefore do not include the effect of resonance absorptions discussed in Sec 7.1; however, it is believed that the general shapes of the curves in Figs. 7.4 and 7.5 would not be altered even though resonance absorptions were considered.

7.3 HEAT GENERATION RATES IN HRE-3 CORE VESSEL

Revised heat generation rates in the core tank of HRE-3 type reactors for several conditions are presented in Table 7.4. The total heat generation rates shown are lower than the values

Table 7.4. Heat Generation Rates in Core Tank of HRE-3 Type Reactors[a]

Case	Core Fuel Type	Core Power (Mw)	Blanket Power (Mw)	Blanket Thorium Concentration (g/liter)	Blanket Uranium Concentration (g/liter)	Core Poison (%)	Blanket Poison (%)	Heat Generation (w/cc)	
								Core-Wall Capture Gammas	Total
1	Solution	50	0	1000	0	0	0	0.57	9.10
2	Solution	50	11.6	1000	3	0	0	0.60	9.84
3	Solution	50	20.2	1000	5	0	0	0.63	10.4
4	Solution	50	0	1000	0	6	0	0.53	8.93
5	Solution	50	10.9	1000	3	6	2	0.56	9.63
6	Solution	50	0	500	0	0	0	0.75	9.53
7	Solution	50	12.6	500	3	0	0	0.80	10.4
8	Solution	50	22.7	500	5	0	0	0.84	11.1
9	Solution	50	0	500	0	6	2	0.70	9.37
10	Solution	50	11.9	500	3	6	2	0.74	10.2
11	Solution	50	0	0	0	0	0	2.5	10.7
12	Solution	50	0	0	0	6	0	2.3	10.6
13[b]	Solution	367.9	117.6	1000	4	8	3.4	2.5	28.1
14	Slurry[c]	50	11.7	1000	3	6	2	0.15	6.08
15	Slurry[c]	55.6	5.3	1000	3	6	2	0.17	6.76
16	Slurry[c]	50	8.1	1000	5	6	2	0.16	6.22
17	Slurry[c]	50	14.3	500	3	6	2	0.22	6.59
18	Slurry[c]	50	0	0	0	0	0	0.77	7.96
19[b]	Slurry[c]	444.8	40.7	1000	4	8	2.7	0.60	17.3

[a]Core diameter, 4 ft; ID of pressure vessel, 9 ft; core-tank thickness, ½ in.; moderator, D_2O. See footnote (*b*) for exception.

[b]Core diameter, 6 ft; ID of pressure vessel, 10 ft.

[c]200 g of Th per liter.

previously reported[8] by about 10% for blankets containing thoria and by about 25% for pure D_2O blankets. The results presented here are based on a more refined method of calculating the heat generation rate resulting from core-wall capture gammas. (There is no change in the energy contribution resulting from gammas originating in the core and blanket.) The previously reported values were obtained by accounting for buildup by dividing all attenuation coefficients by 1.2. In the present calculation the buildup factor was explicitly calculated by means of a technique that permitted the buildup factor to vary as a function of the number of relaxation lengths. The details of this method are presented elsewhere.[9]

[8]P. R. Kasten *et al.*, *HRP Quar. Prog. Rep. Oct. 31, 1957*, ORNL-2432, p 41.

[9]H. C. Claiborne and T. B. Fowler, *Heat Generation Rates in Core Tank of HRE-3*, ORNL CF-57-12-45 (Dec. 12, 1957).

The revised values for the core-wall capture-gamma contribution are given in Table 7.4 and are 62% lower than the previous values. Two additional cases (cases 13 and 19 in Table 7.4) are presented to illustrate the magnitude of the heat generation rate in power reactors utilizing either a solution- or slurry-type core. Results are for a total power of 485.5 Mw and show that a reduction from 28 to 17 w/cc (38%) occurs by substituting a slurry core for the solution core.

7.4 PHYSICAL CHEMISTRY OF SLURRIES

7.4.1 Thorium Oxide Preparation

The properties of an oxide produced by precipitation and subsequent calcination may be influenced by the length of time the precipitate is allowed to stand in the supernatant liquid. Digestion of the precipitate allows fine particles to dissolve and redeposit. If, by this process, crystallites were filled, more compact and structurally stronger particles could result. Thorium oxalate which was digested for 48 hr and then filtered and dried at 120°C had a surface area of 4.6 m^2/g, as compared with 12.7 m^2/g for thorium oxalate which was not digested. Also, digestion of freshly precipitated thorium oxalate in supernatant liquid followed by filtration, drying, and stepwise calcination to 800°C resulted in thoria particles more resistant to degradation in a Waring Blendor than those particles prepared without digestion. Thoria produced from digested precipitates had a lower cake resuspension index (CRI)[10,11] than did thoria prepared from undigested precipitates. This is shown in Table 7.5, along with other thoria properties (the CRI is low if the oxide particles are resistant to degradation).

Data obtained to date indicate that thoria with a CRI of zero will not form cakes or spheres during circulation; therefore the use of digestion in oxide preparation may alleviate the thoria caking problem.

7.4.2 Influence of Surface-Active Agents on Thoria Slurry Properties

Prior investigation[12] has established that some surface-active agents such as silicate exert a favorable influence on thoria slurry properties. The effect of sodium aluminate has been evaluated on a laboratory scale. Addition of $NaAlO_2$ (about 1 wt % based on ThO_2) to a flocculated slurry having a high yield stress resulted in a slurry having nearly Newtonian properties. No evidence of diminution of the dispersing effect was detected after four days of autoclaving at 250°C. In another test, slurry treated with sodium aluminate was placed in a rocking quartz tube at 280°C; during

[10] C. S. Morgan, *Status Report on ThO_2 Caking Studies*, ORNL CF-57-9-102 (Sept. 26, 1957).

[11] R. B. Korsmeyer *et al.*, *HRP Quar. Prog. Rep. July 31, 1957*, ORNL-2379, p 56; *April 30, 1957*, ORNL-2331, p 64.

[12] P. H. Hayes and D. G. Thomas, *Thermal Stability of Sodium Silicate Treated Thorium Oxide Slurry in Dynamic Tests (100-A Loop Run T-79)*, ORNL CF-56-11-2 (Nov. 12, 1956).

Table 7.5. Effect of Digestion Time upon Thoria Properties

Digestion Time (hr)	Time in Waring Blendor (hr)	Cake Resuspension Index	Crystallite Size (Å)	Surface Area (m^2/g)	50% Size, After Waring Blendor (μ)
0	1.16	7	178	10.7	0.7
1	1.16	5.7	202		0.6
16	1.16	0	182		0.9
48	1.16	0	186	9.3	1.0
112	5	0	213		

three weeks of observation the slurry remained fluid. In other tests, slurry prepared from 800°C-calcined thoria was placed in a Waring Blendor having a stainless steel plate suspended above the blade. (The method of evaluating the tendency of ThO_2 to plate out during circulation by Waring Blendor tests was developed at the Pennsylvania Advanced Reactor Project by G. R. Taylor and A. Biancheria.) With no additives present, a heavy thoria film formed on the surface of the plate; however, with slurry containing sodium aluminate additive, the thickness of the resulting oxide film decreased with increasing $NaAlO_2$ concentration as shown in Fig. 7.6. The ThO_2 film had almost vanished at 0.44 wt % $NaAlO_2$; in further tests, with $NaAlO_2$ at concentrations up to 3.5 wt %, there was virtually no film formation. The influence of $NaAlO_2$ additive in preventing film formation was not altered by nine days of autoclaving at 300°C.

7.5 SLURRY HEAT TRANSFER

Laminar heat transfer coefficients obtained from data taken in the series of tests previously reported[13] were found to be greater than the conventional Newtonian-fluid coefficients by a factor of $[1 + (g_c \tau_y D/24\eta V)]^{1/3}$. This agrees with the correlation proposed by Bailey,[14] as illustrated in Fig. 7.7. The nominal concentration of the slurry used was 685 g of Th per kg of H_2O.

7.6 TEST OF A HYDROCLONE FOR PARTIAL SIZE CLASSIFICATION OF THORIA PARTICLES

Results from various toroid and loop tests indicate that only those thorium oxide particles greater than some critical diameter (3–10 μ) are effective in causing abrasive attack when fluid velocities are less than 30 fps. In these studies a hydroclone was tested to determine its usefulness in separating the coarse-particle-size fraction from the as-produced material.

A 0.50-in. hydroclone was tested to determine whether it would remove the larger particles from a 1600°C-fired oxide when operated as a particle-size classifier rather than as a liquid-solid separator.[15] A photograph of the test

[13] R. B. Korsmeyer *et al.*, *HRP Quar. Prog. Rep. Oct. 31, 1957*, ORNL-2432, p 57–59.

[14] R. V. Bailey, *Forced Convection Heat Transfer to Slurries in Tubes*, ORNL CF-52-11-189 (Nov. 24, 1952).

[15] P. A. Haas *et al.*, *Hydraulic Cyclones for Application to Homogeneous Reactor Chemical Processing*, ORNL-2301 (Nov. 18, 1957).

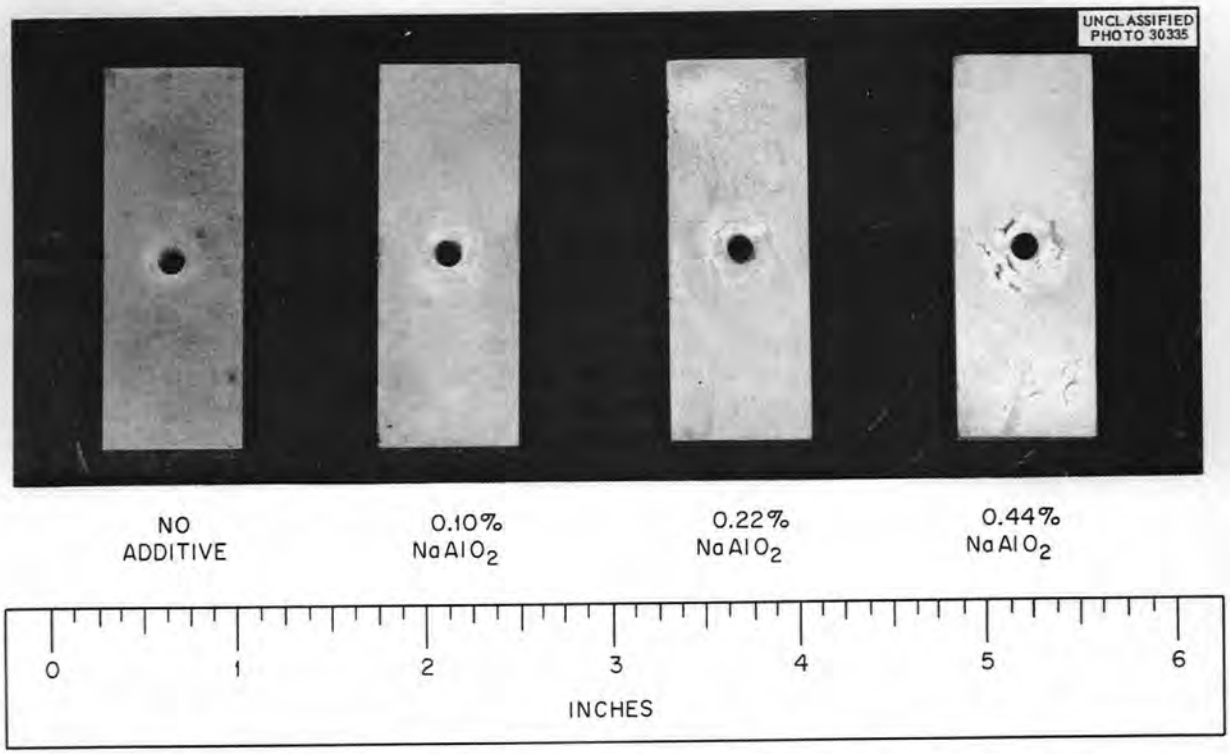

Fig. 7.6. Influence of $NaAlO_2$ Concentration on Thoria Film Deposit on Stainless Steel Plates.

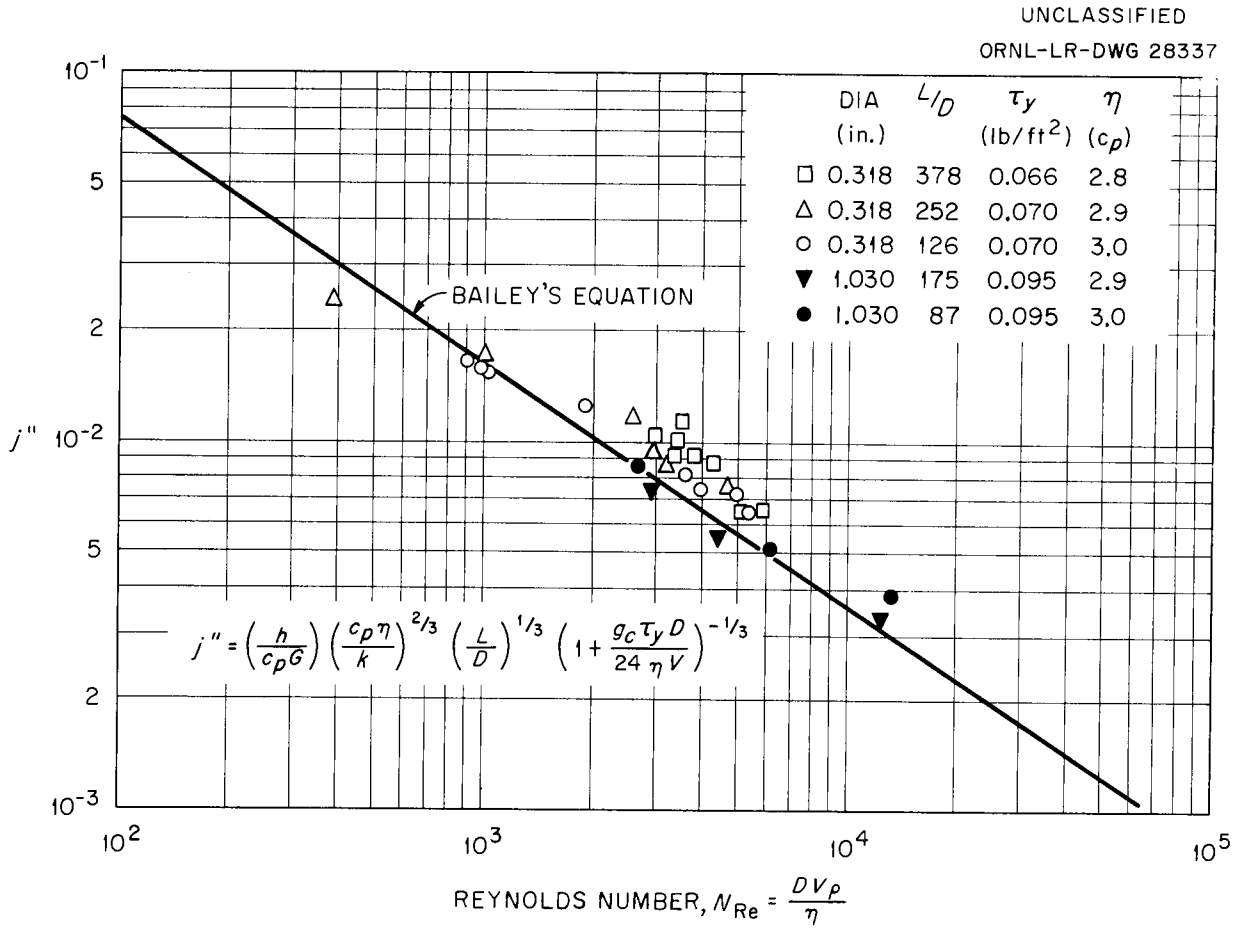

Fig. 7.7. Laminar Heat Transfer Characteristics of Thoria Slurries.

setup is shown in Fig. 7.8, and the hydroclone dimensions are given in Table 7.6. The hydroclone discharged to a receiver at atmospheric pressure.

It was shown[16] that a single pass through this hydroclone would reduce the material greater than 10 μ from 12 wt % to less than 1 wt %, while the mean diameter was reduced from 1.7 to 0.9 μ. When the overflow (fine) fraction was again pumped through the hydroclone, 98 wt % of the overflow solids from the second pass were less than 2 μ in diameter. The mean diameter was reduced from 0.9 to about 0.7 μ by the second pass. Typical results, shown in Fig. 7.9, were obtained with a 25-psi pressure drop

Table 7.6. Hydroclone Dimensions

Item	Size (in.)
Hydroclone inside length	3.00
Hydroclone ID at feed port	0.500
Feed-port width	0.10
Feed-port height	0.15
Underflow-port diameter	0.125
Overflow-port diameter, vortex-finder ID	0.100
Vortex-finder OD	0.125
Vortex-finder length, extension into hydroclone	0.250

[16] L. L. Bennett and D. G. Thomas, *Hydraulic Cyclones for Thorium Oxide Size Classification*, ORNL CF-58-1-35 (in press).

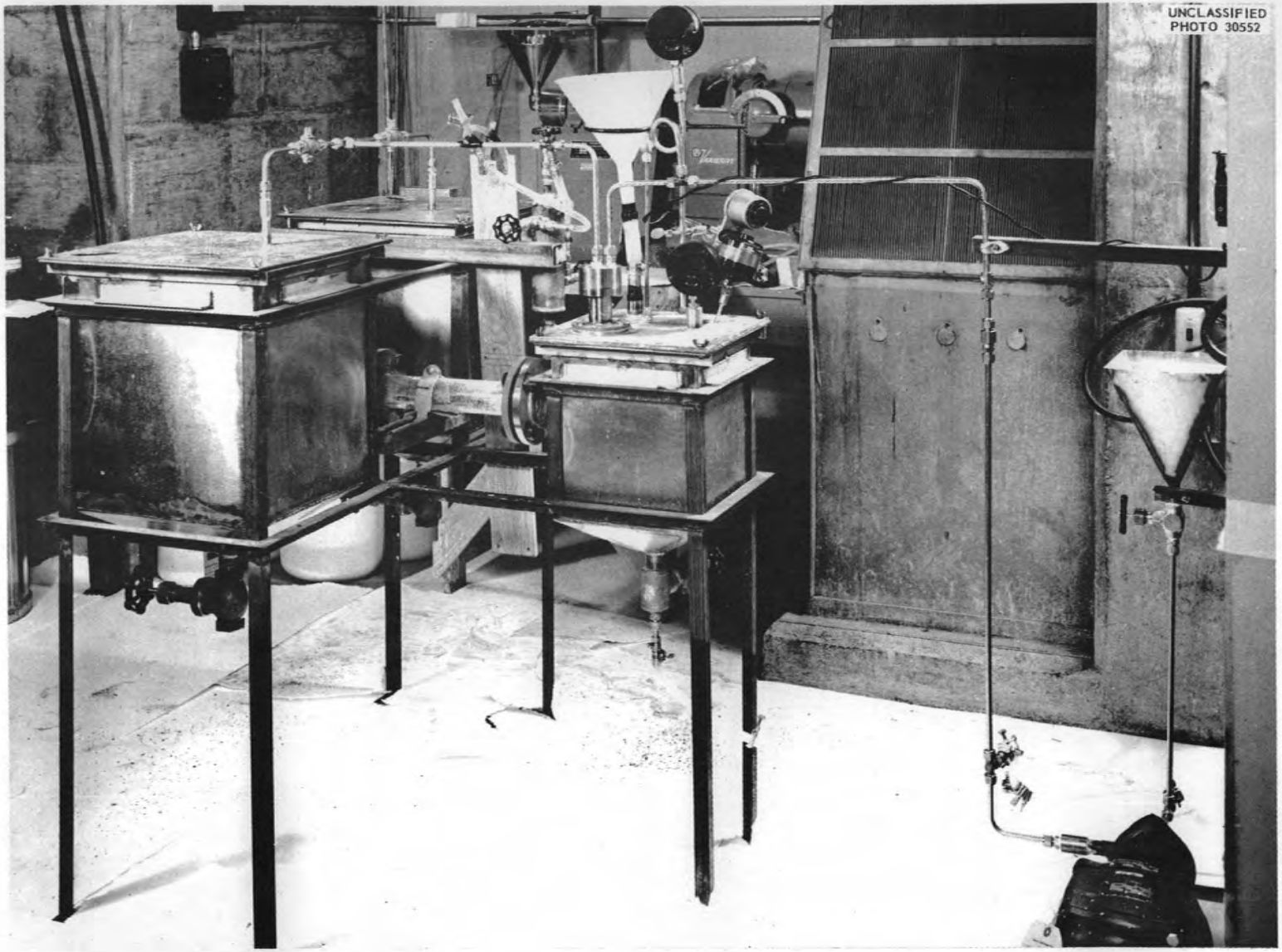

Fig. 7.8. Hydroclone Test System.

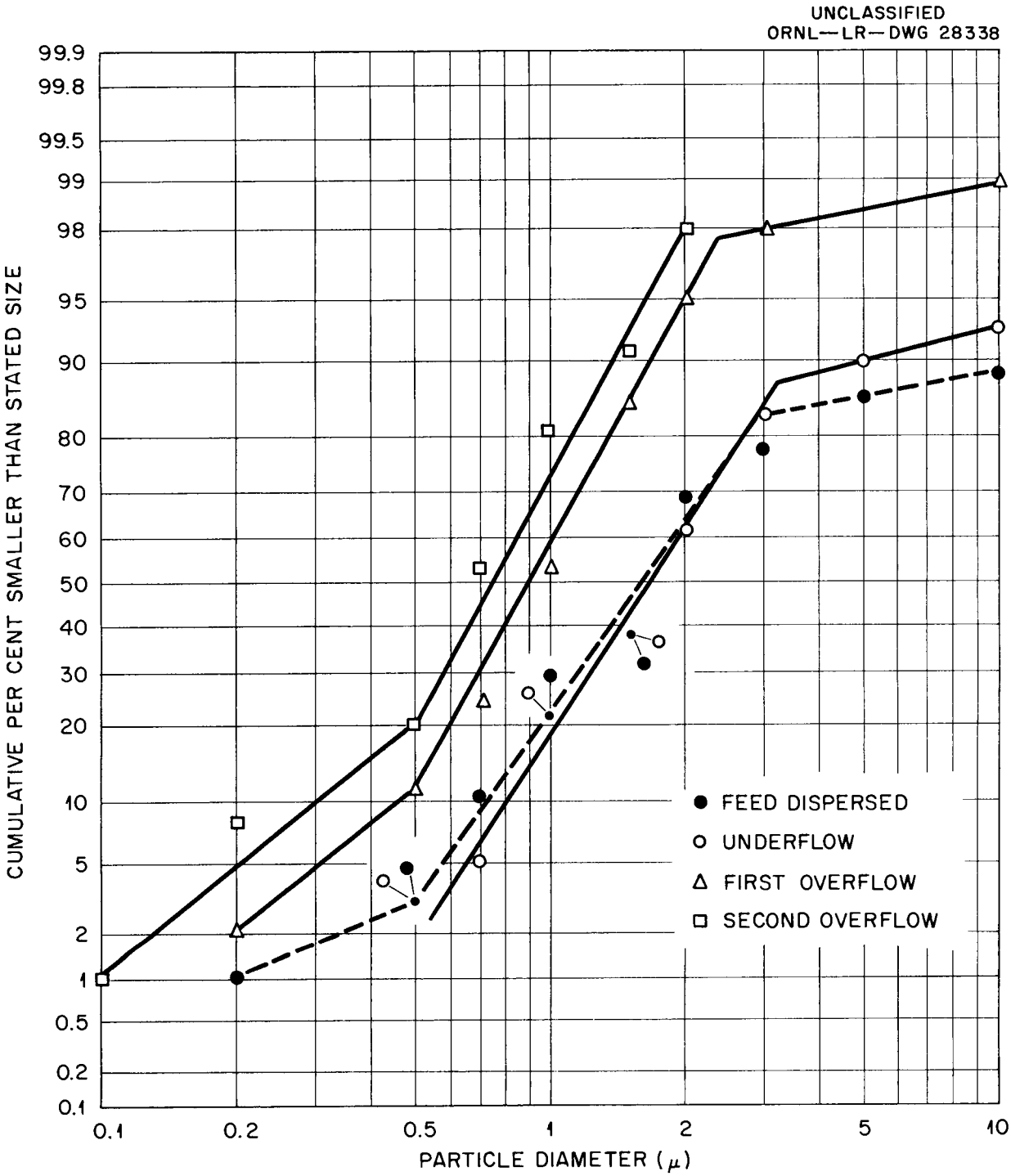

Fig. 7.9. Typical Particle-Size Distribution of Thoria Obtained from Hydroclone Test System.

across the hydroclone (feed to overflow) and with a feed concentration of 500 g of ThO_2 per liter of water; sodium silicate solution was added as a dispersing agent.

An overflow-material yield of 5–7 wt % of feed solids and an overflow ratio (ratio of overflow volume to feed volume) of 0.25–0.30 were observed during the tests. This corresponds to a yield of about 5 kg/hr of classified fine material. Although the percentage yield is quite low, it could be increased by:

1. operating hydroclones in series and recycling underflow to feed;
2. decreasing underflow-port diameter to about 0.09–0.10 in.;
3. operating with lower feed-to-overflow pressure drop (about 15–20 psi).

7.7 SLURRY RHEOLOGY

Figure 7.10 shows the vertical-tube viscometer system as the piping approached completion. The slurry feed tank is located on the 13-ft platform, and the 3.5- and the 9.0-ft-long viscometer tubes discharge at the 6.5-ft and the first-floor levels, respectively. The first phase of operation will employ the cooler-sampler system previously described,[17] wherein the hot slurry from the viscometer tubes passes through a cooling coil and needle valve and is collected at atmospheric pressure.

[17] R. B. Korsmeyer *et al.*, *HRP Quar. Prog. Rep. April 30, 1957*, ORNL-2331, p 68.

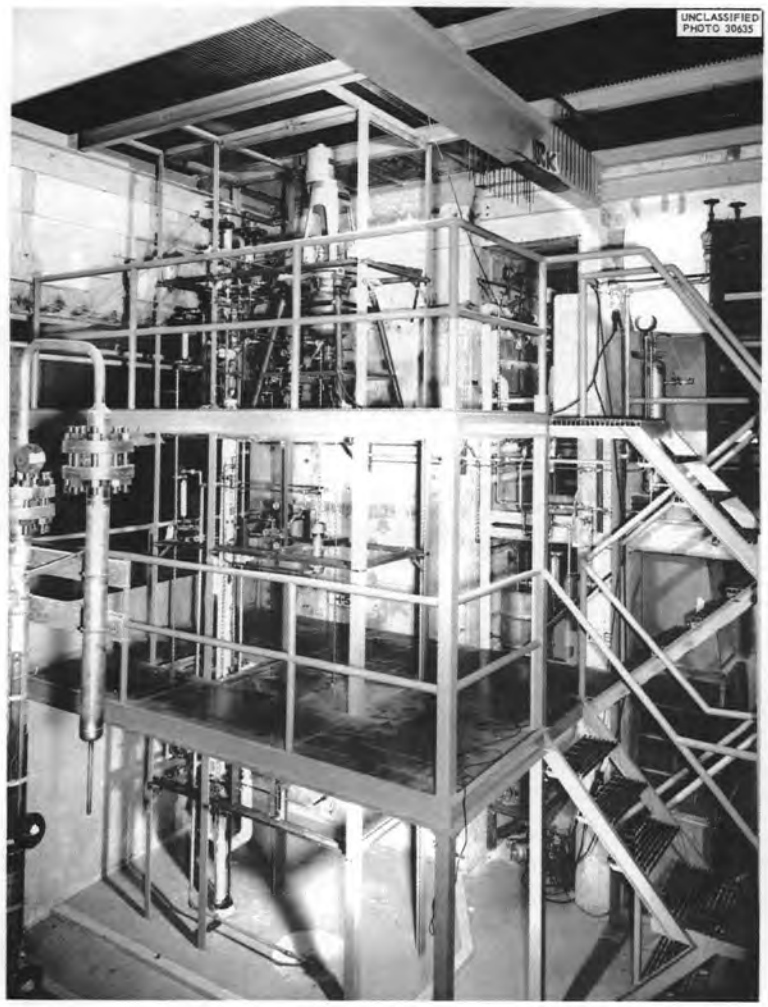

Fig. 7.10. Vertical-Tube-Viscometer System.

8. HRE-3 INSTRUMENTATION AND CONTROLS SYSTEM DESIGN

D. S. Toomb

J. R. Brown R. L. Moore

8.1 PLANT POWER DISTRIBUTION SYSTEM

A conceptual one-line diagram and associated bus-load survey for HRE-3 were made, indicating an expected plant electrical operating load of about 2200 kva, an installed load of about 3900 kva, and showing a generator with a capability of 20,000 kw delivering power to the transmission line at 13.8 kv. The plant distribution voltage was indicated as three phase, 460 v, derived from three 1250-kva forced-air-cooled 13.8 kv/460 v, three-phase transformers whose secondaries could be interconnected by bus ties in case of breaker or transformer failure. The suggested grouping of loads on buses was indicated, and d-c control supplies of 125 and 48 v were shown derived from batteries charged by motor-generator sets. The 48-v d-c supply would be used for process control, and the 125-v system would supply turbine auxiliaries, emergency lighting, and switchgear power.

8.2 CONCEPTUAL ELECTRICAL EQUIPMENT LAYOUT

The layout of an electrical equipment room to house the substation transformers, switchgear, motor starters, and small distribution transformers was also made for HRE-3, primarily to indicate the building space required if the major electrical equipment were to be located in one room. Free-standing modular motor-starting equipment was assumed in order to minimize the conduiting necessary and to provide maximum flexibility.

8.3 CONCEPTUAL CONTROL-ROOM LAYOUTS

Conceptual layouts of instrumentation and control panels in a main control room and an auxiliary instrument room were made for HRE-3. About 1500 ft^2 was shown to be necessary for all this equipment. The main control room would house only those instruments and controls necessary for startup and operation of the reactor, to minimize operation confusion. Data-collection instruments, auxiliary transducers, thermocouple patch panels, solenoid-valve cabinets, nuclear-instrument amplifiers and power supplies, etc., would be located in the auxiliary room, which should be in proximity to the main control room.

Part III

ENGINEERING DEVELOPMENT

R. N. Lyon

9. DEVELOPMENT OF FUEL-SYSTEM COMPONENTS

I. Spiewak

J. M. Baker
R. Blumberg
J. S. Culver
B. D. Draper
C. H. Gabbard
B. A. Hannaford
J. K. Hayes
E. C. Hise
P. P. Holz
C. G. Lawson
J. E. Mott
J. C. Moyers
I. K. Namba
H. R. Payne
H. C. Roller
D. L. Snyder

9.1 RECOMBINER DEVELOPMENT

9.1.1 High-Pressure Recombiner

Reconstruction of the high-pressure recombiner loop was completed, with Inconel being used in regions where stainless steel had previously suffered caustic cracking. The system operated at 600 psi for 500 hr, including 310 hr with the steam containing 5% of a stoichiometric mixture of hydrogen and oxygen and with a recombiner temperature of 500°C. The run was terminated as a result of failures in two nozzle attachment welds on the stainless steel boiler.

Specimens of titanium and zirconium alloys and of Croloy 16-1 were removed for metallographic examination. Two specimens of crystal-bar zirconium exposed to superheated vapor had disintegrated, although Zircaloy-2, similarly exposed, was visually intact. Titanium-jacketed thermocouple wells indicated the same temperature as stainless steel reference wells; phase transformations noted in previous specimens apparently cannot be attributed to local high temperatures generated by $Ti\text{-}H_2\text{-}O_2$ interaction.

Operation of the loop will be resumed after installation of an Inconel boiler. A 1500-psi natural-circulation recombiner is also being constructed for testing in this system.

9.1.2 Syracuse Contract

Syracuse University has confirmed the existence of explosive reactions, involving very weak pressure rises, in steam containing as little as 6% stoichiometric $H_2\text{-}O_2$. Experiments in a 1-in. tube showed that variations in the method of ignition did not affect the reaction limits or the developed pressures.

9.2 CENTRIFUGAL PUMPS

9.2.1 20-cfm Allis-Chalmers Blower

The 20-cfm canned-motor blower was operated for 428 hr with thorium oxide slurry used as the hydrostatic bearing fluid. However, the solids did not remain suspended and the concentration averaged only 2 g/liter, in spite of the fact that an external circulator was used in an attempt to sweep slurry out of stagnant areas. No measurable bearing wear was noted.

The blower loop is currently being prepared for a long-term run at elevated temperature and pressure.

9.2.2 4000-gpm Byron Jackson Pump

A series of runs was completed in which motor heat removal and fluid mixing were investigated for the Byron Jackson 4000-gpm pump. It was found that the external heat exchanger in which heat is transferred from motor-bearing water to cooling water is essential in preventing motor overheating. The mixing flow between motor fluid and pump fluid, shown in Fig. 9.1, was found to vary between 36 liters/hr at zero purge flow and 0.2 liter/hr at 136 liters/hr of purge. The high mixing rate at zero purge is attributed to recirculation around the outside edge of the thermal barrier and through the shaft seal. This recirculation is blocked at high purge rates when back pressure on the motor side increases. It is concluded from these tests that purge rates of 60 to 150 liters/hr would be adequate for this particular pump. However, no general conclusions can be drawn about purge requirements of this pump design because the size of the recirculation path is dependent on close tolerance fits.

The loop has been shut down for an extended period for conversion to slurry operation.

9.2.3 Reliance 6000-gpm Pump

The preliminary hydraulic and electrical design of the Reliance 6000-gpm pump, a prototype of the HRE-3 fuel pump, was completed. The motor will be a single-winding, reconnectable two-speed machine designed to operate at 3600 and 1800 rpm. The lower speed will be used to bring the system

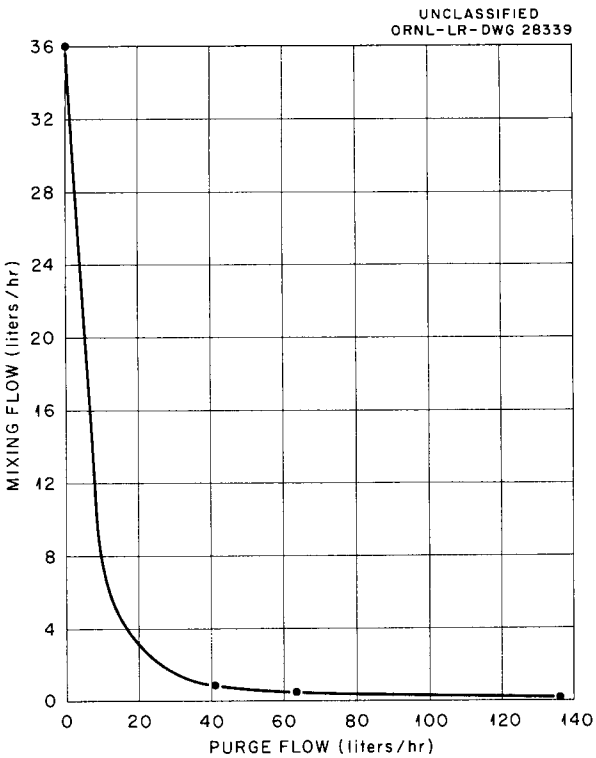

Fig. 9.1. Effect of Purge Rate on Mixing Rate in 4000-gpm Byran Jackson Pump.

up to temperature and pressure at reduced flow. Pump and motor characteristics are shown in Fig. 9.2 and Table 9.1.

The proposed mixed-flow impeller should be operated between 5000 and 6000 gpm because the efficiency drops off rapidly outside these limits, as shown in Fig. 9.2. The decrease in efficiency is caused by turbulence and recirculation within the impeller channels, which would probably result in reduced pump life.

Three insulation-test stators, which will be irradiated by ORNL, have been delivered by Reliance Electric & Engineering Co. They were built with the proposed insulation system of the 6000-gpm pump, as well as that of the HRT pumps. The first was installed in the HRT, and the other two will be irradiated in a Co^{60} source. Measurements will be made of electrical resistance, breakdown voltage, and hydrogen buildup vs radiation dosage.

9.3 OXYGEN COMPRESSORS

The Pressure Products Industries diaphragm compressor has continued its satisfactory service on the HRT mockup.

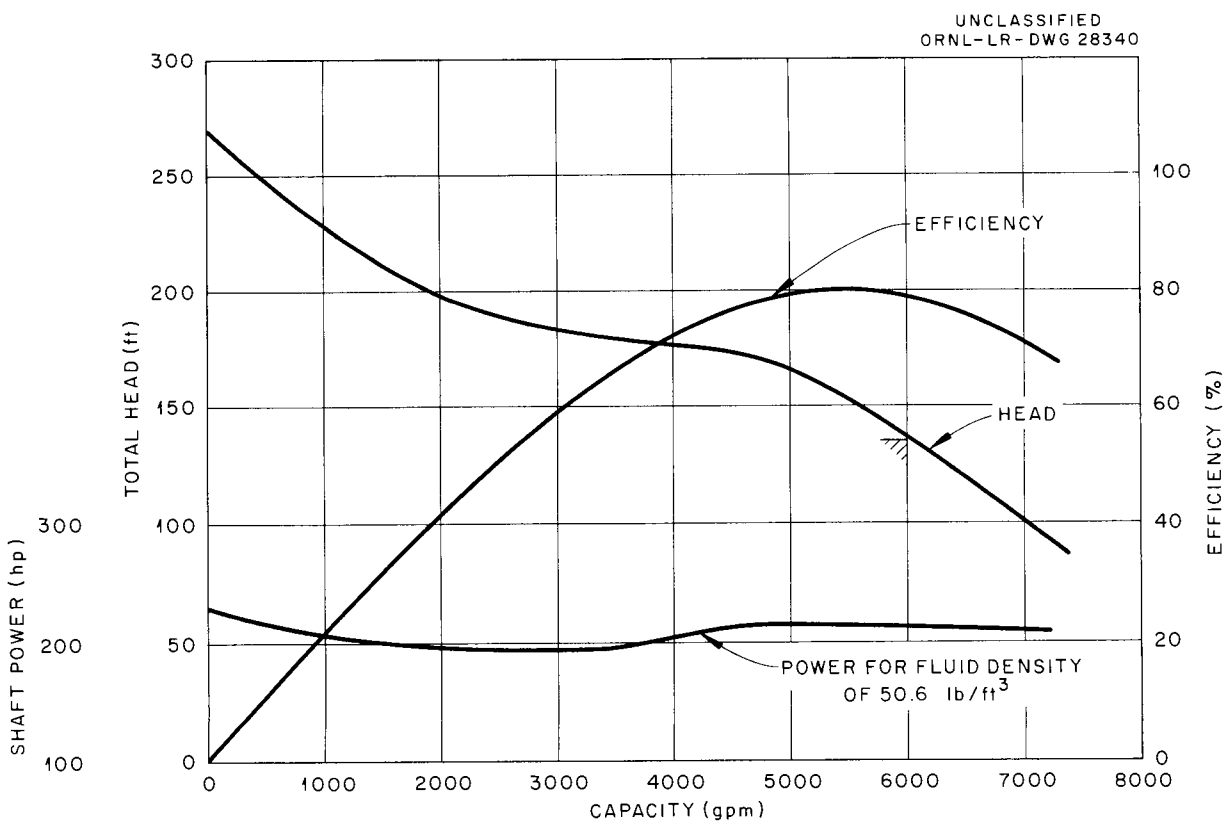

Fig. 9.2. Characteristics of 6000-gpm Pump.

Table 9.1. Predicted Performance of 6000-gpm-Pump Motor

	Two-Pole Performance	Four-Pole Performance
Horsepower	250	31.3
Efficiency, %	80	76
Power factor, %	86.8	61.7
Speed at full load, rpm	3452	1762
Slip, %	4.08	2.1
Starting torque (% of full load)	76	178
Breakdown (max) torque, %	214	424
Full-load current, amp	351	61
Starting current, amp	1367	344

An order has been placed with Pressure Products Industries to construct a remotely driven, three-stage, diaphragm compressor capable of delivering 2 scfm of contaminated oxygen from 15 to 2500 psia. Delivery is expected in July 1958.

9.4 FUEL FEED PUMPS

The Roth turbine pump, which had operated successfully with water, failed very quickly in fuel solution as a result of severe impeller corrosion in two instances. It was found that the manufacturer had supplied a type 316 stainless steel impeller inadvertently nitrided and a type 17-4 PH impeller improperly heat treated. Other test impellers are on order.

Testing of the Stellite-piston pump was terminated after 757 hr of fuel service, owing to gross wear of the Stellite No. 3 cylinder and the Haynes alloy 25 rings.[1] This concept has been eliminated from consideration.

A diaphragm head containing screen tubes of 20-μ Poroloy[2] has operated satisfactorily on the multipump loop for 476 hr. These filters should provide complete protection of the diaphragm against dirt.

A double-diaphragm feed pump, shown in Fig. 9.3, was designed and built and was operated for 500 hr on the multipump loop. The assembly consists essentially of two "standard" heads with a common solution header. Use of multiple-head feed pumps of this type in future reactors would represent a very simple extrapolation of HRT technology. The test pump supplied 2 gpm at 2000 psi. Its operation was interrupted by a screen plug-weld failure, attributed to poor weld fitup and material.

9.5 DUMP-VALVE TRIM

Responsibility for operation of the valve test loop was transferred from the Instrument Section to the Component Development Section in October 1957. Since then, five valve trims have been tested: a palladium plug, which failed in less than 10 dumps because of mechanical misalignment; tungsten carbide flame-coated on type 347 stainless steel, which had excessive leakage after 450 dumps; two Allegheny Ludlum AM-355 stainless steel plugs, which were deeply eroded after 20 to 25 dumps (the alloy may not have received proper heat treatment); a valve with a gold ring seal, which has retained its integrity after 2000 dumps. A photograph of the gold trim is shown in Fig. 9.4. This extremely promising valve will be subjected to further tests.

The future program will consist mainly of long-term tests of the more promising valve materials.

9.6 TITANIUM PROGRAM

Crane Company completed the fabrication of test pieces of titanium-lined 3½-in. and 20-in. carbon-steel pipe. However, welds in both pieces failed during hydrostatic testing at 1100 psi and 200 psi, respectively. Crane is attempting repairs.

Chase Brass & Copper Company has extruded a second length of 3½-in. A-110AT titanium pipe, which is believed to be satisfactory for use in a boiling uranyl sulfate pressurizer. The interior of this section must be bored before it can be used.

Of the four A-110AT caps ordered to mate with this pipe, only one has been fabricated successfully; the others are being remade.

An all-titanium letdown heat exchanger was constructed for the HRT mockup from A-55 pipe

[1] E. C. Hise, *Stellite Piston Pump*, ORNL CF-57-12-75 (Dec. 16, 1957).

[2] I. Spiewak *et al.*, *HRP Quar. Prog. Rep. Oct. 31, 1957*, ORNL-2432, p 52.

and fittings. Recently developed titanium–stainless steel ring-joint transition flanges[3] were used to join the exchanger into the system.

9.7 FLANGE TEST PROGRAM

The titanium-to-stainless-steel transition joint,[2] after passing four series of thermal cycles (100 to 635°F) with ferruled bolts, was subjected to a series of cycles with standard bolts. No difference in behavior was observed.

Additional tests of type 347 stainless steel ring-joint flanges without bolt ferrules confirmed that leakage was not affected by elimination of the ferrules. However, bolt stresses are not known accurately at the present time owing to malfunction of the gaging equipment. This difficulty is being corrected.

[3]B. D. Draper and H. C. Roller, *Design and Development of a 1/2-inch Titanium to Stainless Flange*, ORNL CF-57-11-140 (Nov. 27, 1957).

9.7.1 Bolting-Material Program

Several materials are being studied as possible bolting materials suitable for use in contact with UO_2SO_4 fuel solution systems. The requirements

UNCLASSIFIED
T-11887

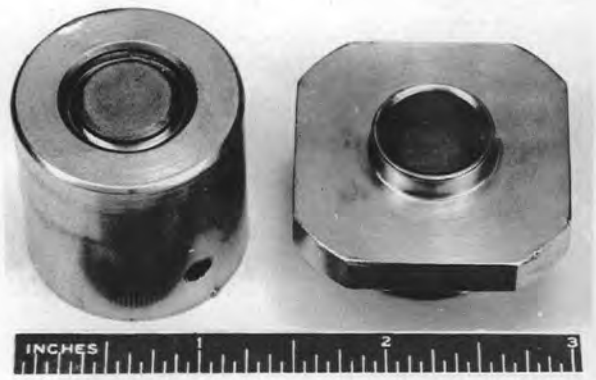

G-4 AFTER TEST

Fig. 9.4. Gold Valve Trim After 2000 Dumps.

UNCLASSIFIED
ORNL-LR-DWG 28341

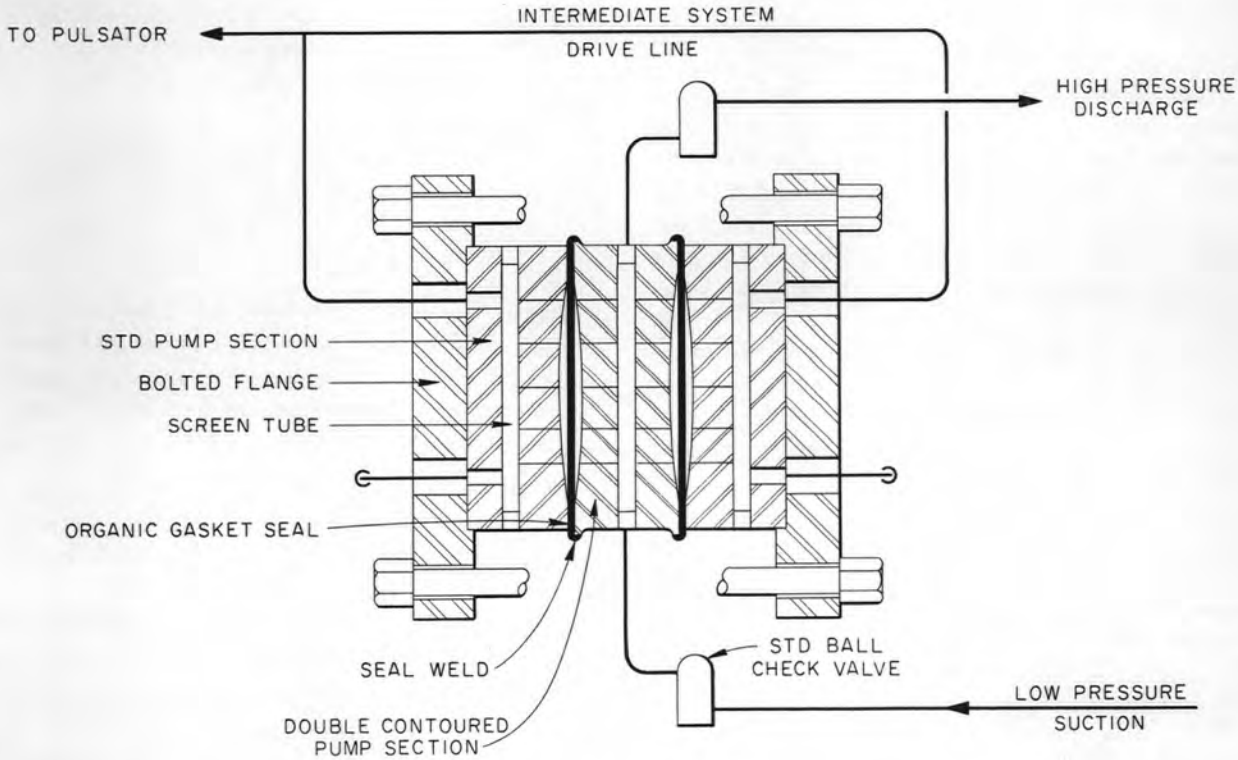

Fig. 9.3. Double-Diaphragm Pump.

of such a material are high strength, corrosion resistance, nongalling characteristics, and preferably a coefficient of expansion close to that of type 347 stainless steel.

Earlier work indicated that Armco 17-4 PH had most of the required properties, except for a low coefficient of expansion. However, recent tests in which stressed specimens were suspended in the liquid or in the vapor above UO_2SO_4 solution at 250°C showed severe cracking.

Presently being investigated are Allegheny Ludlum AM-355, Universal-Cyclops 19-9 DL, and Timken 16-25-6 stainless steels. Both stressed and coupon samples are being tested to observe the corrosion behavior of these materials.

In addition, solution corrosion tests are being run on a work-hardened 18-8 stainless steel thread insert, which is commercially available.

9.8 THERMAL-CYCLE FACILITY

The thermal-cycle facility, which is designed to subject large equipment items to cyclic testing between 380 and 580°F, has been constructed and operated. A schematic diagram is shown in Fig. 9.5. The cycling operation is regulated by a steam throttling valve which controls the pressure, and consequently the temperature, of the saturated steam in the test system. The Besler boiler is operated at a manually adjusted constant steaming

UNCLASSIFIED
ORNL—LR—DWG 28342

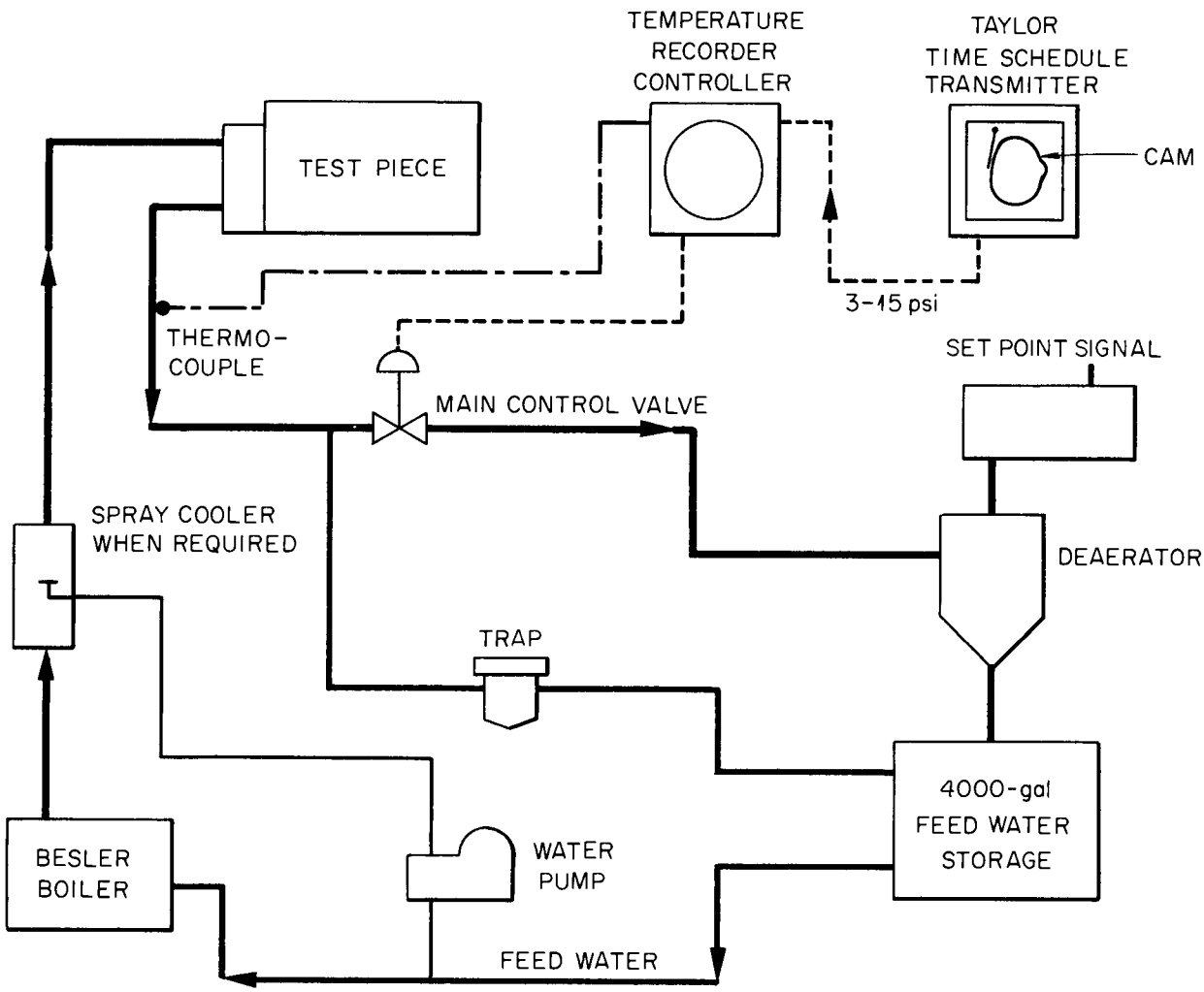

Fig. 9.5. Thermal-Cycle Facility.

rate, the magnitude of which is determined by the heat capacity of the test piece and the desired heating rate. Water may be mixed with the steam during the cooling cycle if rapid cooling is required.

A large autoclave has been used as a test piece in preliminary runs and has been subjected to 19 thermal cycles to date. The desired cycle conforms to that proposed for the HRT spare heat exchanger,[4] which is shown in Fig. 9.6; shown also are typical experimental cycles, which fall within specification limits. Minor adjustments in control instrumentation have produced significant improvement in the ability to control the cycle.

9.9 HEAT EXCHANGERS

9.9.1 Tube-Joint Test

Two of five tube bundles were removed after 2700 hr of thermal cycling in an environment containing 50 ppm Cl^- and 10–25 ppm O_2 in 200°C boiler water. There was no visible evidence of cracking in the type 347 stainless steel tubes, which are joined to a clad carbon-steel tube sheet. Testing of the remaining three units is continuing.

9.9.2 Heat Exchanger Test Facility[5]

Contract negotiations for fabrication of heat exchangers for the heat exchanger test facility are nearly complete. One conventional U-tube unit will heat fuel solution from 250 to 300°C, and four experimental tube bundles will cool the solution by generating steam. The four test pieces are mounted in a common steam system. Delivery of this equipment is expected in the fall of 1958.

9.10 HRE-3 PRESSURIZER DEVELOPMENT

9.10.1 Titanium Equipment for Containing Boiling UO_2SO_4 Solutions

A long-term test to determine the effect of boiling HRT fuel solution upon a titanium container has continued for more than 1200 hr at 1500 psi and 313°C. No deleterious effects have been observed to date.

9.10.2 Heating and Cooling of Steam-Oxygen Mixtures

The stainless steel natural-circulation loop built to determine heating and condensation coefficients of steam-oxygen mixtures and to obtain vapor corrosion information was placed in operation. The system pressure was maintained at 1500 psi, while the partial pressure of oxygen was increased gradually from 0 to 385 psi. The heating and cooling data obtained under the above conditions are being analyzed. Additional measurements will be taken at higher oxygen partial pressures.

[4]HRP Specification 1113a.

[5]I. Spiewak *et al.*, *HRP Quar. Prog. Rep. July 31, 1957*, ORNL-2379, p 49.

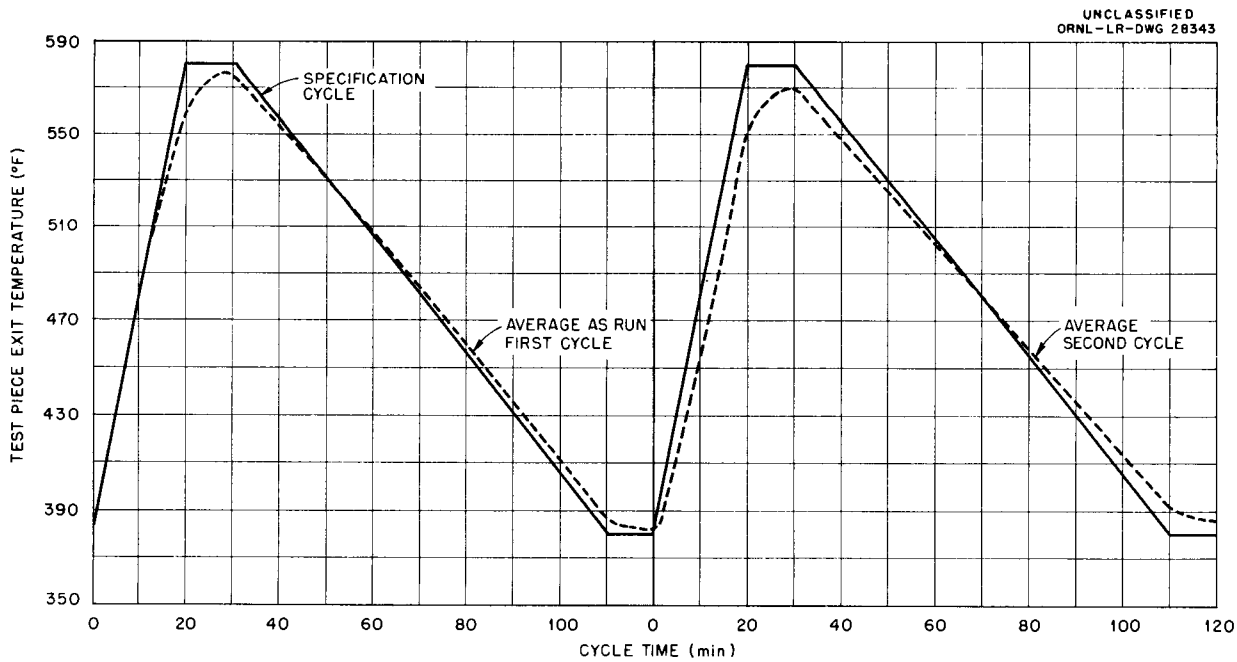

Fig. 9.6. Typical Thermal Cycles of Test Autoclave.

9.10.3 Gas Dissolving Efficiency of Eductor

In the proposed HRE-3 gas pressurizer design, a jet eductor is used to contact the pressurizer vapor with circulating fuel solution to prevent deuterium buildup in the pressurizer. An eductor manufactured by Penberthy Injector Co., for use in the 300A pump loop,[6] was tested at atmospheric pressure while contacting water and oxygen. Results are shown in Fig. 9.7. Although a contacting efficiency of 60% was obtained at the design flow of 25 gpm of liquid (which pumped about 1.5 cfm of gas), the efficiency fell off rapidly at lower flow rates.

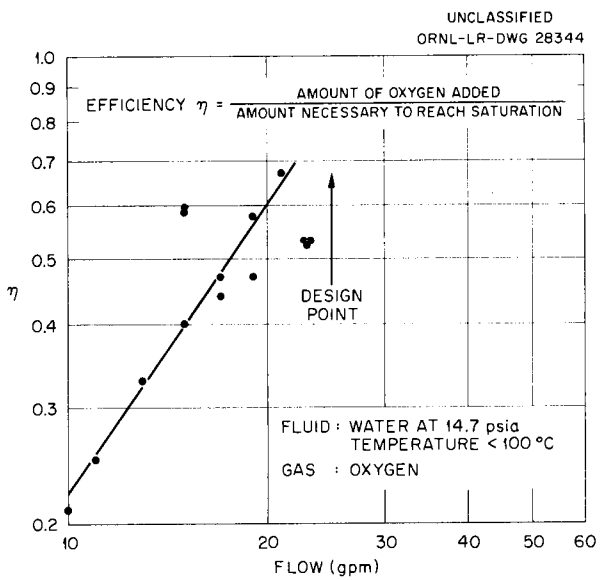

Fig. 9.7. Gas Dissolving Efficiency of Jet vs Flow Rate.

9.11 HEAT TRANSFER FROM HRE-3 CORE WALL TO CORE SOLUTION

Measurements to determine the heat transfer rates from the HRE-3 core wall to the circulating fuel solution are being made. Preliminary measurements on a 4-ft-dia core, at a point located on an azimuth 150 deg from the concentric inlet-outlet, with water at room temperature indicated a forced-convection heat transfer coefficient in excess of 2000 Btu/hr/ft^2/°F at a flow of 6000 gpm. The heat transfer coefficient varied with the velocity to the 0.75 power over the flow rate range of 1500 to 6000 gpm. Tests are being conducted to determine the forced-convection heat transfer coefficient as a function of position on the core wall. The effect of surface irregularities introduced by the measuring equipment will also be examined.

If HRE-3 surface coefficients were actually to be 2000 or above, the core-tank surface would be very close to fluid temperature.

9.12 DEVELOPMENT OF SLURRY COMPONENTS

9.12.1 300A Slurry Loop

Fabrication of the main piping for the 300A slurry loop was completed, and completion of auxiliary piping, electrical work, and instrumentation is expected shortly.

A full-scale glass model of the loop was operated with water and with thorium oxide slurry, primarily to check the operation of the pressurizer. Flow studies with water and dye injection showed that, with a net downward flow in the pressurizer, there were no undesirable vortices or stagnant regions. With no flow through the pressurizer, transient vortices were observed extending up about 6 in. from the T-connection between the pressurizer and the loop.

Operation of the system with slurry prepared from 1600°C-fired ThO_2 at a concentration of 1000 g of Th per kg of H_2O revealed that downward flow was necessary to prevent stagnation and sedimentation in the pressurizer.

The only problem uncovered in the flow tests was the carry-under of small gas bubbles, which may affect pump operation adversely, at downward flows greater than 0.13 fps.

9.12.2 Feed Pumps

The problem of feeding high-concentration ThO_2 slurry is being approached by two methods. A diaphragm head having a contour on the intermediate side and a recessed chamber on the pumping side is being constructed. It is so arranged that the diaphragm will operate only from the intermediate contour to center, thus avoiding the possibility of trapping slurry particles between the diaphragm and contour face and thus deforming or overstressing the diaphragm. A remote-leg test facility is being constructed, in which the check valves are mounted at some distance below a standard head and connected thereto by a glass

[6] I. Spiewak *et al.*, *HRP Quar. Prog. Rep. Oct. 31, 1957*, ORNL-2432, p 51.

vertical leg. It will be used to determine whether it is possible to maintain a water-slurry interface in the oscillating vertical column and to pump slurry through the check valves while the diaphragm operates in water.

A slurry multipump facility, consisting of a storage tank, a circulating pump, and a low-pressure piping loop with twelve flanged entries, has been designed. It is intended to provide a well-agitated, constant-concentration supply of slurry to the suction of test feed pumps and a receiver for the discharge after it has been let down to low pressure.

9.12.3 Slurry Check-Valve Material Test

The test facility for evaluation of slurry check-valve materials was charged with a 1600°C-fired slurry containing about 200 g of Th per liter. This slurry, however, contained an excessive amount of solids larger than 10 μ. Check-valve seats of type 347 stainless steel failed in 17 hr; Stellite No. 1, in 100 hr; and the Stellite Star J balls suffered severe uniform weight loss. Balls and seats of Kennametal K501 (platinum-bonded tungsten carbide) appeared to be in excellent condition after 160 hr. Testing was suspended for loop revisions aimed at resolving problems of slurry settling.

The revised system was started up with Al_2O_3 valve trim under test. Other materials to be tested are boron carbide, 17-4 PH stainless steel, titanium, three grades of tungsten carbide, and two grades of titanium carbide

9.12.4 Separation of Water from ThO_2 Slurry

Several approaches to the problem of supplying purge water for slurry systems are being investigated as alternates to the obvious evaporation method.

A small sintered stainless steel filter has been constructed and will be tested as soon as a suitable system is available.

A 57-in.-long, 12-in.-dia horizontal settling tank has been constructed for testing in the glass model of the 300A loop. Twenty-five gallons per minute of slurry will pass through this section, and it is hoped that 1 gpm of clear water can be withdrawn from the top of the exit end.

A continuous centrifuge will also be tested.

9.12.5 30-in. Low-Pressure Model of HRE-3 Blanket

Design and fabrication of a 30-in. HRE-3 blanket model were begun. Figure 9.8 shows the layout of this vessel. Slurry enters at a nominal 300 gpm through a jet eductor, which increases the apparent throughput, and flows upward between the shroud and the core vessel. Slurry leaves the vessel at either the top or the bottom.

Discussions with vendors indicate that approximately 2.5 times the input flow should circulate through the shroud.

Subassembly tests of the jet and the shroud are planned so that spacing in the final assembly can be optimized. The proper angle for the bottom cone will also be determined experimentally.

9.12.6 Slurry Dump Tanks and Evaporators

A slurry dump-tank–evaporator model was designed and is being built. The model is a vertical 6-in.-dia glass pipe 6 ft long containing a 2-in.-dia 4-ft-long stainless steel draft tube with holes drilled in the side to permit cross flow of slurry at low-level operation. A steam coil for heating and boiling the slurry is located within the bottom 18 in. of the draft tube. A condenser is located in the vapor space. The equipment will be used to determine (1) the feasibility of the design concept for a slurry dump tank, (2) the foaming tendency, if any, of slurry steam mixtures, and (3) under what heat flux condition, if any, a submerged steam-heated tube will cause slurry dehydration.

UNCLASSIFIED
ORNL-LR-DWG 28345

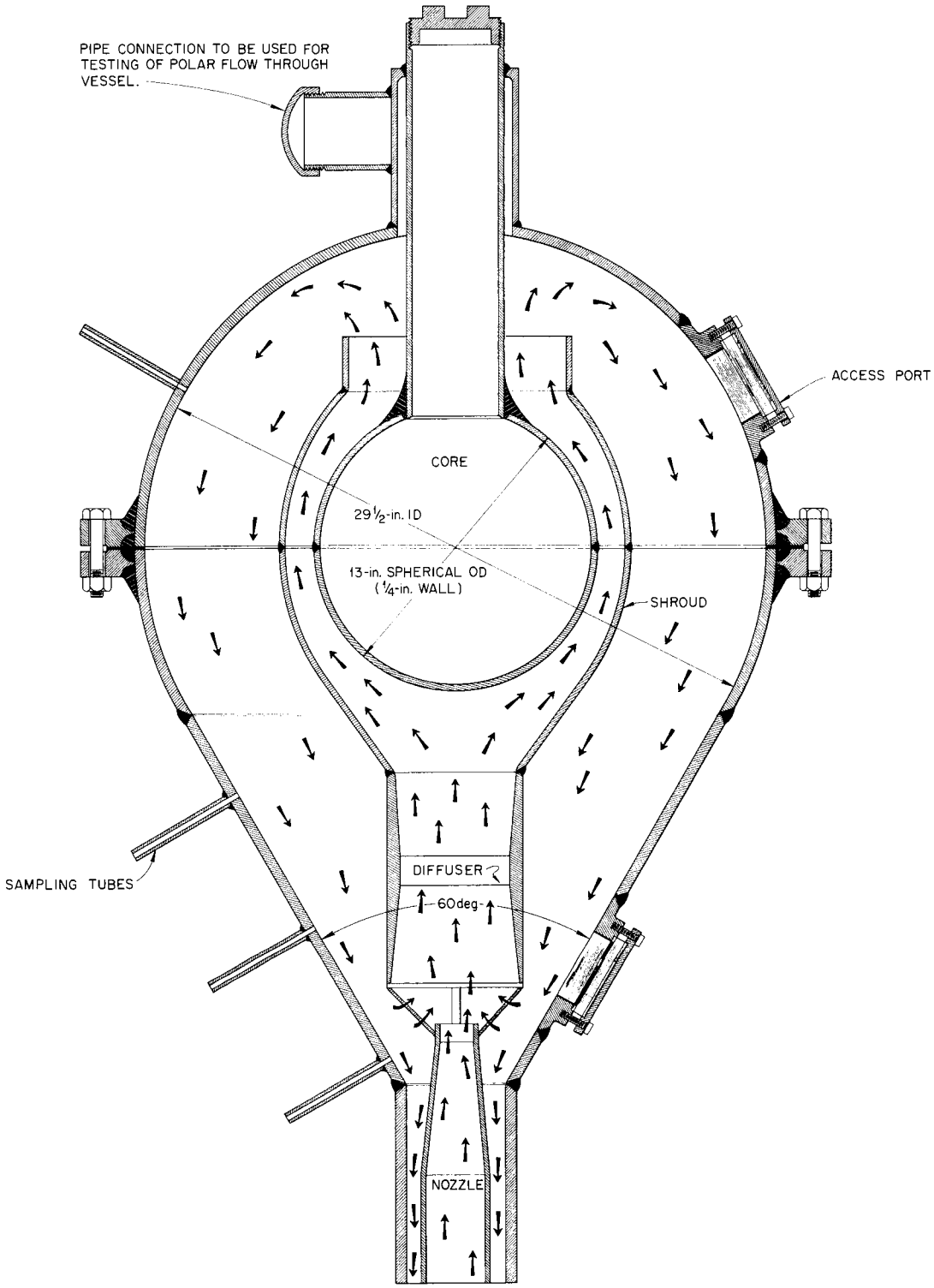

Fig. 9.8. 30-in. Low-Pressure Model of HRE-3 Blanket.

10. DEVELOPMENT OF REACTOR SLURRY SYSTEMS

R. B. Korsmeyer F. N. Peebles

D. G. Davis V. L. Kenyon A. N. Smith
R. B. Gallaher L. F. Parsly C. F. VandenBulck[1]
C. H. Gibson M. Richardson R. P. Wichner[2]

10.1 CIRCULATING-SLURRY BEHAVIOR

Slurry and water were circulated in S, T, and 200A loops for over 4103 hr during the quarter. These runs are summarized in Table 10.1.

10.1.1 200-gpm-Loop Operation

Run 200A-14, conducted in order to determine the degradation characteristics of 1600°C-fired oxide, was terminated after 3787 hr at 300°C and 2000 psig. During the last 1000 hr of circulation the mean particle size was 1.8 μ, as compared with 2.5 μ during the first 1500 hr. However, the nitrogen adsorption surface area was constant at 1.6 m^2/g for the entire run. Spheroidal particles observed earlier disappeared with continued circulation. The iron-to-thorium ratio increased linearly during the entire run according to the equation $Fe/Th = 0.0024t + 0.1$, where t is the time in hours, Fe/Th is grams of iron per kilogram of thorium, and the constant term represents the iron contamination in the oxide as charged.

When the run was terminated, the slurry was easily removed from the loop; no cakes or films were found. The impeller, which lost 80 g out of a total of 2073 g, had no areas of extreme wear (Figs. 10.1 and 10.2). However, the scroll liner was heavily eroded near the seal rings (Fig. 10.3). The upstream side of the 1⅛-in. orifice had a hammered appearance (Fig. 10.4), but there was only negligible attack on the downstream face. The 1½-in. orifice showed similar attack except to a lesser extent.

The lower Graphitar radial bearing was worn approximately 0.038 in. uniformly along its length (not a bell-shaped worn area as in run 200A-11). The upper Graphitar radial bearing was worn 0.012 in. Very little wear, less than 0.002 in., was observed on the Graphitar thrust runner. Figure 10.5 shows the good condition of the cast Stellite-19 Kingsbury shoe. Both the cast Stellite-19 journals were damaged to some extent (Fig. 10.6). The upper bearing appeared to have run dry at some time during the run and had small cracks in a band around the journal. At the corresponding location the upper Graphitar bearing had failed. The lower cast Stellite-19 journal showed oxidation attack at the lower end, apparently because it operated at approximately 180°C. The rotor was out of balance rather badly (static imbalance = 12 g/in., tolerance <g/in.) at the end of the run, which probably contributed to the excessive bearing wear.

10.1.2 100-gpm-Pump Thrust Bearing

A thrust bearing designed for the Westinghouse 100A pump operated satisfactorily for 573 hr on water in the S-loop pump but failed during a test with 1200°C-fired spheres of thoria (run S-109). After a modification in operating techniques, a 384-hr test with slurry (run S-110) was successful, and another run is now in progress (run S-111).

10.1.3 100-gpm-Loop Operation

Thoria spheres prepared by circulating 800°C-fired oxide in the 200A loop (run 200A-12) were refired at 1200°C for 6 hr, mulled to break up the light clinker, and loaded into S loop (run S-109) in order to determine the particle integrity and circulation characteristics of this material. The slurry settled rapidly into a bed which was extremely difficult to resuspend and was difficult to load and sample. Pump failure terminated the run 7.8 hr after the slurry was charged into the loop. All evidence indicated that most of the slurry did not circulate in the loop. A small amount of cake formed in the vanes of the impeller.

[1]On loan from Union Carbide Nuclear Co., New York office.

[2]Attending Oak Ridge School of Reactor Technology.

Table 10.1. High-Temperature Slurry Circulation – Run Summaries

	Run No.										
	200A-14	S-107	S-108	S-109	S-110	S-111	T-93	T-94	T-95	T-96	T-97
Test dates	7/18 to 12/27	10/2 to 10/14	10/25 to 10/31	11/13	11/29 to 12/16	1/6 to I*	9/10 to 10/23	11/7 to 11/14	12/4 to 12/18	12/23 to 1/7	1/14 to I*
Running time, hr	3787	288	133	440 on water; 7.8 on slurry	384	I	976	167	331	342	I
Objective	To determine the circulation and degradation characteristics of 1600°C-fired ThO_2	To determine rate of disappearance of solids from dilute-slurry circulating stream	To test new thrust-bearing assembly on water	To determine the particle integrity and circulation characteristics of 1200°C-fired spheres	To determine the effect of MoO_3 on caking and sphere-forming tendencies of 800°C-fired ThO_2 (rerun of T-94)	To determine the effect of uranium on caking and sphere-forming tendencies of 800°C-fired ThO_2 (rerun of T-95)	To determine the circulation characteristics of sulfated slurry containing uranium and molybdenum	To determine the effect of MoO_3 on caking and sphere-forming tendencies of 800°C-fired ThO_2	To determine the effect of uranium on caking and sphere-forming tendencies of 800°C-fired ThO_2	To determine the effect of molybdenum and uranium on caking and sphere-forming tendencies of 800°C-fired ThO_2	To determine the effect of molybdenum and uranium on caking and sphere-forming tendencies of 800°C-fired ThO_2 at 1000 g Th/kg H_2O
Charge											
ThO_2, kg	30 (LO-22, refired)	Incremental amounts of LO-7		6.6 (LO-20)	6.8 (LO-23)	4.05 (LO-23)	15.4 (LO-23)	7.3 (LO-23)	7.1 (LO-23)	6.0 (LO-23)	12.4 (LO-23)
Water, kg	71	12.5	12.5	12	12	12.1	14.5	15.3	15.3	15.5	14.8
Additives	75 liters O_2	25 liters O_2	25 liters O_2	25 liters O_2	43 g MoO_3 25 liters O_2	29 g $UO_3 \cdot H_2O$ 25 liters O_2	86 g $Th(SO_4)_2$ 197 g $UO_3 \cdot H_2O$ 97 g MoO_3 25 liters O_2	45 g MoO_3 25 liters O_2	45 g $UO_3 \cdot H_2O$ 25 liters O_2	39 g $UO_3 \cdot H_2O$ 39 g MoO_3	76 g $UO_3 \cdot H_2O$ 76 g MoO_3
Temperature, °C	300	250	255	290	290	290	290	290	290	290	290
Pressure, psig	2000	1600	1600	1600	1600	1600	1600	1600	1600	1600	1600
Average circulating concentration, g of Th per kg of H_2O	585			149	679	I	1132	725	720	685	I
Reason for termination	Vibrations in pump; shut down before failure	Scheduled shutdown	Inspection of thrust bearing	Noise in the pump; rear thrust bearing failed	Scheduled shutdown	I	Scheduled shutdown	Pump noisy; hydraulic unbalance due to pressurizer-baffles failure	Scheduled shutdown	Scheduled shutdown	I
Equilibrium mean particle size, μ	1.8			17	0.4 (no spheres)	I (no spheres)	0.7 (no spheres)	0.4 (no spheres)	0.4 (no spheres)	0.7 (no spheres)	I
Cake location	No cakes or films	No cakes or films		Small cake in impeller vanes; none in loop	No cakes or films	I	No cakes or films	No cakes or films	No cakes or films	No cakes or films	I
Fe buildup in slurry, g	226	Negligible		8.15	25.4	I	71.6	28.7	36.6	17.07	I
Ni buildup in slurry, g	33.8	Negligible		0.58	4.68	I	12.35	4.80	5.45	2.52	I
Cr buildup in slurry, g	12.9	Negligible		0.31	2.12	I	5.80	7.71	6.44	2.94	I
Impeller weight loss, g	80	Negligible	Not examined	2.5	14.3	I	35.0	24.0	19	25.5	I
Orifice-plate weight loss, g	3.7385 ($1\frac{1}{8}$ in.) 1.3742 ($1\frac{1}{2}$ in.)	0.1261	Not examined	Negligible	1.4707	I	1.0724	0.2948	2.0727	0.8230	I

*Incomplete (still running).

Seven runs were made in the 100A loops this quarter to determine the effect of additives on the caking and sphere-forming tendencies of 800°C-fired thorium oxide. For these tests a batch of oxide, LO-23, was chosen which had formed spheres in all previous runs (runs 200A-13, T-91, and T-92) in which there were no additives.

Run T-93 was loaded for a concentration of 1000 g of Th per kg of H_2O, along with 2500 ppm of sulfate, 1 wt % U, and 1.16 mole % MoO_3 (based on the thorium oxide) and was operated for 976 hr. No spheres or cakes were found. In two tests at a concentration of 500 g of Th per kg of H_2O, along with 1.16 mole % MoO_3

UNCLASSIFIED
PHOTO 30503

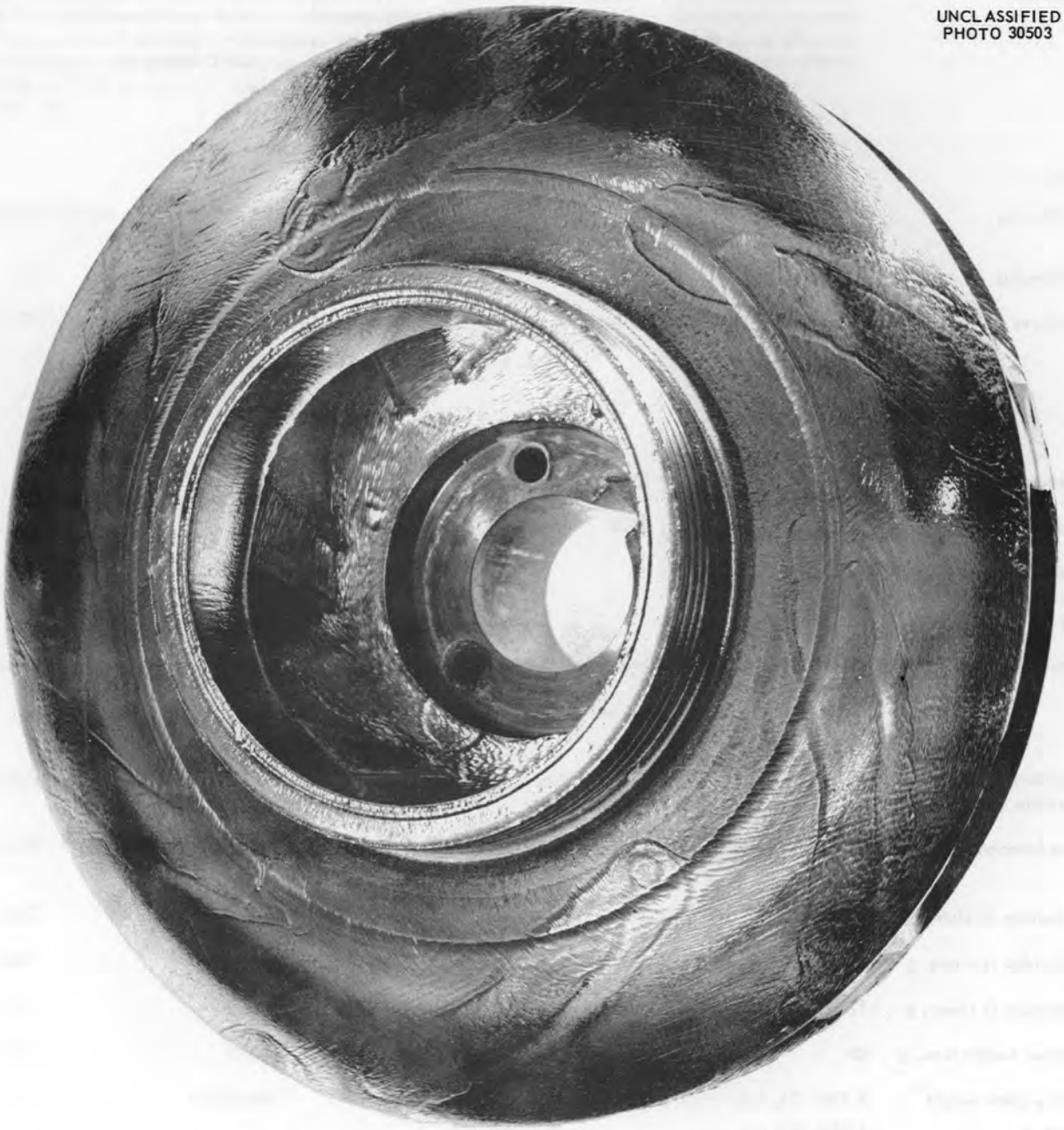

Fig. 10.1. Pump Impeller After Run 200A-14 (Front).

(runs T-94 and S-110), no spheres or cakes were observed. In two tests at a concentration of 500 g of Th per kg of H_2O, but with ½ wt % U (run T-95 and S-111), no spheres were observed, and no cake was found in T-95. Run S-111 is still in progress. Next, the two additives were combined and tested: first, at a concentration of 500 g of Th per kg of H_2O (run T-96), and then at a concentration of 1000 g of Th per kg of H_2O (run T-97). No spheres or cakes were formed during run T-96; run T-97 is still in progress. Apparently the presence of ½ wt % of uranium as $UO_3 \cdot H_2O$, 1.16 mole % of MoO_3, or 2500 ppm of sulfate as $Th(SO_4)_2$, singly or combined, is sufficient to prevent the formation of spheres and cakes in a slurry which has been observed to form cakes and spheres with no additives.

10.1.4 Laminar Flow at Elevated Temperatures

During the determination of the rheological properties of the slurry in run T-93[3] the preheater

[3] R. B. Korsmeyer *et al.*, *HRP Quar. Prog. Rep. Oct. 31, 1957*, ORNL-2432, p 57–58.

UNCLASSIFIED
PHOTO 30502

Fig. 10.2. Pump Impeller After Run 200A-14 (Back).

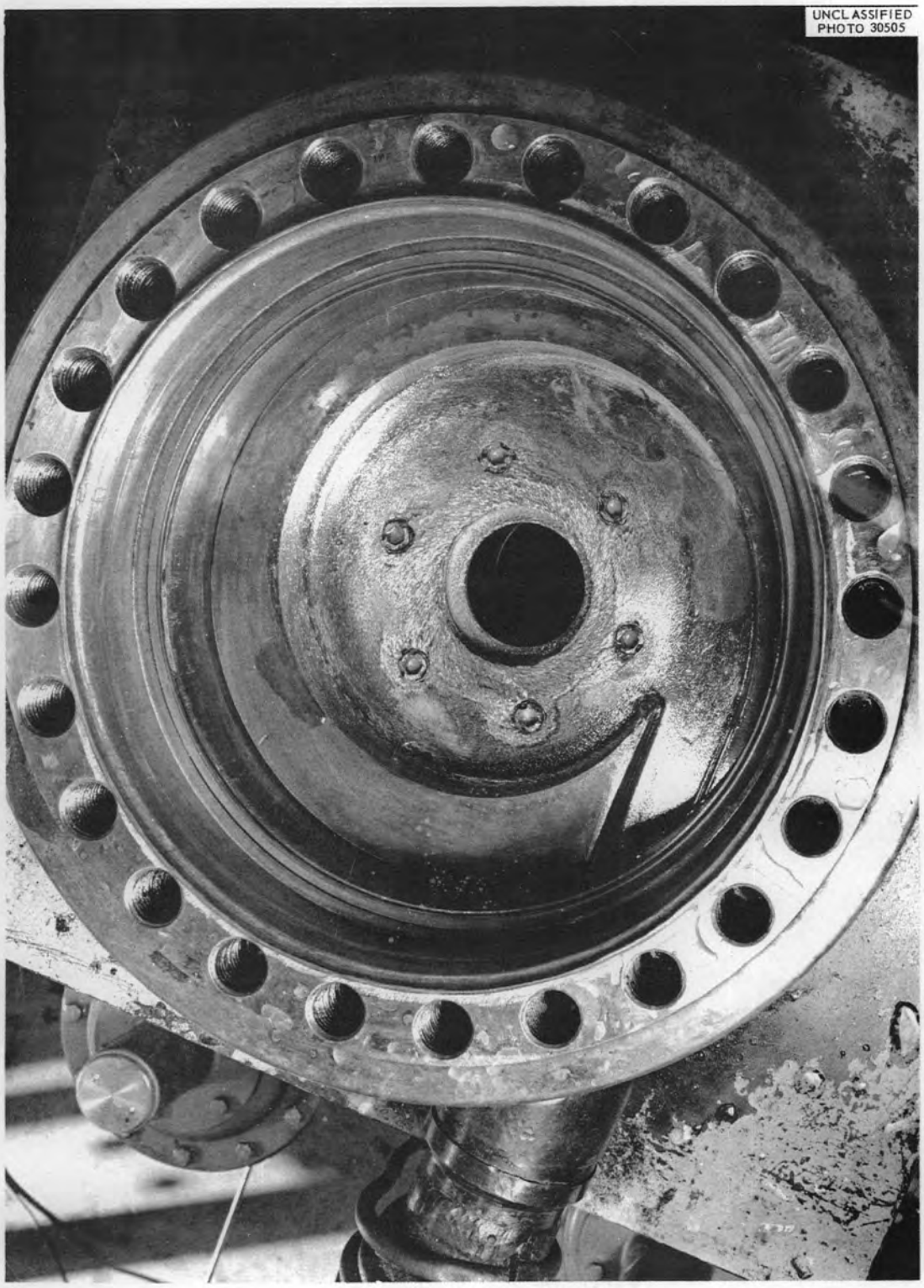

Fig. 10.3. Pump Scroll Liner After Run 200A-14.

of the capillary sampler-viscometer[4] proved inadequate. A new preheater was constructed, allowing operation of the viscometer at temperatures up to 300°C. The viscometer was recalibrated with water, and determination of the rheological properties of the slurry of run T-97 is now in progress.

[4]R. B. Korsmeyer *et al.*, *HRP Quar. Prog. Rep. July 31, 1957*, ORNL-2379, p 52–54.

10.2 HRT BLANKET SYSTEM DEVELOPMENT

Run SM-4, begun last quarter, was continued to a total of 2400 hr. The principal reason for shutting down was that the iron pickup, indicating attack on the pressure vessel, was approaching a predetermined limit. In addition, difficulties were encountered with the pressurizer at the higher thorium concentrations employed during the latter part of the run; these difficulties

UNCLASSIFIED
PHOTO 30498

Fig. 10.4. Orifice Plate After Run 200A-14 (Upstream Face).

prevented additional charging of thorium and indicated the need for modifying the pressurizer design.

10.2.1 Slurry Distribution Studies

Figure 10.7 shows the temperature, frequency, pump flow, charged concentration, and circulating and blanket concentrations plotted as a function of running time, thus indicating the slurry behavior and the system response to changes in operating conditions.

During the period from 800 to 1000 hr, the loop was run at 200°C with variable-frequency power supply to the pump in the range 46–50 cycles. Data were taken on thorium distribution both by spot sampling and by gamma surveys. A second

UNCLASSIFIED
PHOTO 30504

Fig. 10.5. Kingsbury Bearing Shoes After Run 200A-14.

UNCLASSIFIED
PHOTO 30509

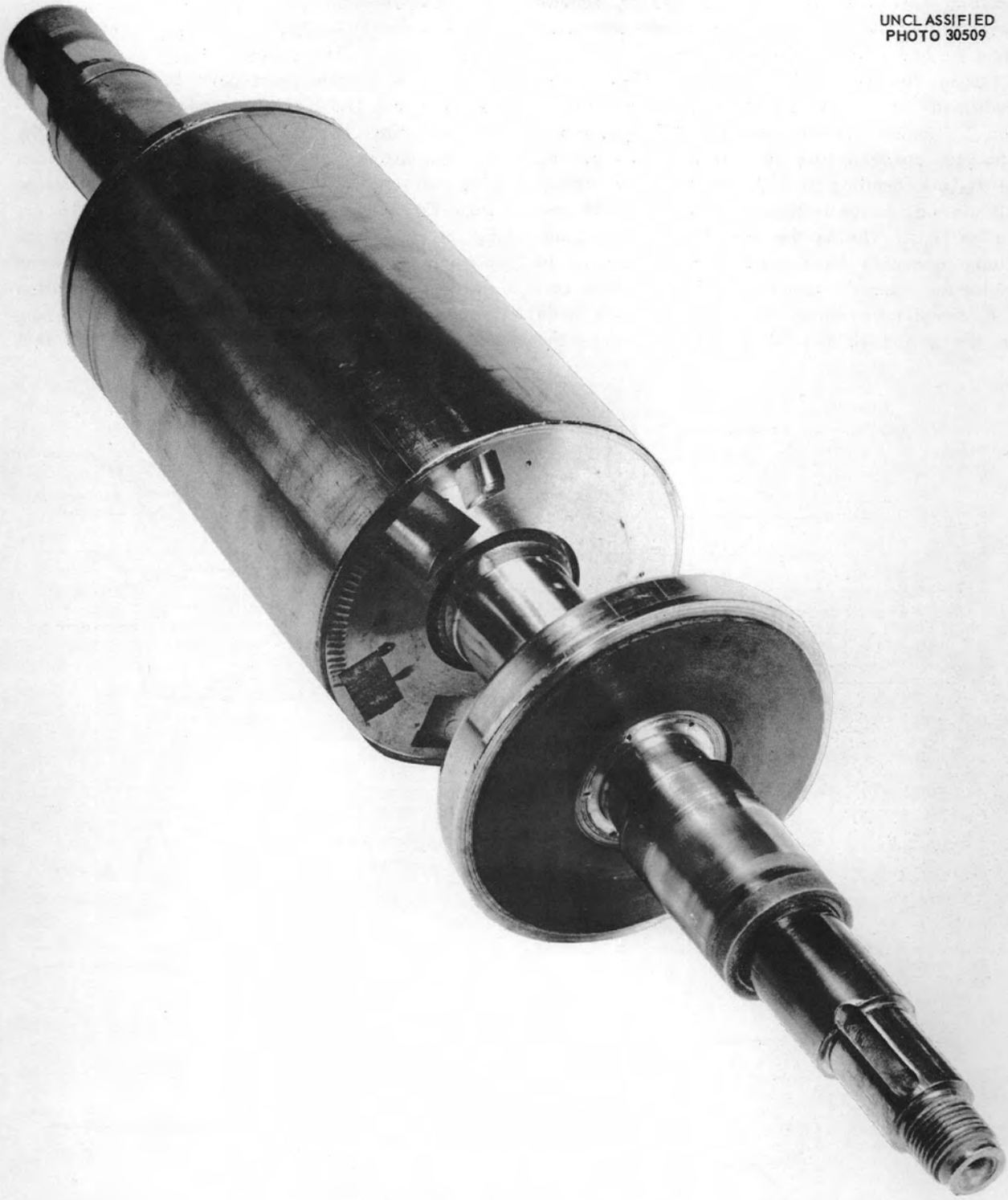

Fig. 10.6. Pump Rotor After Run 200A-14.

settling test was carried out at 975 hr, and an inventory of 546 kg in the blanket was estimated from the bed volume and concentration.

During the period from 1000 to 1220 hr, an additional 483 kg of thorium was charged to the loop, bringing the inventory to 1013 kg and the charged concentration to 720 g of Th per kg of H_2O. Sampling at 1230 hr showed an actual circulating concentration of 710 g of Th per kg of H_2O. During the last 70 hr of charging, slurry appeared for the first time in the liquid withdrawn from the upper part of the pressurizer.

A complete sampling of the system was made in the period 1300–1350 hr. The mean for the 36 samples from the blanket was 623 g of Th per kg of H_2O; the circulating concentration was 647 g of Th per kg of H_2O, and the lower pressurizer sample point gave 1410 g of Th per kg of H_2O. The blanket samples indicated high-concentration regions on the core wall at the top and on the pressure-vessel wall at the bottom. The average blanket concentration estimated from the gamma surveys was 655 g of Th per kg of H_2O, with the heaviest concentration indicated near the top. The discrepancy between the charged and the circulating concentration amounted to approximately 80 kg of thorium. In all probability, one-third to one-half of this

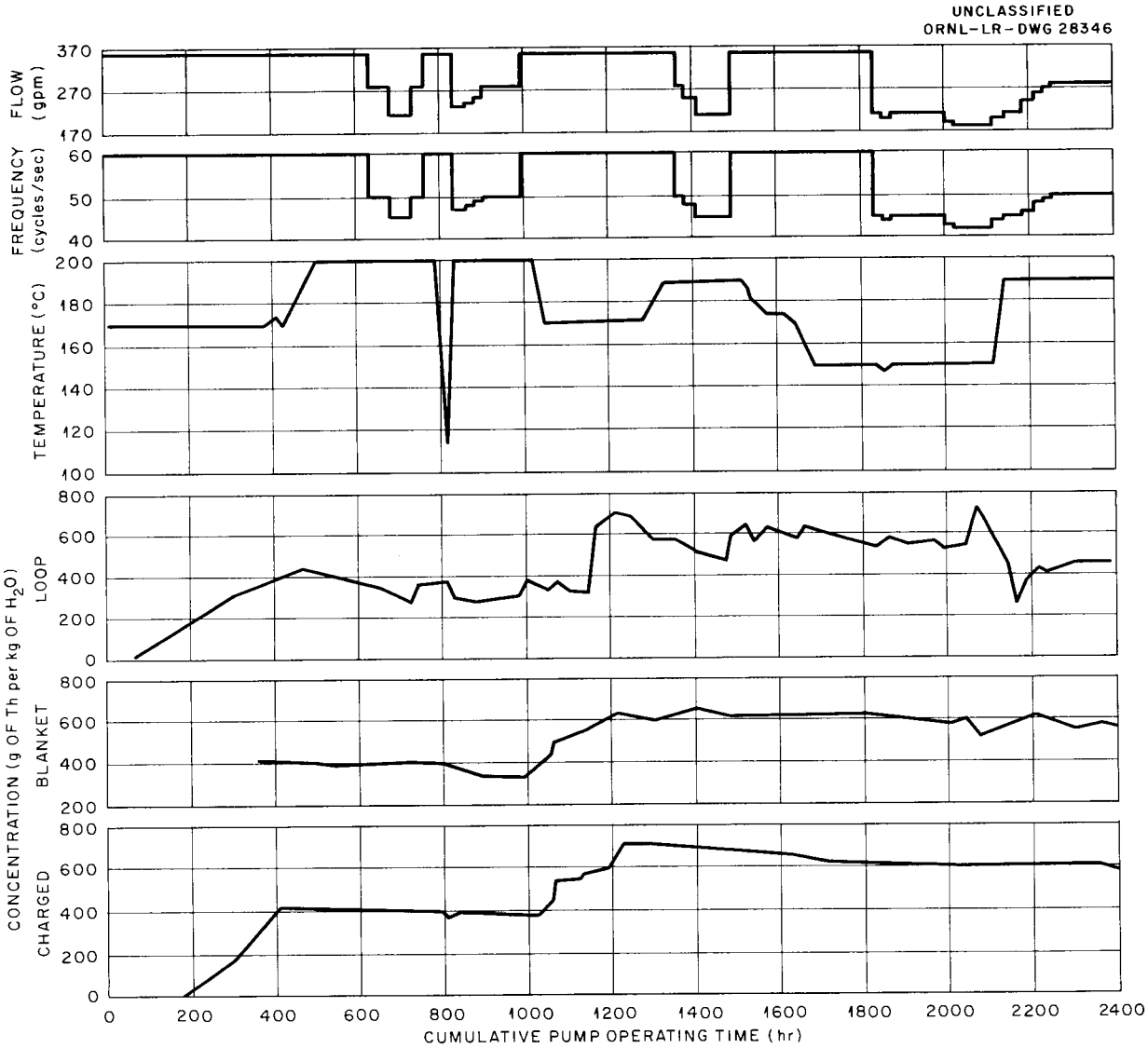

Fig. 10.7. Slurry Blanket Test, Run SM-4.

material was in the pressurizer, and the remainder was in the blanket, either on the core wall or on the bottom. The latter material might not be picked up by sampling, either because the sampling devices did not extend into the heavy layer or because a true sample was not obtained from the heavy layer. Effects observed during settling tests and dumping operations indicate that there is a tendency for dilute material to flow out of very heavy beds. This is illustrated by data from a settling test taken at 1350 hr (see Table 10.2). The low values of the 2-hr samples represent this effect.

Table 10.2. Blanket Settling Test at 1350 hr (Run SM-4)*

Time After Pump Shutdown	Concentration (g of Th per kg of H_2O)		
	At Wall	6 in. into Blanket	12 in. into Blanket
15 min	1358	1329	1342
1 hr	1730	1551	1420
2 hr	361	1111	345

*Samples taken from bottom row of samplers.

Over a period of 130 hr following the completion of charging, the circulating concentration decreased by approximately 100 g of Th per kg of H_2O, representing the removal of 140 kg of thorium from the circulating system.

After the settling test at 1350 hr, reduced-frequency operation was resumed, the frequency being reduced to 50, 48, and 46.5 cycles. The circulating concentration gradually dropped to approximately 470 g of Th per kg of H_2O. Operation at 60 cycles was then resumed to determine whether the slurry could be brought back into circulation. Approximately 15 min after shifting to 60 cycles, the circulating concentration had increased to 593 g of Th per kg of H_2O, and 24 hr later it was 624 g of Th per kg of H_2O, as compared with a calculated charge of 685 g of Th per kg of H_2O at the time. The temperature was then gradually reduced from 190 to 150°C over a period of 175 hr. No significant change in the discrepancy between charged and circulating concentration was observed; the discrepancy ranged from 30 to 60 g of Th per kg of H_2O throughout the entire temperature range.

Reduced-frequency operation was again started at 1825 hr. The frequency was maintained at 46 cycles until 1970 hr, at 44 cycles until 2020 hr, and at 42 cycles until 2160 hr, the temperature being increased from 150 to 190°C at 2070 hr. The discrepancy between the charged concentration and the circulating concentration gradually increased as operation continued at these lower frequencies at 150°C. It appeared to be a function both of the frequency and of the time after the frequency change. When the temperature was raised to 190 at 42 cycles, a very large discrepancy between charged and circulating concentration developed: 267 g of Th per kg of H_2O circulating vs 626 g of Th per kg of H_2O charged. Blanket samples averaged 493 g of Th per kg of H_2O. Similar results were obtained in run SM-2 under somewhat similar conditions.

Between 2160 and 2235 hr, the frequency was raised from 42 to 50 cycles, with the temperature being kept at 190°C. The discrepancy between the charged and circulating concentration decreased with each frequency increase and leveled out at approximately 125 g of Th per kg of H_2O after approximately 72 hr at 50 cycles.

In the period of 2300–2400 hr, two uranium additions were made to the system in order to determine the interchange of slurry between the circulating stream and the blanket contents. One 700-g addition was charged into the circulating stream, and 48 hr later a second charge was injected into the lower pressurizer sample point.

Figure 10.8 shows the results of these experiments. The first addition was to the circulating stream at a point several feet upstream of the pump suction. The UO_3 slurry was placed in a 1-liter bomb and displaced into the loop by flushing approximately 5 liters of water through the bomb. The net uranium added was determined by subtracting the uranium found in the bomb on subsequent thorough rinsing from the quantity loaded. The apparent disappearance of some of the uranium immediately on its addition and its later appearance in the circulating stream is believed to have been due to its adsorption on a large mass of thoria in the blanket which was stirred up only infrequently by eddies created by the inlet nozzles.

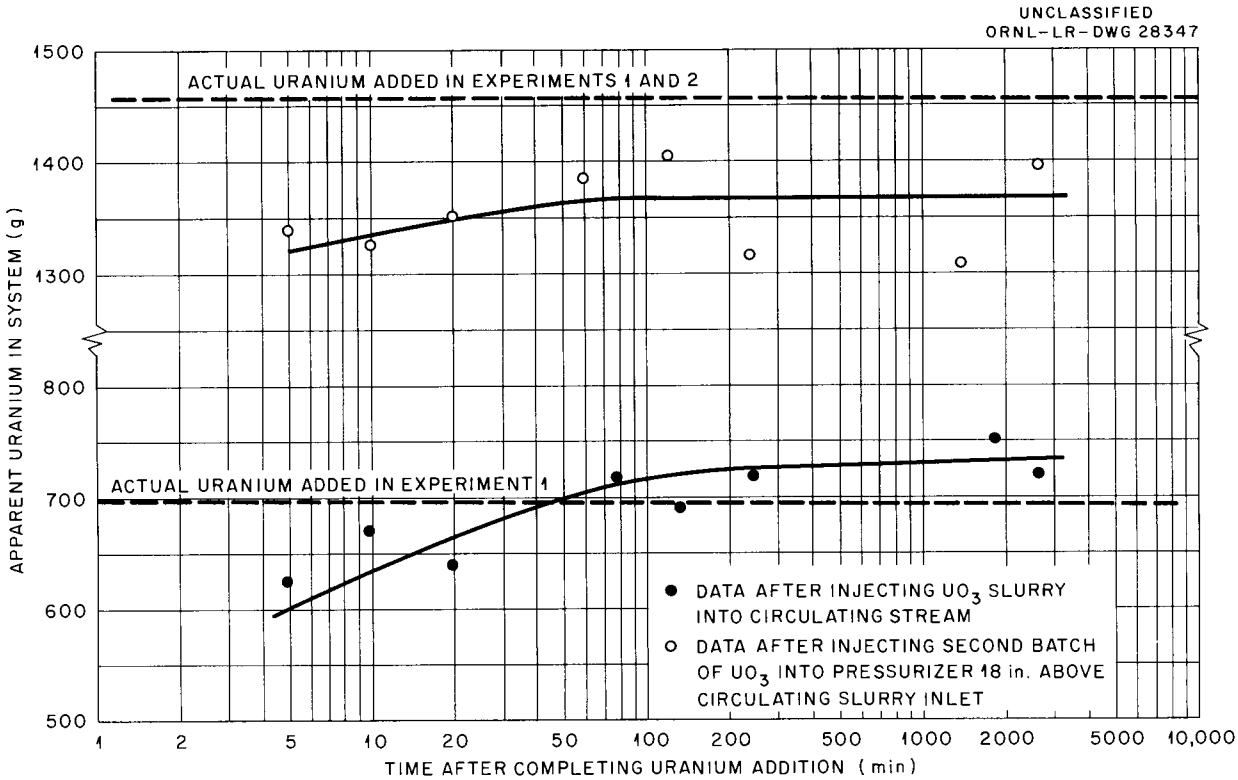

Fig. 10.8. Results of Uranium Addition to Circulating Thoria Blanket.

In a period of 2 hr, equivalent to nearly 100 cycles of the circulating stream around the loop, this mass became largely intermixed with the main stream, and the uranium loop concentration appeared to have leveled off. This hypothesis is supported by the discovery that some material removed from the slurry bed at the bottom of the blanket contained about 2.5 times the uranium concentration found in the circulating stream. Since the apparent uranium exceeds the quantity added, it is believed that some of the thorium in the blanket was not mixing with the circulating stream. This "inactive" thorium is estimated as approximately 25 kg, of which, part was in the pressurizer and the rest in the blanket. Confirmation that some of the thorium in the blanket did not mix completely with the uranium was found after the shutdown; some material removed from the top of the core was comprised of white and yellow regions. The regions were separated and analyzed; the white solids were found to be free of uranium, while the yellow solids contained a substantial quantity.

The second uranium addition was made in a similar manner by injecting the uranium into the lower pressurizer sample point. A total of 760 g of uranium was added, of which approximately 640 g rapidly mixed with the circulating slurry; the rest apparently remained in the pressurizer.

10.2.2 Pressurizer Behavior at Concentrations Above 500 Grams of Thorium per Kilogram of Water

At 1240 hr, the pressurizer wall temperatures in the heated zone started rising and in a short time attained values of over 400°C. In view of the presence of slurry high in the pressurizer, it was suspected that a plug had formed in the heated zone, and corrective action was taken on this premise. The loop was shut down temporarily to determine whether the slurry could be removed from the pressurizer by settling; this proved unsuccessful. After approximately 4 hr, the plug was cleared sufficiently to permit satisfactory operation of the pressurizer heaters (wall temperatures not exceeding 270°C) by opening a ¼-in. bypass line from the pump discharge to the upper pressurizer sample point. This line had been installed for the purpose of venting the pump scroll and discharge line during loop filling operations.

The pressurizer plugging trouble continued intermittently for the rest of the run. In general, it did not recur with the bypass open when the circulating concentration was less than 500 g of Th per kg of H_2O. It could be made to occur rather quickly at any time by closing the bypass. The trouble could be cleared by stopping circulation for about 5 min with the bypass open. The only instrumentation available on the bypass was a thermocouple, which was installed after the pressurizer plugging problem occurred. The behavior of the wall temperature indicated that the bypass carried much more flow with the pump off than with it on. During circulation the wall temperature would drop to about 90°C, and with the pump off it would rise in a very short time to within 10°C of the loop temperature. Since the bypass line connects to the main loop at the pump discharge, it seemed that the pump interfered to some extent with thermal convection.

No gamma-ray transmission survey facilities were available on the pressurizer. However, a number of emission surveys were made during the latter part of the run. These indicated a zone of very high thorium concentration, centered approximately 1 ft below the top of the pressurizer heaters and 8 to 12 in. long. The difference between the pressurizer being "plugged" and "unplugged," as reflected in the wall temperature, was associated with approximately a 10% difference in the gamma-ray intensity in the high-concentration zone. Observations indicated that the zone was capable of several inches of vertical displacement. During one settling test late in the run, the behavior of the level-indicating differential-pressure cell indicated that a vapor space actually developed below the high-concentration zone, while clear liquid was retained on top of it with the bypass closed. At the end of the run, when the pressurizer was opened, a solid layer of thorium oxide was found in the pressurizer at the level of the high-concentration zone. This layer was approximately 8 in. thick. Cake-resuspension-index tests on material from the layer indicated it to be dried slurry rather than true cake. Thus it is inferred that in operation the plug existed as a very heavy thorium oxide mud having a high yield stress. The mechanism by which the plug formed is uncertain, although boiling at the heater surfaces is suspected as the cause.

On a few occasions when plugging was encountered, serious pressure excursions occurred because of the sudden release of the stored heat in the pipe wall into the pressurizer when the heat transfer surfaces were again cleared sufficiently to permit normal heat transfer. In the most extreme case the pressure went to 365 psi (the rupture disk is rated at 375 psi), and at this point it was relieved to the core through the pressure-balancing system which limits the core-to-blanket differential to 50 psi. As experience was gained, the plugging was recognized at an earlier stage and was cleared before the wall temperature became high enough to cause serious pressure excursions.

10.2.3 Dump Operation and Examination of Equipment

The run was terminated by dumping at 2400 hr. For the first time, steam spargers were used to agitate the slurry in the pressure vessel while the dump was in progress. A marked improvement in completeness of dumping was observed. The bed of slurry in the bottom of the vessel lay entirely below the sparger inlets and contained approximately 50 liters as opposed to 200 liters remaining after runs SM-2 and SM-3. Figure 10.9 shows the settled bed in the bottom of the vessel. One of the inlet nozzles can be seen in this picture. On the two previous dumps, at least 6 in. of slurry covered the inlet nozzles. Of 822 kg of thorium estimated to be in the loop at the end of the run, 615 kg was recovered in the initial dump.

Evidence of a considerably thicker layer of slurry on the top of the core than that which existed in previous runs is given in Fig. 10.10, which shows the dried slurry layer in that area. The dried material ranged up to ½ in. thick. From this evidence and the data taken during the run, it is now believed that the lower inlet to the blanket exit baffle assembly was blocked for most of the run, probably from about 375 hr on. Thus the stream intended for sweeping the upper core surface did not exist. Both the sampling and gamma-survey data indicated heavy slurry at the top of the core during the rest of the run.

After the interior of the pressure vessel and pressurizer had been inspected, the openings were closed and rinsing operations were begun. On the first run the pump seized twice, and it was subsequently found that it had not been vented properly. No further pump trouble was experienced. Air was connected to the sparging system and was used for agitation during the draining of all

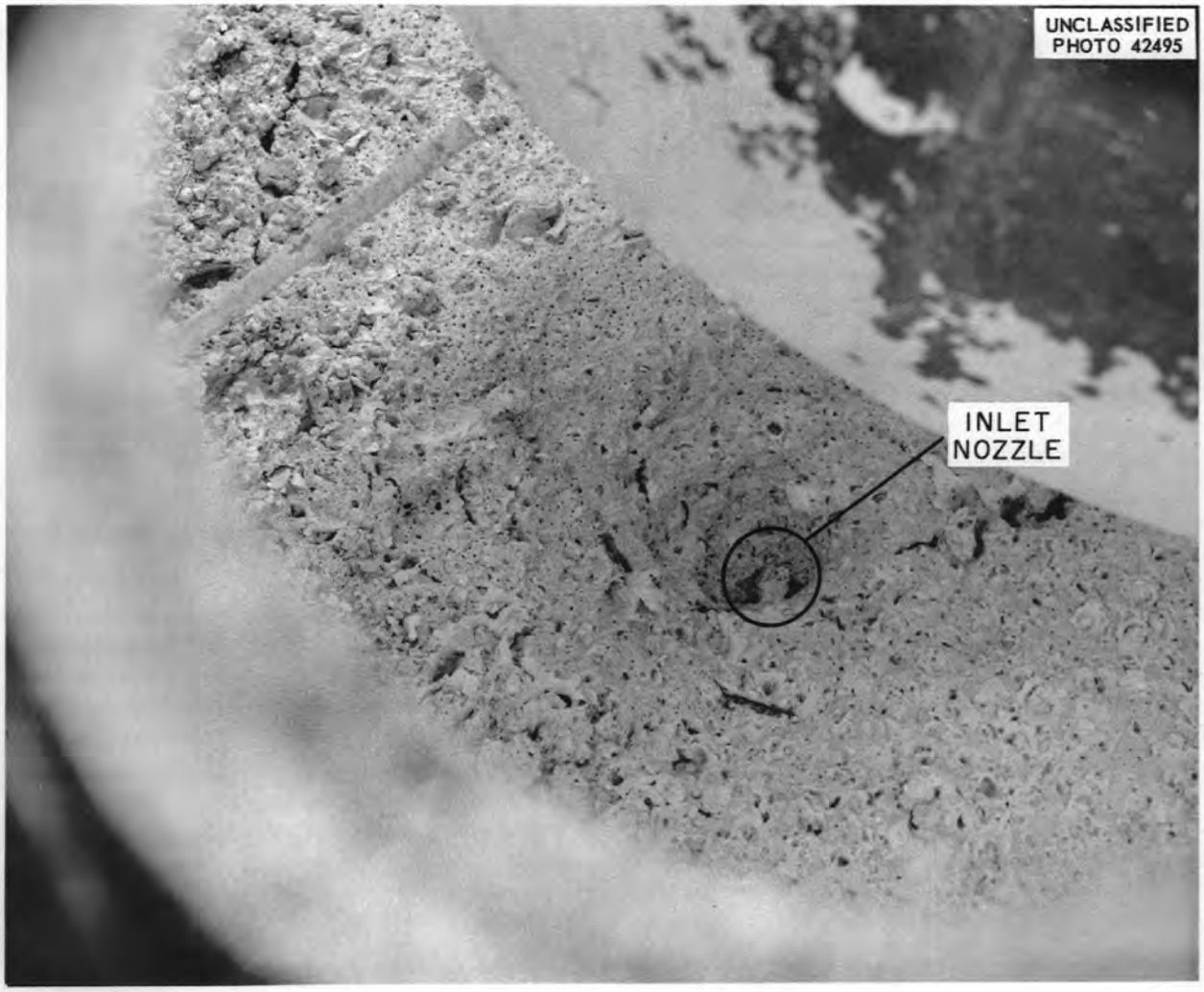

Fig. 10.9. Heel of Thoria Remaining in Blanket After Dump.

but the first of these rinse runs. After the fifth rinse, the blanket inspection ports were again opened, and a thorough inspection was made. Except for a thin cake covering some of the pressure-vessel surface, the vessel was clean down to the sparger inlets. Below the inlets, most of the bottom had a layer of rather fluid slurry approximately $\frac{1}{4}$ in. thick. On the north side, a pile approximately 1 ft long and 6 in. high remained. This material had a density of 3.2 g/cc, or a concentration of 2540 g of Th per kg of H_2O. The pile, located between the high-velocity jet from the west inlet nozzle and the core, was raked into the jet stream, and a sixth rinse run was carried out for approximately 1 hr. At the end of this run, the pressure-vessel ports were again opened, and the slurry remaining was removed by hosing with distilled water. As a very rough estimate, 15 kg of thorium remained in the pressure vessel after the first five rinses, 2 kg after the sixth rinse run, and 100–200 g after hosing.

After the slurry was cleaned out, an inspection of the interior surface of the pressure vessel showed several deep pits. These appear to be as much as $\frac{3}{16}$ in. deep in the $\frac{1}{2}$-in.-thick pressure-vessel shell. All are located in the lower half of the vessel. The stainless steel weld pads laid down in front of the inlet nozzles after run SM-3 were not attacked to any observable extent.

Corrosion experience during the run was similar to that in the preceding runs. Superficial attack rates based on total pickup of corrosion products

Fig. 10.10. Dried Thoria on Core Vessel After Dump.

are meaningless, as attack on all materials tends to concentrate in a few localized areas. This has proved true of carbon steel, stainless steel, and titanium. In almost all cases observed, severe corrosion appears to be associated with flow-separation regions at high free stream velocities.

When the pump was disassembled, it was found generally to be in excellent condition except for a crack in the upper journal, which probably occurred during the first rinse run. Bearing wear was slight; the upper bearing was worn 5 mils; the lower, 10 mils; and the thrust runner, 3 mils. There was no measurable wear on either journal. The impeller lost 18 g and exhibited the typical appearance of titanium impellers after slurry service. It was bright all over and showed slight attack at flow-separation regions and in the lower wear-ring area. The most severe attack occurred on the stainless steel bottom of the scroll (Fig. 10.11). The titanium wear-ring insert, however, showed only slight attack, and its inside diameter had increased only 6 mils. A wear ring of uniform inside diameter, rather than a labyrinth, was installed for this run, and this design appears advantageous.

10.2.4 Conclusions from Run SM-4

The conclusions reached during this run are as follows:

1. Completely uniform thoria suspension was probably not achieved under any conditions, and

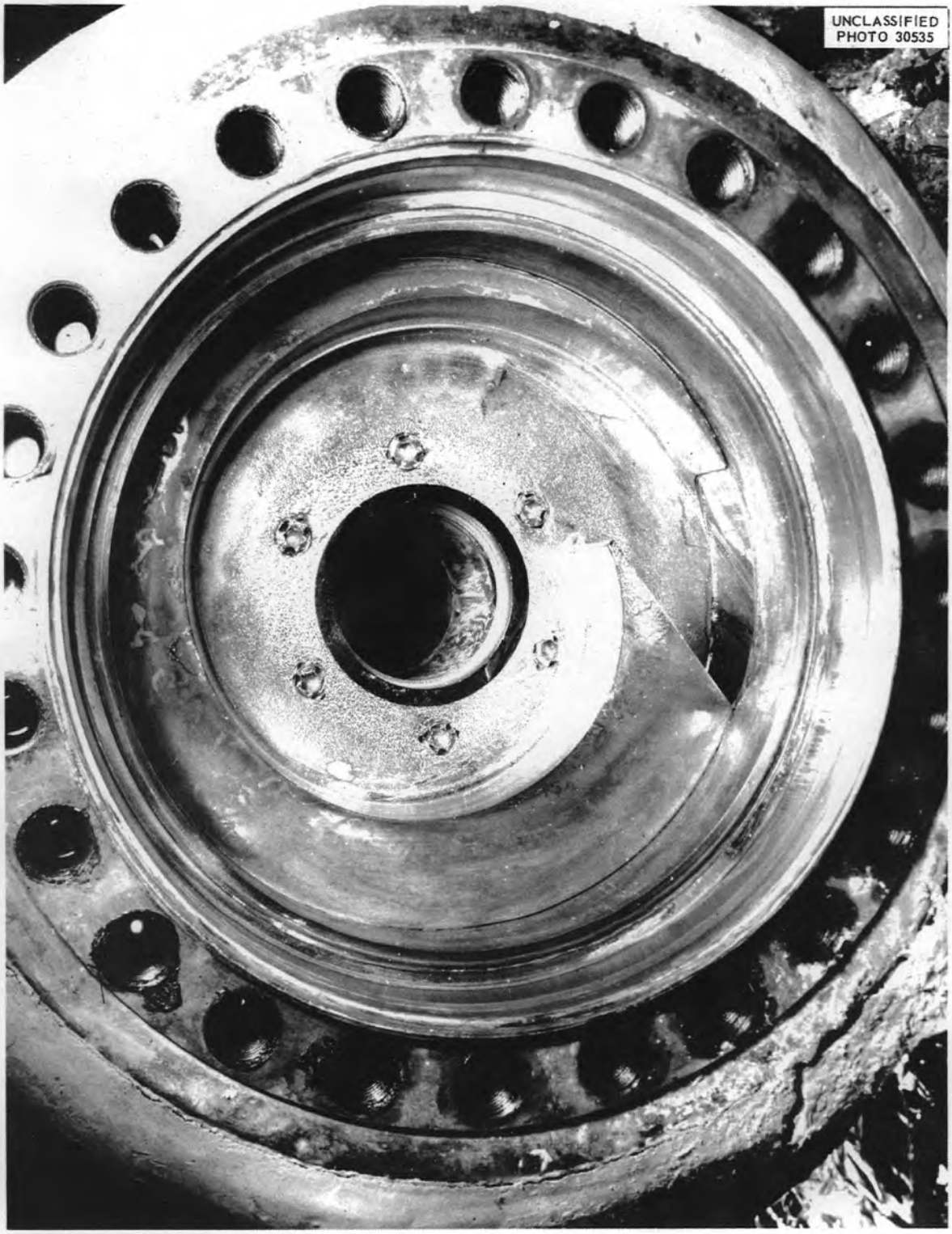

Fig. 10.11. Pump Scroll After Blanket Run SM-4.

there were stagnant regions within the vessel. There was a tendency for thoria to accumulate on the top of the core and at the bottom of the blanket. Some revisions to the exit baffle arrangement may be required to correct the core accumulation.

2. At concentrations above 500 g of Th per kg of H_2O, there was a tendency for thoria to accumulate in the pressurizer, and a rather tenacious mass developed near the top of the pressurizer heaters. This behavior was also observed[5] in run CS-41.

3. At comparable conditions of flow and temperature, suspension achieved with the 1½-in. inlet nozzles appeared better than that achieved with the 2-in. nozzles installed in the HRT. The 2-in. nozzles are being reinstalled prior to the next run to confirm this conclusion.

4. Steam or gas sparging is required to maintain the slurry in suspension during dumping operations.

[5]E. L. Compere *et al.*, *HRP Quar. Prog. Rep. Oct. 31, 1957*, ORNL-2432, p 92.

11. INSTRUMENT AND VALVE DEVELOPMENT

D. S. Toomb

A. M. Billings
E. H. Bell
R. L. Moore
J. A. Russell
H. D. Wills

11.1 INSTRUMENT DEVELOPMENT

11.1.1 High-Temperature Radiation-Resistant Differential Transformers

The development of differential transformers for sensing motions of instrument primary elements and capable of operating for long periods of time at high temperatures and in nuclear radiation fields is continuing. Tests performed on the units previously described[1,2] have yielded the following information:

1. ORNL design, Sprague Electric Co. Ceroc-T-insulated copper wire, silicone-varnish vacuum impregnated. – These transformers have been found capable of continuous operation at 250°C, but will fail when operated continuously at 280°C. The transformers exhibit a 2% zero shift and negligible null-voltage change at 250°C.
2. G. L. Collins Co. model LMT-78201, asbestos- and ceramic-insulated copper wire, hermetically sealed. – Two of these transformers have failed at 250°C owing to melting of the solder at the lead-through terminals.
3. Crescent Engineering and Research Co. ceramic-insulated silver wire, hermetically sealed. – Both transformers performed satisfactorily at 300°C insofar as insulation breakdown was concerned. One of the transformers exhibited a zero shift of 6% at 300°C and a null-voltage increase of 2 v, which is considered acceptable. The second unit, however, was found to have a zero shift of 45% at 300°C and a null-voltage increase of 11 v, which is not satisfactory.
4. ORNL design, wound with No. 30 AWG anodized aluminum wire. – One transformer operated for one week at 300°C without insulation breakdown or excessive zero shift or null-voltage increase. The second transformer of this type tested had an acceptable zero shift but an excessive null shift. The reason for the poor performance of the second unit is not apparent, and tests of this coil are continuing. Two aluminum bobbins were wound with the anodized aluminum wire furnished by the Sigmund Cohn Co. and inserted in beam hole 51 of the ORNL Graphite Reactor to determine radiation effects on the wire. Coil construction was such as to simulate that of each half of the ORNL-design differential transformer. The flux in this beam hole is reported as being approximately 8×10^{11} neutrons/cm^2/sec (fast), 5×10^{11} neutrons/cm^2/sec (thermal), and 5×10^5 r/hr of gamma radiation. During ten days in the hole (nine days at power), the primary-to-secondary resistance decreased from 30×10^6 ohms to a minimum of 1.76×10^6 ohms after two days of exposure and then increased slowly to 3.2×10^6 ohms at the end of the run. Total exposure was approximately 6×10^{17} neutrons/cm^2 (fast), 4×10^{17} neutrons/cm^2 (thermal), and 1×10^8 r of gamma radiation. This fast-neutron exposure is estimated to be equivalent to that which would be accumulated in 70 years at the location of the HRT pressurizer liquid-level transmitters.

11.1.2 Solid-State-Component Instrument Systems

A Sarkes-Tarzian Company No. S5017 silicon-junction rectifier was evaluated for possible use as a replacement for the type 6X5 vacuum-tube rectifiers utilized in the Foxboro Company Dynalog instruments used in considerable number in HRP instrument systems. Tests indicate that the increase in B+ voltage because of the lower forward resistance of these inherently more reliable rectifiers is not excessive for the instruments and that the rectifiers will withstand the high surge currents, which occur when the instruments are turned on.

11.1.3 Instrument Alarm-Scanner

An alarm-scanner for process-variable instruments, which is manufactured by Taylor Instrument Companies to ORNL specifications,

[1] D. S. Toomb *et al.*, *HRP Quar. Prog. Rep. July 31, 1957*, ORNL-2379, p 21.

[2] D. S. Toomb *et al.*, *HRP Quar. Prog. Rep. Oct. 31, 1957*, ORNL-2432, p 70.

has been placed in checkout service with simulated signals. This alarm-scanner affords a means of satisfying a dual requirement encountered in instrumenting in-pile loops, where periodic precision readout of pressure is needed and where continuous monitoring of temperatures and pressure is required to ensure that the variables are within limits.

This scanning system is designed to select automatically and sequentially one variable per second and compare it with a high and a low limit, both preselected. If the system is outside the limits, an audible alarm is sounded and a visual indication of its high or low condition is displayed. Provision for manual checking of the lamps and high-low limit operation is built into the instrument, as can be seen in Fig. 11.1, a block diagram of the system. Precision readout is accomplished by manually switching the variable to an expanded-scale self-balancing precision potentiometer.

Figure 11.2 is a photograph of the scanner and associated precision indicator mounted in a standard ORNL modular instrument cabinet. The bottom section contains auxiliary power supplies and Transet potentiometer-transmitters for converting signals from strain-gage-type pressure transmitters to millivolt signals compatible with the scanning system. Temperature signals from thermocouples are fed directly into the scanner.

Most of the system is wired to scan 20 variables, although indication has been provided for only 14 of these. Each of the variables is designated by a number marked on a circular Lucite block located in one of two rows at the top of the panel. Each block has two indicating lamps mounted within, an amber light indicating an off-normal low condition and a red light indicating a high condition. Another amber lamp flashes once per second as the variables are scanned.

The eight electronic chassis, the lamp and manual switch bank, and the high-low limit-setting pinboard which comprise the scanner proper are shown in Fig. 11.3. The separate chassis are interconnected with Varicon connectors so that any unit may be removed from the cabinet for maintenance without the unsoldering of wires.

UNCLASSIFIED
ORNL-LR-DWG 28348

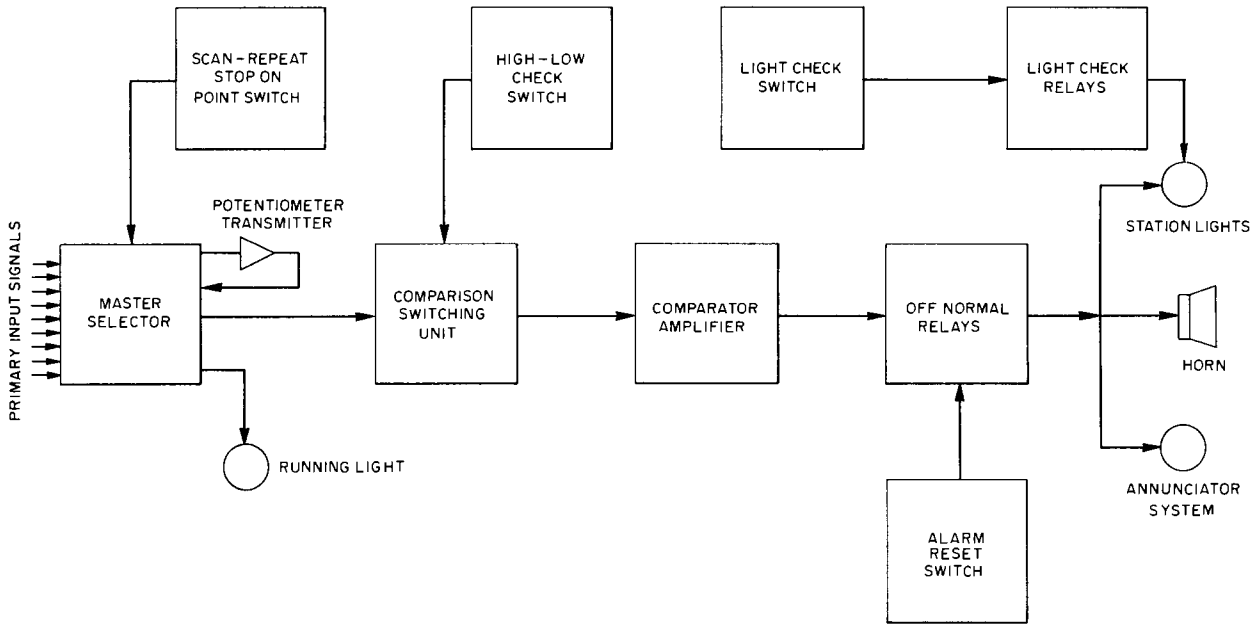

Fig. 11.1. Alarm-Scanner – Block Diagram.

UNCLASSIFIED
PHOTO 30257

Fig. 11.2. Alarm-Scanner and Precision Indicator.

11.1.4 Airborne-Alpha-Contamination Monitor

To provide leak detection and personnel protection in areas near slurry loops, two monitoring instruments sensing airborne alpha contamination have been constructed. The monitors, which are patterned after a prototype developed by the ORNL Health Physics Division, have given excellent service.

Referring to Fig. 11.4, operation is as follows: Air drawn by a rotary carbon-vane vacuum pump from the area to be sampled passes through a filter-paper tape, which is periodically advanced by a motor-driven spool to a position where any alpha radioactivity in the collected sample is counted, by a scintillation-type detector, consisting of a zinc sulfide crystal and a photomultiplier tube. The millivolt output pulses from the photomultiplier tube are amplified by a preamplifier immediately adjacent to the photomultiplier and fed to a counting-rate circuit, which, in turn, drives a recorder and a contact-making milliammeter alarm circuit. Figure 11.5 is a photograph of the instrument, which is housed in a portable cabinet, in operation near a slurry pump test loop.

The instrument, which is built from readily available standard subassemblies, can be duplicated for about $2500.

The electronic circuits are periodically standardized by counting known samples deposited on metal strips which are inserted in the light-tight slit normally occupied by the sample tape in the scintillating-crystal assembly.

11.2 VALVE DEVELOPMENT

11.2.1 Solution-Valve Trim

Operation of the valve test loop was turned over to the Component Development Section after 4776 hr of operation. During this operation the following valve trim materials were the most satisfactory in high-temperature uranyl sulfate.[3]

Plug	Seat
Armco 17-4 PH hardened to 35–40 Rockwell C	Type 347 stainless steel
Type 347 stainless steel with a gold-gasketed groove	Type 347 stainless steel with tongue

[3] A. M. Billings, *Valve Test Loop Operation – Nov. 23, 1955 thru Oct. 18, 1957*, ORNL CF-57-12-57 (Dec. 12, 1957).

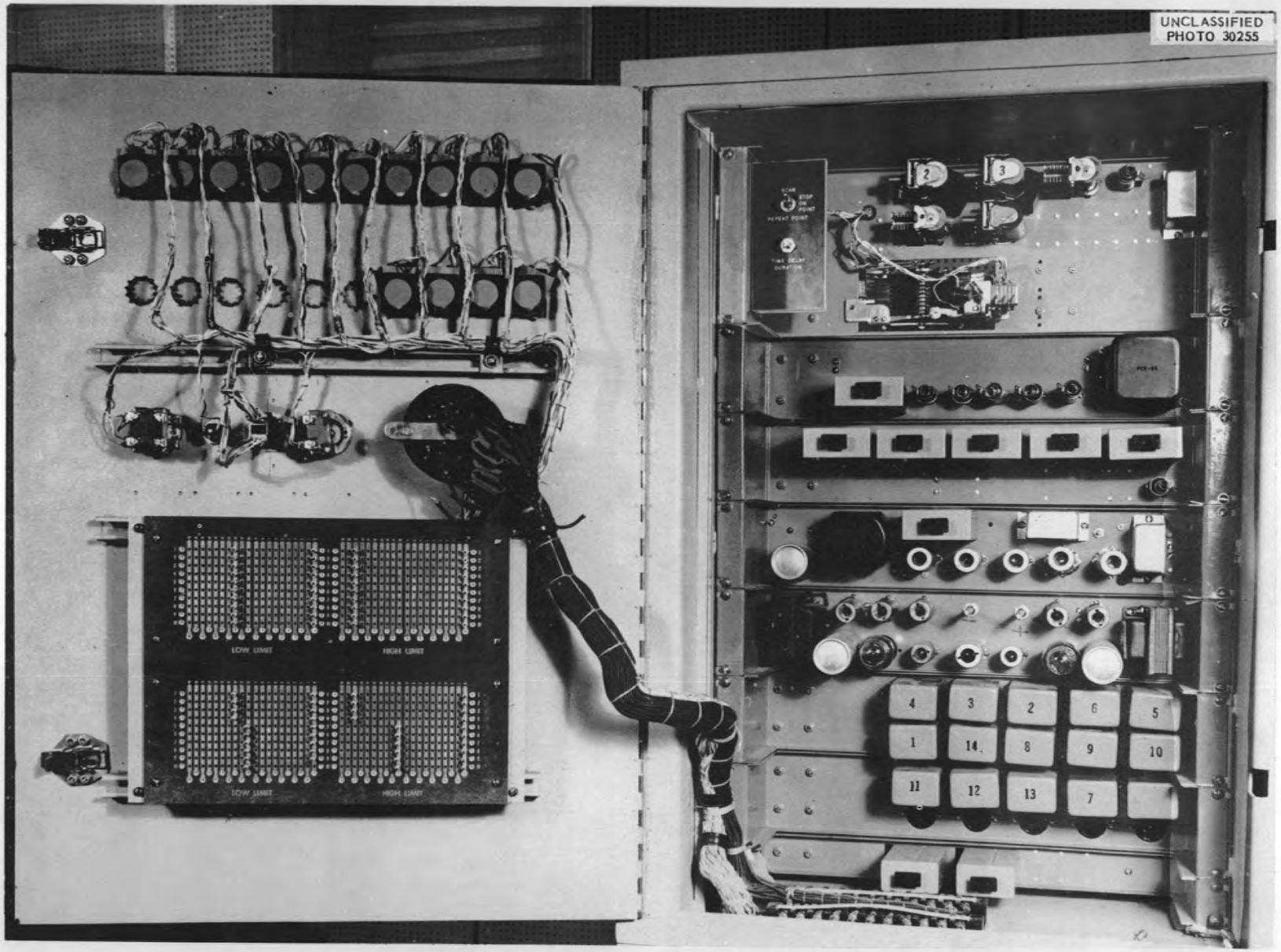

Fig. 11.3. Alarm-Scanner Chassis and Pinboard.

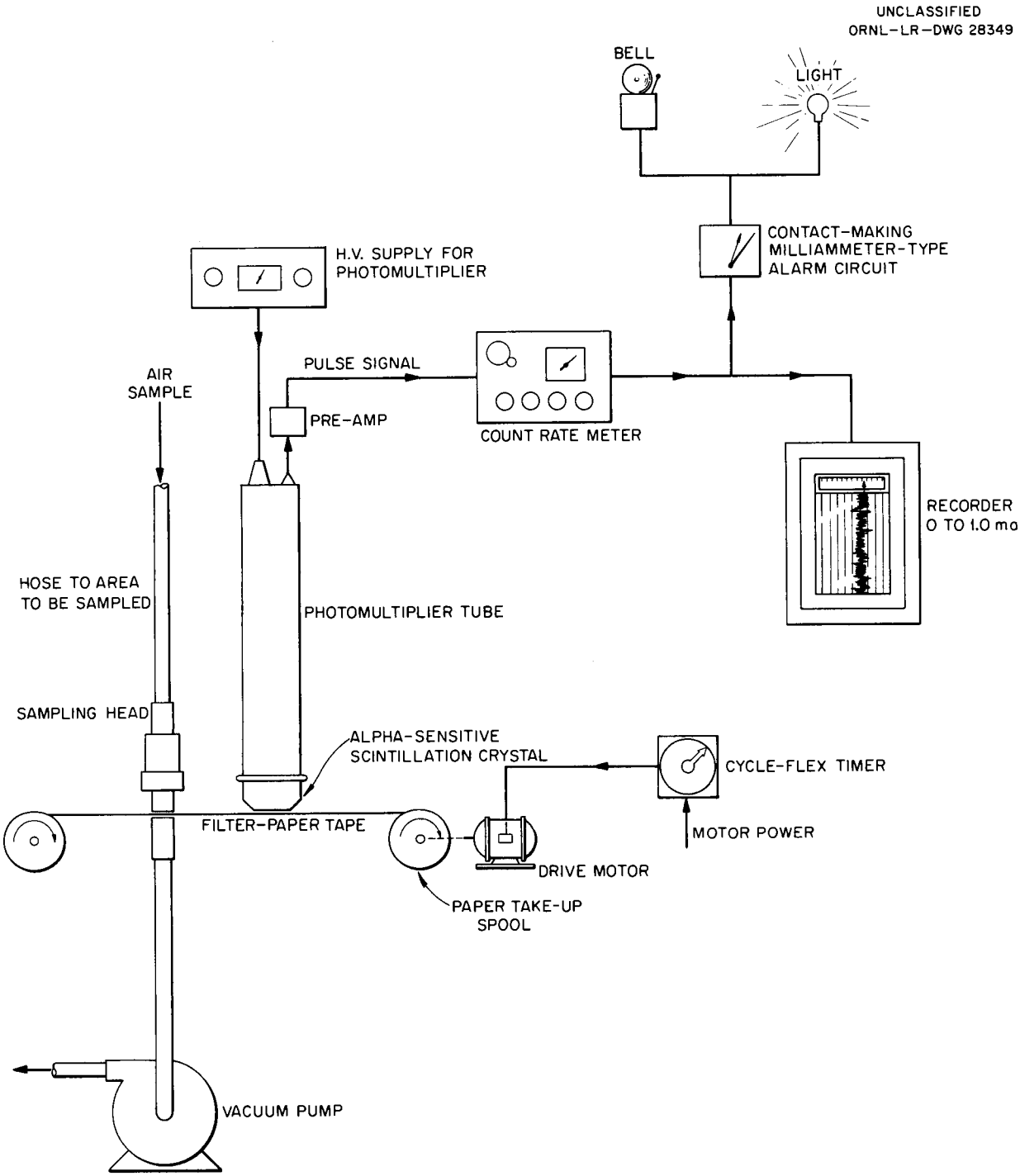

Fig. 11.4. Airborne-Alpha-Contamination Monitor – Simplified Schematic Drawing.

UNCLASSIFIED
PHOTO 30317

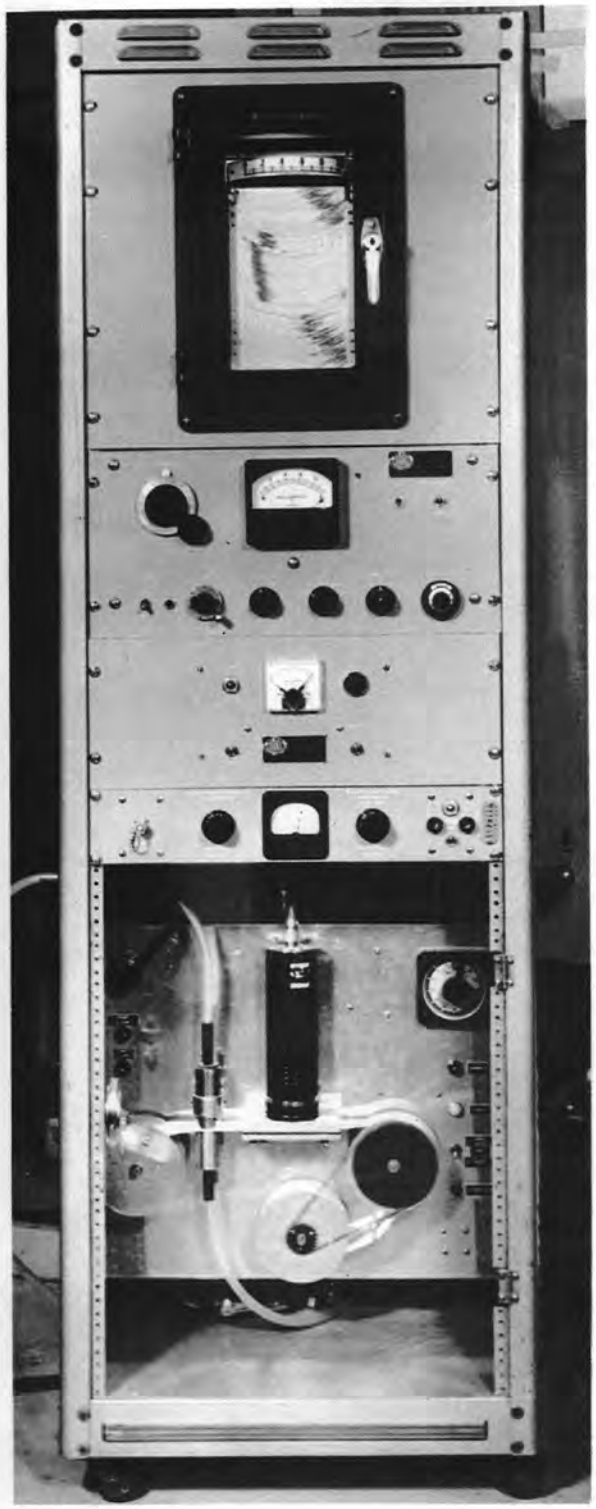

Fig. 11.5. Airborne-Alpha-Contamination Monitor.

11.2.2 Valve Actuators

A prototype pneumatic actuator for large valves was built and tested for proper operation. The unit, pictured in Fig. 11.6, consists of two (more may be used) pneumatically powered metal bellows attached to a common shaft and connected in parallel to a source of air pressure. The bellows assemblies are Fulton Sylphon Division No. 6745-R2, each with an effective area of 123 in.^{2} and rated for a 1-in. stroke with an actuating pressure of 100 psi.

11.2.3 Stem Sealing Bellows

Gold plating to increase the corrosion resistance of the stainless steel bellows used for control-valve stem seals was not satisfactory. The plates on two bellows cracked upon flexing or pitted when exposed to boiling 10 wt % HCl.[4] Three different plating techniques were tried, but all were unsatisfactory.

11.2.4 Slurry-Service Valves

A valve especially constructed for slurry use was obtained from the Hammel-Dahl Company and will be installed in the 200B slurry loop. The valve, shown in Fig. 11.7, incorporates a long-radius-bend body configuration to minimize erosion by the slurry. The bellows compartment can be purged to prevent slurry from entering through the annulus between the Stellite No. 6 stem guide pads and the Colmonoy hard-faced stem. As the two-ply type 347 stainless steel bellows used in this valve is rated at only 450 psi, provision is made to back-pressurize the bellows when the valve is used in applications above this pressure; the valve body is designed for a working pressure of 2000 psi at 300°C. The plug and seat are fabricated of tungsten carbide, for wear resistance.

11.2.5 Slurry-Valve Trim

Nine Pressure Products Company valves which were used in the slurry blanket test system were inspected. Two of the valves, Nos. V-76 and V-166, exhibited plug erosion of such severity

[4]D. N. Hess, *Evaluation of Gold Plating on Type 347 Stainless Steel Bellows as Determined by Immersion in Boiling 10 wt % HCl*, memorandum to A. M. Billings (Nov. 8, 1957).

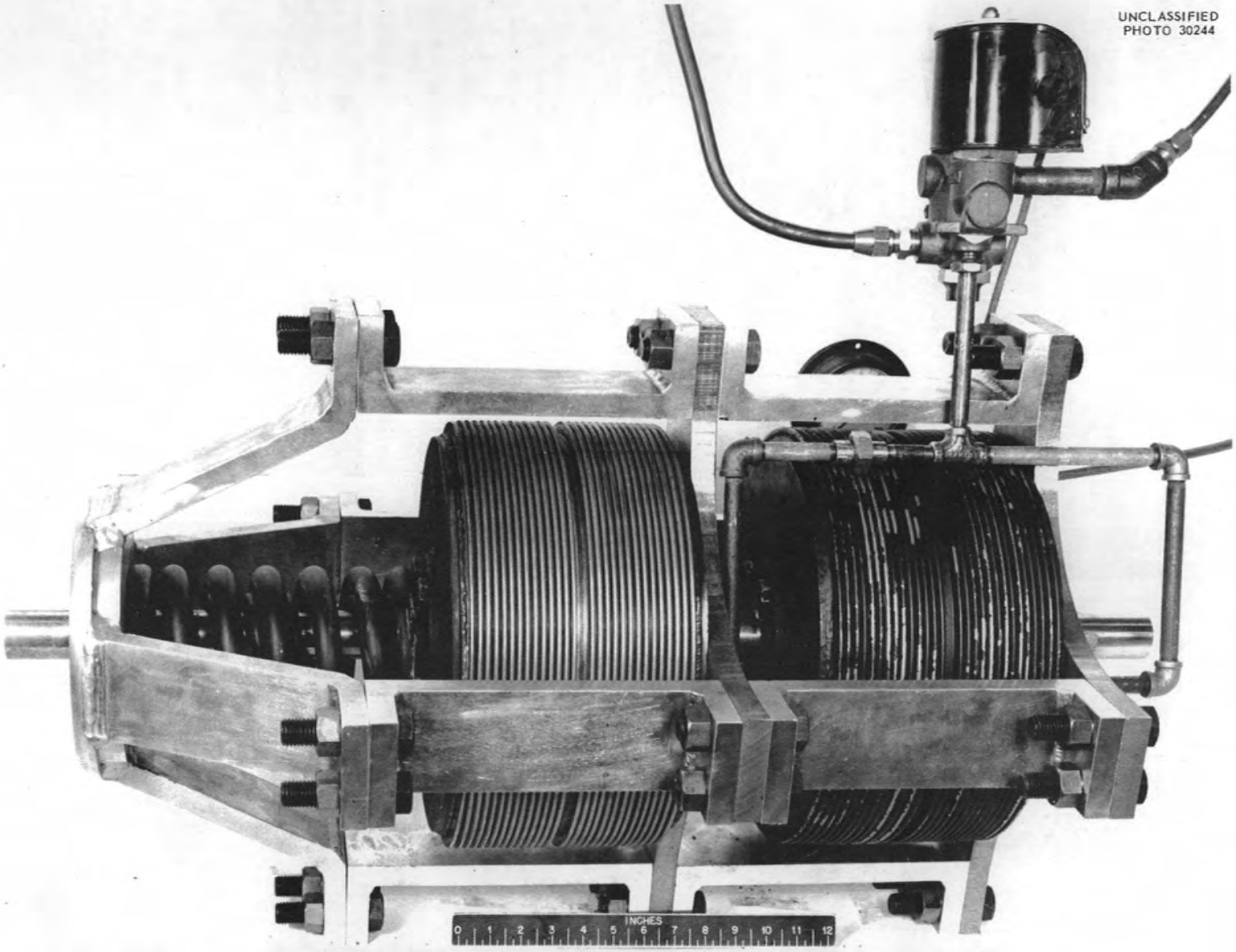

Fig. 11.6. Prototype Actuator for Large Valves.

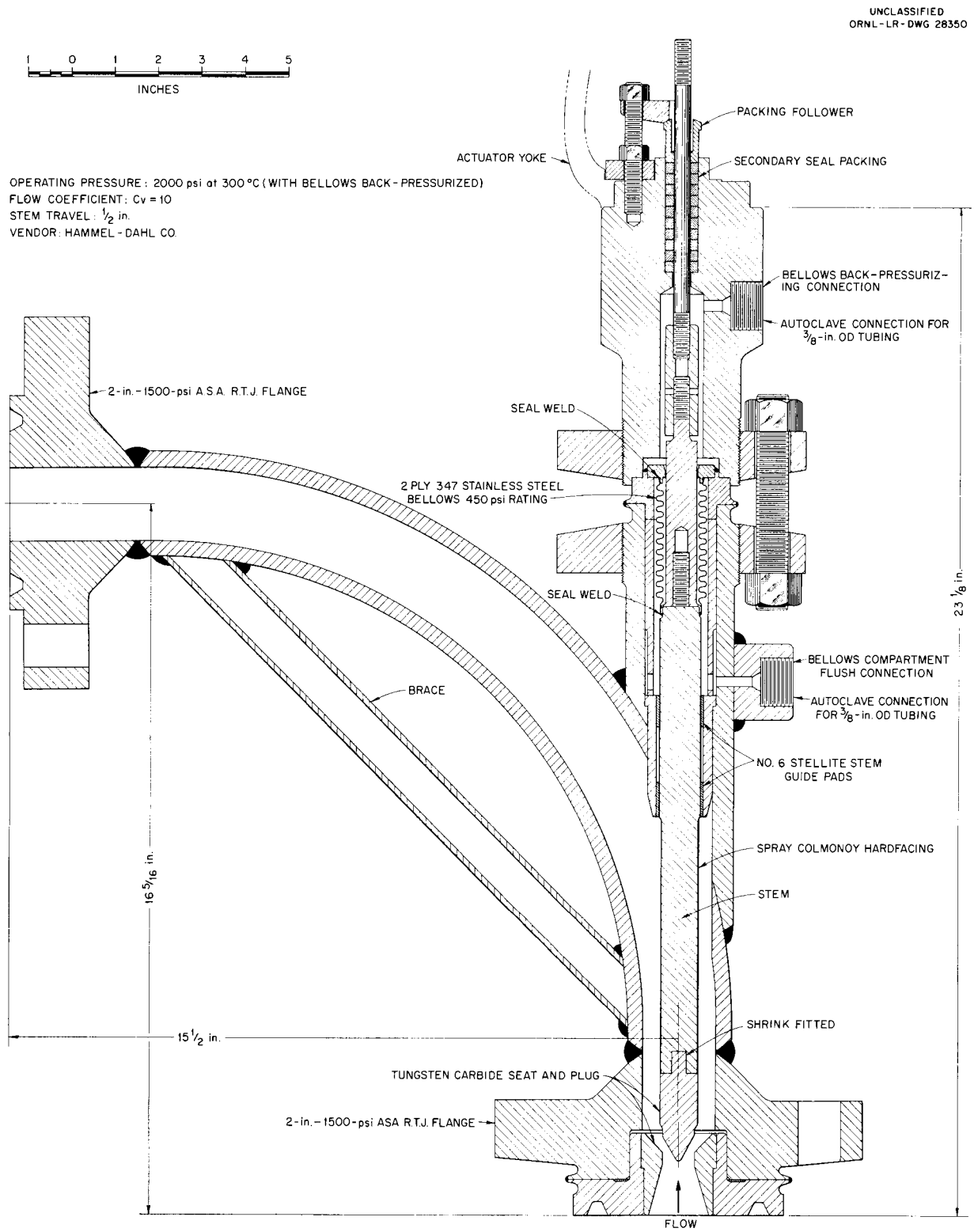

Fig. 11.7. Long-Sweep Angle Valve for Slurry Service.

as to require replacement of the Stellite No. 6 plug and the 17-4 PH seat.

Valve V-166 had been in the system for approximately 3400 hr. During this period some 373 slurry samples were taken through the valve, with a system pressure of 300 psi at a temperature of 150 to 200°C. Since other valves and piping served to reduce the pressure, the actual pressure drop across the valve is unknown. The valve was open approximately 5 min for each sample. Erosion of trim is shown in Fig. 11.8. Three valves, V-75, V-168, and V-169, had substantially the same service history but were found to be in excellent condition.

Valve V-76, the second valve which required plug replacement, was used for 37 samples or approximately 3 hr of actual flow at a pressure drop close to 300 psi. In addition, the valve was used during eight feeding cycles for about 7 hr. During sampling and feeding operations the fluid in the valve was a low-thorium-content slurry.

UNCLASSIFIED
T 14172

V-166 PP-50-1
AFTER 3400 HOURS SERVICE IN SBM LOOP

Fig. 11.8. Eroded Sampling Valve Trim.

For a final cycle of 8 min, the fluid was UO_3 slurry at a negligible pressure drop.

Valve trim of tungsten carbide and of chromium carbide is being procured for test and evaluation in these sampling applications.

Part IV

REACTOR MATERIALS RESEARCH

E. G. Bohlmann

12. SOLUTION CORROSION[1]

J. C. Griess
S. E. Bolt
S. R. Buxton
J. L. English
H. C. Savage
R. S. Greeley
D. N. Hess
P. D. Neumann
W. C. Ulrich

12.1 DYNAMIC SOLUTION CORROSION

12.1.1 Corrosion in Water at 300°C

Since the boiler water in the HRT steam system may contain as much as 2 ppm oxygen due to radiolytic decomposition,[2] several runs were made in order to determine the effect of low oxygen concentrations on the corrosion of carbon and stainless steel in boiler water at 300°C. By use of the letdown system described previously[3] and with fresh solution being added continuously, the water was controlled at pH 9 to 11 with 60 ppm phosphate, as recommended for the HRT steam system.[2]

In 200-hr tests the average corrosion rate of carbon steel grade SA-212-B increased from 4 mpy in the presence of less than 0.1 ppm oxygen to 12 mpy with 2 ppm oxygen and to 22 mpy with 10 ppm oxygen. Type 347 stainless steel corroded at 1.6 mpy or less under these conditions. Although these rates would be expected to decrease with time owing to buildup of film, the carbon steel pitted extensively in the presence of oxygen; thus the actual penetration rates were greater than those quoted above. Every effort should be made to keep the oxygen concentration of the HRT steam-system boiler water as low as possible.

Further tests were made at 300°C similar to those at 250°C reported previously[4] in which no attempt was made to maintain the phosphate concentration or the pH of the water constant by continuous replacement. Oxygen concentrations of less than 0.1, 4 to 11, 50 to 500, and 700 to 1500 ppm were used. Corrosion rates of carbon steels increased with increasing oxygen concentration up to about 25 mpy at 50 to 500 ppm and then decreased slightly at 700 to 1500 ppm. The rates appeared to depend as much on the final pH and chromium(VI) concentration of the solution as on the oxygen concentration. The carbon steels pitted in the presence of oxygen but to a lesser extent than at 250°C. Stainless steels corroded at about 1 mpy or less in each run. Zircaloy-2, titanium RC-55, and niobium were relatively unaffected by oxygen concentration, generally showing weight increases or slight weight losses. Carbon steel AISI type C1010 nickel-plated to a thickness of about 0.002 in. by an electroless process[5,6] gave excellent corrosion resistance, showing rates 10 to 20 times lower than those for unplated AISI C1010.

12.1.2 Corrosion Resistance of Several Alloys at 200 to 295°C in 0.17 *m* UO_2SO_4

The corrosion resistance of a number of alloys not previously tested and of three alloys hardened by appropriate heat treatment was compared with the resistance of the austenitic stainless steels in 0.17 *m* UO_2SO_4 at 200 to 295°C. Table 12.1 lists the weight losses observed for several of the alloys tested. At 200°C all the alloys except Hastelloy B were covered with a partially protective coating at all flow rates. At 250°C most of the alloys exposed at 5 to 11 fps developed protective coatings, but at the higher flow rates either no coating or only a partial coating formed. Those alloys showing low weight losses at 295°C developed protective films, whereas those showing high weight losses did not. If the weight losses of the other alloys are compared with those of

[1] Reported in greater detail by J. C. Griess *et al.*, *Quarterly Report of the Solution Corrosion Group for the Period Ending Jan. 31, 1958*, ORNL CF-58-1-72 (in press).

[2] H. A. McLain, *Treatment of the HRT Steam System Water*, ORNL CF-56-11-132, p 2 (Nov. 29, 1956).

[3] J. C. Griess *et al.*, *HRP Quar. Prog. Rep. July 31, 1957*, ORNL-2379, p 69.

[4] J. C. Griess *et al.*, *HRP Quar. Prog. Rep. April 30, 1957*, ORNL-2331, p 87–88.

[5] A. Brenner, *Metal Finishing* 52(11), 68; (12), 61 (1954).

[6] A. Brenner, National Bureau of Standards, private communication to J. A. Swartout (May 2, 1951).

type 347 stainless steel, it can be seen that equally good corrosion resistance was shown by the following: types 430, 431, 446, AM-350, and Croloy 16-1 stainless steel; Incoloy; Carpenter 10, 20, and 20 Nb; CD4MCu; Hastelloy R-235; Multimet; and Timken 16-25-6. Types 430, 446, and Croloy 16-1 are ferritic steels, whereas the 431 and AM-350 steels are martensitic and hardenable by appropriate heat treatment. In the hardened condition types 431 and AM-350 showed

Table 12.1. Averaged Weight Loss of Different Alloys in 0.17 *m* Uranyl Sulfate Solution at 200, 250, and 295°C for 200 hr

Alloy	Average Defilmed Weight Loss (mg/cm^2)					
	200°C		250°C		295°C	
	5–11 fps	21–43 fps	5–11 fps	21–43 fps	5–11 fps	21–43 fps
347	6.0	6.9	22	69	2.9	11
347 Cr PA[a]		0.87		5.5		120
347 Cr PB[b]		0.78		9.2		120
414 annealed	20	33	21	23	23	27
414 hardened	20	23	13	14	17	17
430	9.2	13	5.5	51	1.5	2.5
431 annealed	9.7	9.7	5.1	6.4	4.0	2.9
431 hardened	12	13	6.0	14	4.2	4.0
446	8.3	10	5.1	10	1.7	2.4
Croloy 16-1	6.4	10	2.8	6.4	1.5	1.7
1515N	12	14	25	97[c]	2.5	13
AM-350 annealed	5.1	6.9	5.5	16, 92[c]	1.8	2.9
AM-350 hardened	4.6	6.9	5.5	13, 110[c]	2.0	2.3
CD4MCu	4.3	4.2	14	83	4.1	78
Carpenter 10	8.3	8.3	12	87	3.0	26
Carpenter 20	3.4	4.1	30	78	6.9	150
Carpenter 20 Cb	3.7	3.7	16	60	9.2	92
Hastelloy B	>2600	>2600				
Hastelloy C	33	36	160	240	360	1100
Hastelloy R-235	6.9	6.4	35	110	13	130
Hastelloy X	8.7	11	64	120	43	270
Haynes 25	6.0	6.0	64	87	280	460
Incoloy	8.3	8.7	24	100	6.9	17
Multimet	6.9	7.4	29	120	7.4	190
Nionel	11	11	32	130	18	190
Timken 16-25-6	4.5	8.7	11	97	3.5	55

[a]Chromium plated 0.0002 in. by Electrolyzing Corp., Chicago Heights, Ill.
[b]Chromium plated 0.0005 in. by Electrolyzing Corp., Chicago Heights, Ill.
[c]Each value for one pin.

no difference in corrosion resistance from that shown in the annealed condition. Incoloy and the Carpenter materials are alloys of possible use in the homogeneous reactor program. CD4MCu is an alloy which may be used as cast or wrought and can be hardened by aging. Hastelloy R-235, Multimet, and Timken are high-strength alloys of possible interest as bolt materials.

Showing greater corrosion resistance than type 347 stainless steel at 200 and 250°C but poorer resistance at 295°C were type 347 stainless steel specimens chromium plated to a thickness of 0.0002 and 0.0005 in. by an electrolyzing process. Showing slightly poorer resistance than type 347 at all temperatures were Nionel and type 1515 N stainless steel; and showing considerably poorer resistance were Hastelloys B, C, and X, Haynes 25, and stainless steel type 414. The compositions of the alloys and the heat treatments given have been listed in other reports.[7,8]

12.1.3 Stability of Dilute Uranyl Sulfate Solutions

Previous work[9] has shown that 0.04 *m* UO_2SO_4 containing 0.005 *m* $CuSO_4$ must be made about 0.02 *m* in H_2SO_4 to prevent hydrolytic precipitation of uranium and/or copper at 300°C. In order to determine whether decreasing the uranium concentration or increasing the copper concentration would affect solution stability, four runs were made (in light-water solution) with 0.02 *m* UO_2SO_4 containing 0.02 or 0.03 *m* $CuSO_4$ and various amounts of sulfuric acid.

A solution containing 0.02 *m* UO_2SO_4, 0.03 *m* $CuSO_4$, and 0.02 *m* H_2SO_4 was stable for 1000 hr at 300°C, whereas 0.02 *m* UO_2SO_4 solutions containing 0.02 or 0.03 *m* $CuSO_4$ with 0.006 to 0.01 *m* H_2SO_4 were not stable within 1000 hr at 300°C. Therefore, since as much sulfuric acid (0.02 *m*) is needed to stabilize these solutions as those studied previously, there appears to be no significant effect achievable through decreasing the uranium concentration by a factor of 2 or through increasing the copper concentration by a factor of 4 to 6. Corrosion of stainless steel likewise was not significantly affected by the changes in uranium or copper concentrations.

12.1.4 Circulation of Uranyl Carbonate Solutions at 250 to 300°C

Previous corrosion tests with dilute uranyl carbonate–lithium carbonate–carbon dioxide solutions have produced very low corrosion rates at 250°C with many materials, including carbon and stainless steels.[10] Similar tests have now been made at temperatures up to 300°C. Corrosion rates of carbon steels were between 1 and 5 mpy and of austenitic and ferritic stainless steels between 0.5 and 3 mpy.

However, the solutions were not stable. In the first run at 300°C with a solution containing initially 0.19 *m* Li_2CO_3 and 0.03 *m* UO_3, precipitation occurred, so that after 24 hr the solution contained only 0.06 *m* Li_2CO_3 and 0.002 *m* UO_3 (about 0.5 g of U per liter). Increasing the carbon dioxide pressure in the system from 200 to 600 psi failed to increase the solubility. In a second run at 300°C, uranium and lithium precipitated from a solution initially containing 0.25 *m* Li_2CO_3 and 0.06 *m* UO_3 (15 g of U per liter); within 150 hr the solution contained only 0.07 *m* Li_2CO_3 and 0.004 *m* UO_3 (1 g of U per liter). In the third run the temperature was increased stepwise from 250 to 260, 265, 270, and 280°C. The uranium concentration fell successively from 0.03 *m* to 0.01, 0.005, 0.002, and 0.001 *m*, respectively, in a solution containing initially 0.2 *m* Li_2CO_3. Therefore the uranyl carbonate–lithium carbonate system does not appear to be useful for operation at temperatures much above 250°C.

12.1.5 Circulation of 0.04 *m* UO_2SO_4 Containing 0.04 *m* $BeSO_4$

It was reported previously that corrosion rates of type 347 stainless steel in 0.04 *m* UO_2SO_4 containing 0.04 *m* $BeSO_4$ and 0.005 *m* $CuSO_4$ were lower at 200 to 250°C than in HRT solution (0.04 *m* UO_2SO_4 + 0.02 *m* H_2SO_4 + 0.005 *m* $CuSO_4$)

[7] Alloy compositions are given by J. C. Griess *et al.*, *Quarterly Report of the Solution Corrosion Group for the Period Ending April 30, 1957*, ORNL CF-57-4-55, p 18; *July 31, 1957*, ORNL CF-57-7-121, p 55; *Jan. 31, 1958*, ORNL CF-58-1-72 (in press).

[8] Heat treatments are given by J. C. Griess *et al.*, *Quarterly Report of the Solution Corrosion Group for the Period Ending Jan. 31, 1958*, ORNL CF-58-1-72 (in press).

[9] J. C. Griess *et al.*, *HRP Quar. Prog. Rep. July 31, 1957*, ORNL-2379, p 73.

[10] J. C. Griess *et al.*, *HRP Quar. Prog. Rep. April 30, 1956*, ORNL-2096, p 82.

but that the specimens did not film over during 200-hr tests.[11] In order to determine whether stainless steel specimens would film over after longer times, 500- and 1000-hr runs were made with the beryllium-containing solution at 200°C, and 500-hr runs were made at 225 and 250°C. The specimens did film over within 500 hr at each temperature, up to a critical velocity of 15 to 20 fps at 200 and 225°C and of 20 to 30 fps at 250°C. Corrosion rates above the critical velocity were lower by a factor of 5 than rates in HRT solution at the same temperature. However, the film formation at 200°C appeared to depend on a buildup of chromium(VI) in solution. Since chromium(VI) is apparently not stable in radiation fields, it is not known whether stainless steel specimens would develop protective films in reactor experiments.

In order to determine the stability of the above beryllium-containing solution, a 1000-hr run was made at 300°C. The loop was thermally cycled to 200°C twice to find out whether any precipitates would redissolve at the lower temperature. The uranium and copper concentrations were constant within ±5 and ±15%, respectively. However, beryllium precipitated at 300°C and redissolved at 200°C, and the room-temperature pH of the solution changed reversibly from 2.0 at 300°C to 3.0 at 200°C. Although the solution was not stable at 300°C (with regard to beryllium only), it is possible that the solution would be stable at 280°C; or it may be possible by adjustment of the beryllium sulfate concentration to develop a solution that would be stable at 300°C. The fact that the addition of sulfate ions to uranyl sulfate solutions substantially reduces the in-pile corrosion of Zircaloy-2 (and possibly other alloys) seems to warrant further studies in the beryllium sulfate–uranyl sulfate system.

12.1.6 Combustion of a Titanium Nipple in Oxygen at Room Temperature

Recently, in the course of readying an all-titanium loop for a run, about 175 psig oxygen pressure was applied to the inside of the loop at room temperature to aid in forcing out a small piece of Teflon which had previously become wedged into a $\frac{3}{8}$-in. titanium nipple on the loop. When the piece of Teflon was being pried out with a short file, a spark was observed, and the Teflon piece became dislodged suddenly. As the oxygen rushed out, $\frac{3}{8}$ in. of the titanium-75A nipple was consumed in a flash of flame.

The incident is an example of a titanium-oxygen reaction at moderate pressure and room temperature. In work being performed on subcontract to the Laboratory, these reactions are being investigated in more detail.[12]

12.2 LABORATORY CORROSION STUDIES

12.2.1 Stress-Corrosion Cracking in Uranyl Sulfate Solution

(a) Effect of Solution Components. – Previous tests have demonstrated that stressed type 347 stainless steel is susceptible to cracking in boiling solutions containing 0.04 *m* UO_2SO_4, 0.02 *m* H_2SO_4, 0.005 *m* $CuSO_4$, and 25 to 500 ppm chloride.[13,14] Tests have been conducted recently to determine what component of the solution other than chloride is responsible for stress corrosion.

Each test solution contained 50 ppm chloride added as potassium chloride and was run at atmospheric boiling with aeration. Duplicate or triplicate stress specimens were used in each test. In two tests potassium sulfate replaced the uranyl sulfate, and in other tests only selected components of the HRT core solution were present.

The results of the tests are reported in Table 12.2. In control tests with a 0.04 *m* UO_2SO_4–0.02 *m* H_2SO_4–0.005 *m* $CuSO_4$ solution containing 50 ppm chloride, five of six stress specimens cracked during a 400-hr exposure; four of the five specimens cracked during the first 50 hr. The specimens in solutions containing potassium in place of uranyl ions did not crack during a 2500-hr test. Similarly, no cracking was experienced in the UO_2SO_4–H_2SO_4, UO_2SO_4–$CuSO_4$, H_2SO_4, or $CuSO_4$ solutions after periods from 200 to 1500 hr. However, in the solution containing 0.04 *m* UO_2SO_4, three of eight specimens cracked during the initial 50 hr of the 200-hr test.

[11] J. C. Griess *et al.*, *HRP Quar. Prog. Rep. April 30, 1957*, ORNL-2331, p 84–85.

[12] See, for example, G. M. Adamson *et al.*, *HRP Quar. Prog. Rep. Oct. 31, 1957*, ORNL-2432, p 137.

[13] J. C. Griess *et al.*, *HRP Quar. Prog. Rep. April 30, 1957*, ORNL-2331, p 90–91.

[14] J. C. Griess *et al.*, *HRP Quar. Prog. Rep. Oct. 31, 1957*, ORNL-2432, p 82–83.

Table 12.2. Effect of HRT Core Solution Components on Stress-Corrosion Cracking Behavior of Type 347 Stainless Steel: Atmospheric Boiling with 50 ppm Chloride

Solution	No. of Specimens	Total Time (hr)	Cracking
0.04 *m* UO_2SO_4 0.02 *m* H_2SO_4 0.005 *m* $CuSO_4$	6	400	Observed on 5 specimens; 4 of 5 specimens cracked in 50 hr or less
0.04 *m* K_2SO_4 0.02 *m* H_2SO_4 0.005 *m* $CuSO_4$	2	2500	None observed
0.04 *m* K_2SO_4 0.02 *m* H_2SO_4	2	2500	None observed
0.04 *m* UO_2SO_4 0.02 *m* H_2SO_4	2	1000	None observed
0.04 *m* UO_2SO_4 0.005 *m* $CuSO_4$	3	300	None observed
0.02 *m* H_2SO_4	2	1000	None observed
0.005 *m* $CuSO_4$	3	200	None observed
0.04 *m* UO_2SO_4	8*	200	Observed on 3 specimens

*Two separate tests.

Thus, in the presence of chloride, the preliminary experimental data indicate that cracking of type 347 stainless steel can be initiated in two systems at atmospheric boiling, namely, the 0.04 *m* UO_2SO_4–0.02 *m* H_2SO_4–0.005 *m* $CuSO_4$ solution and the 0.04 *m* UO_2SO_4 solution. Cracking has not been observed thus far in other solutions of the compositions listed in Table 12.2. Additional testing will be required in the latter cases, however, before final conclusions may be reached.

Additional evidence pointing to the uranyl ion as having an important role in the stress-corrosion cracking process was obtained from the K_2SO_4-H_2SO_4-$CuSO_4$ test. Upon completion of the 2500-hr exposure, during which no cracking was observed, the duplicate stress specimens were acid-pickled to expose fresh surfaces and were returned to the original solution. Uranyl sulfate was added to make the solution 0.04 *m*, and the test was continued at atmospheric boiling. During the initial 200 hr, one of the two specimens cracked; the test is being continued.

(*b*) **Effect of Preformed Films.** – Additional information has been obtained on the effect of preformed films on the stress-corrosion cracking behavior of type 347 stainless steel in chloride-containing HRT core solution. Preliminary results have been reported.[14] It was found that no cracking occurred on U-bend stress specimens whether the specimens were prefilmed in chloride-free, boiling HRT core solution (0.04 *m* UO_2SO_4–0.02 *m* H_2SO_4–0.005 *m* $CuSO_4$) before or after stressing.

Present tests consisted of exposing stressed specimens for periods of 50, 200, and 500 hr in boiling and aerated chloride-free HRT core solution. The specimens were then placed in a similar solution to which 50 ppm of chloride was added.

Seventeen stress specimens treated in the above manner have been exposed for periods ranging from 200 to 2000 hr in the chloride-containing environment. Thus far, none of the specimens have exhibited any evidence of cracking. In control tests with stress specimens not subjected

to the prefilming treatment, 75% of the specimens cracked in 50 hr or less; 85% of the specimens cracked in 400 hr or less. It appears, on the basis of the preliminary data, that a preformed film is effective for protecting type 347 stainless steel (and presumably other austenitic grades) from chloride-induced cracking in boiling uranyl sulfate solution. Future work will be concerned with the effect of temperature on the effectiveness of the prefilming process.

12.2.2 Stress-Corrosion Cracking in Chloride-Containing Water

(*a*) **Effect of Oxygen.** – Previous work[15,16] has demonstrated that distilled water containing 25 to 100 ppm chloride at pH values of 2.8 to 10.5 can produce cracking in stressed type 347 stainless steel in the temperature range of 150 to 300°C. Furthermore, the time to the appearance of cracks appeared to be independent of the dissolved-oxygen concentration in the range from 10 to 1200 ppm.

In order to determine the susceptibility of type 347 stainless steel to cracking in chloride-containing water in the absence of oxygen, tests were run at 300°C in solutions containing 100 ppm chloride at adjusted pH values of 2.8, 6.5, and 10.5. After the stress specimens and solution had been placed in the autoclave, a double freezing–vacuum-degassing treatment was used to remove the oxygen. After 400 hr, four of six U-bend specimens in solutions with initial pH values of 2.8 and 10.5 had cracked. No cracks were observed after 400 hr in specimens exposed to the pH 6.5 solution.

Since some doubt exists with regard to the efficiency of the degassing operation, it cannot be stated with certainty that the cracking occurred in the absence of oxygen. Tests are being run in which sodium sulfite has been added to solutions (pH = 6.5 and 10) as an oxygen scavenger. To date, the testing time has been 300 hr, and no cracks have appeared. Residual sulfite concentrations of 15 to 80 ppm at the end of each 100-hr period indicate the complete removal of oxygen. The tests are being continued.

U-bend test specimens exposed to a solution containing 25 to 500 ppm chloride at a pH of 2.8 and boiling in air (100°C) showed no tendency to crack after 3000 hr. Since the solution was boiling in the presence of only 3 psi oxygen, the concentration of dissolved oxygen in the solution was very low. To see what effect additional oxygen would have at 100°C, eight specimens were exposed in the same solution as above in an autoclave to which 150 psi oxygen was added. The test was run at 100°C. After 400 hr, seven of the eight specimens had developed cracks. These experiments demonstrate the importance of oxygen in the cracking process under the conditions of test.

(*b*) **Effect of Preformed Films.** – The effect of preformed films in eliminating the incidence of cracking in type 347 stainless steel exposed in boiling, chloride-containing uranyl sulfate solution was described previously. To determine whether similar results could be produced in high-temperature distilled water containing chloride, stress specimens were prefilmed in chloride-free distilled water at 300°C for 100 hr and in a 500-ppm chromate (as sodium chromate) solution at 300°C for 100 hr. Upon exposure at 200°C to distilled water containing 100 ppm chloride, all stress specimens cracked in less than 100 hr. Thus films formed at high temperature are not effective in protecting type 347 stainless steel from stress-corrosion cracking in chloride-containing water at 200°C. The effectiveness of films formed at lower temperatures will be tested next.

(*c*) **Effect of Alloy Composition.** – The results reported thus far have been concerned with the behavior of type 347 stainless steel only. To determine the effect of the alloy composition on the susceptibility to cracking, several different alloys have been tested in water containing 100 ppm chloride at 300°C. All tests were run (or are being continued) in the presence of oxygen. The pH of the solution was adjusted with either hydrochloric acid or sodium hydroxide. The conditions of the tests and the results obtained to date are shown in Table 12.3. The condition of the alloy refers to the condition prior to stressing.

All the austenitic stainless steels except type 309 SCb have shown evidence of transgranular cracking in 300 hr or less. Even the cracks in

[15] J. C. Griess *et al.*, *HRP Quar. Prog. Rep. July 31, 1957*, ORNL-2379, p 69, esp 78–79.

[16] J. C. Griess *et al.*, *HRP Quar. Prog. Rep. Oct. 31, 1957*, ORNL-2432, p 83.

Table 12.3. Stress-Corrosion Cracking Behavior of Various Alloys at 300°C in Distilled Water with 100 ppm Chloride (Saturated with Air at Room Temperature)

Alloy Type	Condition	Solution pH	Test Time (hr)	Observations
304	Annealed	2.8	100	Cracked
304	Annealed	10.5	100	Cracked
304	Sensitized	2.8	100	Cracked
304	Sensitized	10.5	100	Suspected cracks
304 ELC	Annealed	2.8	300	Surface crazing; few pits
309 SCb	Annealed	2.8	200	No cracks
316	Annealed	2.8	200	Cracked
321	Annealed	2.8	200	Cracked
321	Annealed	10.5	200	No cracks
Carp. 7-Mo	Annealed	2.8	300	Suspected cracks; moderate generol corrosion
Carp. 7-Mo	Annealed	10.5	300	No visible cracks; thin hard film
Carp. 7-Mo	Full hard	2.8	100	Cracked; moderate general corrosion
Carp. 7-Mo	Full hard	10.5	100	No visible cracks
Croloy 16-1	Annealed	2.8	600	Severe pitting; thick scale; no cracks
	Annealed	6.5	200	Severe pitting; no cracks
	Annealed	10.5	400	Severe pitting; no cracks
Incoloy	Annealed	2.8	500	Severe pitting; heavy corrosion; cracked
	Annealed	6.5	100	Light general corrosion; no cracks
	Annealed	10.5	300	Few small pits; light corrosion; no cracks
Nionel	Annealed	2.8	200	Heavy loose scale; no cracks
	Annealed	6.5	100	Deep pits; thick scale; no cracks
	Annealed	10.5	100	Light general corrosion; no cracks

sensitized type 304 stainless steel were predominantly transgranular. Further testing with type 309 SCb stainless steel is in progress. Carpenter 7-Mo stainless steel showed evidence of cracking both in the annealed and in the hardened condition when the solution pH was 2.8, but no cracks have been observed in the solution at a pH of 10.5 during the relatively short test periods. Both Nionel and Incoloy are reportedly more resistant to cracking in chloride environments than are the austenitic stainless steels, and the present tests seemed to confirm this. Cracks were found only in Incoloy exposed at a pH of 2.8 (Fig. 12.1). The pitting and general attack of the alloys were dependent on the pH of the solution. Croloy 16-1 stainless steel did not crack during the 600-hr test period, but pitting was appreciable at all pH values. Exposure of Croloy 16-1 to boiling 42% $MgCl_2$ for 100 hr did not produce any cracks visible at 15X magnification. However, metallographic examination at higher magnification located two transgranular cracks in the specimen (Fig. 12.2).

The results to date substantiate data obtained from the boiling 42% $MgCl_2$ tests and indicate that the class of alloys most susceptible to

Fig. 12.1. Stress-Corrosion Cracks in Incoloy After Exposure for 500 hr to Oxygenated Distilled Water Containing 100 ppm Chloride at pH 2.8. 250X.

Fig. 12.2. Stress-Corrosion Cracks in Croloy 16-1 After Exposure for 100 hr to 42% $MgCl_2$ Solution at 154°C. 250X.

stress-corrosion cracking in chloride environments is the austenitic stainless steels. Increasing the nickel content appeared to reduce the susceptibility to cracking, and in the case of Nionel (40% Ni) no cracking was observed. Croloy 16-1 is not austenitic and was not expected to crack.

12.2.3 Corrosion Behavior of Electroless Nickel Plate

The corrosion resistance of carbon steel in oxygenated steam or in water can be markedly improved by depositing on the surface of the steel a thin layer of nickel by means of a nonelectrolytic process developed by the National Bureau of Standards.[17] Coupons of SAE 1045 carbon steel plated to a thickness of 2 mils by this method were tested at 300°C in distilled water under various pH conditions. After 200 hr, all corrosion rates were less than 1 mpy. No significant pitting was observed, but the plate was chipped at some of the sharp corners, indicating the necessity of careful design and preparation of parts to be protected by this method. Shallow pitting attack developed at the areas where the nickel coating was chipped.

12.2.4 Miscellaneous Corrosion Tests

The corrosion behavior of a number of materials of possible interest to the Homogeneous Reactor Project was examined in several reactor-related environments. The materials included Incoloy; AM-350 stainless steel; Stellites 1, 3, and 98M2; Rexalloy 33; and type 202 stainless steel.

(a) Incoloy. – Incoloy was examined because of its resistance to stress-corrosion cracking. Present tests were concerned with the general corrosion resistance and the stress-corrosion cracking behavior of the alloy in oxygenated 0.04 *m* UO_2SO_4–0.02 *m* H_2SO_4–0.005 *m* $CuSO_4$ solution at temperatures of 100, 200, and 300°C and in boiling 5% HNO_3 and 42% $MgCl_2$ solutions. The alloy exhibited excellent corrosion resistance in the uranyl sulfate solution at all temperatures; the average 1000-hr corrosion rates were not greater than 1 mpy. Stressed specimens exposed at 300°C showed no tendency to crack. In boiling 5% HNO_3 solution the observed rate was only 0.1 mpy.

[17] A. Brenner, National Bureau of Standards, private communication to J. A. Swartout (May 2, 1951).

Stress specimens were exposed in boiling 42% $MgCl_2$ solution and in boiling uranyl sulfate solution containing 50 ppm chloride. After 1000 hr in the uranyl sulfate solution, there were no visible cracks on the Incoloy. The 42% $MgCl_2$ test was run for 100 hr, during which period no cracking occurred. Examination at 90X of specimens from both tests disclosed an appearance which suggested a superficial crazing, however.

Thus in static systems Incoloy seems to have a general corrosion resistance comparable with that of type 347 stainless steel and a resistance to stress-corrosion cracking in chloride-containing environments superior to that of type 347.

(b) Type AM-350 Stainless Steel. – Although not classed as a true precipitation-hardening alloy, type AM-350 stainless steel is nevertheless considered as a member of this group.[18] The nominal composition of the alloy is 0.10% C max, 16.25 to 17.25% Cr, 4 to 4.5% Ni, 2.5 to 3% Mo, and balance iron. In the present tests, the corrosion behavior of the material in four different conditions of heat treatment was examined in simulated HRT core solution (0.04 *m* UO_2SO_4–0.02 *m* H_2SO_4–0.005 *m* $CuSO_4$) at temperatures of 100, 200, and 300°C, and in boiling 5% HNO_3 solution. All specimens were annealed at 1950°F and air cooled before receiving subsequent treatment. The various heat treatments produced hardnesses ranging from 92 Rockwell B to 49 Rockwell C. Results of the tests appear in Table 12.4.

In all conditions tested in oxygenated uranyl sulfate solution at 100 and 300°C, corrosion rates after 1000 hr were 0.6 mpy or less. Several weld specimens in the cooled and tempered condition (AM-350 welded to type 347 stainless steel) corroded at slightly higher rates of 0.7 and 1.5 mpy. Corrosion attack on the heat-treated alloy at 200°C in uranyl sulfate solution was greater; rates ranged from 5 to 11 mpy after 1000 hr. Corrosion rates of the alloy in the annealed and subzero-cooled conditions in boiling 5% HNO_3 solution during 1000-hr tests did not exceed 0.5 mpy. Specimens in the aged condition corroded at a rate of 3 mpy, however. The alloy in the subzero-cooled and tempered (750°F) condition was found to be susceptible to stress-corrosion cracking in boiling and oxygenated HRT core solution containing 50 ppm chloride; cracking in a stress specimen occurred during the first 50 hr of test. No cracking took place on a stress specimen in a similar heat-treated condition during 1000 hr in boiling, chloride-free HRT core solution.

(c) Stellites 1, 3, and 98M2 and Rexalloy 33. – Four materials of interest to the HRP injection-pump program were tested in boiling and aerated 0.04 *m* UO_2SO_4 solution containing 0.02 *m* H_2SO_4 and 0.005 *m* $CuSO_4$. The materials included Stellites 1, 3, and 98M2 and Rexalloy 33. All

[18] D. B. Roach and A. M. Hall, *The Engineering Properties of Precipitation-Hardenable Stainless Steels, TML-48*, p 6 (July 20, 1956).

Table 12.4. Corrosion Behavior of Type AM-350 Stainless Steel in Reactor-Related Environments

(Test Time: 1000 hr)

Heat Treatment	Hardness (Rockwell C)	Corrosion Rate (mpy)			
		5% HNO_3	HRT Core Solution		
		100°C	100°C	200°C	300°C
Annealed	92 Rockwell B	0.5	<0.1	11.0	0.4
– 100°F (2 hr)	39	0.3	0.1	4.8	0.6
– 100°F (2 hr)	49*		0.5		
750°F (1 hr)					
1350°F (1 hr)	32	3.0	0.3	6.5	0.3

*Observed values higher than literature-reported value of 41 Rockwell C.

the materials are cobalt-base alloys containing 2.0 to 2.5% carbon, 30 to 33% chromium, and 12 to 17% tungsten. The Stellite 98M2 corroded at the highest rate, 5 mpy, after 1000 hr in the uranyl sulfate solution. Corrosion rates for the other three alloys ranged from 0.5 to 1.3 mpy. The surfaces of the Stellite 98M2 specimens were uniformly coated with golden-colored crystals; spectrographic analysis showed the major constituent to be tungsten. Hence all the above materials, with the possible exception of Stellite 98M2, showed adequate corrosion resistance to the static uranyl sulfate solution at its boiling point.

(*d*) **Type 202 Stainless Steel.** – A comprehensive series of tests on type 202 stainless steel in sensitized, welded, and annealed conditions is in progress. With one significant exception, the preliminary corrosion data show the alloy to be comparable with type 347 stainless steel in reactor-related environments; in the sensitized condition, severe blistering and intergranular attack accompanied by reduction of copper were observed in a boiling HRT core solution.

13. SLURRY CORROSION

E. L. Compere
S. E. Bolt
J. W. Brown
V. A. DeCarlo
G. W. Eckerd[1]
D. A. Gardiner[2]
D. W. Hubbard
D. T. Jones
H. C. Savage
R. A. Lorenz
S. A. Reed
J. A. Russell, Jr.
W. C. Ulrich
R. M. Warner
L. F. Woo

13.1 100A PUMP LOOP TESTS

13.1.1 Introduction

Current developments in the production of high-fired thoria and in the control of particle-size range by sedimentation classification are related to tests made on the 100A pump loops. Recent circulation tests in both 100A pump loops and toroids have demonstrated that superior handling characteristics and moderate attack of materials of interest for thorium breeder reactor construction are obtainable with aqueous slurries of 1600°C-calcined thoria.[3,4] Further, it has been shown that, in addition to the effect of concentration and flow velocity, the attack of materials by flowing slurries is strongly dependent upon the particle size of the thorium oxide and its rate of attrition during circulation.[5,6] Because 1600°C-calcined thoria undergoes little, if any, degradation during circulation,[3,7] it is essential that the method of preparation of the thoria provide a small-sized material.

Currently, two investigations of production of suitable material are being conducted by the Chemical Technology Division. Associated evaluation studies are being done in the Materials Research Section and are reported below. One production method has been concerned with controlling the particle size of the thorium oxalate, to be subsequently calcined, by adjusting the precipitation conditions as the thorium nitrate and oxalic acid solutions are mixed. Also included are techniques to circumvent sintering during calcination. A second method is concerned with controlling the particle size by means of mechanically degrading the thoria before preparing the slurry.

13.1.2 Effect of Classification on Corrosion by Slurries of High-Fired Thoria Prepared from Jet-Precipitated Thorium Oxalate

Preliminary pilot-plant tests made by the Chemical Technology Division to study the precipitation, filtration, and washing techniques for preparing thorium oxalate for firing to thorium oxide showed that a jet-mixer precipitator produced thoria of small particle size and that varying conditions gave varying particle sizes.[8] Moderate attack rates were observed with one such experimental preparation in screening tests in toroids which employed slurries of thoria of 0.5 to 0.9 μ mean particle size produced by calcining jet-precipitated thorium oxalate at temperatures of 650 to 1600°C.[8] As a result of these tests it was of interest to observe the handling characteristics and the corrosion-erosion attack of slurries of these preparations in larger scale loop tests.

Part of the first pilot lot, batch JP-1, jet-precipitated thorium oxide calcined 4 hr at 1600°C, was circulated in 100A loop run CS-42 in the as-received condition.

As compared with previous batches of 1600°C-calcined thoria which had been tested, batch JP-1 was unique. Although the mean particle size of the preparation determined by sedimentation

[1] Engineering and Maintenance Division.

[2] Mathematics Panel.

[3] E. L. Compere *et al.*, *HRP Quar. Prog. Rep. Oct. 31, 1957*, ORNL-2432, p 87.

[4] *Ibid.*, p 97.

[5] E. L. Compere *et al.*, *HRP Quar. Prog. Rep. Jan. 31, 1957*, ORNL-2272, p 95.

[6] E. L. Compere *et al.*, *HRP Quar. Prog. Rep. Oct. 31, 1956*, ORNL-2222, p 84.

[7] E. L. Compere *et al.*, *HRP Quar. Prog. Rep. July 31, 1957*, ORNL-2379, p 92–93.

[8] J. P. McBride *et al.*, *HRP Quar. Prog. Rep. July 31, 1957*, ORNL-2379, p 152.

analysis was 1.3 μ, unlike previous preparations the batch was composed of particles which were 61% by weight ≤ 2 μ and 28% by weight >10 μ. The latter fraction consisted largely of what appeared to be, by microscopic examination, loose sinters. Previous batches whose mean particle sizes varied from 1.3 to 1.9 μ were composed of particle sizes which followed a more normal distribution curve, that is, the bulk of the material was 1 to 3 μ.

A portion of the original JP-1 batch was used for run CS-42. Eight kilograms of the oxide was injected into the loop while the system was operated under steam pressurization with oxygenated water at 200°C. The charge provided a calculated concentration of 521 g of Th per kg of H_2O.

It was necessary to stop the test after only 5 hr of slurry circulation because of dynamic imbalance of the circulating pump. Subsequent inspection showed this to be due to severe wear of the type 347 stainless steel seal rings and the Graphitar bearings used in the pump.

Attack data of pin and coupon corrosion specimens which were exposed in run CS-42 are shown in Table 13.1. Attack of all materials was high, owing principally to the pronounced erosion of

Table 13.1. Corrosion by Circulating Thorium Oxide Slurries in Loop Tests

	Run Number		
	CS-42	CS-43	BS-19
Hours	5	42	309
Temperature, °C	200	200	280
Concentration, g Th/kg H_2O			
Charged	521	521	427
Average	443	441	323
Calcination temperature, °C	1600	1600	1600
Thoria batch No.	JP-1	LO-25-1	JP-1 classified
Additives	None	None	None
Atmosphere	O_2	O_2	O_2
Average particle size, μ			
Prerun	1.3	1.7	1.7
Postrun	1.3	1.5	1.5
Impeller weight loss, g	11	12	1.5
Loop corrosion rate, mpy	63	9	1.5
Range of pin attack rates, mpy, at given flow velocity			
Velocity, fps			
		Austenitic Stainless Steels	
18 (coupons)	5–74	0.6–2	
22–25	27–57	3–6	0.7–1.0
38–44	150–320	13–24	7–10

Table 13.1 (continued)

	Run Number		
	CS-42	CS-43	BS-19
		Ferritic Stainless Steels	
22–25	34–110	2–5	0.8
38–44	120–180	7–14	4
		Carbon Steels	
18 (coupons)	490–820	82–94	
22–25	560	100	
38–44	590	200	
		Titanium Alloys	
18 (coupons)	2–5	0.5–1.1	
22–25	60–66	3–4	0.3–0.6
38–44	240	16	3–4
		Zirconium Alloys	
12–18 (coupons)	0.0–47	0.1–1.4	
22–25	8–97	1–5	0.0
38–44	310–700	11–34	1.1
55–63 (coupons)	220–330	18–45	
		Gold and Platinum	
22–25	96–120	5–8	0.0–0.5
38–44	630–650	42–47	2–7
		Stellites	
22–25	0.0–32	0–9	
38–44	0.0–100	14–26	
		Hastelloys	
22–25	57–110	9–45	
38–44	300–330	27–80	

the specimens. The over-all system attack rate, calculated from elements detected in the single sample withdrawn from the loop during the 5-hr test, was 63 mpy. The type 347 stainless steel impeller, which was fitted with a Zircaloy-2 front hub, lost 11 g. The front impeller surface and Zircaloy-2 hub both were heavily eroded.

No detectable degradation of the thoria particles occurred during circulation.

The severe abrasion attack noted in run CS-42 was attributed primarily to the high weight fraction of large sinters in the JP-1 thoria which did not degrade during circulation. Therefore the remainder of the batch was classified to remove particles larger than 5 μ before charging to the subsequent test, run BS-19.

The classification was made at room temperature by batch sedimentation with oxalic acid as a

dispersant. The settling interval was estimated by use of Stokes' law. Optimum dispersions were effected by adding sufficient thoria to 0.004 *M* oxalic acid solution to provide a slurry concentration of 250 g of Th per kg of H_2O. The suspension was then blended for 20 min with a Lightnin mixer. After agitation was stopped, the slurry was allowed to settle for 20 min, at which time the upper half of the suspension was siphoned off. The remaining slurry was recycled once again by the same technique.

The thoria was recovered by adjusting the oxalic acid concentration of the suspension to 0.008 *M*, which flocculated the slurry and hastened settling. The supernatant liquid containing considerable fines was then decanted, and the settled solids were dried and ignited at 800°C for 2 hr to remove residual oxalic acid.

A 72% yield of product, which contained 2% by weight of particles $\geq 5\ \mu$, was obtained by the sedimentation classification. The mean particle size of the material was 1.7 μ.

Eight kilograms of the separated product was charged to run BS-19 to provide a calculated circulating slurry concentration of 427 g of Th per kg of H_2O. The test was terminated on schedule after 309 hr of continuous operation with gas pressurization at 280°C.

Attack of pump components and corrosion specimens exposed to the oxygenated slurry in run BS-19 was markedly lower than that observed in run CS-42. The average loop corrosion rate was 1.5 mpy. The type 347 stainless steel impeller used in the circulating pump lost only 1.5 g in the 309-hr period. Wear of other pump components was negligible.

Corrosion rates of BS-19 pin specimens, shown in Table 13.1, were also moderate. At a flow velocity of 22 fps the average attack rate of austenitic stainless steel and titanium-alloy specimens was <1 mpy. There was no detectable attack of Zircaloy-2. At a velocity of 44 fps the average attack of austenitic stainless steels was 8 mpy; titanium alloys, 3.5 mpy; and Zircaloy-2, 1 mpy. There was no detectable degradation of the thoria particles during the circulation period.

Microscopic examination showed no abrasive attack of the specimens exposed at 22 fps. All pins other than those of the noble metals were uniformly covered with a thin adherent corrosion film. Specimens exposed at 44 fps were mildly eroded, principally on the upstream surfaces; however, the eroded areas were filmed over when the specimens were removed from the test loop.

It is clearly evident from the results of runs CS-42 and BS-19 that the particle size of 1600°C-calcined ThO_2 is a major variable in the corrosion-erosion attack by aqueous slurries of these preparations. Large aggregates of the oxide, formed by sintering during a 4-hr firing period at 1600°C, were not readily degraded in the test loop during circulation. A moderate weight fraction of these sinters caused intolerably high attack of materials suitable for reactor construction.

13.1.3 Circulation of Slurry of 1600°C-Calcined Thoria Prepared from Thorium Oxalate Precipitated at 25°C

Batch LO-25-1 thoria, the charge to run CS-43, was prepared by calcining thorium oxalate which was made by batch precipitation of thorium nitrate with oxalic acid at 25°C. The 1600°C-fired product was degraded by passing the dry powder once through a Mikro-pulverizer. The mean particle size of the material was 1.7 μ; however, 15% (by weight) of the particles composing the batch were greater than 5 μ. The large particles, like those in batch JP-1, appeared to be aggregates of smaller particles which had sintered during calcination.

A charge of 17 kg of batch LO-25-1 ThO_2 was injected into the test loop while the system was operated with steam pressurization on oxygenated water at 200°C. The charge provided a calculated circulating slurry concentration of 521 g of Th per kg of H_2O.

The test was stopped after 42 hr of slurry circulation because of excessive vibration in the circulating pump, determined by subsequent examination to be due to severe wear of the seal rings and Graphitar bearings in the pump.

Three slurry samples were withdrawn from the test loop during the short run. From particle-size distribution curves, prepared from sedimentation analysis data of the samples, a sharp decrease in the percentage of particles $>5\ \mu$ was noted during the early period of circulation. After 1.4 hr of circulation 60% of the particles $>5\ \mu$ had been degraded. Little change in particle distribution was observed thereafter.

The incremental system corrosion rate changed accordingly. The attack rates, calculated from corrosion products detected in the samples, were:

53 mpy after 1.4 hr of circulation, 6 mpy for the next 18 hr, and 8 mpy for the following 23 hr, until the test was terminated.

The principal attack was on the type 347 stainless steel impeller and seal rings in the circulating pump. The Zircaloy-2 front hub on the pump impeller was also deeply grooved.

Attack rates of pin and coupon corrosion specimens exposed in the test were relatively high. The data are presented in Table 13.1. In general, all but the carbon steel and Hastelloy specimens displayed moderate rates up to 25 fps. Coupon specimens showed lower attack rates than duplicate pin specimens of the same alloys at comparable velocities. Attack rates of all specimens increased markedly at flow velocities above 25 fps. All specimens were severely eroded at the higher velocities.

The severe initial system attack rate in run CS-43 appeared to be directly attributable to the aggressive erosive action of the large sintered particles of thoria in the slurry. After the sintered material was degraded, corrosion diminished.

A 4% weight fraction of particles $>5\ \mu$ was still present in the slurry when the test was terminated. By microscopic examination, they appeared to be discrete particles rather than loose sinters. It is probable that these particles contributed heavily to the 6- to 8-mpy attack rates observed during the latter period of the run.

In this test and those reported above, no advantage was noted for jet or batch precipitation or for Mikro-pulverization after calcination. However, elimination of particles above $5\ \mu$ was found to result in a much less aggressive slurry.

13.2 TOROIDS

13.2.1 Introduction

Toroid tests during the quarter were concerned with pilot tests of a production batch of jet-precipitated thoria, with early runs in a series of exploratory tests of basic slurry corrosion variables, and with evaluation tests of special and unusual thoria preparations.

13.2.2 Tests with Thorium Oxide Prepared from Jet-Precipitated Thorium Oxalate

Tests were continued during the quarter to evaluate slurries of thorium oxide prepared by calcining jet-precipitated thorium oxalate. Oxygenated slurries of two experimental preparations, one calcined at 1600°C for 4 hr and a second calcined at 1800°C for 1 hr, were circulated at 250 and 280°C in toroids for 300 hr at 26 fps. In one test the proposed recombination catalyst, MoO_3, was added. Corrosion specimens of type 347 stainless steel, titanium 75A, Zircaloy-3A, and SA-212-B carbon steel were exposed in each test.

Corrosion rates, as shown in Table 13.2, were moderate with slurries of 1600°C-calcined preparations at concentrations of 250 to 1000 g of Th per kg of H_2O. At a slurry concentration of 1000 g of Th per kg of H_2O, the addition of 0.05 *M* MoO_3 had no significant effect on attack rates of type 347 stainless steel, titanium 75A, and Zircaloy-3A, but the attack of SA-212-B carbon steel increased approximately sevenfold.

A moderate decrease in the mean Stokes diameter of the thoria particles occurred during circulation.

Corrosion-erosion attack produced by slurries of 1800°C-calcined thoria was generally higher than that which occurred with slurries of 1600°C-calcined thoria at comparable concentrations. This may have been associated with the large (12 μ) original average particle size. A significant change in particle size was noted in the tests employing the 1800°C-calcined material. By sedimentation analysis the mean Stokes diameter of the thoria was reduced from 12 μ to approximately 0.5 μ during the 300-hr circulation period (see Table 13.2). The apparent crystallite size of the oxide, determined by x-ray line broadening, was also markedly reduced during the circulation tests from > 2500 Å to ~ 300 Å. Preliminary data from similar tests employing other oxide preparations calcined at 1800°C support these observations. Additional tests are currently in progress to study the mechanism of degradation of these oxides.

13.2.3 Effect of Atmosphere, Circulation Temperature, and Thoria Calcination Temperature on Attack by Aqueous Slurries

A series of tests has been initiated to study the effect of operating temperature, thoria calcination temperature, and gaseous atmosphere on the corrosion-erosion attack of selected alloys by circulating aqueous slurries in toroids. Slurries of 550, 650, 800, and 1600°C-calcined thoria at a concentration of 1000 g of Th per kg of H_2O are

Table 13.2. Attack by Slurries of Thoria Prepared from Jet-Precipitated Thorium Oxalate

Time: 300 hr
Velocity: 26 fps
Atmosphere: oxygen

Thorium Oxide Batch	Calcination Temperature (°C)	Operating Temperature (°C)	Concentration (g Th/kg H_2O)	Attack Rate* (mpy)				pH, Postrun	Mean Particle Size (μ)	
				347 SS	Ti-75A	SA-212-B Steel	Zircaloy-3A		Prerun	Postrun
JP-1	1600	280	250	2	<1	10	2	6.1	1.3	0.6
JP-1	1600	280	500	1	1	5	2	5.0	1.3	1.1
JP-1	1600	280	1000	4	3	4	2	4.9	1.3	0.8
JP-1 (+ 0.05 *M* MoO_3)	1600	280	1000	3	2	30	3	5.5	1.3	0.5
Jett	1800	250	210	3	2	4	4	5.8	12	0.5
Jett	1800	250	1000	14	9	5	6	11.3	12	0.4
Jett	1800	280	1000	4	8	11	11		12	0.6
Jett	1800	280	1000	6	7	11	12		12	0.6

*Not corrected for slug flow.

being circulated in hydrogen and oxygen atmospheres at circulation temperatures of 100, 150, 200, 250, and 280°C in 300-hr tests. Pin specimens of type 347 stainless steel, Zircaloy-3A, titanium 75A, and SA-212-B mild steel are exposed in each test.

In the oxygenated series, oxygen overpressures are provided by the thermal decomposition of hydrogen peroxide. In the hydrogenated series, the toroids are purged with hydrogen for 15 min and then sealed.

The results of four of the tests which have been completed are presented in Table 13.3.

Type 347 stainless steel, titanium 75A, and SA-212-B steel generally exhibited higher attack rates in hydrogenated tests than in oxygenated tests, irrespective of the test temperature or thoria preparation, whereas attack rates of Zircaloy-3A were not often significantly affected.

The attack of type 347 stainless steel increased moderately in hydrogenated tests with increasing

Table 13.3. Summary of Toroid Experiments Studying the Effects of Hydrogen and Oxygen Atmospheres in Relation to Calcination Temperature and Operating Temperature

Time: 300 hr
Relative velocity: 26 fps
Concentration: 1000 g of Th per kg of H_2O

	Attack Rates (mpy)				pH, Postrun	Average Particle Size (μ)	
	347 SS	Ti-75A	SA-212-B Steel	Zircaloy-3A		Prerun	Postrun
LO-17R (550°C calcined)							
Temperature, 100°C							
Oxygen	0.6	Wt gain	7.1	0.8	7.7	2.3	0.7
Hydrogen	0.9	0.1	51.2	0.5	9.0	2.3	0.6
Temperature, 150°C							
Oxygen	0.8	0.8	6.0	0.8	8.2	2.3	0.7
Hydrogen	4.8	1.3	109	1.8	8.3	2.3	
Temperature, 200°C							
Oxygen	Wt gain	Wt gain	Wt gain	Wt gain	7.4	2.3	0.8
Hydrogen	1.0	0.3	124	0.7	8.9	2.3	0.7
LO-18 (650°C calcined)							
Temperature, 100°C							
Oxygen	0.3	0.2	11.4	0.4	7.6	3.3	0.7
Hydrogen	0.8	0.5	81.4	0.6	8.6	3.3	0.5
Temperature, 150°C							
Oxygen	1.7	0.0	9.3	0.6	7.4	3.3	0.6
Hydrogen	4.4	0.6	173	3.1	7.9	3.3	
Temperature, 200°C							
Oxygen	0.6	0.6	1.2	0.1	7.1	3.3	0.4
Hydrogen	5.8	2.3	126	1.5	7.9	3.3	1.0

Table 13.3 (continued)

	Attack Rates (mpy)				pH, Postrun	Average Particle Size (μ)	
	347 SS	Ti-75A	SA-212-B Steel	Zircaloy-3A		Prerun	Postrun
LO-2A (800°C calcined)							
Temperature, 100°C							
Oxygen	0.1	0.1	10.7	0.1	7.7	1.4	0.7
Hydrogen	Wt gain	Wt gain	155	0.4	7.6	1.4	0.8
Temperature, 150°C							
Oxygen	0.7	2.3	3.8	0.2	7.3	1.4	0.8
Hydrogen	1.7	4.4	124	3.3	7.3	1.4	0.8
Temperature, 200°C							
Oxygen	3.4	4.8	5.9	1.9	6.1	1.4	0.8
Hydrogen	5.7	1.3	69.7	1.0	7.3	1.4	1.0
TO-10-1000 (1600°C calcined)							
Temperature, 100°C							
Oxygen	Wt gain	Wt gain	18.4	0.1	7.4	1.2	1.2
Hydrogen	0.5	Wt gain	3.8	0.6	8.4	1.2	1.8
Temperature, 150°C							
Oxygen	0.2	0.3	2.7	0.4	7.0	1.2	2.0
Hydrogen	0.8	8.4	3.9	1.7	8.1	1.2	1.6
Temperature, 200°C							
Oxygen	0.4	0.4	0.5	1.9	6.2	1.2	0.8
Hydrogen	2.1	0.5	2.7	0.6	8.8	1.2	3.2

circulation temperature. Such an effect was not noted in the oxygenated runs.

Titanium 75A displayed higher attack rates in hydrogenated slurries at 150°C than at 100 or 200°C in three of the four tests. No notable differences in attack rates were observed with titanium in the oxygenated runs at the three temperatures.

No significant trends in the attack of Zircaloy-3A were noted in oxygenated tests at the various operating temperatures. However, with hydrogenated slurries, Zircaloy-3A, like titanium 75A, showed highest rates in runs made at 150°C.

Corrosion rates of SA-212-B mild steel in oxygenated tests decreased with increased circulation temperature. A similar trend was not seen in the hydrogenated system; the attack rates in general were higher than in the oxygenated systems.

No effect of thoria calcination temperature was noted.

Observations of the handling properties (pourability) of the postrun slurries are noteworthy. Without exception, postrun slurries of the 1600°C-calcined thoria used in the tests poured readily from the toroids. Slurries of the 550, 650, and 800°C-calcined preparations which were circulated

at 100°C could not be poured. Recovery of the slurries which had been circulated at 150 and 200°C increased with increasing thoria calcination temperature. No cakes or films of thoria were formed in any of the tests.

13.2.4 Toroid Tests with Slurries of Arc-Fired and Flame-Fired Thoria

Several tests were made during the quarter to evaluate slurries of thoria produced by two new firing techniques. The materials, furnished by the Ceramics Group of the Metallurgy Division, were prepared in an effort to produce fire-polished thoria spheres.[9]

One group of oxides was prepared by passing 800°C-calcined thorium oxide, thorium oxalate, or thorium formate through an electric arc produced between two graphite electrodes. The products were composed of three general particle shapes: hollow spheres, teardrops, and porous irregular sinters. The mean particle sizes of the materials ranged from 21 to 140 μ. A photograph of the arc-fired thoria is shown in Fig. 13.1.

The second group of oxides was prepared by passing thorium oxalate and thorium formate through an oxyacetylene flame using a Metco metallizing gun. The flame-fired products appeared more dense in structure and were generally irregular in shape. Many of them had been sintered together into aggregates. The particle size of these materials ranged from 15 to 140 μ.

Toroid tests of 300 hr duration were made at 250 and 280°C and 26 fps with slurries of each of the preparations at a concentration of 1000 g of Th per kg of H_2O. Specimens of type 347 stainless steel, titanium 75A, Zircaloy-3A, and SA-212-B steel were exposed in each run. The results of the tests are shown in Table 13.4.

During circulation all the arc-fired thoria preparations were degraded and produced high metal attack rates. After circulation the mean particle sizes of the oxides were 0.5 to 0.6 μ.

The flame-fired thorium oxides were degraded to 1.2–2.5 μ during circulation. The slurry of oxide made from thorium formate produced moderate

[9] C. E. Curtis, *HRP Quar. Prog. Rep. Oct. 31, 1957*, ORNL-2432, p 139.

Table 13.4. Attack in Toroids by Slurries of Arc-Fired and Flame-Fired Thoria

Time: 300 hr
Relative velocity: 26 fps
Atmosphere: oxygen
Concentration: 1000 g of Th per kg of H_2O

Thorium Preparation	Calcination Conditions	Operating Temperature (°C)	Attack Rates* (mpy)				pH, Postrun	Mean Particle Size (μ)	
			347 SS	Ti-75A	SA-212-B Steel	Zircaloy-3A		Prerun	Postrun
Thorium formate	Arc fired 3 times	250	8.9	11	10	11	6.4	91	0.6
Thorium oxide	Arc fired 3 times	250	4.0	7.3	5.0	17	3.2	104	0.5
Thorium oxalate	Arc fired 3 times	250	7.9	9.2	7.8	18	9.4	104	0.6
Thorium formate	Arc fired 1 time	250	3.1	4.3	22	5.3	5.5	21	0.5
Thorium formate	Flame fired	280	3.2	2.0	2.0	Wt gain	5.4	>10	1.2
Thorium oxalate	Flame fired	280	13	2.1	157	2.0	5.6	>10	2.5

*Not corrected for slug flow.

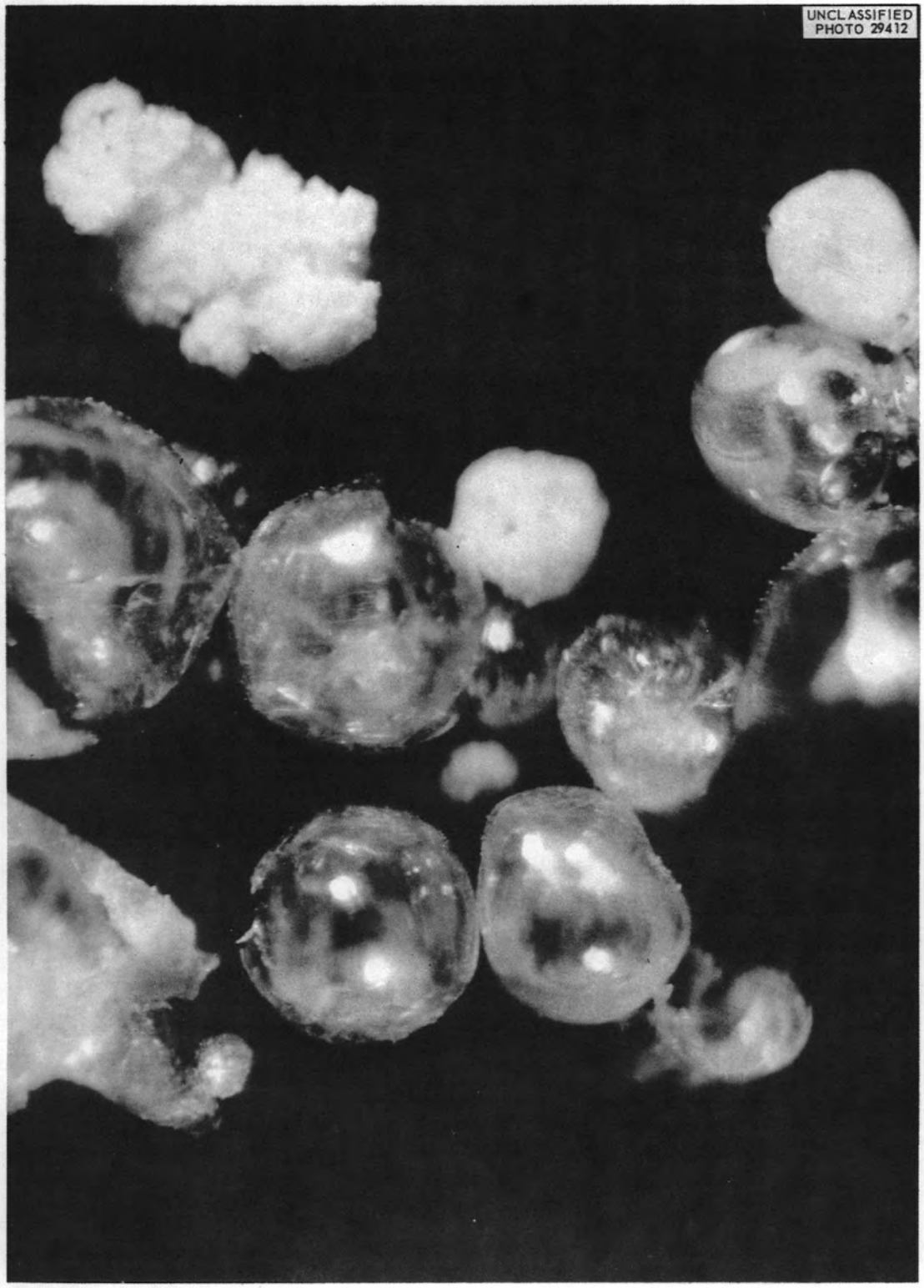

Fig. 13.1. Thoria After Three Passes Through the Carbon Arc. 140X.

attack rates. Attack by the slurry of oxide made from thorium oxalate was high.

13.2.5 Circulation of Slurries of ThO_2-CaO Mixed Oxides

The integrity of certain oxide refractories is often improved by the addition of small amounts of another oxide which forms a solid solution with the matrix. Such an effect has been observed by adding small amounts of calcium oxide to thoria.[10]

One series of ThO_2-CaO mixed oxides, made by the Ceramics Group of the Metallurgy Division, has been evaluated in toroids. The mixed oxides were prepared by dry-blending 800°C-calcined thoria with varying amounts of calcium oxide and subsequently refiring the mixtures at temperatures of 1600 to 1800°C. The fired products were then degraded in a hammer mill and screened through a 250-mesh sieve. Oxygenated aqueous slurries of these compounds were circulated in toroids at concentrations of 500 g of Th per kg of H_2O, at 26 fps and 250°C. For comparison, companion toroids circulated slurries of the pure thoria which was fired at 1600 and 1800°C. Pin corrosion specimens of type 347 stainless steel, titanium 75A, Zircaloy-3A, and SA-212-B carbon steel were exposed in each 300-hr test. The results of the runs are shown in Table 13.5.

Each of the preparations was markedly degraded during circulation. The slurries of ThO_2-CaO mixed oxide were strongly alkaline after circulation, which suggested that the CaO had hydrolyzed during the tests. All postrun slurries were highly flocculated.

Attack rates were not excessive in view of the large particle sizes of the prerun thoria. Major attack of all specimens exposed in the eight tests was due to localized erosion on the upstream surfaces of the pins.

It appears evident from the results of these tests that the addition of CaO to thoria to improve its resistance to attrition is of no value in aqueous systems at elevated temperature because of the reaction between the CaO binder and water.

[10] C. E. Curtis and J. R. Johnson, *Interim Report – Properties of Thorium Oxide Ceramics*, ORNL-1809 (Nov. 29, 1954).

Table 13.5. Attack by Slurries of Thoria Containing Calcium Oxide

Time:	300 hr
Temperature:	250°C
Relative velocity:	26 fps
Concentration:	500 g of Th per kg of H_2O
Thorium oxide:	batch CYT-1143 800°C-calcined

CaO Added (mg CaO/g ThO_2)	Recalcination		Attack Rates* (mpy)				pH, Postrun	Mean Particle Size (μ)	
	Temperature (°C)	Hours at Temperature	347 SS	Ti-75A	SA-212-B Steel	Zircaloy-3A		Prerun	Postrun
None	1600	4	2.4	2.0	4.3	1.9	6.0	12	1.4
None	1800	1	7.1	11	8.2	17	7.0	59	1.6
1.56	1700	2	5.5	2.0	2.9	2.5	6.5	50	2.1
3.16	1800	1	4.7	5.2	3.8	7.5	7.1	48	1.9
3.51	1700	2	4.9	3.1	6.4	3.8	12	59	1.8
6.86	1800	1	5.4	4.0	7.7	5.0	11	50	1.2
7.22	1700	2	4.9	4.2	4.9	6.6	11	58	2.3
10.35	1800	1	4.7	4.7	7.6	9.1	12	58	0.6

*Uncorrected for slug flow.

13.2.6 Tests with Slurries of Silica-Coated Thoria

Eight toroid tests have been made to study the circulation characteristics and corrosion-erosion attack by aqueous slurries of silica-coated thoria.[11] Silica-coated slurries have the desirable property of being Newtonian in their flow characteristics. Seven laboratory preparations, furnished by the Chemical Technology Division, were circulated as oxygenated aqueous slurries at 250 and 280°C. Test variables and corrosion data for the series are presented in Table 13.6.

After being silica-coated, all oxide preparations were recalcined at 650, 900, or 1200°C for 4- or 6-hr periods, as indicated in Table 13.6. The SOB-10 thoria was calcined at 1600°C before silica coating. The other preparations were calcined at 650°C before coating.

In the group of tests made with SOB-10 material, slurries were circulated in both hydrogen and oxygen atmospheres. For comparison, tests were run simultaneously using oxygenated and hydrogenated water to which silica was added as sodium metasilicate.

In the tests with SOB-10 thoria, made at circulating concentrations of 264 and 1000 g of Th per kg of H_2O with hydrogen and oxygen additions, respectively, a pronounced increase in attack of type 347 stainless steel and titanium 75A occurred with the hydrogenated slurries. Attack rates of SA-212-B carbon steel and Zircaloy-3A were comparable in both hydrogenated and oxygenated tests.

In the tests made at 280°C, attack of all alloys, except SA-212-B steel in three experiments, was low. The increased attack of mild steel in those tests was attributed to the presence of 100–500 ppm of chloride in the slurry.

All postrun slurries were well dispersed, were fluid, and settled slowly. Recovery of slurries in all tests was 90% or above.

[11] J. P. McBride and E. V. Jones, *Chem. Tech. Monthly Prog. Rep. Sept. 1957*, ORNL-2416, p 65 (classified).

13.3 IN-PILE AUTOCLAVE SLURRY TESTS – LITR

13.3.1 Introduction

An important factor potentially affecting slurry corrosion in thorium breeder reactors is reactor radiation. The effects of radiation and of radiation in conjunction with other variables remain to be evaluated. The program and experiments described below represent the first parts of an effort to explore the effect of radiation on high-temperature aqueous slurry corrosion. These utilize the in-pile autoclave facility HB-6 of the LITR.

Equipment and general techniques were those of the Solution Radiation Corrosion Section which have been described by Warren and Davis.[12]

[12] K. S. Warren and R. J. Davis, *In-Reactor Autoclave Corrosion Studies – LITR. I. Outline of Methods and Procedures*, ORNL CF-57-5-110 (May 22, 1957).

Table 13.6. Attack by Slurries of Silica-Coated Thoria

Velocity: 26 fps

Thorium Oxide Preparation	Final Calcination		SiO_2 (mg/g ThO_2)	Toroid Operating Conditions			Slurry Concentration (g Th/kg H_2O)	Pin Attack Rates* (mpy)				pH, Postrun	Particle Size (μ)	
	Temp. (°C)	Time (hr)		Atmos.	Time (hr)	Temp. (°C)		347 SS	Ti-75A	SA-212-B Steel	Zircaloy-3A		Prerun	Postrun
None			None	Oxygen	309	250	0	Wt gain	Wt gain	1.4	Wt gain			
None			12.74**	Hydrogen	309	250	0	Wt gain	Wt gain	1.0	Wt gain	11.9		
SOB-10-1600-DF	1200	4	50	Hydrogen	309	250	264	5.9	5.9	3.0	Wt gain	11.2	1.1	
SOB-10-1600-DF	1200	4	50	Oxygen	309	250	1000	2.5	2.5	3.5	0.1	5.7	1.1	
P-10-225-650-DF	650	6	21.67	Oxygen	498	280	500	1.8	Wt gain	61.7	0.3	5.7	0.5	0.6
P-10-225-650-DF	900	6	26.07	Oxygen	498	280	500	0.3	Wt gain	30.5	0.1	4.5	0.5	0.5
P-10-225-650-DF	1200	6	6.79	Oxygen	498	280	500	Wt gain	Wt gain	Wt gain	Wt gain	4.3	12.5	0.3
Th-10-650-DF	650	6	14.82	Oxygen	498	280	500	0.2	Wt gain	18.7	Wt gain	6.5	1.9	1.9
Th-10-650-DF	900	6	18.11	Oxygen	500	280	500	0.7	0.5	1.7	Wt gain	5.2	2.3	
Th-10-650-DF	1200	6	5.13	Oxygen	500	280	500	0.1	1.8	2.1	4.4	4.4	2.9	

*Uncorrected for slug flow.
**Milligrams of SiO_2 per gram of H_2O, added as sodium metasilicate.

A series of experiments has been planned,[13] as shown in Table 13.7, with increasingly severe levels of radiation and fission power density. Essentially duplicate experiments are to be performed in and out of radiation with pure thoria, with thoria containing 0.005 mole fraction enriched uranium, and with thoria containing 0.05 mole fraction enriched uranium. The lower uranium concentration is approximately that estimated by Rosenthal[14] as the equilibrium U^{233} concentration for HRE-3. However, fission power densities (0.9 w/ml estimated) will not be at HRE-3 levels because of the relatively low flux (8×10^{12} estimated) in LITR beam hole HB-6. To achieve higher fission densities, the thoria slurry of increased enriched-uranium content is to be used. All thoria-uranium preparations, determination of catalyst concentrations, and handling of irradiated thoria will be done by the Chemical Technology Division.

[13]E. L. Compere, *Notes on Proposed In-Pile Slurry Autoclave Experiments*, ORNL CF-57-11-27 (Nov. 6, 1957).

[14]M. W. Rosenthal and T. B. Fowler, *Nuclear Computations for HRE-3 Design: Equilibrium Results*, ORNL CF-57-7-23 (July 10, 1957).

13.3.2 Development, Construction, and Operation

As the first in-pile test in the above series, an HB-6 type rocking-autoclave experiment,[15] L6Z-121S, containing a thorium slurry was operated in beam hole HB-6 of the LITR during the past quarter. This was the first in-pile slurry experiment in this facility. Experiment L6Z-121S operated satisfactorily for 319 hr (including 16 hr

[15]G. H. Jenks *et al.*, *HRP Quar. Prog. Rep. July 31, 1957*, ORNL-2379, p 115, Fig. 14.8.

Table 13.7. Proposed Series of In-Pile Rocking-Autoclave Slurry Experiments

Temperature:	280°C
Concentration:	1000 g of Th per kg of D_2O
ThO_2 particle size:	1–2 μ
ThO_2 surface area:	1–2 m^2/g
Overpressure:	300–500 psi O_2/25°C
Fill:	75% at 280°C
Duration:	300–500 hr

	Status							
	Performed		Scheduled		Tentative			
Experiment No.: L6Z-	120S	121S	122S					
Radiation (LITR HB-6)	No	Yes	Yes	Yes	No	Yes	Yes	Yes
Enriched uranium in thoria, mole fraction	0	0	0.005	0.05	0	0	0	0
Natural uranium in thoria, mole fraction	0	0	0	0	0	0	0	0.005
MoO_3, *m*	0	0	0.02	0.20	0	0	0.02	0.02
Specimens								
Zircaloy-2	3	3	2	2	3	3	2	2
Zr-15Nb, β quenched	1	1	1	1	1	1	1	1
Zr-15Nb, heat aged			1	1			1	1
Zr-15Nb-2Pd, β quenched	1	1	1	1	1	1	1	1
Zr-15Nb-5Mo, β quenched	1	1	1	1	1	1	1	1

of pretreatment) at 280°C (261 hr with the reactor at 3 Mw).

The only difficulty encountered was the result of a slight misalignment of the rocking plug in the Oilite bronze bearings in the shielding plug. This misalignment caused wear and, in turn, galling between the plug and bearings. After 319 hr of operation the rocking plug jammed in the bearings, and the run was terminated. The bearing difficulties did not affect the operation of the experiment for the 319 hr prior to shutdown.

The autoclave used in this test was fabricated from Zircaloy-2 and contained six pin-type corrosion specimens – three of Zircaloy-2, one of Zr–15% Nb (beta quenched), one of Zr–15% Nb–5% Mo, and one of Zr–15% Nb–2% Pd. The autoclave was loaded with dry thoria and part of the required D_2O. Gaseous oxygen was subsequently added to the autoclave. No effort was made in these experiments to remove the air originally in the autoclave. After the oxygen addition was made, a predetermined amount of D_2O was pumped into the autoclave through the capillary tubing connecting the pressure cell to the autoclave. The D_2O pumped in was estimated to be sufficient to fill the capillary and to bring the slurry concentration in the autoclave to 1000 g of Th per kg of D_2O, with a fill estimated to be 75% at 280°C. The oxygen pressure was 380 psi at 25°C. By means of a freeze-plug technique the capillary tubing, pressure cell, and valves were checked for leaktightness and absence of gas bubbles.

The addition of gaseous oxygen to the slurry autoclave represented a departure from the loading procedure normally used for the solution-containing experiments, in which the initial oxygen overpressure was obtained by the thermal decomposition of H_2O_2 solution. The gaseous oxygen was used primarily to prevent dilution of the D_2O by the H_2O_2-H_2O solution.

The autoclave was operated in the out-of-pile mockup for approximately 16 hr at 280°C and 1700 psia as a final test before insertion in the LITR.

An out-of-pile rocking-autoclave test, L6Z-120S, of 480 hr duration at 280°C, but otherwise identical to the in-pile autoclave test L6Z-121S, was also conducted as a means of comparing corrosion rates.

The thorium oxide used in both these experiments was from batch TO-10-1000, which was recalcined at 1600°C and subsequently pumped for approximately 200 hr at 300°C in 100A loop runs BS-15 and BS-16. This material had previously been tested for feasibility in the HB-6 autoclave assembly and found to be satisfactory.[16]

13.3.3 Computation of Gas Data

In order to use gas pressure measurements to estimate the amount of oxygen which had disappeared from the system, and thus to estimate general metal corrosion rate, it was necessary to establish a relationship between the pressure and gas quantity. This was done by establishing a material-balance relationship according to the following equation:

$$\frac{\text{moles } O_2}{P_{O_2}} = \frac{V_g}{Z_{O_2}RT} + \frac{W_{liq}}{M_{liq}K_{Henry}} + \sum \frac{V^*_{ext}}{Z_{O_2}} \frac{\left(P_{tot} - S_{T^*}\right)}{RT^*\left(P_{tot} - S_T\right)} ,$$

where

V_g = actual gas space in autoclave, ml,

V^*_{ext} = volume of any external gas-containing space, ml,

P_{tot} = observed total pressure, psi,

P_{O_2} = partial pressure of oxygen, psi,

W_{liq} = mass of liquid in autoclave, g, based on material and volumetric balance for liquid and vapor in autoclave,

M_{liq} = molecular weight of liquid, g/mole,

K_{Henry} = Henry's gas solubility constant, psi/mole fraction,

R = gas constant, 1206 psi ml/g-mole/deg K,

Z = compressibility factor for gas at temperature and partial pressure of region,

T = absolute temperature of autoclave, °K,

T^* = absolute temperature of external region, °K,

S_{T,T^*} = saturation pressure of D_2O vapor at indicated temperature.

[16] E. L. Compere *et al.*, *HRP Quar. Prog. Rep. Oct. 31, 1957*, ORNL-2432, p 104.

This equation is based on a model which regards the system as consisting of a heated autoclave containing solids, liquid, and vapor, connected to an essentially cool liquid-filled pressure-measuring cell by liquid-filled capillary lines in which a small gas volume may develop. This volume, V^*_{ext}, occurs as a result of liquid compression and thermal expansion or contraction, pressure-cell expansion, and any neglected fill that exists. It is assumed that any gas driven from the autoclave into this volume is at the total pressure and that liquid condensed from this gas does not alter this volume appreciably.

Thermal expansion of the autoclave, volume of solids, and compression of the liquid by gases present are taken into account in arriving at the volume of the gas space and the mass of liquid present.

The above expression should be expanded to account for a more complex series of external volumes at differing external temperatures where this is necessary.

Experimentally, all parts of the system were carefully calibrated, and the quantities of all materials added were carefully observed. Values of the ratio mole O_2/psi O_2 were calculated for various typical assumed temperatures and pressures for the autoclave and its particular loading. A correction factor for the effect of temperature variations on the total gas-plus-steam pressure was estimated for each assumed temperature, and the steam (D_2O) pressure at this temperature was subtracted to give the oxygen partial pressure. From this the quantity of oxygen present was computed using the above equation.

The treatment of the *P-V-T* relationship in the gas phase is compatible with that given by Syracuse University Research Institute studies for the systems steam-helium[17] and steam-oxygen,[18] in which it is shown that partial pressures may be regarded as additive and that compositions may then be computed in terms of the vapor densities of the individual gases at the given temperature and partial pressure.

13.3.4 Discussion of Results: Pressure Measurements

Only data based on pressure measurements during operation of experiments L6Z-121S (in-pile) and L6Z-120S (out-of-pile) are available at the present time. Pressure observations at 280°C were taken with the autoclave rocking. Shift-average values of computed oxygen quantity plotted vs time for these runs are shown in Fig. 13.2. Values for run L6Z-121S with the reactor operating and reactor down are shown. The difference is attributed to error of the control thermocouple resulting from gamma heating when the reactor was operating. Values for out-of-pile run L6Z-120S are also shown. The similarity of levels indicates nearly identical loading relative to experiment L6Z-121S.

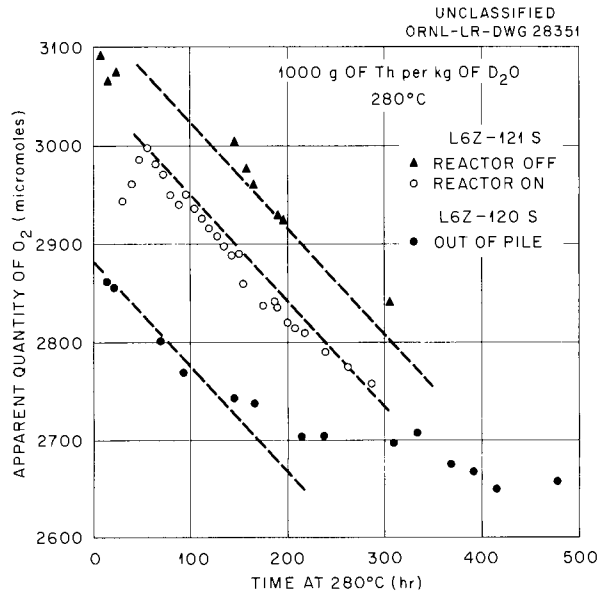

Fig. 13.2. In-Pile and Out-of-Pile Corrosion of Zircaloy-2 by Thoria Slurries in Autoclave Tests at 280°C As Estimated from Oxygen Consumption.

Guide lines of 1-mpy slope indicate that each experiment showed an initial corrosion rate of approximately 1 mpy. The rate in the out-of-pile experiment diminished in the latter part of the run. Corrosion rates for these bombs were computed from the expression mpy = 0.93 × micromoles of O_2 per hr.

An increase in the zero pressure reading of the Baldwin pressure cell of 14 psi was found at the conclusion of in-pile run L6Z-121S. The plotted

[17] J. A. Luker and T. Gniewek, *Saturation Composition of Steam-Helium-Water Mixtures PVT Data and Heat Capacity of Super Heated Steam-Helium Mixtures*, SURI-Ch. E.-273-557F (July 29, 1955).

[18] J. A. Luker and T. Gniewek, *Determination of PVT Relationships and Heat Capacity of Steam-Oxygen Mixtures*, SURI-Ch. E.-273-558F (Aug. 2, 1955).

values do not include this correction as the time of occurrence is not known. The rise in gas quantity indicated in the early part of run L6Z-121S may have been a result of this zero shift, or may have been due to generation of a small amount of radiolytic gas (less than 30 psi), or to other causes. Similar phenomena have been noted in certain in-pile autoclave solution corrosion experiments. Postrun examinations of the specimens, thoria, and autoclaves will be made.

13.4 IN-PILE SLURRY TOROID

13.4.1 Development Engineering

During the past quarter the double-arm in-pile toroid rotator model[19] was fitted with heavy-duty spherical bearings in the gimbal frames and a constant-velocity universal joint in place of the fork-and-tee type. Mechanical vibrations were eliminated by positioning counterweights along the rotator arms. While the spherical bearings performed satisfactorily, the universal joint overheated after short periods of continuous operation at speeds as low as 200 rpm. This was attributed to the combination of high tensile stress in the joint during rotation, created by the centrifugal force of the toroid rings, the counterweights, and the universal-joint weight, along with the large amount of displacement required of the joint in this application.

Meanwhile, a single-arm in-pile toroid rotator model has been designed and fabricated as shown in Figs. 13.3 and 13.4. In this model the universal joint provides a pivot for the rotator arm and prevents the arm from rotating about its

[19] E. L. Compere *et al.*, *HRP Quar. Prog. Rep. Oct. 31, 1957*, ORNL-2432, p 104.

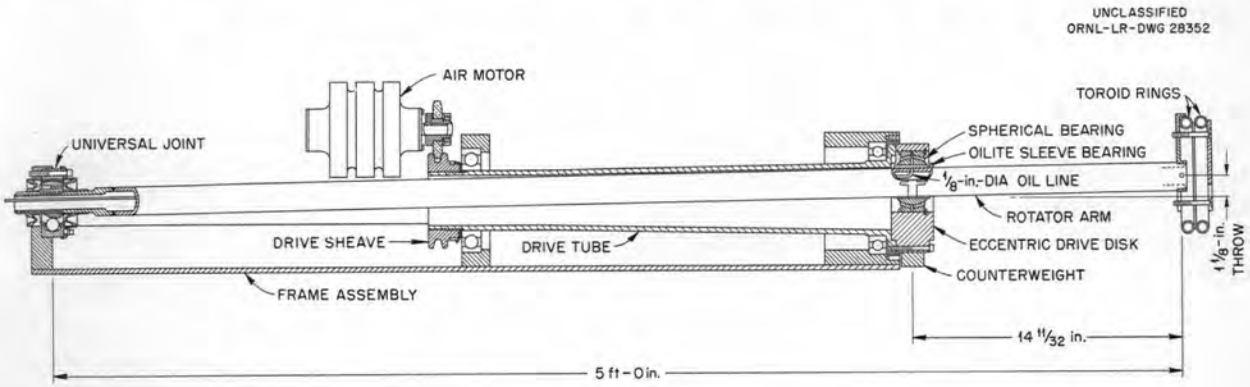

Fig. 13.3. Single-Arm In-Pile Toroid Rotator Model.

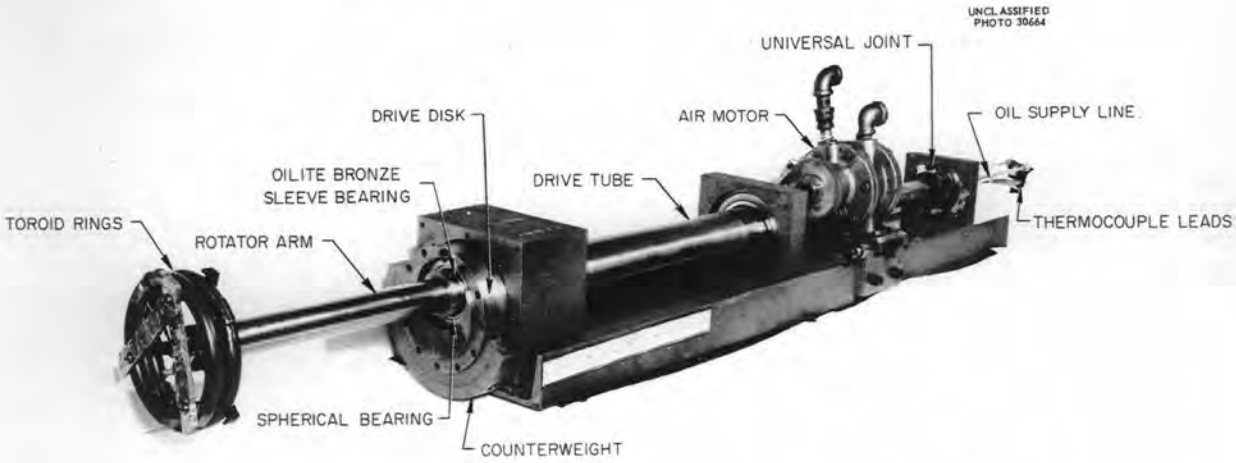

Fig. 13.4. Experimental Model of Single-Arm In-Pile Toroid Rotator.

longitudinal axis. The air motor rotates the drive tube which, in turn, rotates an eccentric-drive disk. The rotator arm has an Oilite bronze bearing fitted to the arm inside the spherical bearings. As the disk turns, the desired circular motion is imparted to the toroid ring. Tests have demonstrated that the spherical bearing cannot withstand rotation in this application; hence, an Oilite bronze sleeve bearing was added to take the rotation, and the spherical bearing merely compensates for any misalignment and/or deflection of the rotator arm during operation. A $\frac{1}{8}$-in. tube passing through the hollow rotator arm and terminating at the drive disk provides a continuous oil supply to the Oilite sleeve bearing. Tests have indicated that this provision is required for satisfactory sleeve-bearing service. The hollow rotator arm is used to route thermocouple leads and capillary tubing from the toroid rings to the rear of the rotator with a minimum of flexure of the leads during rotation.

Preliminary testing of this model has been so encouraging that further development work on other models has been curtailed. Suitable dynamic balance of the machine at speeds up to 1000 rpm was achieved by attaching a counterweight on the front of the drive disk opposite the rotator arm.

A method of heating and cooling which encloses the toroid bundle within an ambient whose temperature is controlled and adjusted with air-water and/or steam mixtures seems the most suitable for in-pile operation.[19] The instrumentation for automatic temperature control of this type of system has been designed and fabricated for test and evaluation.

Work on the in-pile toroid rotator was curtailed during this quarter because of increased effort on the HRT core and blanket corrosion specimen assemblies.

13.5 IN-PILE SLURRY LOOP

13.5.1 Loop Development

During the past quarter, development work was resumed on adaptation of the 5-gpm in-pile solution loop to slurry operation. Essentially no work had been done on this since that last reported for the quarter ending October 31, 1956. This cessation of effort was a result of the inability to circulate the thorium oxide slurries then available in the small loop.[20] However, the improved handling properties, demonstrated[21] in 100A loop run BS-18, of the recently available thorium oxide of small particle size calcined at 1600°C offered promise for use of the 5-gpm pump loop for in-pile slurry studies.

The experimental loop now under test is essentially the same as the one that was used previously.[20] It is similar to the in-pile loops presently operated in beam holes HB-2 and HB-4 of the LITR to obtain radiation-corrosion data with uranyl sulfate solutions. The major difference is the use of a vertical rather than a horizontal pressurizer to prevent slurry settling in the pressurizer.[22] For slurries previously tested (calcined at 800°C), it was also necessary to provide an increased flow rate through the pressurizer.

The loop in which earlier tests were made[22] was further modified for runs made during the past quarter by removing the core, in which flow velocities are low. The core was replaced with a U-bend section of $\frac{3}{8}$-in. sched-40 pipe; this is the same size as the remainder of the main loop piping. The circulation pump was an ORNL 5-gpm model equipped with aluminum oxide bearings and journals and was identical to the pumps used in the in-pile solution loops.[23] The loop also was fitted with a slurry addition tank.

During the past quarter this experimental in-pile slurry loop was operated for a total of 680 hr at 250°C and 675 psia (oxygen partial pressure of 100 psi) circulating a thorium oxide slurry of approximately 550 g of Th per kg of H_2O. The thorium oxide used had been pumped previously in 100A loop runs BS-17 and BS-18. It was prepared originally as mixed batches TO-10-1000 and LO-17, each recalcined at 1600°C, and having a mean particle size of 0.7 μ. The loop flow rate was approximately 7 gpm ($\sim$12 fps in the $\frac{3}{8}$-in. sched-40 main loop piping), as determined from measurements made with water at room temperature. The

[20] E. L. Compere *et al.*, *HRP Quar. Prog. Rep. Oct. 31, 1956*, ORNL-2222, p 88.

[21] E. L. Compere *et al.*, *HRP Quar. Prog. Rep. Oct. 31, 1957*, ORNL-2432, p 88–91.

[22] E. L. Compere *et al.*, *HRP Dynamic Slurry Corrosion Studies: Quarter Ending April 30, 1956*, ORNL CF-56-4-139, p 20–21, Fig. 1.3.1.

[23] G. H. Jenks *et al.*, *HRP Quar. Prog. Rep. July 31, 1957*, ORNL-2379, p 104, Fig. 14.4.

entire loop flow was routed through the bottom section of the vertical pressurizer. A water purge of 15 ml/sec from condensate produced in the pressurizer was maintained to the pump rotor cavity to minimize bearing damage from the thorium oxide slurry. However, with the slurry presently under test, and with the aluminum oxide pump bearings, it may be feasible to substantially reduce or eliminate the bearing purge as described below.

Based on these encouraging preliminary results, development work will continue with two objectives: (1) to modify the loop for possible use in an existing reactor experimental beam-hole facility – either HB-2 or HB-4 of the LITR – for radiation-corrosion studies and (2) to provide a small-scale slurry loop requiring approximately 1 liter of slurry for operation to supplement the larger scale 100A dynamic slurry corrosion test loops which require 15–20 liters of slurry.

13.5.2 Slurry Pump Test

A test is being made to evaluate the need for the pump-bearing purge when aluminum oxide bearings are used and slurries of satisfactory quality are circulated. A water purge is normally used to prevent bearing wear by the thorium oxide slurry when Graphitar pump bearings are used. Eliminating the need to make condensate in the loop pressurizer for pump purge would greatly simplify the design and operation of an in-pile slurry loop.

A standard ORNL 5-gpm pump[23] equipped with aluminum oxide bearings and journal bushings[24] is circulating a thorium oxide slurry at a concentration of ~500 g of Th per kg of H_2O without the use of water as a bearing purge. Operation is at a slurry flow rate of 5 gpm at 40°C and 25 psig. An air overpressure of 25 psi is maintained to prevent pump cavitation. The thorium oxide used is the same as that described in Sec 13.5.1 for the in-pile slurry loop. After operation with thorium oxide slurry for more than 650 hr, there was no evidence of radial bearing wear, but 0.0045 in. wear was measured on the forward thrust bearing when the pump was disassembled for inspection. This thrust wear, although not necessarily significant, was unexpected in view of the lack of wear on the radial surfaces of the bearings and since the thrust load was not considered excessive. Samples of slurry removed from the rear of the pump during operation showed essentially the same concentration of thorium oxide as that in the loop piping.

[24] H. C. Savage, *Sintered Alumina as a Pump Bearing and Journal Material*, ORNL CF-57-11-122 (Nov. 26, 1957).

14. RADIATION CORROSION

G. H. Jenks H. C. Savage

A. L. Bacarella
J. E. Baker
S. J. Ball
J. C. Banter
S. E. Bolt
J. W. Brown
R. J. Davis
V. A. DeCarlo
D. T. Jones
F. A. Knox
R. A. Lorenz
J. R. McWherter
A. R. Olsen
J. A. Russell
M. D. Silverman
W. C. Ulrich
F. J. Walter
R. M. Warner
K. S. Warren
S. H. Wheeler
W. C. Yee

14.1 IN-PILE LOOPS

14.1.1 Development and Construction

(a) HB-2 Loop Package. – Loop L-2-21 has been assembled and is undergoing out-of-pile operational tests prior to insertion into beam hole HB-2 of the LITR. This loop is a modification of the loop previously designated as L-4-21.[1] After 100 hr of out-of-pile operation with a uranyl sulfate solution, one of the corrosion coupons in the core section of L-4-21 became dislodged from the holder and was carried into the first stage of the Byron-Jackson 5-gpm pump,[2] and the pump was damaged beyond repair. The pump was replaced with a three-phase, 220-v ORNL 5-gpm pump.[1] Several changes were made in the sample arrays, and the loop was reassembled for operation in the higher flux installation in HB-2, which had become available as a result of the termination of loop experiment L-2-19.

Zircaloy-2 tapered-channel coupon holders in the core and line positions contain Zircaloy-2, titanium 110AT, and type 347 stainless steel corrosion samples. Stress specimens of titanium 110AT and type 430L stainless steel are installed in the pressurizer. Seven low-velocity coupon holders[3] in the core and three in the line contain a variety of zirconium alloys with different heat treatments. One Zircaloy-2 and one type 347 stainless steel coupon are mounted in the forward section of the core, the region of highest neutron flux. Two cobalt-aluminum flux monitors encased in type 347 stainless steel tubing are located in the core.

(b) ORR Loop Package. – All the loop components except the core section have been fabricated for the first ORR loop package, O-1-20. A transparent plastic model of the core was tested by use of dye-injection techniques to ensure that the flow distribution would be as designed, and the core is now being fabricated. Auxiliary equipment is being assembled for testing of the loop package.

14.1.2 General Description of In-Pile Loop Experiment L-2-17

Except for metallographic examination of specimens, stainless steel loop experiment L-2-17 has been completed. This was the thirteenth in-pile loop experiment and the fourth to be irradiated in the HB-2 beam hole at the LITR.

The objective of this experiment was to obtain corrosion data at 300°C. Light water was used as the solvent, but otherwise the loop solution was similar to the HRT solution.

One set of 24 corrosion coupons in Zircaloy-2 tapered-channel coupon holders was installed in the core and one set in the in-line position. Each set contained eight titanium 55A, eight Zircaloy-2, and eight type 347 stainless steel coupons. The coupon arrangement was identical in each channel holder. Twelve ladder arrays (each containing 15 coupons) were mounted in the loop: six arrays in the core annulus, four in the in-line position, and two in the pressurizer. One of the pressurizer ladder arrays was located in the liquid phase and the other in the vapor phase. Of the 180 coupons in the ladder arrays, 31 were fabricated from titanium alloys, 82 from stainless steel alloys, and 67 from alloys of zirconium. Eight of the ladder coupon holders were fabricated of type 347 stainless steel, three of Zircaloy-2, and one of titanium 55A. The location of the arrays and the types of materials contained in the arrays are given in Table 14.1.

---

[1] G. H. Jenks *et al.*, *HRP Quar. Prog. Rep. Oct. 31, 1957*, ORNL-2432, p 106.

[2] G. H. Jenks *et al.*, *HRP Quar. Prog. Rep. July 31, 1956*, ORNL-2148, p 92 (classified).

[3] G. H. Jenks *et al.*, *HRP Quar. Prog. Rep. July 31, 1957*, ORNL-2379, p 99.

Table 14.1. Alloy Specimens Contained in Experiment L-2-17*

I. Alloys contained in core and line channel holders

Type 347 stainless steel
Zircaloy-2
Titanium 55A

II. Alloys contained in ladder coupon arrays

Core

Array ZB-1 (Zircaloy-2 holder)

Zircaloy-2
Zr (crystal bar)–15% Nb (A, B, C, D)*
Zr (sponge)–15% Nb (A, B, C, D)

Array ZB-2 (Zircaloy-2 holder)

Zr (crystal bar)–20% Nb (E)
Zr (sponge)–15% Nb (A, B, C, D)
Zr (crystal bar)–15% Nb–2% Pd (A)
Zr (crystal bar)–15% Nb–1% Fe (A, B, C, D)

Array SA-4 (type 347 stainless steel holder)

Type 347 stainless steel

Array SA-5 (type 347 stainless steel holder)

Type 430 L stainless steel
Type 430 stainless steel
Type 431 stainless steel
Type 17-4 PH stainless steel (F)

Array SA-6 (type 347 stainless steel holder)

Type 347 stainless steel
Zircaloy-2
Ti-55A

Array TB-1 (titanium 55A holder)

Ti-55A
Ti–3% Al
Ti-110AT

In-line

Array ZB-3 (Zircaloy-2 holder)

Zr (crystal bar)–15% Nb (A, B, C, D)
Zr (sponge)–5% Nb (A, B, C, D)
Zr (crystal bar)–15% Nb (A, B, C, D)
Zr (crystal bar)–2% Pd (A)
Zr (crystal bar)–20% Nb (E)
Zircaloy-2

Array SA-7 (type 347 stainless steel holder)

Type 347 stainless steel

Array SA-8 (type 347 stainless steel holder)

Type 430 stainless steel
Type 430 L stainless steel
Type 431 stainless steel
Type 17-4 PH stainless steel (F)

Array SA-9 (type 347 stainless steel holder)

Type 347 stainless steel
Zircaloy-2
Ti-55A

Pressurizer

Array SA-10 (vapor phase) (type 347 stainless steel holder)

Type 347 stainless steel
Type 430 L stainless steel
Zircaloy-2
Zr (crystal bar)–15% Nb (A)
Ti-55A

Array SA-11 (liquid phase) (type 347 stainless steel holder)

Type 347 stainless steel
Type 430 L stainless steel
Zircaloy-2
Zirconium (crystal bar) (A)
Ti-55A

*Heat treatments:

A: beta quenched (1000°C for 2 hr, water quenched)
B: 600°C for 2 weeks, air cooled
C: 500°C for 2 weeks, air cooled
D: 400°C far 2 hr, water quenched
E: beta quenched, preoxidized
F: hot rolled and annealed

In addition, a type 347 stainless steel "core spider coupon" was attached to the high-flux end of the core tapered-channel coupon holder in a bracket fabricated from 0.010-in.-thick type 347 stainless steel sheet.

The structure of the loop was essentially the same as in previous HB-2 experiments. The 5-gpm ORNL pump was of the outboard-bearing design and contained Kearfott aluminum oxide bearings and journal bushings. The rear bearing housing was pinned to the rear of the pump diaphragm. In addition, both front and rear bearings were pinned to the bearing housings by means of setscrews which seated in grooves in the outside surface of the aluminum oxide bearings.

During out-of-pile pretreatment and tests, the loop was operated for short periods with five different solutions. A 4-hr run with 3% trisodium phosphate solution was made at 95°C and was followed by a 25-hr run with a 5% nitric acid solution at the same temperature. After the acid solution was drained from the loop, water was circulated for 21 hr at 300°C in the main stream and 315°C in the pressurizer. After the H_2O run, two runs with natural-uranium solutions were made at the same temperatures. The solutions, of identical composition, were 0.04 *m* UO_2SO_4, 0.025 *m* H_2SO_4, and 0.005 *m* $CuSO_4$. The first run was for 98 hr, and the second was for 89 hr. The over-all loop corrosion rates during the natural-uranium runs were 2.7 and 3.3 mpy, respectively, based on oxygen consumption, and 1.9 and 0.8 mpy, respectively, based on the amount of nickel found in the solutions.

The enriched-uranium solution initially charged to the loop for in-pile operation was 0.04 *m* UO_2SO_4, 0.025 *m* H_2SO_4, and 0.005 *m* $CuSO_4$. The makeup solution differed only in that it was 0.065 *m* in excess H_2SO_4 and contained 100 ppm chromium. The additional H_2SO_4 was included to replace acid consumed in corrosion, and the chromium was included to inhibit corrosion of the type 420 stainless steel valve stems in the process lines during solution addition. The main-stream temperature during the in-pile run was 300°C, and the pressurizer temperature was 315°C. The only previous loop experiment with 0.04 *m* UO_2SO_4 solution, loop L-2-10,[4] was conducted with a main-stream temperature of 280°C.

Enriched-uranium solution was circulated for about 57 hr in the loop before neutron irradiation was initiated. After a total of 610 hr of circulation time, the loop was drained in order to replace valve No. 30 which was plugged. The loop was then recharged with fresh solution, and operation was resumed. The experiment was terminated when the loop circulating pump failed after 1147 hr of circulation. The energy output of the LITR during the inserted time was 2625 Mwhr, essentially all of which was liberated with the reactor at 3 Mw.

Current and voltage measurements were made on the electrical windings and the power supply during attempts to restart the pump.[5] The results of these measurements, together with those of resistance measurements of the pump start and run windings, indicated that there were turn-to-turn or winding-to-winding shorts in the run windings.

The average fission power during operation of the loop at the 3-Mw reactor level, determined from Cs^{137} analyses, was 522 w during operation with the first solution charge and 780 w during operation with the second solution. The average total fission power during the entire exposure was 604 w. The over-all average total fission and gamma heat at the 3-Mw reactor power level was 1255 w.[5] During operation with the second fuel solution, there was a general upward trend in fission and gamma heat that could not be correlated with changes in the reactor fuel-element loading. The temperature of the core end cap was observed to rise steadily during this period from about 309 to about 311°C.[5]

The thermal-neutron fluxes to which core specimens were exposed were determined from measurements of the induced activities of representative coupons from the core channel and core annulus arrays. The coupons measured were selected from those fabricated from Zircaloy-2, Zr–15% Nb, and Zr–15% Nb–1% Fe. The determinations indicated an axial but no radial flux gradient in the experiment. The fluxes in the core ranged from 1.9×10^{13} neutrons/cm^2/sec at the location of the leading core channel coupon to 4.25×10^{12} neutrons/cm^2/sec at the location of the rear coupon. The thermal-neutron fluxes at the core nose and at the stainless steel coupon in the spider were estimated to be 2.45×10^{13} and

[4] G. H. Jenks *et al.*, *HRP Quar. Prog. Rep. Jan. 31, 1957*, ORNL-2272, p 104.

[5] F. J. Walter, *HRP In-Pile Corrosion Test Loops, Operation of In-Pile Loop L-2-17*, ORNL CF-57-8-112 (Aug. 30, 1957).

2.09×10^{13} neutrons/cm^2/sec, respectively, by extrapolation of the coupon data. Fission power densities at the specimens were calculated by using the thermal fluxes as determined.

The solution power density at a given position was corrected to include the estimated power density associated with moderation of the fast neutrons at the position. The corrected power densities ranged from 6.5 w/ml for the leading core channel coupon to 1.5 w/ml for the rear coupon. These included estimated contributions from fast-neutron moderation of 0.5 and 0.1 w/ml, respectively. The estimated solution power densities were 8.4 w/ml at the nose of the core and 7.2 w/ml at the core spider coupon.

Thermal-neutron fluxes in the core were also measured by means of a cobalt-aluminum flux monitor encased in type 347 stainless steel. Values determined in this manner were 1.7×10^{13} neutrons/cm^2/sec at the nose of the core and 3.3×10^{12} neutrons/cm^2/sec at the location of the rear channel coupon. They are only about 75% of those obtained by analyses of the zirconium specimens.

The calculated free-acid concentration was maintained reasonably constant throughout the run. No evidence of solution instability was observed. The over-all stainless steel corrosion rate was 0.8 mpy based on oxygen consumption and 0.5 mpy based on the nickel in solution.

14.1.3 Qualitative Results of Inspection and Evaluation of Loop L-2-17

The dismantling operations on loop L-2-17 were conducted without difficulty. The components removed from the loop included the core, the two in-line sample holders, the pressurizer, two sections of the pressurizer heater, a section of the main loop piping adjacent to the pump outlet, and the pump.

As with previous loops, all the components outside the core region were covered with a uniform dark-brown, rust-colored scale. This scale was very thin in the vapor region of the pressurizer. There was no evidence of localized attack on any of the components examined. The pump was not completely dismantled as there was evidence of adequate end-play and the impeller rotated freely.

All the in-line channel coupons were uniformly covered with the rust-like scale. All the stainless steel, titanium, and Zircaloy-2 coupons in the in-line ladder arrays were also covered with this scale. However, some of the zirconium alloys in the in-line ladder arrays exhibited scale formations which strongly resembled grain patterns. This resemblance showed as slight changes in color in what appeared under the stereomicroscope to be a relatively uniform scale deposit. This appearance is shown in Fig. 14.1.

Two identical ladder arrays of coupons were exposed in the pressurizer, one in the liquid and one in the vapor phase. All the coupons in the liquid phase were covered with a heavy, dark-brown, almost black scale. Scale on the three beta-quenched Zr–15% Nb alloy coupons flaked quite readily, and some of it broke off in handling. Coupons in the vapor phase showed distinctive films. Figure 14.2 is a photograph of this array. Both the type 347 and type 430L stainless steels were covered with a thin rust-like scale. The

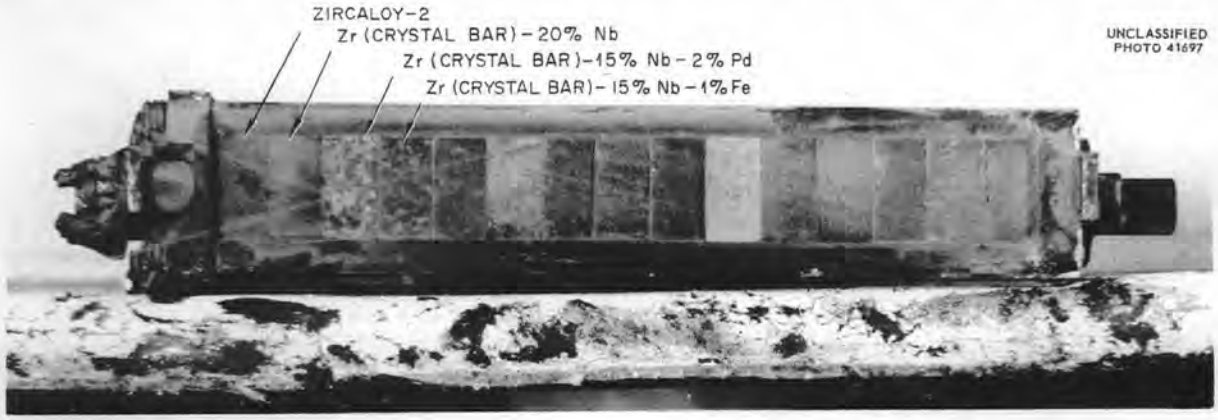

Fig. 14.1. Loop L-2-17 In-Line Ladder Array, ZB-3, As Removed from the Loop.

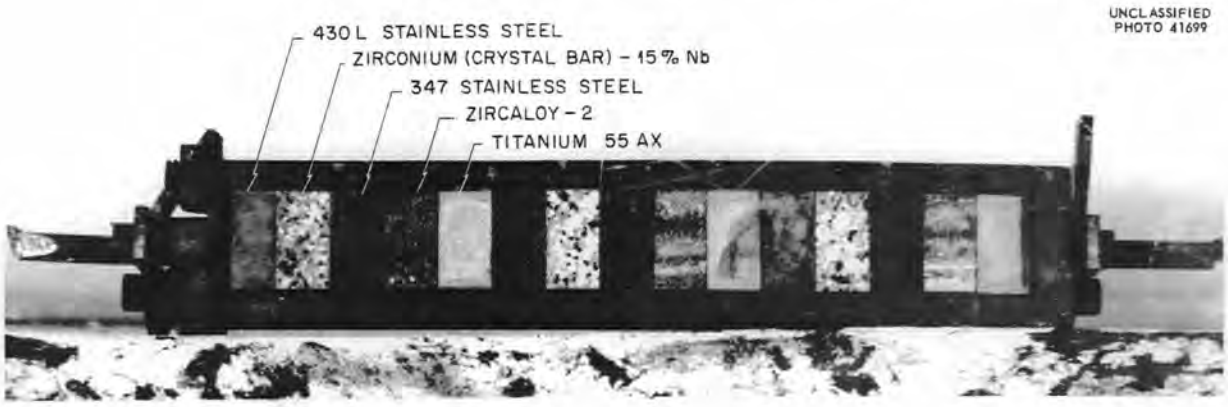

Fig. 14.2. Loop L-2-17 Pressurizer Ladder Array, SA-10 (Vapor Phase), As Removed.

titanium was covered with a thin, uniform bronze-colored film. The Zircaloy-2 was covered with a uniform dark-gray scale. Again, only the Zr–15% Nb alloy coupons did not have a uniform scale. The scale on those coupons was heavy but divided into three different thicknesses. This difference in thickness appeared to be associated with grain orientation, as one thickness persisted over any single grain. The thinnest scale was rough and was dark gray, almost black, in color. The scale of medium thickness was smooth, shiny, and dark brown. The heaviest scale was smooth, shiny, and brass colored and was very similar to the scale found on Zircaloy-2 coupons from the in-pile autoclaves before drying. The thicker scales tended to lap over the other scales, and, where two scales of similar thickness met at a grain boundary, pressure ridges were produced. One of the Zr–15% Nb alloy coupons from the vapor phase was not defilmed but was retained for further examination by the metallurgy group. Another Zr–15% Nb alloy coupon from the vapor phase was tested to determine the stability of the various scale layers. There was no apparent change in weight or appearance during the usual defilming operation. Following this operation, the coupon was soaked in acetone for 30 min and dried at 110°C for 48 hr. This treatment also produced no change in specimen weight or appearance. The coupon was then soaked in 10% (by weight) Aerosol in distilled water for 24 hr, rinsed with acetone, placed in a weighed container, and dried for 17 days in an oven at 110°C. During this period the specimen was observed periodically. The specimen lost 0.8 mg and the thickest scale appeared to have been partially removed in this treatment, while the two thinner scales were apparently unaffected. A small quantity of scale flaked from the specimen and was accumulated in the container. The scale has been submitted for chemical analysis. The coupon was given to the metallurgy group for further examination.

As with previous loops the standard cathodic defilming technique was only partially effective on the zirconium-alloy and titanium coupons. In contrast with previous loop experiments, some of the type 347 stainless steel coupons also retained scale even after repeated defilming treatments.

The interior surface of the type 347 stainless steel core body was covered with a rust-like scale ranging from a deep-red color at the high-flux end, through brown, to almost black at the low-flux end. The scale increased in thickness gradually with decreasing flux. There was no evidence of localized attack. The locating ledge machined into the core cap retained its sharp edge, and there was no evidence of attack in the cap-to-body weld region. The Zircaloy-2 coupon holder from the core is shown in Fig. 14.3. Some scale was retained in spots on the exterior surface of the holder on the high-flux end. This scale accumulation gradually increased to a heavy uniform coating at the low-flux end. The interior of the tapered-channel holder was free from any scale except at the extreme low-flux end. Most of the channel surface was covered with a typical dark-gray film gradually increasing in thickness with decreasing flux. Examination of the Zircaloy-2 holder under the microscope revealed two short

cracks along the edge of the channel at the low-flux end. The fractures were clean and bright. The center portion of the holder was folded inward. Since the holders had been clamped in a vise during the disassembly procedure, it was concluded that the fractures were a result of excessive pressure during this clamping operation. Figure 14.4 is a photograph of the core array as removed from the loop. In general, the surface appearances of the various coupons and fixtures of a given material in the core region were peculiar to that material. All coupons at the low-flux end retained some of the dark rust-like scale. The titanium coupons were covered with a thin, uniform, shiny bronze-colored film, which varied in shade depending on the alloy. The stainless steel spiders and clamping bands and all the stainless steel coupons in the core region were covered with a rust-like scale. The thickness and color of this scale ranged from relatively thin and rust red at the high-flux end to heavy and dark brown, almost black, at the low-flux end. The Zircaloy-2 coupons were covered with the typical dark-gray film. The other zirconium alloys, in general, were covered with a darker gray, oily-appearing film. The nature of this film was more strongly dependent on the heat treatment the coupons had received than on the particular alloy content. There was some evidence of the original grain structure, particularly with the beta-quenched samples, but it was not distinct as in the case of the line annulus and pressurizer samples.

Most of the zirconium-alloy coupons and many of the titanium and stainless steel coupons from different locations in the loop were transferred to the Solid State Division for metallographic examination. In addition to the usual loop component sections (core cap, pressurizer, pressurizer

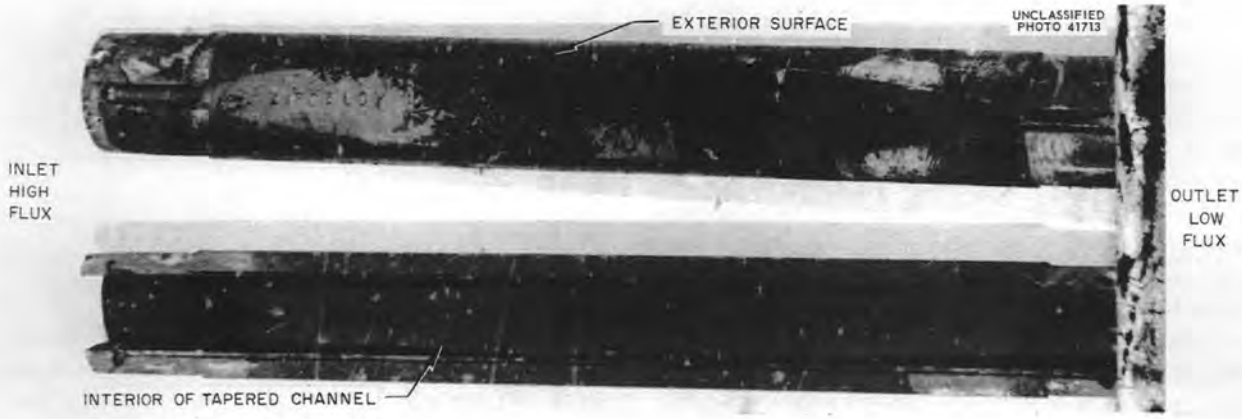

Fig. 14.3. Loop L-2-17 Zircaloy-2 Core Coupon Holder As Removed.

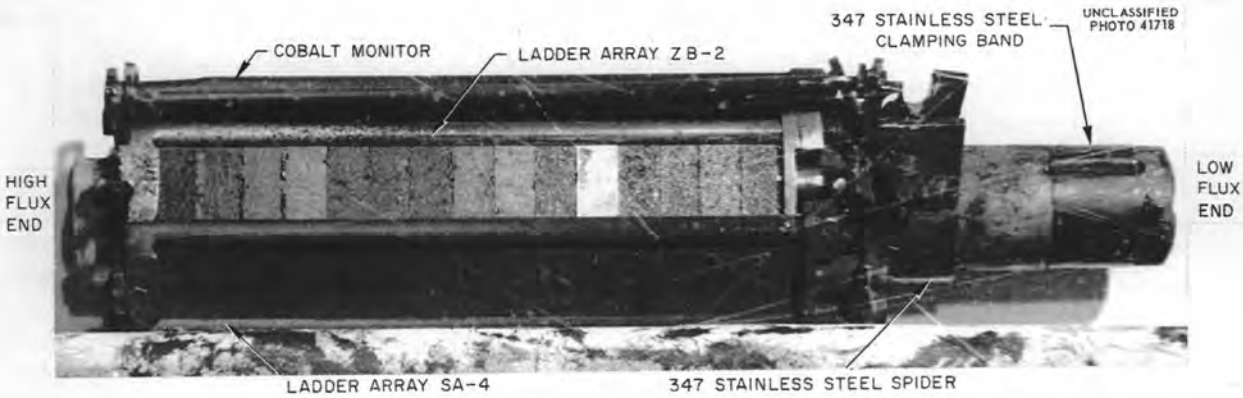

Fig. 14.4. Loop L-2-17 Core Coupon Array As Removed.

heater, and main loop piping), a section of the core-cap-to-core-body weld was also submitted for metallographic examination.

14.1.4 Quantitative Inspection, Results, and Discussion of Loop L-2-17

(a) Analyses of Scale from Low-Power-Density Regions. – (1) *Procedure and Results.* – Continuing the effort to determine the distribution of corrosion products and uranium throughout the loop system, samples of the bulk scale were removed from the core wall, the in-line annulus holder, the pressurizer, the pump volute, and the channel area of the core coupon holder for chemical analyses. The samples were analyzed for U, Zr, Cr, Fe, Ni, Cu, and SO_4. Results of these analyses are shown in Table 14.2. Amounts of each constituent are listed as percentages by weight of the entire sample. Also shown, in the final column of the table, is the weight per cent of each scale sample not represented by the listed constituents.

A material balance of Fe, Cr, Ni, and Zr was attempted, with the use of these results together with the results of oxygen, nickel, and weight measurements. The scale sample from the core channel holder was excluded from this consideration. The average of the other samples was employed as representative of the average scale in portions of the loop outside the core. The amount of scale in the core was considered negligible. The method of testing the balance and the assumptions involved are the same as those previously employed and described for the L-4-16 experiment.[6] The results are presented in Table 14.3 in the manner employed with L-4-16. The value for the excess of nickel listed in the final column is the difference between the sum of the values for the nickel in solution and scale and the total amount of nickel oxidized, as calculated from oxygen data when it is assumed that no constituent of the steel was selectively oxidized.

(2) *Discussion of Results.* – The scale sample from the core channel was excluded from the material balance because it is believed unlikely that scale in the high-flux region is similar in composition to that found outside the core. Furthermore, the analytical results for the sample from the core are open to question because the summation of the percentages for the various constituents is greater than 100. Probably, the value for SO_4 is erroneously high and accounts for most of this discrepancy.

The results for the other samples indicate that the composition of the scale from different locations differs more in this loop experiment than in the previous loop experiment L-4-16 for which similar data are available.[6] In general, however, the results of the material balance are the same as for L-4-16. The results indicate that nearly all the zirconium that was oxidized in the core was transported to portions of the loop outside the core and deposited in the scale. The ratio of

[6] G. H. Jenks *et al.*, *HRP Quar. Prog. Rep. July 31, 1957*, ORNL-2379, p 110.

Table 14.2. Analyses of Scale from Loop L-2-17

Source of Scale	Scale Weight (mg)	Amount in Scale (wt %)							
		U	Zr	Cr	Fe	Ni	Cu	SO_4	*
Rear of core	63.7	0.09	6.3	0.06	30.7	3.9	1.3	0.4	57
In-line annulus holder	3.4	0.12	20.6	0.0	38.6	5.0	8.0	4.0	24
Pressurizer	45.3	0.05	1.5	0.43	8.5	7.7	6.7	2.0	73
Pump volute	4.1	0.54	4.9	0.0	23.3	16.8	1.4	7.8	45
Core channel surface	1.2	0.67	0.0	0.0	25.0	5.9	0.0	93.0	

*Weight per cent of scale not represented by listed constituents.

Table 14.3. Material Balance of Scale Constituents

Element	Mass Ratio of Element to Iron in Scale	Mass Ratio of Element to Iron in Stainless Steel	Element Oxidized During In-Pile Exposure (g)	Element in Scale Based on Iron (g)	Excess of Element in Scale over Amount Calculated from Corrosion Data (g)
Zr	0.33		1.08[a]	1.59	0.51
Cr	0.005	0.26	1.21[b]	0.024	−1.19
Ni	0.33	0.15	0.68[b]	1.59	1.37[c]
Fe	(1)	(1)	4.83[b]	(4.83)	(0)

Stainless Steel Oxidized During In-Pile Exposure

Basis of Calculation	Weight Oxidized (g)
Oxygen consumption	6.79
Dissolved nickel	4.6[d]

[a]Based on weight-loss data.
[b]Based on oxygen data.
[c]Nickel in scale plus nickel in solution less nickel oxidized based on oxygen data.
[d]Extrapolated to end of run.

chromium to iron in the scale is less than should be expected if there was no preferential oxidation of any steel component. The nickel in the scale is much greater than expected with no selective oxidation. Thus it appears that nickel is leached or oxidized from the metal more rapidly than iron. A large part of this nickel remains in the scale, but some goes into solution. In some cases, as in L-4-16,[6] the amount in solution is about that expected with no selective oxidation and with complete solution of the nickel. In other cases, as in the L-2-17 experiment, the amount in solution is less than expected on the same basis. As a result, the amount of nickel in solution cannot be regarded as an accurate measure of the amount of steel which has been oxidized.

(*b*) Analyses of Scale from Surfaces of Zirconium Alloys Exposed in the Loop L-2-17 Core. – (1) *Procedure and Results.* – A correlation of in-pile autoclave results in terms of uranium content of the scale was discussed in the previous quarterly report.[7] Specimens exposed in loops, at appreciable fission power densities, do not retain scale of the type encountered with autoclave specimens. However, as was mentioned in the previous report,[8] an extension of the correlation to loop results suggests that, in some cases at least, uranium is sorbed on Zircaloy-2 surfaces exposed in loops and that the quantities sorbed are sufficient to influence the corrosion behavior.

Analytical measurements of the uranium sorbed on two Zircaloy-2 specimens from the core of loop L-2-17 have been carried out. One specimen, ZB-103, was from the channel and was exposed at a solution power density of about 3 w/ml and a solution velocity of about 30 fps. The other, ZB-127, was from the core annulus; the power density was about 4 w/ml and the velocity was about 1 fps. The analytical method was developed and measurements were carried out by the In-Pile Loop Analyses Group in the Analytical Chemistry Division. In outline, the analytical method is the following: A specimen, as removed from the loop, is treated with fuming H_2SO_4. The scale, film,

[7]G. H. Jenks *et al.*, *HRP Quar. Prog. Rep. Oct. 31, 1957*, ORNL-2432, p 120.

[8]G. H. Jenks *et al.*, *HRP Quar. Prog. Rep. Oct. 31, 1957*, ORNL-2432, p 118.

and some metal are dissolved in this treatment. Aliquots of the H_2SO_4 solution are then analyzed for various constituents. The uranium is determined by a fluorometric method. The sensitivity and accuracy of the method are such that 10^{-9} g of uranium in an aliquot can be determined with an accuracy of ±20%.[9] The aliquots which were employed contained about 10^{-9} g of uranium.

In addition to the above-described measurements, an analysis was made of the combined solutions which resulted from the pickling, in preparation for neutron activation analyses, of 12 zirconium-alloy core specimens. Six of the specimens were of Zr-Nb alloys and six of Zircaloy-2. Three of the Zircaloy-2 specimens were from the channel; the remainder of the specimens were from the annulus. All were from locations in the rear, low-flux portion of the core.

The results of the various analyses are given in Table 14.4. The percentages in column 5 are not the true percentages of the element in the respective scales since, in the dissolution of the scale and film, a considerable amount of underlying metal was also dissolved. Values for the total weight of a given element in the scale which are calculated from the analytical results are listed in column 6. Values for the total weight per unit area are listed in the final column. A correction has been applied in these values for the quantities of iron, chromium, and nickel in the analytical samples which can be attributed to the dissolution of the metal sample. For the estimation of these corrections, the following weight percentages in the Zircaloy-2 were assumed: Fe, 0.12%; Cr, 0.1%; Ni, 0.05%.

[9]U. Koskela, private communication to A. R. Olsen.

Table 14.4. L-2-17 Core Specimen Scale Analyses

Specimen	Type	Weight Dissolved (mg)	Element	Element in Sample (%)	Total Element in Scale (μg)	Element in Scale (μg/cm^2)
ZB-103	Core channel coupon	121.5	U	0.01	12	5.5
			Fe	0.17	110	50
			Cr	0.09	20	9.1
			Cu	0.0	0	0
			Ni	0.05	20	9.1
			Zr	70.78		
ZB-127	Core annulus coupon	66.12	U	0.07	46	21
			Fe	0.16	60	27
			Cr	0.10	22	9.1
			Cu	0.07	46	21
			Ni	0.05	12	4.6
			Zr	68.06		
L-2-17 pickling solution		1441.4	U	0.18	2.6×10^3	100
			Fe	20.8	3.0×10^5	1.1×10^4
			Cr	0.0	0	0
			Cu	0.09	1.3×10^3	49
			Ni	0.22	2.7×10^3	100
			Zr	64.00		

(2) *Discussion of Results.* – In order to compare contributions of uranium in solution and uranium in the film to the effective power density at the specimen surface, the total amounts of uranium contributing fission fragments to the surface from the two respective regions were calculated on the basis of 1 cm^2 of area at 280°C. The films from specimens ZB-103 and ZB-127 contained 5.5×10^{-6} g and 2.1×10^{-5} g of uranium per square centimeter, respectively. Considering the uranium in solution which contributes fission fragments to the surface to be contained in the layer extending 30 μ (the fission-fragment range in the solution) from the surface, the solution effectively contained 2.25×10^{-5} g of uranium per square centimeter. Geometrical and theoretical considerations indicate that, for equal amounts of uranium in the film and solution, the amount in the film is about five times as effective in depositing fission-fragment energy in the wall as is that in solution. If corrections in power densities are made on this basis, the points for the two specimens fall between the rate-vs-power-density curve for L-2-15 and L-4-16 (0.17 *m* UO_2SO_4, 0.015 *m* $CuSO_4$, and 0.03 *m* H_2SO_4) and that for L-2-14. The L-2-14 experiment was run with 0.4 *m* sulfuric acid and is of interest for comparison since high acid concentration may suppress uranium sorption on a Zircaloy-2 surface.

Dividing the total weight of uranium from the L-2-17 pickling solution by the number of coupons involved and by the area of the coupons, it is found that 1×10^{-4} g of uranium per square centimeter was contained in the film. This amount is significantly higher than that found on the two Zircaloy-2 coupons. Since there were equal numbers of Zircaloy-2 and zirconium-niobium coupons involved in this analysis, this difference might be attributed to a greater affinity of the zirconium-niobium alloys for the uranium. There is, however, another factor which may account for this difference. All the specimens in this group were located in the rear portion of the core. As was described in Sec 14.1.3, the scale becomes progressively heavier in passing from the high- to the low-flux regions of the core. This heavier scale in the low-flux region may be expected to provide additional surface for sorption of uranium. As an additional point of interest, the presence of a large amount of iron in the pickling solution suggests that this heavier scale is transported iron oxide.

(c) Results of Specimen Weight Measurements and Discussion. – (1) *General.* – Unless otherwise stated, all corrosion-rate values reported below were calculated from weight-loss data, with the exposed specimen area and total radiation time (equivalent to 875 hr of LITR operation at 3 Mw) used as the bases for the calculations. Average solution velocities across the coupons contained in the tapered-channel holders were from 8.7 to 41.2 fps. Solution velocity across the ladder coupon arrays was estimated at 1 fps. Power-density values for the core specimens include the estimated contributions from fast neutrons at the specimen positions.

(2) *Zircaloy-2.* – The results of weight measurements (presented as corrosion rates) for Zircaloy-2 core specimens are listed in Table 14.5 and plotted in Fig. 14.5. For comparison, the L-2-10 results are also plotted in Fig. 14.5. The exposure conditions in these two experiments were similar, except that the temperature was 280°C in L-2-10 and 300°C in L-2-17. The line in Fig. 14.5 is that previously drawn through the L-2-10 data.

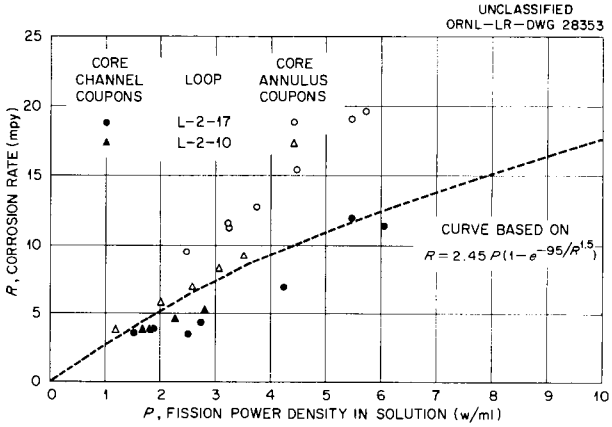

Fig. 14.5. Corrosion Rates of Zircaloy-2 Core Coupons in Loop L-2-17 Based on Exposed Area and Radiation Time.

All specimens from the in-line and pressurizer positions which were measured exhibited weight gains after being defilmed.

As plotted in Fig. 14.5, qualitative agreement is indicated between the results of L-2-17 and L-2-10. However, the agreement may be better, quantitatively, than indicated. If total specimen areas rather than exposed specimen areas are employed in the calculation of corrosion rates, the annulus

Table 14.5. L-2-17 Core Coupon Corrosion Rates

Core Channel Coupons			Core Annulus Coupons			
Power Density (w/ml)	Velocity (fps)	Corrosion Rate (mpy)	Array	Power Density (w/ml)	Velocity (fps)	Corrosion Rate (mpy)
			Zircaloy-2			
6.03	9.4	11.3	ZB-1	5.79	~1.0	19.5
5.68	10.2	11.9	SA-6	5.46	~1.0	19.0
4.14	18.2	6.8	SA-6	4.48	~1.0	15.4
2.85	41.2	4.2	SA-6	3.76	~1.0	12.7
2.68	37.3	3.5	ZB-1	3.09	~1.0	11.6
1.96	13.8	3.8	SA-6	3.09	~1.0	11.4
1.63	10.0	3.6	SA-6	2.56	~1.0	9.6
			Type 347 Stainless Steel			
5.40	11.2	11.4	SA-4	5.79	~1.0	4.5
5.00	12.4	9.8	SA-4	5.47	~1.0	4.2
4.45	15.7	6.9	SA-4	5.10	~1.0	3.6
3.72	27.1	3.5	SA-4	4.80	~1.0	3.3
3.04	37.2	1.4	SA-4	4.45	~1.0	2.9
2.22	18.7	1.1	SA-4	4.17	~1.0	2.5
1.84	12.3	33.4	SA-4	3.96	~1.0	2.0
1.52	9.2	1.5	SA-4	3.76	~1.0	2.0
			SA-4	3.49	~1.0	1.2
			SA-4	3.29	~1.0	1.0
			SA-4	3.09	~1.0	0.70
			SA-4	2.90	~1.0	0.70
			SA-4	2.73	~1.0	0.50
			SA-4	2.56	~1.0	0.50
			SA-4	2.40	~1.0	0.50
			SA-6	5.10	~1.0	4.8
			SA-6	4.17	~1.0	3.5
			SA-6	3.49	~1.0	1.9
			SA-6	2.90	~1.0	1.1
			SA-6	2.40	~1.0	0.60
			Titanium-55A			
6.48	8.7	0.77	SA-6	5.79	~1.0	0.56
4.75	13.8	0.68	SA-6	4.80	~1.0	0.56
3.87	21.6	0.68	SA-6	3.96	~1.0	0.56
3.23	34.3	0.55	SA-6	3.29	~1.0	0.43
2.53	27.8	0.50	SA-6	2.73	~1.0	0.25
2.36	22.4	0.31	TB-1	5.79	~1.0	0.31
2.10	15.9	0.50	TB-1	4.80	~1.0	0.37
1.74	11.0	0.00	TB-1	3.96	~1.0	0.25
			TB-1	3.29.	~1.0	0.19
			TB-1	2.73	~1.0	0.00

rates as well as the channel rates in the two experiments are in agreement as shown in Fig. 14.6. This difference in rate values resulting from the two methods of calculation arises because annulus specimens of two different types were employed in the two experiments. In L-2-10, the ratio of total to exposed area for the annulus coupons is 1.12; in L-2-17 this ratio is 1.57. In the past, the usual practice has been to employ exposed areas in rate calculations.

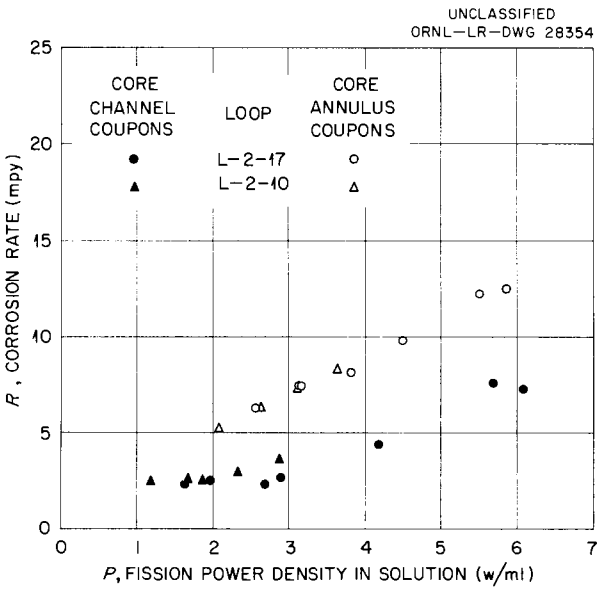

Fig. 14.6. Corrosion Rates of Zircaloy-2 Core Coupons in Loop L-2-17 Based on Total Area and Radiation Time.

Recent results obtained with experiment L-2-19 have indicated that the use of total area yields more consistent and, hence, probably more valid rate values. Coupons of two different types were employed in L-2-19; one with a ratio of total to exposed area of 1.07, the other with the usual ratio of 1.57. Preliminary data show that the rates based on exposed area are greater for the coupons of the usual type than for the ones with a smaller unexposed area. When total areas are employed in rate calculations, the rates for the different types of specimens are in near agreement. From these considerations, it appears likely that the corrosion attack at a given solution power density in the 300°C experiment, L-2-17, is about the same as that in the 280°C experiment, L-2-10.

The L-2-17 results as plotted in Fig. 14.5 or Fig. 14.6 support the postulate, discussed in the previous quarterly report,[8] that the corrosion rate at a given solution power density decreases with increasing solution velocity. The rates posted for the low-velocity annulus coupons are greater than those for the higher velocity channel specimens. Furthermore, the results for the channel specimens indicate that the rates for the central coupons are less than expected when compared with the rates for the specimens located either in the front or back portions of the channel holder. These front and back specimens are exposed to solution velocities of about 10 fps. The central coupons are exposed to velocities as high as 40 fps. The results, which are presented and discussed in Sec 14.1.4(*b*), show that appreciable amounts of uranium are sorbed on surfaces of both the channel and the annulus specimens. The results also indicate that the amounts sorbed on the annulus specimens are greater than those on the channel specimens. It appears likely that uranium sorption on a given Zircaloy-2 specimen is responsible for an appreciable fraction of the total corrosion attack on a given specimen both in L-2-10 and in L-2-17, and that differences in the amount of uranium which is sorbed at different velocities result in the apparent beneficial effect of increasing solution velocity.

(3) *Zirconium Alloys Other Than Zircaloy-2.* – Corrosion rates observed on the core annulus coupons of crystal-bar zirconium alloyed with 15% Nb, 15% Nb–2% Pd, and 15% Nb–1% Fe; sponge zirconium–15% Nb; and crystal-bar zirconium–20% Nb are compared in Table 14.6 with the corrosion rates observed on the Zircaloy-2 core annulus coupons. The data are presented as ratios of the observed zirconium-alloy corrosion rate to the observed Zircaloy-2 corrosion rate, at similar power densities. The Zircaloy-2 rates used for the comparisons are the averages of the rates observed on the coupons in annulus arrays ZB-1 and SA-6. The results are plotted in the usual manner in Fig. 14.7. Alloys subjected to the beta-quench heat treatment exhibited the best corrosion behavior, and the rates for all alloys with this heat treatment are about 70% of those for Zircaloy-2.

All in-line and pressurizer samples which were measured exhibited weight gains after being defilmed.

(4) *Type 347 Stainless Steel.* – The results for core channel specimens are listed in Table 14.5 and plotted in Fig. 14.8. The power-density values

Table 14.6. Relative Corrosion Rates of Zirconium-Alloy Core Annulus Coupons

Alloy	Power Density (w/ml)	Corrosion Rate*				
		A**	B**	C**	D**	E**
Zr (crystal bar)–20% Nb	3.09					1.03
	5.79					0.84
Zr (crystal bar)–15% Nb–2% Pd	4.17	0.69				
Zr (crystal bar)–15% Nb–1% Fe	2.40				0.86	
	2.56			1.34		
	2.74		0.94			
	2.90	0.70				
	3.29				1.03	
	3.48			1.34		
	3.76		0.87			
	3.96	0.71				
Zr (crystal bar)–15% Nb	3.29				0.85	
	3.49			1.35		
	3.76		0.93			
	3.97	0.79				
	4.48				0.82	
	4.80			1.25		
	5.10		0.88			
	5.46	0.72				
Zr (sponge)–15% Nb	2.40				0.82	
	2.56			1.29		
	2.73		0.95			
	2.90	0.74				
	4.48				0.85	
	4.80			1.24		
	5.10		0.95			
	5.46	0.71				

*Ratio of corrosion rate to that of Zircaloy-2 core annulus coupons at similar power densities.

**Heat treatments:
A: beta quenched (1000°C for 2 hr, water quenched).
B: 600°C for 2 weeks; air cooled.
C: 500°C for 2 weeks; air cooled.
D: 400°C for 2 hr; water quenched.
E: beta quenched; preoxidized.

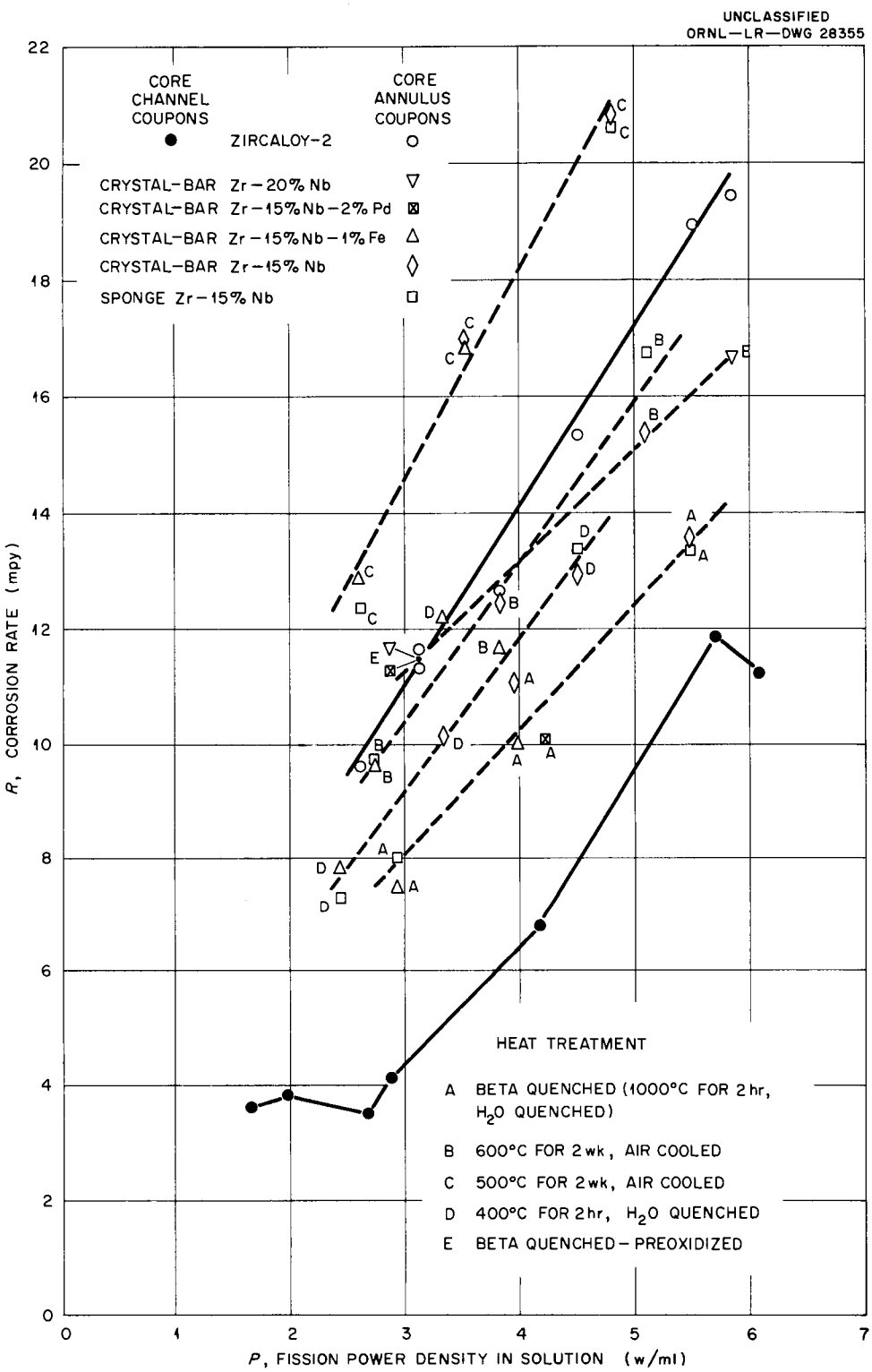

Fig. 14.7. Corrosion Rates of Zirconium-Alloy Core Specimens in Loop L-2-17.

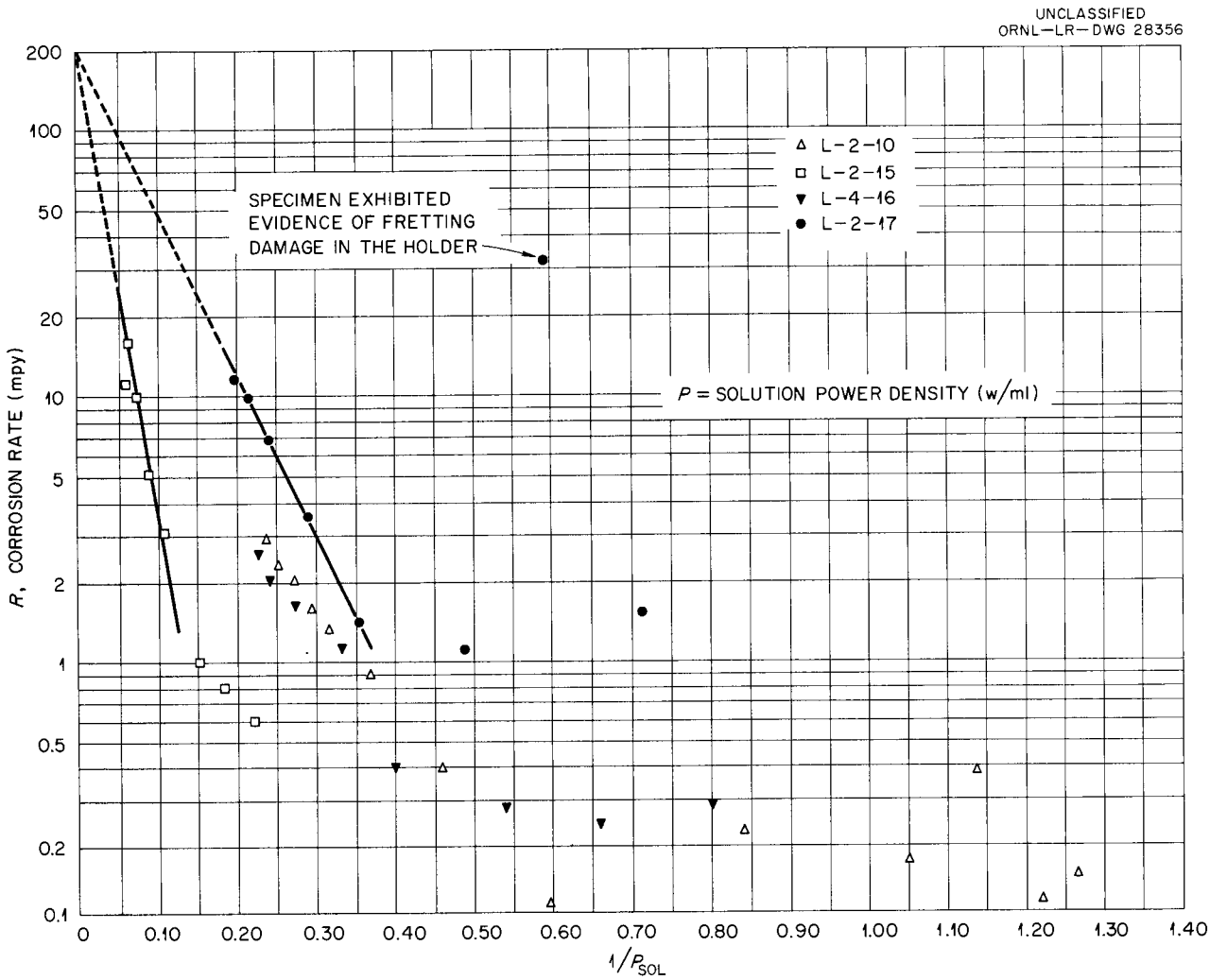

Fig. 14.8. Corrosion Data for Type 347 Stainless Steel in Experiments at 280 and 300°C (Core Channel Specimens).

employed in Fig. 14.8 do not include any contribution from fast neutrons. Core channel data from 280°C loop experiments are included for comparison. The specimen which showed a weight loss corresponding to an average rate of about 30 mpy at a solution power density of 1.8 w/ml exhibited evidence of fretting damage in the holder, and the result should be omitted in the consideration of the radiation-induced corrosion. The corrosion of the steel core channel and annulus specimens appeared to be of the usual type encountered under irradiation; shallow pits are formed which spread laterally to give, as a result, fairly uniform attack.[10]

[10] G. H. Jenks *et al.*, *HRP Quar. Prog. Rep. July 31, 1957*, ORNL-2379, p 110.

The results for core annulus specimens are listed in Table 14.5 and plotted in Fig. 14.9.

The manner in which the steel data are plotted in Figs. 14.8 and 14.9 implies that the corrosion-rate–power-density relationship for steel at the higher corrosion-rate values is of the following general form:

$$R = Ae^{-B/P} ,$$

where R is the corrosion rate, P is the solution power density, and A and B are constants for a given experiment. The primary justification for the use of a plot of this form at this time is that the corrosion data for channel specimens in L-2-17 and L-2-15, above rates of 1 or 2 mpy, form straight

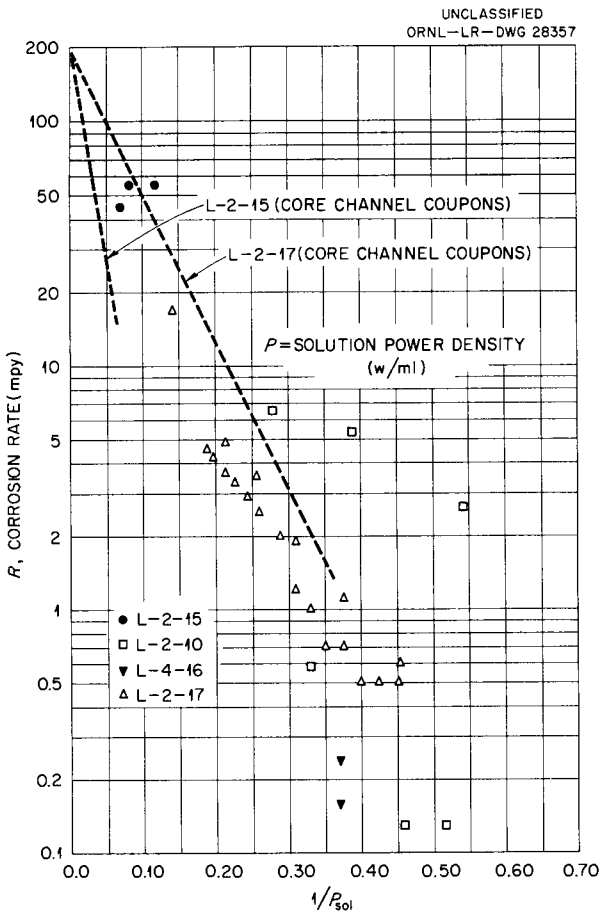

Fig. 14.9. Corrosion Data for Type 347 Stainless Steel in Experiments at 280 and 300°C (Core Annulus Specimens).

lines. However, a model of the corrosion of steel under irradiation has been devised which leads to an equation of this general form. This model will not be discussed here.

The L-2-10 and L-4-16 data do not extend to rates which are sufficiently high to establish the slope for the data. However, it appears from the data available that the value of the constant B in the above equation is smaller for the L-2-17 results than for any of the 280°C results. The exposure conditions for L-2-17 were similar to those for L-2-10 with the exception of temperature. The similarity includes the radiolytic-gas pressures, estimated values of which were about the same in L-2-10 and L-2-17. The channel-holder material in L-2-17 was Zircaloy-2; that in L-2-10 was type 347 stainless steel. However, comparison of the results of L-4-16 and L-2-15 indicated no adverse effect on steel corrosion from the use of a Zircaloy-2 holder; in L-2-15 the holders were of Zircaloy-2, in L-4-16 of type 347 stainless steel. The estimated partial pressure of radiolytic gas in the main stream in L-2-15 was 100 psi; that in L-4-16 was 30 psi.[10]

The annulus results for L-2-17, as shown in Fig. 14.9, indicate that the annulus rates are somewhat less than the channel rates at a given solution power density. The few results available from a given 280°C experiment differ appreciably from those for the channel specimens in the same experiment.

In-line and pressurizer samples showed, after defilming, either weight gains or weight losses that correspond to low rates of corrosion. The data for these specimens are summarized in Table 14.7.

(5) *Stainless Steel Other Than Type 347.* – Corrosion rates observed on the type 17-4 PH, 430, 430L, and 431 stainless steel core annulus coupons are compared in Table 14.8 with the corrosion rates observed on the type 347 stainless steel core annulus coupons. The data are presented as ratios of the observed steel corrosion rate to the observed type 347 stainless steel corrosion rate, at similar power densities. The type 347 corrosion rates used for the comparisons are the averages of the rates observed for the coupons in annulus arrays SA-4 and SA-6. Average corrosion rates for these alloys appear to be somewhat less than those for type 347 stainless steel.

The majority of the stainless steel specimens from the in-line and pressurizer positions lost weight, as measured after defilming. The average corrosion rate as calculated from the weight-loss data is, in each case, less than 1 mpy. The results are summarized in Table 14.7.

(6) *Titanium 55A.* – The results for core channel and annulus specimens of titanium 55A are listed in Table 14.5.

All in-line and pressurizer specimens exhibited weight gains as measured after the defilming operation, with the exception of one of the three pressurizer liquid specimens. The weight loss observed with the exception corresponds to an average corrosion rate of 0.1 mpy.

(7) *Titanium 110AT and Titanium–3% Al.* – Corrosion rates observed on the titanium 110AT and titanium–3% Al core annulus coupons are

Table 14.7. Summary of Data for Steel Specimens from In-Line and Pressurizer Positions, Loop L-2-17

Stainless Steel Type	Position	Array	Number of Specimens	Velocity (fps)	Corrosion Rate (mpy)
347	In-line channel		6	9.2-27.1	*
			1	12.4	0.0
			1	37.2	0.04
	In-line annulus	SA-7	15	1.0	0.0–0.4
		SA-9	5	1.0	0.1–0.4
	Pressurizer vapor	SA-10	3	<1.0	0.3
	Pressurizer liquid	SA-11	3	<1.0	0.3–0.8
17-4 PH	In-line annulus	SA-8	3	1.0	0.1–0.2
430	In-line annulus	SA-8	4	1.0	0.0–0.3
430L	In-line annulus	SA-8	4	1.0	0.1–0.3
	Pressurizer vapor	SA-10	3	<1.0	0.4–0.7
	Pressurizer liquid	SA-11	3	<1.0	0.3–1.2
431	In-line annulus	SA-8	4	1.0	0.04–0.2

*Weight gains, 0.9 to 2.3 mg.

compared in Table 14.9 with the corrosion rates observed on the titanium 55A core annulus coupons. The data are presented as ratios of the observed titanium-alloy corrosion rate to the observed Ti-55A corrosion rate at similar power densities. The titanium 55A corrosion rates used for the comparisons are the averages of the rates observed on the coupons in annulus arrays SA-6 and TB-1. The average rates for the alloys are slightly greater than those for titanium 55A.

14.1.5 In-Pile Loop L-2-19

Irradiation of stainless steel loop L-2-19 has been completed in beam hole HB-2 at the LITR. Total circulation time with enriched solution was 1149 hr, of which 96 hr was accumulated outside the reactor. The energy output of the LITR during the period that the experiment was inserted was 2705 Mwhr. Almost all the energy was liberated at the 3-Mw level. The run was terminated when the circulation pump failed.

Operating conditions and contents were reported previously.[11,12] The solution originally charged to the loop was 0.17 *m* UO_2SO_4 (enriched), 0.02 *m* $CuSO_4$, 0.1 *m* H_2SO_4, and 0.2 *m* Li_2SO_4 (99.9% Li^7) in a light-water solvent. The make-up solution, added to the system to replace solution withdrawn in sampling, was similar to the original solution except that it contained 100 ppm chromium, to inhibit corrosion of the valve stems, and 0.12 *m* H_2SO_4. The calculated free-acid concentration was maintained reasonably constant during the run at about 0.10 *m*, but the calculated sulfate concentration increased gradually from about 47.5 to 49.5 mg/ml at the termination of the run. The main-stream temperature was 280°C, and the pressurizer temperature was 295°C. No evidence

[11] G. H. Jenks *et al.*, *HRP Quar. Prog. Rep. July 31, 1957*, ORNL-2379, p 99.

[12] G. H. Jenks *et al.*, *HRP Quar. Prog. Rep. Oct. 31, 1957*, ORNL-2432, p 119.

Table 14.8. Relative Corrosion Rates of Stainless Steel Core Annulus Coupons

Stainless Steel Type	Power Density (w/ml)	Corrosion Rate*
430	2.56	0.66
	3.29	0.55
	4.17	0.30
	5.47	0.33
430L	2.74	0.75
	3.49	0.50
	4.48	0.56
	5.79	0.37
431	2.40	1.00
	3.09	0.55
	3.96	0.42
	5.10	0.39
17-4 PH	2.90	0.56
	3.76	0.41
	4.80	0.28

*Ratio of corrosion rate to that of type 347 stainless steel core annulus coupons at similar power densities.

of solution instability was observed at these operating conditions. The over-all stainless steel corrosion rate was 1.1 mpy based on oxygen consumption and 0.9 mpy based on the nickel in solution.

14.2 IN-PILE SOLUTION AUTOCLAVE TESTS – LITR

14.2.1 Development, Construction, and Operation

The assembly and operation of rocking-autoclave experiments for radiation-corrosion studies in beam hole HB-5 of the LITR continued. Three experiments, L52Z-110, L53Z-111, and L51Z-105-2, were prepared and operated during the past quarter. In-pile operating times for these three experiments were 231, 165, and 208 hr, respectively. Each of the three autoclaves was operated in a different hole of the HB-5 facility without mechanical difficulty. On this basis it appears that the Oilite bronze sleeve bearings installed in the

Table 14.9. Relative Corrosion Rates of Titanium Alloy Core Annulus Coupons

Alloy	Power Density (w/ml)	Corrosion Rate*
Ti-110AT	2.73	0
	2.90	1.63
	3.49	1.68
	4.17	1.64
	5.10	1.62
Ti–3% Al	2.56	0
	3.09	1.0
	3.76	0.49
	4.47	1.11
	5.46	0.41

*Ratio of corrosion rate to that of Ti-55A core annulus coupons at similar power densities.

fixed plug hole and the ball bearing added to the nose (reactor) end of the autoclave assembly have eliminated the galling noted previously[13] between the rocking plug and the fixed-plug-hole liner.

14.2.2 HB-5 Experiments

Six experiments have been exposed in the new HB-5 facility since it was placed in operation. Results are incomplete for each of these experiments, and only the results of some flux measurements in the facility are discussed. A comparison of flux values from a cobalt flux monitor and from Zr^{95} activity in Zircaloy-2 specimens exposed in autoclave L52Z-107 was made in the previous quarterly report.[14] The values employed in that comparison have been found to be in error. The corrected results are shown graphically in Fig. 14.10. The results of cobalt activation analyses in a second HB-5 experiment, L52Z-110, are included in Fig. 14.10, although the zirconium activation results for this experiment are not yet available.

For each set of data shown in the graph, the indicated flux decreases linearly with increasing

[13] G. H. Jenks *et al.*, *HRP Quar. Prog. Rep. Oct. 31, 1957*, ORNL-2432, p 120.

[14] G. H. Jenks *et al.*, *HRP Quar. Prog. Rep. Oct. 31, 1957*, ORNL-2432, p 127.

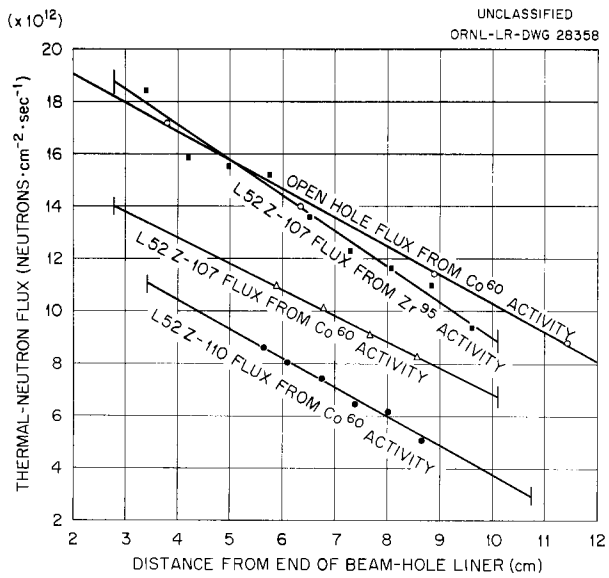

Fig. 14.10. Comparison of Thermal-Neutron Flux Values from Zr^{95} and Co^{60} Activities.

distance from the front of the autoclave. The same linear relationship between position and flux obtains in the experimental facility in the absence of an autoclave, as indicated by the cobalt activation measurement reported previously.[14]

The flux values obtained from cobalt activation measurements in experiment L52Z-107 are about 75% of those derived from zirconium activation measurements. A similar discrepancy between thermal-flux values from Zr^{95} and Co^{60} measurements was observed in in-pile loop experiment L-2-17 (Sec 14.1.2). The source of this discrepancy is unknown, but will be investigated. Corrosion data described below will be discussed in terms of flux values indicated by Zr^{95} measurements. Past results using values indicated by Zr^{95} measurements have been quite consistent, and it is likely that relative values of fluxes from Zr^{95} measurements are valid.

The flux values in experiment L52Z-110, which are indicated by the results of cobalt measurements, are appreciably lower than those in L52Z-107. This lower flux is probably due to the nose bearing, which was employed in L52Z-110 but not in L52Z-107. This bearing is of steel and hence presents an appreciable cross section for neutron absorption. In addition, an experiment employing the bearing must be located about ¼ in. farther from the reactor lattice than one not employing the bearing.

14.2.3 HB-6 Experiments

(*a*) General. – The HB-6 facility is presently being used for radiation-corrosion studies with thorium oxide slurries (see Sec 13.3). No solution autoclaves were operated in HB-6 during the past quarter.

Nearly complete results of several solution experiments previously exposed in the HB-6 facility have recently become available and are presented and discussed. Some of the pertinent information for these experiments is listed in Table 14.10. Preliminary results for some of these experiments have been mentioned in previous reports.

(*b*) Description of Experiments and Results. – (1) *Z-104, Z-106, and Z-112.* – A Zircaloy-2 autoclave containing two type 347 stainless steel, two Zircaloy-2, and two niobium-zirconium specimens was employed in each of these tests. These experiments were planned primarily as part of a series to determine the effect on steel corrosion of radiolytic-gas pressures and of excess acid concentration. However, the interpretation of these steel results will depend upon the results, as yet unavailable, of other experiments in this series. The Zircaloy-2 and zirconium-alloy results can be compared with other results, and, in connection with these, the experiments are described more fully below.

An intention of the experimental design was to provide a system in which the concentration buildup of stainless steel corrosion products would be small by virtue of a large ratio of solution volume to stainless steel surface area. The observed total buildup of nickel in solution was less than 0.01 *m*. However, the increase in the room-temperature pH values of the solutions, as measured after irradiation, was rather large in two of the three autoclaves involved. The pH values were observed as follows: Z-104, pH 1.3 before irradiation, 2.3 after; Z-106, 1.05 before and 1.6 after; Z-112, 1.05 before and 2.9 after irradiation. Chemical analyses indicated about 100 to 150 ppm of chromium in each solution after exposure. The copper concentration in solution was the same in each solution and was at a value calculated to yield a radiolytic-gas pressure comparable with the pressures estimated for the 280°C loop experiments: 100 psi in L-2-15 and

Table 14.10. In-Pile Autoclave Data

Bomb No.	Solution Composition: UO_2SO_4[a] (m)	$CuSO_4$ (m)	H_2SO_4 (m)	Other (m)	Exposure Temperature (°C)	Exposure Time (hr)	Fission Power Density in Solution (w/ml)	Corrosion Rate of Autoclave Material, O_2 Data (mpy)	Corrosion Penetration of Autoclave Material, O_2 Data (mils)	Specimen Data: Specimen Material	Number of Specimens	Corrosion Penetration: Average Value, Weight-Loss Data (mils)	Corrosion Penetration: Average Deviation from Average Value (mils)	Average Corrosion Rate, Weight-Loss Data (mpy)	Uranium in Scale (% U)
L6Z-104	0.173	0.031	0.031		250	20	10.7		0.360	Zircaloy-2	2	0.333	0.004	10.5	
					280	256	10.1	11.0		Zr–15% Nb–1.5% Sn	2	0.172	0.012	5.4	1.1
										347 SS	2	0.227	0.020	7.2	
L6Z-106	0.171	0.031	0.060		280	180	10.2	9.8	0.238	Zircaloy-2	2	0.090	0.087		
										Zr–15% Nb–1.5% Sn	2	0.102	0.002	5.0	2.2
										347 SS	2	0.160	0.040	7.8	
L6Z-112	0.171	0.030	0.060		280	279	11.3			Zircaloy-2	2	0.321	0.014	10.1	2.5
										Zr–15% Nb–1.5% Sn	2	0.197	0.005	6.2	0.6
										347 SS	2	0.284	0.040	8.9	0.5
L6Z-113	0.157[b]	0.037	0.037		280	345	8.2[c]	7.2	0.267	Zircaloy-2	3	0.296	0.012	7.5	
										Niobium	3	0.099	0.002	2.5	25.9
										ZrO_2	2	Decomposed			2.8
L6Z-114	0.168[d]	0.020		0.098 HNO_3	250	150	9.9[e]	7.4	0.178	Zircaloy-2	2	0.178	0.056		
					280	16	9.3[f]			Zircaloy-2 pickled	2	0.216	0.112		3.8
										Zr–15% Nb–1.5% Sn	2	0.278	0.212		14.7
L6Z-115	0.042	0.007	0.020	0.198 Li_2SO_4 (99.9% Li^7)	280	278	~2.5	5.0	0.144	Zircaloy-2	1	0.130		4.1	
										Zircaloy-2 pickled	2	0.117	0.008	3.7	0.1
										Zr–15% Nb	2	0.086	0.007	2.7	0.1
L6Z-116	0.174[g]	0.041	0.041	0.183 Li_2SO_4 (natural)	280	257	~10	5.8	0.283	Zircaloy-2	1	0.282			2.7
					250	212	~10[h]	4.1		Zr–15% Nb	2	0.322	0.055	114% of Zr-2	0.3
										Niobium	2	0.292	0.055	104% of Zr-2	24.8

[a]Enrichment, 93.2% U^{235}.
[b]Final concentration, 0.077 *m*.
[c]4.0 at final uranium concentration.
[d]Final concentration, 0.112 *m*.
[e]6.6 at final uranium concentration.
[f]6.2 at final uranium concentration.
[g]Final concentration, 0.114 *m*.
[h]~6.6 at final uranium concentration.

30 psi in L-4-16 [Sec 14.1.4(*c*)(4)]. In practice, the estimated pressures in the autoclave tests were between 30 and 70 psi.

Values for the average corrosion rate of Zircaloy-2 in each of these experiments as determined from oxygen-pressure measurements and from specimen weight measurements are shown graphically in Fig. 14.11. No reliable results for Zircaloy-2 specimens are available for experiment Z-106 since, through an oversight, the specimens contained fissure defects when installed.[15] In the case of Z-112, discrepancies were observed in the oxygen data, and only the specimen data are considered dependable and are reported. As may be noted in Fig. 14.11, the Zircaloy-2 rates observed in each case are about 20% less than those expected for autoclave systems which are similar to these but which contain no steel specimens. As was mentioned above, the chromium concentration in the irradiated solutions from these autoclaves was 100 to 150 ppm. The indicated reduction in the Zircaloy-2 corrosion rate in the presence of steel is consistent with previous indications of a small beneficial effect of chromium.[16]

[15] G. H. Jenks *et al.*, *HRP Quar. Prog. Rep. Oct. 31, 1957*, ORNL-2432, p 127–128.

[16] G. H. Jenks *et al.*, *HRP Quar. Prog. Rep. Oct. 31, 1957*, ORNL-2432, p 125.

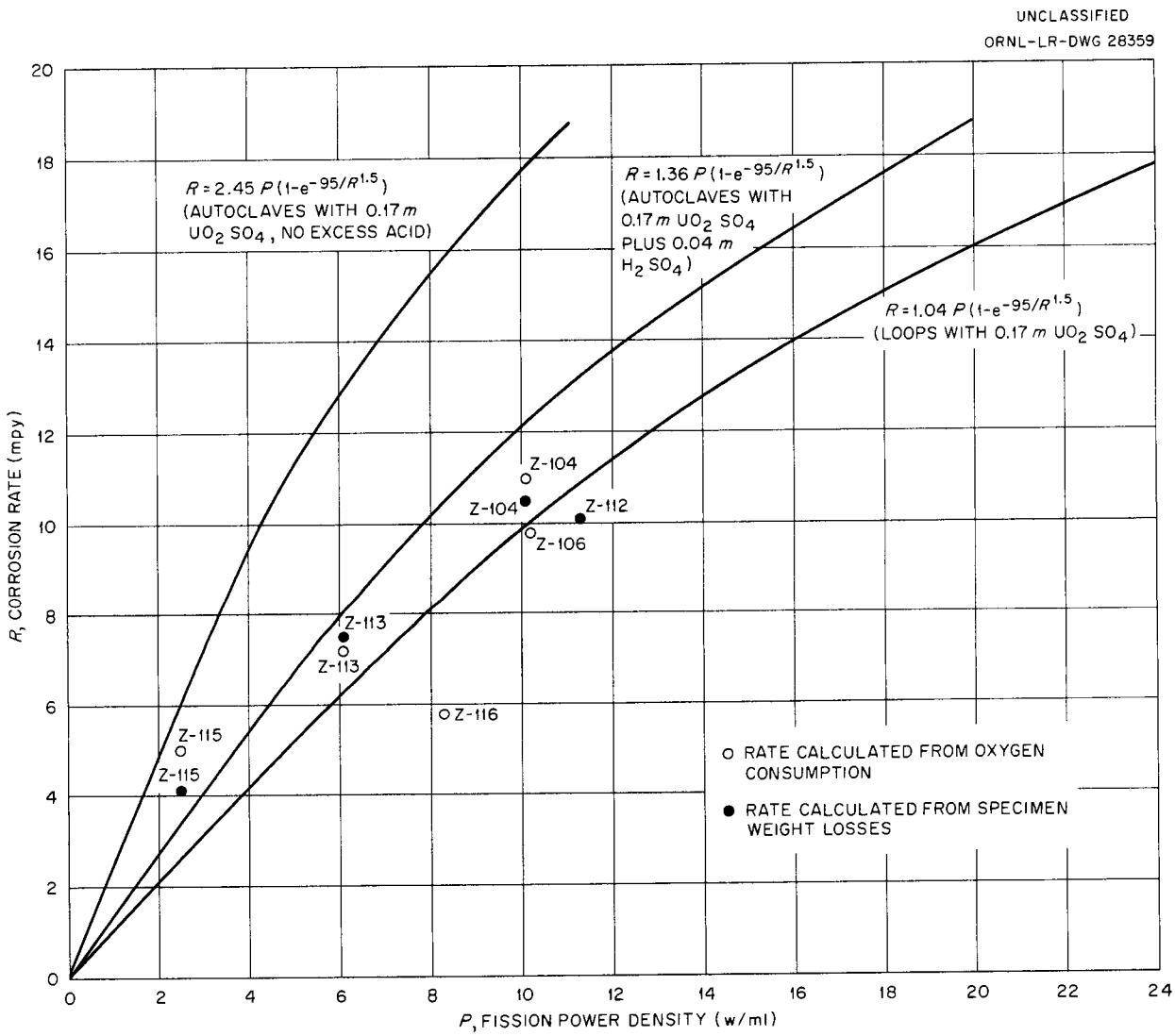

Fig. 14.11. Corrosion of Zircaloy-2 at 280°C in Autoclaves.

The Zr–15% Nb–1.5% Sn alloy specimens in these experiments corroded at an average rate equal to about half that of the Zircaloy-2 specimens.

(2) *Z-113.* – This experiment has been reported previously,[17] but some of the data, in particular the solution power density and the corrosion rate from pressure measurements, were in error. Table 14.10 contains the revised values. The uranium concentration in solution decreased by a factor of about 2 during exposure. Sorption of uranium by the niobium and ZrO_2 specimens probably accounts for this decrease. The effective solution power density in this experiment is uncertain, but for purposes of representing the Zircaloy-2 result in Fig. 14.11, a power-density value corresponding to a uranium concentration intermediate between the initial and final values is employed.

(3) *Z-114.* – This experiment was proposed to investigate further the function of nitrogen in the autoclave systems. Previous data have indicated that a large part of any atmospheric nitrogen enclosed in autoclaves is fixed during irradiation. Many autoclave tests have included sufficient atmospheric nitrogen to yield a 0.05 *N* solution of nitrogenous material in the autoclave if all the included nitrogen were in solution. The Z-114 initial solution was 0.17 *m* in UO_2SO_4 and 0.1 *m* in HNO_3. After irradiation the uranium concentration was 0.11 *m*. The results of analyses for NO_3^-, NH_3, and total nitrogen were inconsistent, but ammonia was found in the irradiated solution, and the pH of the final solution was 2.9 whereas the initial pH was 1.0. The weight-loss results from the three pairs of duplicate specimens show a large disagreement and indicate a correspondence between the corrosion rate of a specimen and the relative orientation of the specimen in the autoclave. The pin specimens were held in a rack with all pins parallel. In cross section, the pins lie at the corners of a hexagon with duplicate specimens located across the hexagon from each other. Three consecutive pins, one of each material, corroded relatively less than the other three. The data are consistent with the interpretation that the three pins in the lower portion of the autoclave witnessed a different medium than the other three, perhaps due to an unstable solution. The average rate for the two Zircaloy-2 specimens which exhibited the smaller amount of attack is 6.0 mpy. This is about the rate expected for a UO_2SO_4 solution containing excess H_2SO_4 but no HNO_3. The average rate for the other two Zircaloy-2 specimens is 14.8 mpy. Results for the Zr-Nb-Sn alloy in this experiment are also of uncertain significance; the average rate for one specimen is 3.4 mpy, and that for the other is 25.9 mpy. The values for corrosion penetration from specimen data listed in Table 14.10 are average values for duplicate specimens.

(4) *Z-115 and Z-116.* – These experiments employed solutions which were 0.04 *m* and 0.17 *m* in UO_2SO_4, respectively. Each was about 0.2 *m* in Li_2SO_4. Zirconium activation data are not yet available, and the power-density values listed in Table 14.10 and shown in Fig. 14.11 are based on estimated flux values. In addition, an appreciable amount of uranium was lost from the Z-116 solution during exposure, and the power-density value plotted in Fig. 14.11 corresponds to a uranium concentration intermediate between the initial and final values. Part of this loss of uranium can be accounted for in the large amount of uranium found in the scale from the niobium specimens.

In the case of Z-116, the addition of the Li_2SO_4 appears to have offered some protection against Zircaloy-2 corrosion at 280°C. The rate at this temperature, as determined from oxygen measurements, is a factor of about 2 less than that expected with a solution which is similar but which contains no Li_2SO_4. At 250°C, the rate observed is only slightly less than that expected for a solution free of Li_2SO_4: 4.1 mpy observed as compared with 4.8 mpy expected without Li_2SO_4. In this connection it may be noted that the Z-26 experiment[18] with added $MgSO_4$ was operated at 250°C, and no beneficial effect of the addition was noted.

The corrosion rate of Zircaloy-2 in Z-115 should be compared with similar 0.04 *m* UO_2SO_4 experiments at 280°C without added Li_2SO_4. These are Z-12 and Z-18 (about 10 mpy at 4.2 and 4.9 w/ml, respectively) and Z-27 (14.5 mpy at 4.3 w/ml). The comparison is not very clear, particularly in view of the fact that the power-density value given for Z-115 is an estimate, but there was probably some reduction in corrosion rate in Z-115 due to Li_2SO_4.

[17] G. H. Jenks *et al.*, *HRP Quar. Prog. Rep. Oct. 31, 1957*, ORNL-2432, p 129.

[18] G. H. Jenks *et al.*, *HRP Quar. Prog. Rep. Jan. 31, 1957*, ORNL-2272, p 110–113.

An empirical correlation of autoclave corrosion data for Zircaloy-2 with the amount of uranium found in samples of the loose scale formed on specimens has been reported.[19] The data for the experiments under discussion do not establish whether the beneficial effect of Li_2SO_4 is due to a reduced sorption of uranium in the scale. The scale from Z-116 is reported to be 2.7% uranium, about the same as the 1 to 3% reported for comparable experiments with excess H_2SO_4 but without Li_2SO_4. However, the final portion of the radiation exposure for this experiment was at 250°C, and at this lower temperature little if any beneficial effect of the additive on the corrosion rate was noted. The Z-115 scale is reported to be only 0.1% uranium. Scales from comparable experiments without Li_2SO_4 have contained 2.5 to 3% uranium. The results of scale analyses from other autoclave experiments with Li_2SO_4 have also been inconclusive.

Specimens of Zr–15% Nb were included in experiments Z-115 and Z-116. In Z-115, the relationship between the observed rates for Zircaloy-2 and the niobium alloy is about that expected for the solution without Li_2SO_4. In Z-116, the rate for the alloy is slightly greater than that for Zircaloy-2 and is about equal to the rate expected for the solution without Li_2SO_4. The explanation for these differences is unknown, but the Z-116 results indicate that the presence of Li_2SO_4 has little effect on the niobium-alloy corrosion under these conditions.

In connection with considerations of the effect of scale uranium on corrosion, it may be noted that in one of these experiments the reported uranium is 0.1%, and in the other, 0.3%. The scales from the Zr-Nb-Sn alloy specimens in experiments Z-112 and Z-114 were also analyzed for uranium; weight percentages of 0.6 and 14.7, respectively, are reported for these. If the latter result obtained under the exceptional solution conditions in Z-114 is disregarded, it appears that the amount of uranium sorbed on the niobium-alloy scales in these experiments is a factor of 5 to 10 less than that usually found in Zircaloy-2 scales. As for Zircaloy-2, there is no clear evidence in these results that the presence of Li_2SO_4 in solution has any appreciable effect on the amount of sorbed uranium.

[19] G. H. Jenks *et al.*, *HRP Quar. Prog. Rep. Oct. 31, 1957*, ORNL-2432, p 120–126.

Niobium metal specimens which were included in Z-116 corroded at about the same average rate as the Zircaloy-2 specimens. In comparison, niobium specimens in experiment Z-113, mentioned above, corroded at an average rate about one-third of that for Zircaloy-2 in that experiment. These results indicate that the radiation corrosion of niobium is not greatly affected by excess Li_2SO_4. In both experiments, the niobium specimens developed a very heavy scale which was about 25% uranium by weight. In Z-116, this percentage of uranium is about a factor of 10 greater than that found in the scale from Zircaloy-2 specimens. The scale from Zircaloy-2 specimens in Z-113 was not analyzed separately, but a concentration of 1–3% uranium is expected under these conditions.

14.3 SUPPORTING RESEARCH

In a manner analogous to experiments previously performed on zirconium and titanium,[20] type 347 stainless steel foil specimens, 0.6 × 0.18 cm, contained in a thermal siphon loop were exposed for approximately 45 hr at 280°C to Van de Graaff electrons. The test-solution composition was 0.04 *m* UO_2SO_4, 0.01 *m* $CuSO_4$, and 0.025 *m* H_2SO_4. Current densities were approximately 40 $\mu a/cm^2$ at the specimen surface, and it is estimated that the power density in the solution adjacent to the specimens was about 60 w/ml.

The specimens were not defilmed after exposure; they were weighed as removed. Weight changes of $+3.3 \times 10^{-5}$ and $+1.4 \times 10^{-5}$ g for the upstream and downstream specimens, respectively, as compared with $+3.1 \times 10^{-5}$ g for the irradiated specimen, were obtained under these experimental conditions. Microscopy revealed little difference between the unirradiated and irradiated specimens.

It appears, therefore, that the effect of Van de Graaff electron irradiation on the corrosion of type 347 stainless steel is a minor one under the experimental conditions employed.

Similar experiments are being made by use of a 23-Mev proton beam supplied by the 86-in. cyclotron at Y-12.

14.4 HRT CORROSION SPECIMENS

A program has been in progress for some time in the Homogeneous Reactor Project to design equipment and facilities necessary for the installation and evaluation of mechanical-property and

[20] G. H. Jenks *et al.*, *HRP Quar. Prog. Rep. Oct. 31, 1957*, ORNL-2432, p 130.

corrosion specimens in the HRT core and blanket regions. Most of the design work has been carried out in the Design Section.[21] The Materials Research Section is conducting the testing program, and the tests will be reported here.

The specimens for use in these tests are in the form of subsize impact and tensile specimens. These are mounted in titanium holders designed to be inserted through existing flanged openings in the core and blanket vessels.[21]

A titanium holder containing a total of 24 of the subsize impact and tensile specimens was installed in the blanket of the HRT on December 30, 1957. The test specimens are fabricated from type 347 stainless steel, titanium A-40, titanium 110AT, Zircaloy-2 (welded), Zr–15% Nb (alpha quenched), and Zr–15% Nb (beta quenched). Installation of the test specimens in the core region of the HRT has been delayed, pending completion of the initial power operation.

Several additional holders and sets of test specimens for both the core and blanket regions have been fabricated. A supply of these assemblies is required since it is planned to remove assemblies for examination during periods of reactor shutdown. New specimen-holder assemblies will then be inserted.

[21] W. R. Gall *et al.*, *HRP Quar. Prog. Rep. Oct. 31, 1955*, ORNL-2222, p 7–10.

15. METALLURGY

G. M. Adamson

R. G. Berggren
E. S. Bomar
F. W. Cooke
W. J. Leonard
M. L. Picklesimer
J. J. Prislinger
P. L. Rittenhouse
R. L. Stephenson
J. K. White
J. C. Wilson
C. H. Wodtke

15.1 PHYSICAL METALLURGY

15.1.1 Zirconium-Alloy Development

Zirconium-base alloys containing niobium have shown the greatest promise in the development of a high-strength corrosion-resistant alloy to replace Zircaloy-2 as the HRP core-tank material. Basic physical-metallurgy studies and in-pile corrosion tests are being used to procure the information necessary for the development of these alloys.

Data on the transformations occurring in the Zr-Nb-*X* alloy systems have been reported in four prior reports,[1–4] and the progress and mechanisms of the transformations were summarized in the last report.[5]

Quench-and-reheat transformation data have now been obtained on all the Zr-Nb-*X* alloys over the range of compositions and temperatures of interest in the alloy development program. Most of the work has been performed on the Zr-15Nb-*X* alloys, with a small amount having been performed on the Zr-20Nb-*X* alloys and on the Zr-Nb binary alloys. The ternary additions have been in the amounts of 2 and 5 wt % for the elements Pd, Pt, and Mo; 1 wt % for Fe, Ni, Al, and Cr; ½ wt % for Cu; 3 wt % for V; 2 wt % for Th; and 5 wt % for Ta. The binary alloys have contained niobium in the amounts of 5, 7.5, 10, 15, 20, 25, and 33 wt %. Data on the oxides (type formed in air at several temperatures and in water and uranyl sulfate at 300°C) have been obtained for essentially all the above alloys, plus a number of binary and ternary alloys containing Ag, Sn, Si, Mn, Y, and Ti.[6] Oxidation rates in air at 600°C have been obtained on a number of the more promising alloys (judged on the basis of in-pile corrosion data and transformation kinetics) and at 700°C on the alloys that showed oxidation resistance better than Zircaloy-2 at 600°C. In-pile loop corrosion data, in the fuel solutions, have been obtained (see Sec 14.1.4) on some of the binary and ternary alloys in several heat-treated conditions. During the past quarter, long-time aging data on several of the ternary alloys were obtained at 400 and 500°C. These data, along with representative portions of the transformation data obtained previously, are summarized in Table 15.1 for the alloys Zr-15Nb, Zr-15Nb-2Pd, Zr-15Nb-5Pd, Zr-15Nb-2Mo, and Zr-15Nb-5Mo. As can be seen from an examination of these data, the addition of 2Pd to the Zr-15Nb base alloy delays the hardening transformation, 5Pd and 2Mo delay it more, and 5Mo almost suppresses it. Aging data for all the test alloys are now being obtained at all temperatures of investigation for times up to and including three weeks.

In general, the ternary additions, except for Ta and O_2, increased the incubation period for the hardening reaction at all temperatures, with Fe, Ni, and Cr having the least effect, Pt and Pd an intermediate effect, and Mo the greatest effect. The additions of Cu and Al drastically reduced the maximum temperature at which the hardening transformation can take place and reduced the temperature at which the hardening transformation takes place at the maximum rate, but did not increase the incubation period for the reaction

[1] G. M. Adamson *et al.*, *HRP Quar. Prog. Rep. Oct. 31, 1956*, ORNL-2222, p 114–116.

[2] G. M. Adamson *et al.*, *HRP Quar. Prog. Rep. Jan. 31, 1956*, ORNL-2272, p 119–123.

[3] G. M. Adamson *et al.*, *HRP Quar. Prog. Rep. April 30, 1957*, ORNL-2331, p 124–138.

[4] G. M. Adamson *et al.*, *HRP Quar. Prog. Rep. July 31, 1957*, ORNL-2379, p 122–126.

[5] G. M. Adamson *et al.*, *HRP Quar. Prog. Rep. Oct. 31, 1957*, ORNL-2432, p 131–133.

[6] O. Zmeskal, *HRP Quar. Prog. Rep. July 31, 1956*, ORNL-2148, p 112–114 (classified).

Table 15.1. Quench-and-Reheat Hardness Data for Various Zirconium-Niobium-Base Alloys

Reheat Temperature (°C)	Reheat Time (hr)	Diamond Pyramid Hardness, 10-kg Load				
		Zr-15Nb	Zr-15Nb-2Mo	Zr-15Nb-5Mo	Zr-15Nb-2Pd	Zr-15Nb-5Pd
Beta quench		210	187	235	185	210
400	0.5*	390	197	227	325	210
	1*	390	193	230	358	209
	2*		191	230		221
	2	400	192	216	395	227
	6		314	221		254
	16		253	216		289
	24	405	279	203	428	304
	48	402	300	210	415	366
	168	398	366	221	435	401
	336	410	339	224	435	417
	504		354	227		429
500	0.5*	250	189	222	188	209
	1*	260	186	225	230	206
	2*		188	227		213
	1	240	187	221	180	199
	2	255	182	221	262	206
	6		187	221		232
	16		219	216		266
	24	280	235	216	255	276
	48	287	240	218	260	283
	168	270	256	232	257	289
	336	255	251	245	210	285
	504		240	256		276

*Specimens run in isothermal transformation machine.
All other specimens run in quartz capsules.

sufficiently to prevent excessive hardening in the heat-affected zone of a weldment. The addition of 5 wt % Ta to the Zr-15Nb base alloy resulted in the formation of a completely martensitic structure on quenching from the beta field, and the addition of oxygen by the use of sponge Zr resulted in an increase in the rate of all transformations. In general, an increase in the amount of the ternary addition resulted in an increase in the effect on the transformations occurring in that system.

An examination of these data, plus the data obtained on the in-pile corrosion resistance to uranyl sulfate, has shown that the future investigations should be confined primarily to the ternary alloys Zr-15Nb-*X* and Zr-20Nb-*X*, with *X* as 2 and 5 wt % Mo and 2 and 5 wt % Pd. Small-scale investigations of the Zr-Pd and Zr-Pt binary alloy systems will be continued because of their apparent promise in in-pile corrosion resistance to the fuel solutions; as yet, insufficient metallurgical data are available to show the complexity of these systems.

Representative binary and ternary zirconium-base alloys under study in the alloy development program have been oxidized in air at 600°C to determine relatively their oxidation resistance. Certain of these alloys which showed good oxidation resistance were oxidized in air at 700°C. Control samples of iodide zirconium and Zircaloy-2 were also oxidized to provide a basis for comparison. Samples approximately

0.060 in. thick by ½ in. wide by 1 in. long were chemically polished, weighed, and inserted into a hot furnace at the desired temperature for a short-time exposure, generally 1 hr. The weight change was determined, and the same samples were reinserted into the furnace for further oxidation. When possible, they were oxidized in steps for a total time of 64 hr. The data are presented in Tables 15.2 and 15.3.

Alloys Zr-15Nb-5Pd, Zr-15Nb-½Cu, and Zr-15Nb-5Mo showed better oxidation resistance than Zircaloy-2 at both 600 and 700°C, while Zr-15Nb-2Pt was slightly better at 600°C and slightly worse at 700°C. The Zr-15Nb-2Mo-2Pd was better than Zircaloy-2 at 700°C. In no case was any alloy comparable with the iodide zirconium at 600°C. Iodide zirconium has not as yet been oxidized at 700°C. The alloys which showed the lower oxidation rates all had glassy-appearing oxides which remained adherent, except for edge cracking, for the entire test period. Those alloys which had poor oxidation resistance in air all showed early spalling and cracking of the oxide films.

Table 15.2. Weight Gain for Zirconium-Base Alloys Oxidized in Air at 600°C

Alloy	Weight Gain (mg/cm^2)			
	1 hr	16 hr	32 hr	64 hr
Iodide Zr	0.23	0.85	1.16	1.50
Zr-15Nb-5Mo	1.80	3.93	5.06	6.82
Zr-15Pt	0.64	2.66	4.31	7.56
Zr-15Nb-5Pd	1.14	2.56	3.75	7.82
Zr-15Nb-½Cu	1.08	2.78	4.53	8.46
Zr-15Nb-2Pt	0.81	2.52	3.77	8.60
Zircaloy-2	0.21	2.96	5.26	9.38
Zr-15Nb-2Mo	1.68	4.02	7.04	10.50
Zr-15Nb-2Pd	0.98	4.18	7.85	15.12
Sponge Zr-15Nb	1.15	4.54	8.81	16.50
Zr-15Nb-3V	0.74	2.35	6.12	21.76
Zr-15Nb	1.15	5.71	12.60	22.00*
Zr-15Nb-1Cr	1.09	4.57	10.50	23.40
Zr-15Nb-2Th	0.68	5.22	12.76	23.75
Zr-15Pd	1.28	7.14	19.70	37.22
Zr-15Nb-1Al	2.71	6.96	8.70	**

*Some oxide was lost, so the weight gain was probably 25 mg/cm^2 or greater.

**Scaling resulting in weight loss at 64 hr.

Table 15.3. Weight Gain of Zirconium-Base Alloys Oxidized in Air at 700°C

Alloy	Weight Gain (mg/cm^2)			
	2 hr	8 hr	16 hr	32 hr
Zr-15Nb-5Pd	2.47	4.02	5.43	7.09
Zr-15Nb-½Cu	2.58	4.77	7.21	13.50
Zr-15Nb-5Mo	3.35	6.65	9.35	13.53
Zr-15Nb-2Mo-2Pd	3.48	7.54	11.06	15.00
Zircaloy-2	2.27	6.22	12.83	28.37
Zr-15Nb-2Pt	2.30	6.25	12.37	28.70

15.1.2 Zirconium-Hydrogen Study

A study has been initiated with the main purpose of developing methods by which thin hydride layers on Zircaloy-2 may be identified and studied. Major unanswered questions concerning a homogeneous reactor system are whether the zirconium core tank will pick up hydrogen from either the corrosion reactions or from dissociation of the heavy water and, if so, how the resulting hydrides will be distributed. Furthermore, it has often been postulated that a hydride layer exists between the metal and the oxide layer formed during the aqueous corrosion of zirconium-base alloys. As yet, however, the existence of such a layer has not been demonstrated experimentally. As a first step in this study, hydride layers of varying thickness are being placed upon Zircaloy-2 specimens, and various techniques are being evaluated to demonstrate the presence of this known layer.

To prepare specimens for study, Zircaloy-2 was hydrided at 400°C in the Seivert's apparatus to a total hydrogen content of 100 and 500 ppm. Since, at these hydrogen levels, the specimens had a sufficient content of hydrogen to produce both alpha zirconium saturated in hydrogen and the hydride, the hydride formed would exist as a surface layer. These specimens were mounted

in Bakelite, with a polyethylene layer being placed between the specimen and the mount for the preservation of the surface edge. "Slant" polishing was used to extend the surface layer sufficiently to permit examination under the optical microscope. After being polished and etched, the specimens were anodized[7] to identify the hydride, both in the surface layer and in the interior of the specimen. A hydride layer was found and examined in the specimen containing 500 ppm H_2. An indication of the existence of a hydride layer was found in the specimen containing 100 ppm H_2, but the layer could not be positively identified or examined because of edge rounding even in the slant-polished specimen. The development of methods for preserving the edge is continuing. New etchants are being examined for sensitivity in revealing the hydride layer, and a technique of replication involving the use of Faxfilm replicas is being tried. Such a technique, if successful, would find its greatest use in the examination of irradiated specimens.

15.2 MECHANICAL METALLURGY

15.2.1 Titanium

To ensure sufficient ductility and reliability of A-40 titanium (35 ppm H_2) as a reactor material, a mechanical-property study is being conducted. Although not thought to be serious, a reduction in impact properties of A-40 titanium has been found[3] in the neighborhood of 250°C. Since this temperature is within the proposed operating range of the reactor, attempts are being made through mechanical testing to understand these phenomena.

In tensile tests Rosi and Perkins[8] have also found a decrease in ductility, as measured by per cent elongation, for high-purity material in the range of 230 to 450°C. With A-110AT, an all-alpha alloy, Makrides and Baldwin[9] also reported a dip in the reduction-in-area curve. Increasing the strain rate from 0.05 in./in./min to 100 in./in./min moved the trough from 370 to 540°C. These investigators suspected a strain-aging phenomenon as the cause of this embrittling.

While tensile and creep tests are planned with A-40 titanium in the range of interest, the first tests were on samples aged in the absence of stress. A group of Charpy V-notched impact samples were aged for 3024 hr at 300°C. The data are plotted in Fig. 15.1, along with the original impact curve. There is very little, if any, significant difference between the two curves, which shows that the trough is not caused by a simple aging mechanism and confirms the data obtained with subsize samples in a previous study on the effect of hydrogen concentration on the aging of titanium.[4]

A mechanical-property study is being made on a plate of A-70 (400 ppm H_2) titanium to determine what may be expected of this and other contaminated material. Such data should also be helpful in the long-range study of brittle fracture in hexagonal metals.

With the transition temperature for this alloy occurring above 100°C, it was not possible to use the standard drop-weight procedures, since at these high transition temperatures the hydrogen in the brittle crack-starter deposit goes into solution. For these drop-weight tests the crack-starter deposit was made by depositing a layer of titanium from a rod which had previously been contaminated with oxygen.

In Fig. 15.2 are presented Charpy V-notch impact curves for two specimen orientations, the nil ductility transition (NDT) temperature from the drop-weight test being indicated. The impact transition is more definite, with an abrupt change in slope which occurs at a much higher temperature than for the uncontaminated alloys. The NDT temperature for this material occurred at the break in the curve, while with comparable but uncontaminated alloys it was on the flat portion of the curve at a lower temperature than the impact transition. This new position more nearly corresponds to what is found with steels than do the previous locations. In contrast to most previous titanium samples, with this material a rather marked change in fracture appearance occurs within a narrow temperature range at what corresponds to the NDT temperature in the drop-weight test. It seems likely that the transition temperature for this contaminated A-70

[7] M. L. Picklesimer, *Anodizing as a Metallographic Technique for Zirconium-Base Alloys*, ORNL-2296 (May 24, 1957).

[8] F. D. Rosi and F. C. Perkins, *Trans. Am. Soc. Metals* 45, 972–992 (1953).

[9] N. Makrides and W. M. Baldwin, Jr., *High Temperature Brittleness in Titanium Alloys*, WADC-TR-57-251(Pt I) (March 1957).

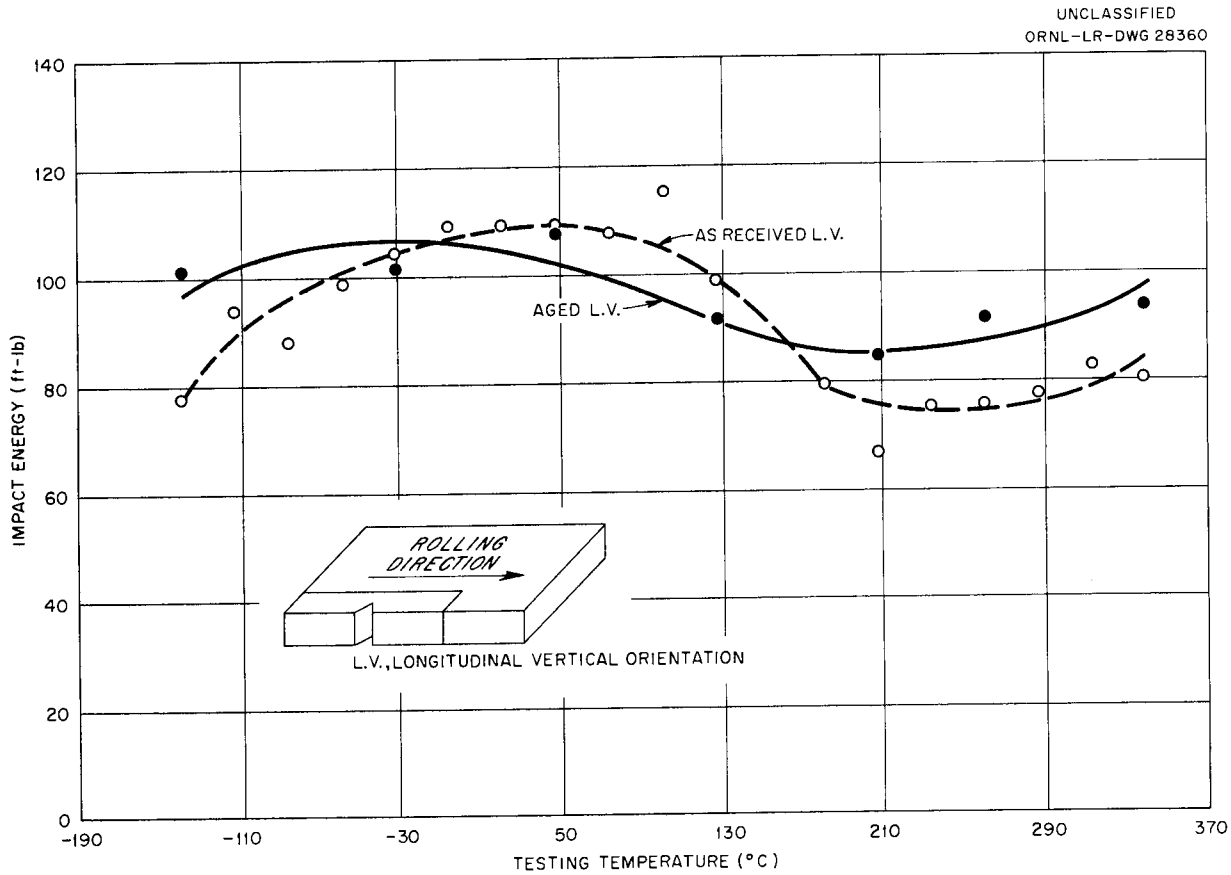

Fig. 15.1. Charpy Impact Strength of As-Received and Aged A-40 Titanium.

titanium is related to the brittle hydride going into solution.

15.2.2 Zirconium Alloys

A program on the mechanical properties of zirconium alloys has been scheduled to obtain the mechanical-property data required by the designers and to understand better the meaning of the mechanical properties of the hexagonal metals. With a hexagonal metal, the effect of preferred orientation is likely to be greater than it is for the common cubic metals.

Full-size Charpy V-notch impact specimens were cut from four different orientations in a ½-in. plate of Zircaloy-2, fabricated by the Bureau of Mines. This plate contained 16 ppm of hydrogen and was fabricated (forged and rolled at 850°C) by essentially the same procedure used for the HRT core-tank plates. As shown by the divergence in the four curves presented in Fig. 15.3, considerable anisotropy was present in this plate. The orientation of the notch seems to have a greater effect than the specimen orientation. Specimens cut from both plate directions but with horizontal notches showed no definite transition region either in fracture appearance or in energy values. The energy values are fairly low for all temperatures; yet all the specimens showed shear lips, which are normally considered a mark of a ductile fracture. The specimens with a vertical notch gave curves that seem to indicate a transition region, but all energy values are higher than with the horizontal notch. The specimens with the vertical notch broke with a very unusual S-shaped fracture. The height of the S decreased with decreasing temperature. These tests well illustrate the premise that the usual brittle fracture relationships cannot be applied to hexagonal metals.

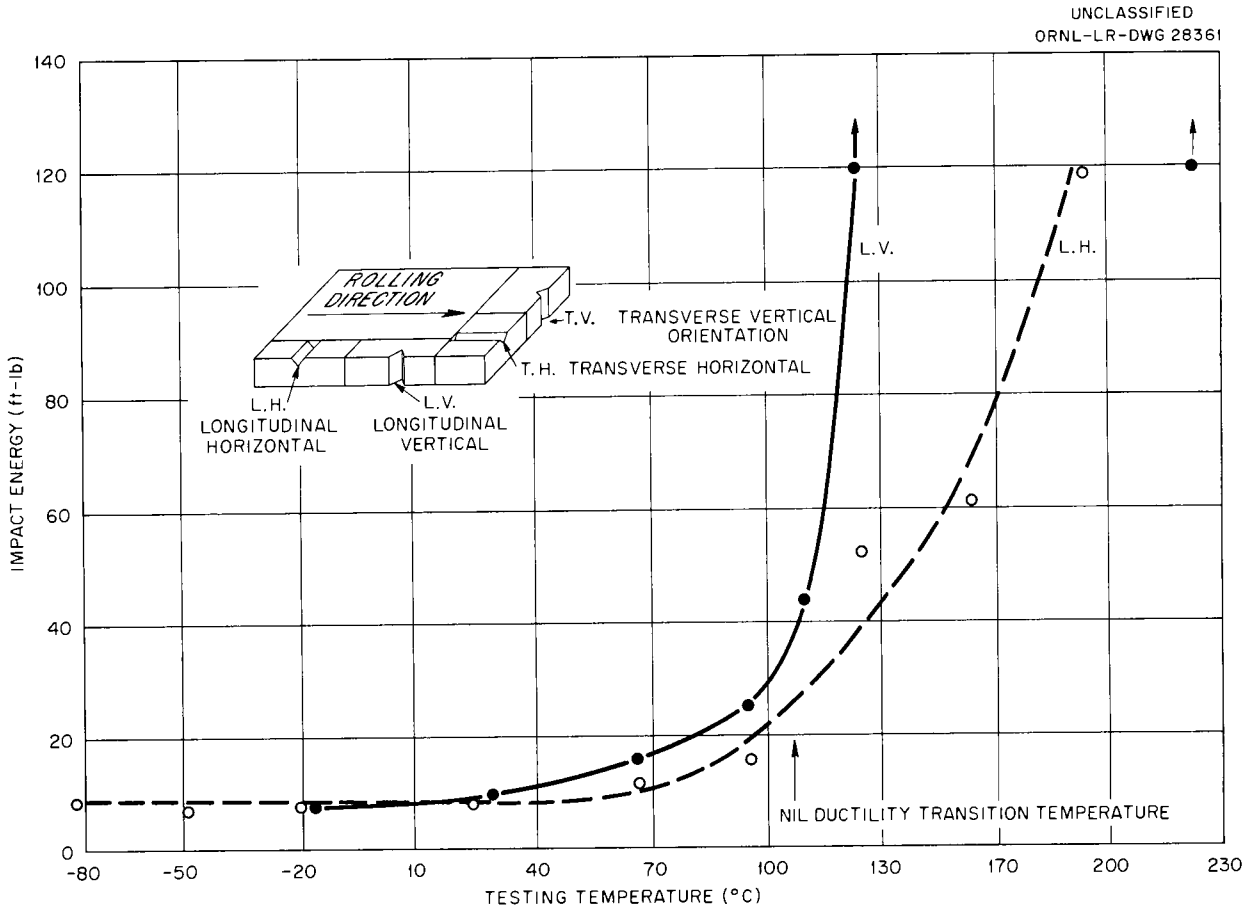

Fig. 15.2. Charpy Impact Strength for Two Specimen Orientations of Contaminated A-70 Titanium.

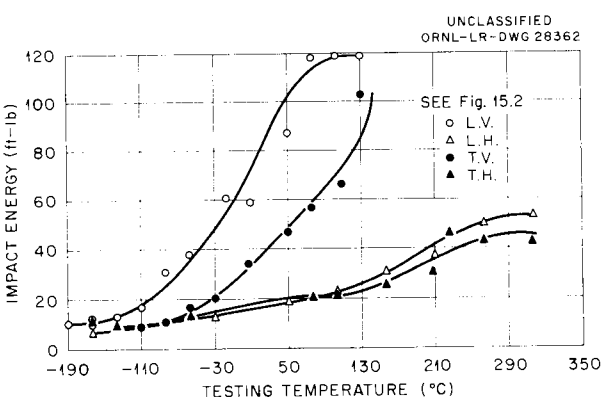

Fig. 15.3. Effect of Specimen Orientation on Impact Properties of Zircaloy-2.

15.2.3 Mechanical Properties of Irradiated Titanium Alloys

Various titanium-base metals of interest to the Homogeneous Reactor Project are being tested in in-pile uranyl sulfate corrosion loops to determine whether any changes occur in the mechanical properties as a result of either hydrogen pickup or neutron irradiation.

During this period, A-40 and C-130AM titanium tensile specimens from in-pile loop L-2-14 were broken.[10] No large change in properties of either alloy was noted. There does seem to be a small

[10] G. H. Jenks *et al.*, *HRP Quar. Prog. Rep. April 30, 1957*, ORNL-2331, p 118.

increase in tensile and yield strengths and, at least with A-40, a decrease in ductility. More exact data will be presented in the next report when information is available on the reproducibility of the subsize tensile tests with these metals.

15.2.4 Creep Studies

Preliminary creep tests are being conducted on Zircaloy-2 and titanium 45A and A-110AT. The purpose of these tests is to provide experience with the equipment and to determine the reliability of the data obtained. Data for time-deformation curves are presently being collected for stress levels in the vicinity of the short-time yield strength at 600°F. As expected, the data indicate that for times below 1000 hr the above-mentioned materials are quite creep-resistant at 600°F. The tests are continuing to determine the time required before third-stage creep begins.

15.3 WELDING DEVELOPMENT

15.3.1 Titanium-Alloy Welding

Alpha-titanium alloys are simple, stable alloys which possess much better mechanical properties than the unalloyed grades and which, unlike most titanium alloys, are considered to be weldable. Attempts are now being made to develop procedures by which such alloys may be field-welded to produce welds of reactor quality.

Two weldments were made in 3-in.-dia pipe having $\frac{1}{16}$-in. wall thickness. This pipe was prepared by seam-welding $\frac{1}{16}$-in. sheet stock of titanium A-110AT alloy which had been roll-formed. The joint design and procedure used were the same as those that have been developed and are now being tested for the air-welding of commercial titanium.[11] Owing to the lack of rigidity and slight out-of-roundness of the rolled sheet, the fitup of the joint prior to welding did not meet specifications. However, the joints were welded to study contamination and the mechanical properties of the weldment.

Visual examination of the first weld revealed intermittent lack of penetration, while visually the second one was acceptable. Radiography indicated fine-to-medium porosity throughout the first weld, with some areas of heavy porosity; again, the second weld was acceptable. The mechanical properties of samples removed from the welds are listed in Table 15.4. With the exception of a reduction in the per cent elongation, from 16% for the base metal, the mechanical properties for the first three samples were equivalent to the properties of the base metal. The duplicate sample from the second weld broke in the heat-affected zone outside the intended area; therefore the values must be regarded as only approximate.

A microscopic examination confirmed the presence of the porosity indicated by radiography. Microhardness surveys showed average diamond pyramid hardnesses (DPH) in the weld deposits of 321 and 339 (10-kg load), while the base metal was 305 DPH. These surveys showed consistently higher hardnesses in the filler passes near the face of the weld. While these welds are not up to the usual HRP standards, it does appear likely that with minor modifications in procedure titanium A-110AT may be welded satisfactorily in air.

[11] HRP Welding Specification No. 7 – Inert-Gas Shielded-Arc Welding of Commercially Pure Titanium (Dec. 7, 1956).

Table 15.4. Mechanical Properties of Titanium A-110AT Weldments

Specimen No.	Ultimate Tensile Strength (psi)	Yield Strength (psi)	Per Cent Elongation in 1 in.	Bend Test, $2\frac{1}{2}T$ Radius	
				Bend Angle (deg)	Remarks
1A	133,290	117,770	10	5–10	Ruptured
1B	135,045	118,995	11	5–10	Ruptured
2A	132,670	122,390	12.5	20–30	Ruptured
2B	144,665	131,325	10	110	Cracks appeared

15.3.2 Zirconium-Alloy Welding

The Zircaloy-2 core tank in the HRT was successfully welded by use of specially fabricated trailers to prevent contamination; however, this procedure is slow and expensive and not readily adaptable to field-welding. Efforts are now being made to develop tungsten inert-gas-shielded air-welding techniques suitable for use with Zircaloy-2. Present efforts are being directed at modifying developed titanium procedures[11] so that they may be used with zirconium.

Two welds were made in air on Zircaloy-2 plates of $\frac{1}{2}$-in. thickness using $\frac{3}{32}$-in. filler wire. Both welds were satisfactory as determined by visual inspection. The first weld contained fine porosity with some scattered medium porosity, determined by radiography and confirmed by microscopy. In a microhardness traverse the base metal gave an average hardness of 172 DPH (10-kg load), while the weld metal had an average hardness of 228 DPH. The radiograph on the second weld indicated fine porosity, which was also confirmed by metallographic examination. The average weld-metal hardness was 224 DPH (10-kg load). No mechanical-property tests have been made on these welds.

15.4 NONDESTRUCTIVE-TESTING DEVELOPMENT

15.4.1 Weld Inspection

Development of a reliable ultrasonic inspection of stainless steel welds has been a goal of the Nondestructive-Testing Development Group for some time. Such an inspection would be better adapted to remote inspection than presently accepted methods and also could be less expensive than radiography. A number of inspectors in this country and abroad use a straightforward pulse-echo ultrasonic technique with an angle-beam search for weld inspection. This has proved reliable in some specific applications, but several drawbacks are apparent for HRP applications.

A large part of HRP weld inspection is concerned with type 347 stainless steel. In type 347 weldments, the weld metal and the base metal differ in composition; thus there is a possibility of a reflection of ultrasound from the interface between weld and base metals, even in a good weld. Any such reflection might well be misinterpreted as a weld defect and could mask a real defect if it lay close to the interface. Fortunately, no such reflections have so far been identified with HRP type 347 stainless steel weldments.

Type 347 weld metal attenuates ultrasound rapidly. In order to evaluate this attenuation, holes of various sizes were drilled through and half-way through 2-in. pipe which had been butt-welded. The drill holes, located both in the weld metal and about $\frac{1}{2}$ in. away from it, were then "viewed" with ultrasonic waves which had not passed through any weld metal, which had traversed half the weld, and which had penetrated the entire weld. By comparing reponse amplitudes of these three groups of readings, a good estimate of attenuation could be made. Table 15.5 records these readings. It can be be seen that the attenuation is indeed high. For frequencies of over 2.25 Mc, attenuation in type 347 stainless steel welds is inordinately high, but, even at low frequencies, it would be very desirable to be able to introduce more power into small-diameter pipe. Maximum instrument sensitivity was necessary for all measurements on the 2-in. pipe. This can be ascribed to low power inputs due to losses from the use of a flat transducer on the curved pipe surface and to the small reflecting surface provided by a drilled hole. Several types of plastic shoes as well as larger transducers were tried. The 1-in. transducer without shoes proved best able to introduce energy into small pipe having better than average surface finish. Heat treatment is being investigated as a method of improving transmission characteristics of type 347 weld metal.

A high or irregular face or root bead can cause spurious indications. For the purpose of evaluating these indications, ultrasonic surveys were made of a $\frac{5}{16}$-in.-thick weld specimen, before and after all face reinforcement was ground off. If an echo was eliminated or reduced to background level by the surfacing operation, it was attributed to the bead. Radiography had been unable to detect any voids in the reinforcement. It was shown that the reflections from the reinforcement may be a considerable portion of the total. While some welds may be ground to remove the excess metal, many field welds are not adaptable to grinding; so this cannot be

Table 15.5. Propagation of Ultrosonic Waves Through Weld Beads in Type 347 Stainless Steel Pipe

Values given are in instrument scale divisions

Defect (in.)	Through Parent Metal	Through Half of Weld	Through Full Weld
5-Mc ½-in. × ½-in. SW Transducer – Full Sensitivity			
0.040	0.6	NRD[a]	NRD
0.096	0.6	0.5	0.7
0.128 (½ way)	0.6	NRD	NRD
0.128	0.6	NRD	NRD
0.185 (½ way)	0.4	0.2	NRD
0.185	0.5	0.6 to NRD	NRD
2.25-Mc ½-in. × ½-in. XW Transducer – Full Sensitivity			
0.040	1.6	NRD	NRD
0.096	2.8	2.0	NRD
0.128 (½ way)	2.5	1.8	1.6
0.128	2.0	1.8	NRD
0.185 (½ way)	2.2	1.1	NRD
0.185	2.7	3.2 to 1.1	NRD
2.25-Mc 1-in. × 1-in. SW Transducer – Full Sensitivity			
0.040	1.8	NRD	NRD
0.096	2.5	2.0 to 1.0[b] NRD[c]	NRD
0.128 (½ way)	2.0	NRD	NRD
0.128	2.6	1.4	NRD
0.185 (½ way)	1.6	1.5	NRD
0.185	2.9	2.0 to 1.0	NRD

[a]NRD = not reliably detected.
[b]Through one-third of weld.
[c]Through two-thirds of weld.

considered as a final solution to the problem. Some investigators have used a low angle of approach or a large refracted angle of the ultrasound to solve the problem. This method would not detect defects in the weld reinforcement; with type 347 weldments, defects are quite likely to be found in the root reinforcement. Such a method also requires very large power inputs.

15.5 ACTIVE-METAL REACTIONS

15.5.1 Titanium

Under an ORNL subcontract, Stanford Research Institute is studying combustion reactions of titanium with aqueous solution or vapors. The purpose of the study is to establish the limiting conditions for such reactions. The work discussed

below is summarized from Stanford's quarterly report.[12]

Titanium rods were broken in tension while confined in a pressure vessel filled with mixtures of oxygen and helium or oxygen and steam at various pressures and temperatures. Autoignition of the titanium occurred when the mixture was sufficiently rich in oxygen. Ignition occurred at 350 psi in pure oxygen, at 500 psi in 90% oxygen, at 1000 psi in 65% oxygen, and at 1700 psi in 50% oxygen. In a similar set of runs, ½-in.-wide strips of 0.012-in. titanium foil were used instead of ¼-in. rod; essentially identical values were obtained in the two series. The diluent used for most runs was helium, but for a number of runs steam was used; this substitution had no gross effect on the limits of this reaction.

Somewhat different results were obtained under dynamic conditions. In these runs a titanium rupture disk sealed off the gas mixture in the pressure vessel. The rupture disk was broken by piercing it with a spring-loaded plunger, resulting in escape of the gases past the broken surface. Under these conditions autoignition occurred even more readily, requiring only 50 psi with pure oxygen, 500 psi with 60% oxygen, 1000 psi with 45% oxygen. The curves delineating the area of combustion under both static and dynamic conditions and plotted with percentage of oxygen against oxygen pressure and total pressure are shown in Figs. 15.4 and 15.5. Combustion will occur in environments represented by the regions above the curves. The dynamic or lower curve appears to become asymptotic at about 35% oxygen, indicating that autoignition will not occur (at this velocity and at room temperature) below this concentration, regardless of pressure. However, it is likely that the location of these curves will vary with the velocity.

Changes in the ratios of fresh to undisturbed titanium surface did not result in major shifts of the limits of this reaction. For most runs a ¼-in. round specimen was used, notched by reducing its diameter to ⅛ in. Samples in which the notched area was reduced to 1/16 in. in diameter ignited equally readily; so did a 1-in. round poppet machined to simulate the original poppet used

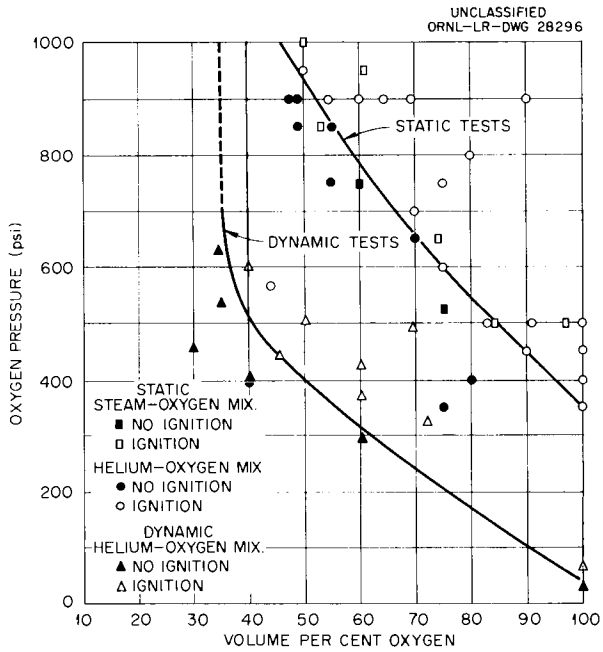

Fig. 15.4. Reactions of Titanium with Helium-Oxygen and Steam-Oxygen Mixtures. Dependence on oxygen pressure.

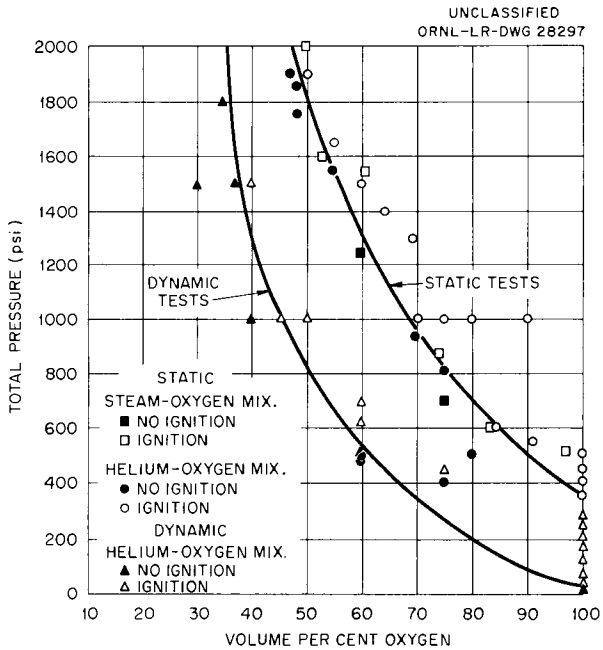

Fig. 15.5. Reactions of Titanium with Helium-Oxygen and Steam-Oxygen Mixtures. Dependence on total pressure.

[12] F. E. Littman, *Reactions of Titanium with Water and Aqueous Solutions*, Stanford Research Institute Quarterly Report No. 3, September 16–December 15, 1957.

in the test loop, when a $\frac{1}{8}$-in.-dia appendix was broken off.

Earlier experiments had shown that titanium samples broken under water did not react. To see if titanium once ignited in oxygen would continue to react with water, the bottom of the pressure vessel was filled with water. The results indicated that the major effect of this was to quench the reaction. A small amount of reaction with water did occur under these conditions, as was indicated by the presence of hydrogen in the residual atmosphere. Whether this was due to a specific reaction of the metal with water or just to thermal decomposition of water by the hot melt could not be determined.

An exploratory survey indicated that of the metals tested, only titanium and zirconium were capable of autoignition upon exposure of a fresh surface to an oxygen atmosphere. Neither aluminum, magnesium, iron, stainless steel, tantalum, niobium, nor molybdenum showed any signs of autoignition under these conditions.

15.5.2 Zirconium

Aerojet General Corporation, on a subcontract, is comparing the reactions of zirconium alloys with water and with oxygenated aqueous solutions of uranyl sulfate.

No differences were found either in the room-temperature dynamometer tests or in high-temperature, high-pressure molten-wire tests.[13] Experimental difficulties prevented the obtainment of comparative data in the high-pressure, high-temperature injection tests.

15.6 CERAMIC DEVELOPMENTS[14]

15.6.1 Calcination of Thorium Oxide at 1600°C

The Chemical Technology and Engineering Research Groups have employed one Ceramic Laboratory kiln since December 17, 1957, for calcining thorium oxide at 1600°C for 4 hr. The average production rate was only 16 lb per day, owing mainly to loss of kiln space while consideration was being given to the problems of firing schedule and of containers for the thoria powder. Chief considerations concerned container materials suitable from the standpoint of low contamination of the thoria, of resistance to destruction during continued recycling at 1600°C on a fast heating schedule of 6 hr from room temperature to 1600°C, of ready availability, and of sizes suitable for maximum use of kiln space. Containers of various shapes have been obtained from Chas. Taylor Sons Co., Electric Auto-Lite Company, and Norton Company, and some were fabricated in this laboratory. It is now agreed that containers high in aluminum oxide are suitable from temperature and contamination standpoints, but the other questions have not received a final answer.

It appears that a production of 40 lb per day per kiln may soon be possible.

15.6.2 Calcining Techniques for Thorium Oxide

Apparently the simplest procedure in thorium oxide calcination from the standpoint of dispersibility and small particle size of the product is obtained by packing the powered thorium oxide loosely in the container. Tentative tests of other techniques point to the following conclusions:

1. Effect of compaction. – Tamping the dry thorium oxide by hand into the container or by dry pressing at 1300 psi into bars results in hard-sintered products.
2. Effect of steam. – When steam was passed through powdered thorium oxide during heating to 1600°C for 2 hr, coarse particles (over 5 μ) were obtained, comprising 69 to 70 vol %.
3. Effect of burn-out material. – Firing thorium oxide containing 10 wt % of thorium oxalate resulted in many coarse particles (30 to 50 vol % larger than 5 μ). Thorium oxalate by itself, whether loosely or densely packed, burned out to form easily dispersed particles (3 to 6 vol % over 5 μ). Thorium oxide blended with an equal weight of the oxalate and 10% of cellulose powder produced only 5 to 15 vol % coarse particles.

15.7 EFFECTS OF RADIATION ON STRUCTURAL METALS AND ALLOYS

15.7.1 Equipment and Facilities

Experiments ORNL-10-6 (lattice irradiation) and 10-9 (Charpy and subsize Izods in hole HB-3) are still being irradiated in the MTR. Withdrawal is scheduled for February 10, 1958. ORNL-10-8 was returned from the MTR.

[13] H. M. Higgins, *Reaction of Zircaloy-2 with Water and with Uranyl Sulfate Fuel Solution, Monthly Progress Report No. 4, October 1 Through October 31, 1957*, AGC-AE-39.

[14] This section was submitted by C. E. Curtis of the Ceramics Section of the Metallurgy Division.

A series of full-size Charpy specimens was irradiated to approximately 5×10^{18} fast neutrons/cm^2 in the LITR at 200 and 575°F. Testing is in progress on A-285, A-301, and two heats of A-212B steels. One of the A-212B steels was cut from a 6-in.-thick plate of material that had been normalized in the full thickness.

A variety of steel specimens was canned for insertion in the source-tube facility in the blanket of the HRT. These specimens will be subjected to approximately the same temperature and flux conditions as the pressure vessel during the operation of the reactor.

Several hundred specimens have been run successfully in the remotely operated, subsize Izod machine. Thermocouples have failed on several occasions, but replacement units are kept on hand so that little time is lost in replacement.

15.7.2 Steels and Iron

The variables affecting sensitivity to radiation effects in ferrites are being investigated in a high-purity iron. The results are not yet complete, but several conclusions are possible. A shift upward in transition temperature of 225°F was observed in fine-grained (subcritical anneal) iron at about 10^{19} neutrons/cm^2 (energy >1 Mev). This is the largest shift ever observed for such a small neutron dose. This information confirms earlier observations, based on tensile data at room temperature, that ferritic structures are more sensitive to irradiation than pearlitic structures.

A change of 75°F in transition temperature was observed in the iron that had been subjected to a supercritical anneal and thus had a large grain size. This grain-size effect is contrary to the data for 0.24% carbon steel,[15] for which the fine-grained material was found to be less sensitive to radiation effects.

For the same iron in the as-received, cold-rolled condition, no definite transition-temperature shift was observed after irradiation, but the transition-temperature range appeared to be narrowed. The fractures in this material were most unusual. Fracture at the lower temperatures took place on two successive intersecting planes about 90 deg apart. Normally, fracture proceeds from the base of the notch directly across the specimen in a plane perpendicular to the plane of the notched face. In the irradiated specimen the fracture propagated downward at a 45-deg angle from the notched face until halfway through the specimen; at this point the plane of fracture changed direction 90 deg and emerged from the specimen at the normal position opposite the notch. The results can be tentatively rationalized on the basis of the predominant (100) [011] rolling texture in iron and the increased susceptibility to cleavage fracture caused by irradiation.

15.7.3 Zirconium Alloys

Notch-impact specimens of Zircaloy-2 irradiated in excess of 10^{20} neutrons/cm^2 (energy >1 Mev) as part of the Phillips-ETR materials program were tested. Energy absorption was *increased* by irradiation. The orientation of the specimens with respect to the plate was not known, and this probably has an important bearing on the results. The impact strength, as shown by energy absorption, increased by about a factor of 4 at some temperatures.

---

[15] R. G. Berggren and J. C. Wilson, *Recent Data on the Effects of Neutron Irradiation on Structural Metals and Welds*, ORNL CF-56-11-1 (Jan. 30, 1957).

Part V

CHEMICAL ENGINEERING DEVELOPMENT

D. E. Ferguson

16. URANYL SULFATE FUEL PROCESSING

R. A. McNees S. Peterson

16.1 SOLIDS BEHAVIOR

A limited accumulation of solids occurred on small test pins of type 347 stainless steel which were in contact with dilute slurries of simulated HRT corrosion-product solids for several hundred hours at temperatures of 25 to 100°C. Solids buildup on the pins was measured by counting techniques, Fe^{55}-Fe^{59} or Zr^{95} tracers being used in the preparation of the simulated HRT solids. The test pins were immobilized in glass cylinders containing the slurry of solids in 0.04 *m* UO_2SO_4–0.02 *m* H_2SO_4 solutions and were tumbled end over end. Solids accumulation was at a maximum in about 120 hr, after which time solids were slowly lost from the pins.

No effect attributable to temperature variation between 25 and 100°C could be seen, and the studies are being extended to 275°C. Unfilmed test pins that had been electropolished picked up only about 10% of the amount of solids picked up by pins left in the machined state. On the unfilmed pins, Zr^{95} activity was more strongly adsorbed than Fe^{59} activity, while on passivated pins the reverse was true. Increasing the slurry concentration increased the solids accumulation on the pins somewhat, but the effects were not proportional to slurry concentration changes.

Solids accumulation on the pins ranged from 10 $\mu g/cm^2$ on electropolished untreated pins in slurries containing 100 mg of solids per liter to a single value of 1 mg of solids per square centimeter in the case of a slurry containing 1210 mg of solids per liter. With the exception of this single value, the solids concentration on the pins ranged from 10 to 50 $\mu g/cm^2$. It should be noted that even the largest value observed represents a film thickness of only about 0.05 mil, and the important observation is made that in such a system an equilibrium condition is attained in which a continuing buildup of solids on the metal surfaces does not occur.

A hydroclone operating on loop F at Y-12 consistently removed solids from the loop, but, owing to uncertainties about the rate of corrosion, estimates of its efficiency are not possible. More solids were separated during periods of loop thermal cycling than during periods in which the temperature of the loop remained constant.

16.2 IODINE CHEMISTRY

Laboratory tests have repeatedly shown that small-diameter (1-in.) absorption beds filled with silvered Yorkmesh are less efficient than the same beds filled with $\frac{1}{8}$-in.-dia silvered-alundum pellets because of channeling in the mesh-packed bed. In two tests in the HRT mockup loop, 6-in.-dia absorption beds packed with silvered Yorkmesh removed iodine very efficiently from gas streams at 120°C. A bed packed to a density of 22 lb/ft^3 removed 97% of the iodine passing through it, and a bed packed to a density of 29 lb/ft^3 removed 99.6%. The distribution of iodine in the two Yorkmesh beds and a silvered-alundum bed under the same conditions is shown in Fig. 16.1.

Samples of the silvered Yorkmesh to be used in the HRT iodine absorption bed were subjected to various radical treatments to determine the effect of possible HRT operating conditions on the behavior of the Yorkmesh and the iodine absorbed on it. The Yorkmesh used had a surface area of 0.07 m^2/g as measured by nitrogen adsorption and contained 21.4 wt % silver.

In repeated experiments with the silvered Yorkmesh, after about 2% of the silver had been consumed by iodine, the rate of iodine absorption decreased by a factor of about 10 (Fig. 16.2). For the run, a constant weight of steam-oxygen-iodine mixture passed through the gauze per unit time, but the iodine picked up by the gauze dropped from about 40 mg per 30 min (2 $mg/m^2/min$) to 4 mg per 30 min (0.2 $mg/m^2/min$). After a gauze that was absorbing iodine at the slower rate was heated to 600°C for a few minutes, it would pick up another 10 mg of iodine in less than 30 min, after which the iodine absorption rate would again drop to 4 mg per 30 min. This behavior was observed each time after the gauze had been heated to 600°C and suggests that at 120–140°C the diffusion of iodine through the mass of silver is the rate-controlling step in the reaction. With silvered alundum under the

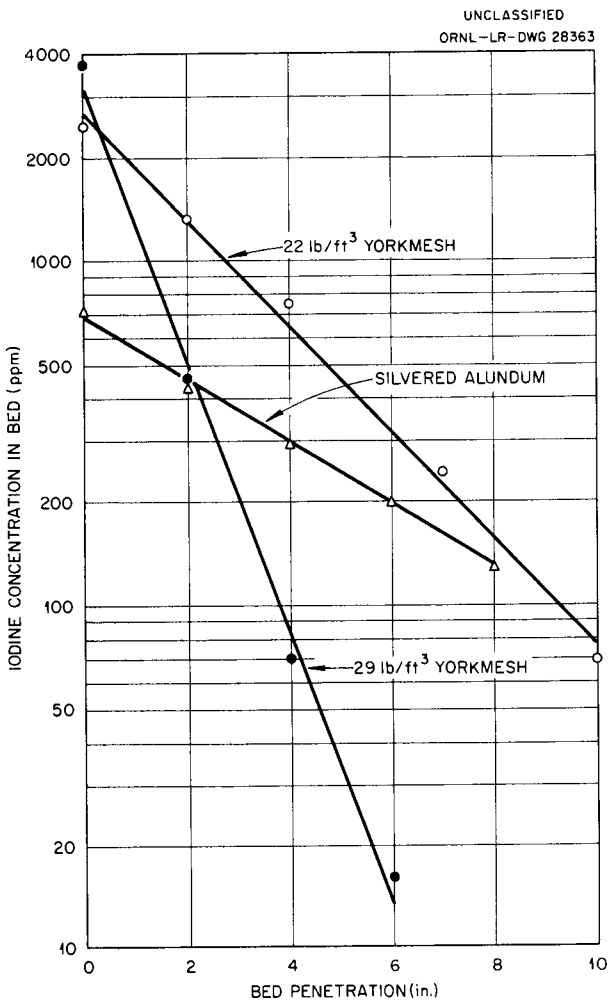

Fig. 16.1. Comparison of Iodine Penetration of Three Absorption Beds.

same conditions of temperature, gas flow, and gas composition, diffusion was not observed to be the rate-controlling step, and 100% saturation of the silver was easily obtained.

Silvered Yorkmesh gauzes loaded with iodine to 0.4, 0.8, and 4.0% of saturation were subjected to rapid temperature cycling between 30 and

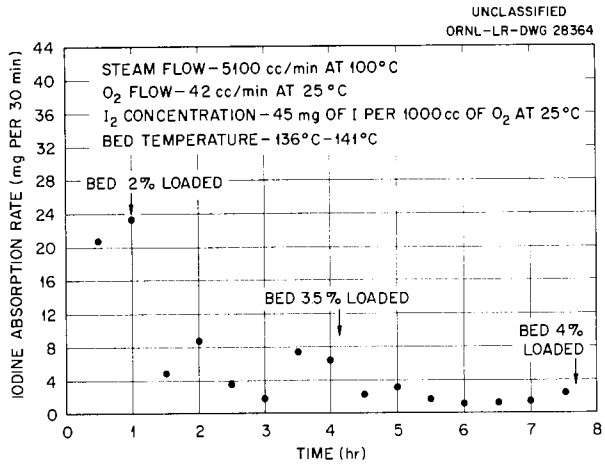

Fig. 16.2. Variation of Iodine Absorption Rate with Time for Silvered Yorkmesh.

400°C. No appreciable amount of iodine was lost from the gauzes after 10 cycles.

Another iodinated gauze was heated to 170°C and then rapidly immersed in boiling 0.04 *m* UO_2SO_4–0.02 *m* H_2SO_4 solution. After 10 cycles the uranyl sulfate solution contained only 0.01% of the iodine originally on the gauze. The uranyl sulfate solution did not wet the gauze, and solid uranyl sulfate was not deposited on the gauze. Attempts to form such deposits were unsuccessful.

Other iodinated gauzes were heated to 600°C in streams of oxygen and steam-oxygen mixtures. No iodine could be detected in the gases passing through the gauze. A slight darkening of the pyrex tube in the areas in contact with the test gauzes indicated a very small amount of reaction with the silver of the gauze, but the absence of I^{131} in such areas indicated that iodine was not a factor in that reaction. Samples of the gauze wire from this test and from the other treatments have been submitted for metallographic examination.

17. GASEOUS FISSION-PRODUCT DISPOSAL

W. E. Browning
R. E. Adams
R. A. McNees
M. H. Lloyd

17.1 DYNAMIC STUDIES

In additional experiments[1] on the adsorption of xenon by Columbia grade G charcoal, xenon was adsorbed 16.5 times as strongly as krypton at room temperature but only 7.9 times as strongly at 100°C. The experimental techniques have been described elsewhere.[2]

Preliminary results in an evaluation of other adsorber materials showed four types of Linde molecular-sieve material to be considerably less efficient than Columbia grade G charcoal in holdup of krypton at room temperature (Table 17.1).

Table 17.1. Comparison of Solid-Adsorbent Efficiencies for Holdup of Krypton

Material	Efficiency Compared with That of Charcoal (%)
Linde molecular sieves	
4A	14
5A	14
10X	28
13X	36
Columbia grade G charcoal	100

Ninety per cent of the iodine adsorbed by a 12-in.-long Columbia grade G charcoal trap was in the first $\frac{3}{8}$ in., but only 55% was in the same portion of a trap containing molecular sieve 13X ($\frac{1}{16}$-in.-dia pellets). After 20 hr of operation the traps contained 99.95% of the iodine passed into them in the gas stream. That the iodine was held more strongly by the charcoal than by the molecular sieve was shown by the fact that the distribution of iodine on the charcoal did not change during the test, but the distribution on the molecular sieve did change slightly. For the experiment I^{131} was selected as typical of the iodine isotopes resulting from uranium fission. Palladium iodide, synthesized from I^{131}, was heated and decomposed to generate I^{131} vapor, which was swept into the 0.5-in.-dia traps by an air stream of 7 liters/min.

Holdup tests on the HRT charcoal beds by means of the technique reported previously[3] were completed. The results indicate that the beds should perform adequately for the disposal of fission gases, provided that the heating of the charcoal in the inlet of the bed by decay of the adsorbed fission gases does not produce a temperature exceeding the ignition temperature of charcoal in oxygen, about 360°C.

17.2 EQUILIBRIUM STUDIES

Equilibrium adsorption isotherms for krypton on various inorganic adsorbents have been determined at 2 and 28°C and are compared in Figs. 17.1 and 17.2 with HRT charcoal. Data for two different grades of charcoal and two Linde molecular sieves, 10X and 13X, at 2 and 28°C are shown in Figs. 17.3 and 17.4. For comparison, isotherms of molecular sieves 10X, 13X, 4A, and 5A, as well as Columbia grade G activated charcoal, are shown in Fig. 17.5. Isotherm data clearly show that, under static equilibrium conditions, except for charcoal the 5A material is the strongest adsorbent for krypton, while the dynamic studies reported in Sec 17.1 indicate that the 13X material is best for holding up krypton in a flowing stream of oxygen.

Activated charcoal in contact with mercury vapor at 28°C adsorbed 0.60 mg of mercury per gram. The krypton adsorption characteristics were not affected by the mercury.

The adsorption isotherms for xenon on Columbia grade G activated charcoal and Linde molecular sieve 5A have been measured and are shown in Fig. 17.6. Comparison of these data with similar data for krypton at 28°C indicates that xenon is adsorbed 11 to 12 times more strongly than krypton.

[1] R. A. McNees *et al.*, *HRP Quar. Prog. Rep. Oct. 31, 1957*, ORNL-2432, p 147.

[2] W. E. Browning and C. C. Bolta, *Measurement and Analysis of the Holdup of Gas Mixtures by Charcoal Adsorption Traps*, ORNL-2116 (Aug. 10, 1956).

[3] W. D. Burch *et al.*, *HRP Quar. Prog. Rep. Oct. 31, 1957*, ORNL-2432, p 23.

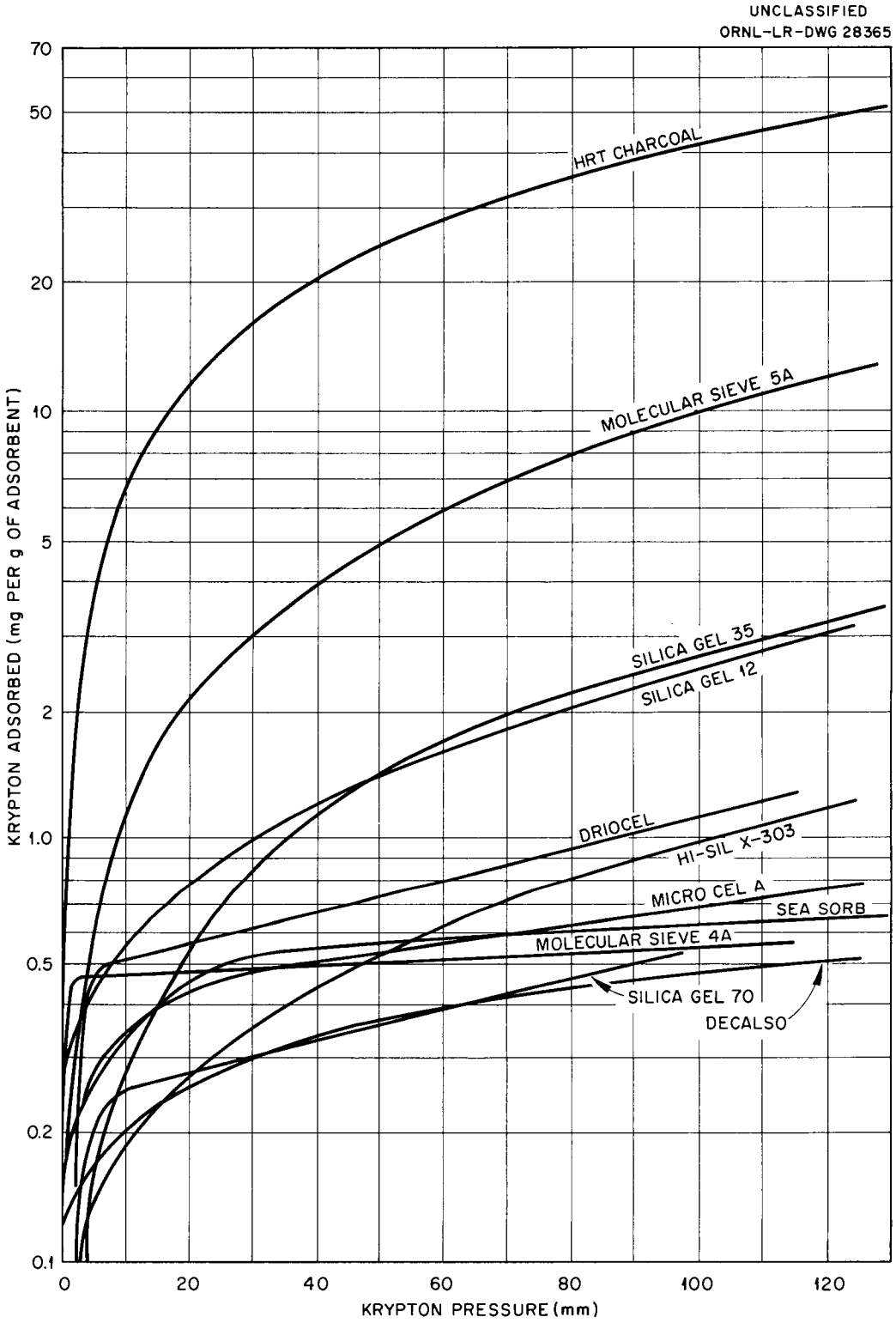

Fig. 17.1. Adsorption of Krypton on Various Materials at 2°C.

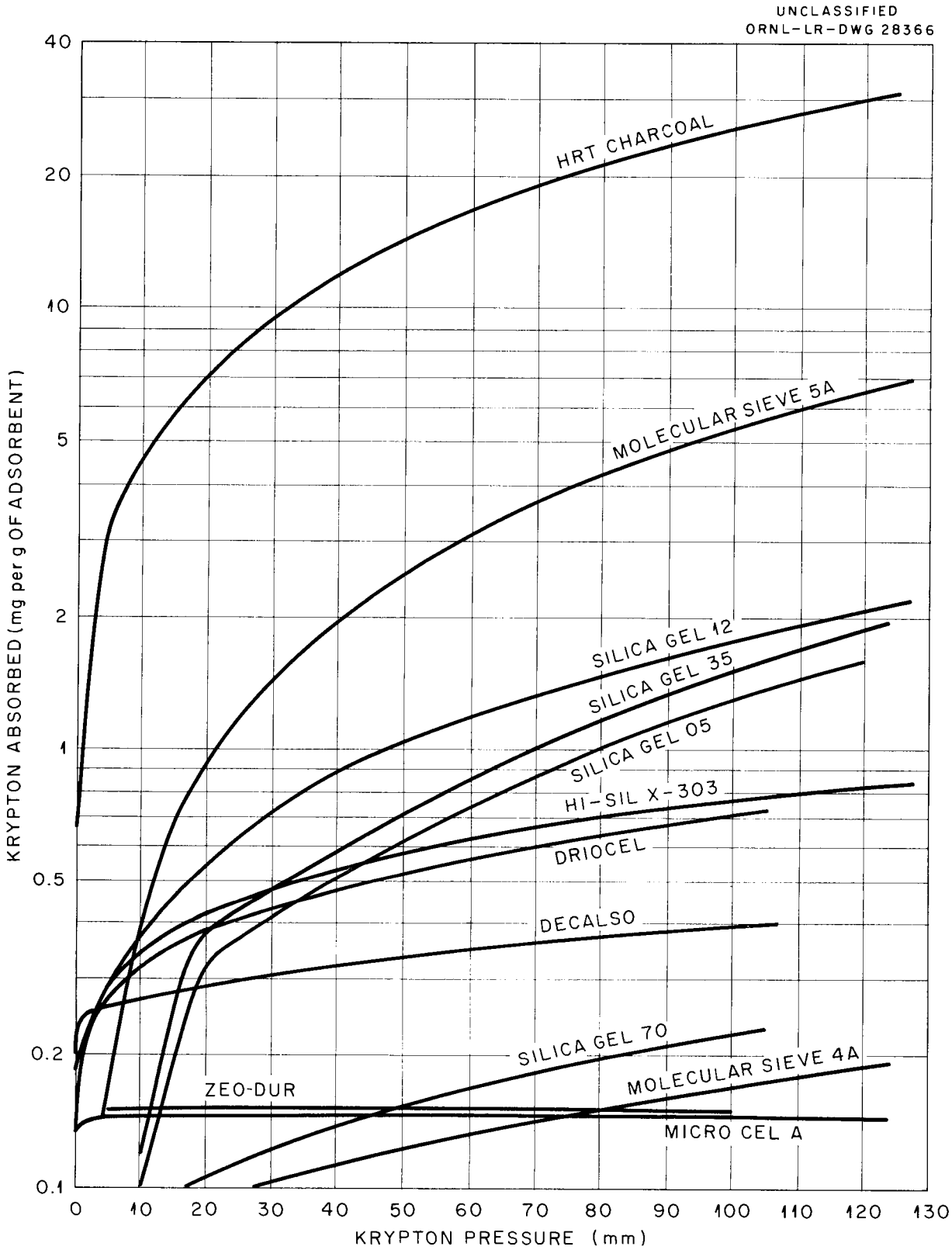

Fig. 17.2. Adsorption of Krypton on Various Materials at 28°C.

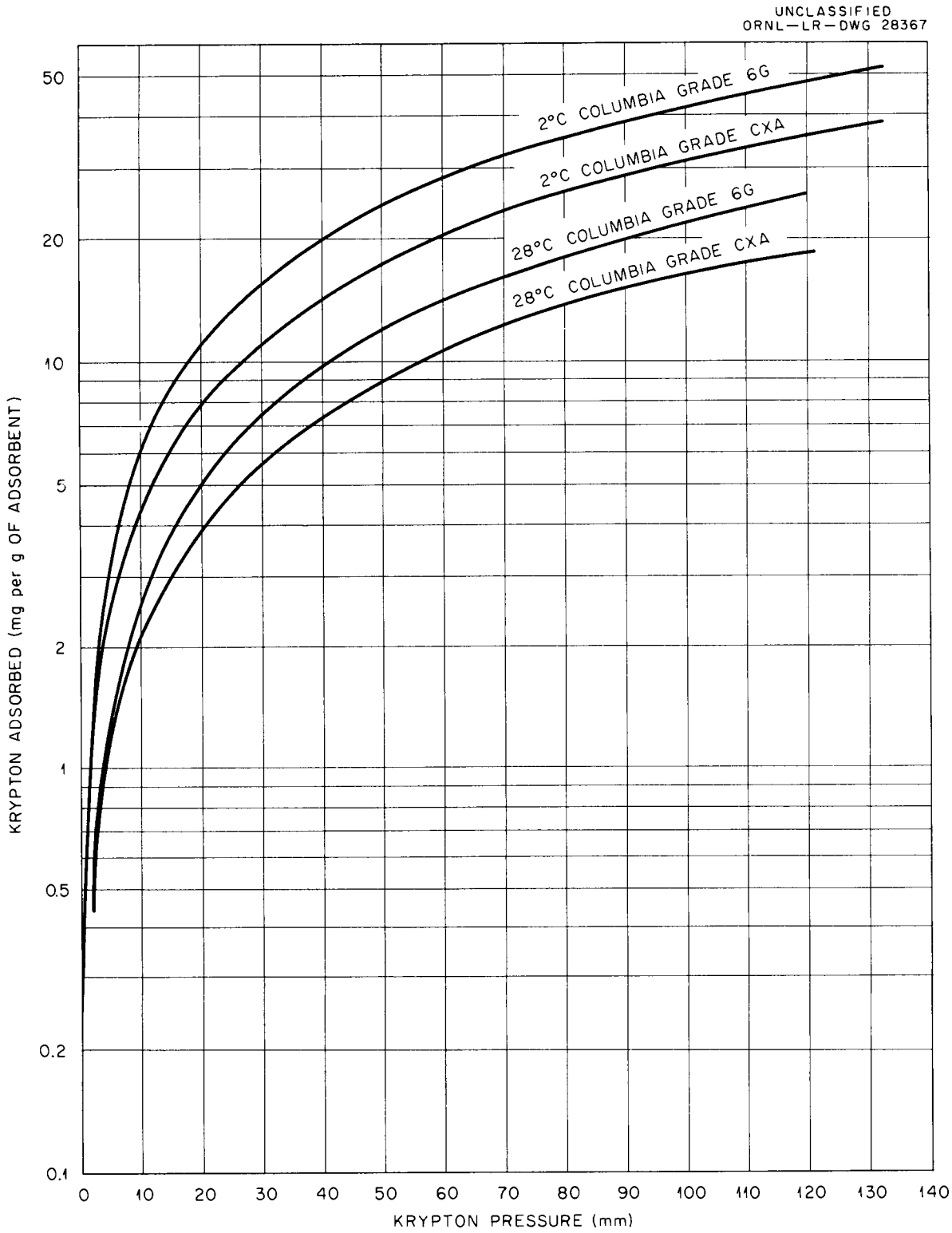

Fig. 17.3. Adsorption Isotherms for Krypton on Two Grades of Columbia Charcoal.

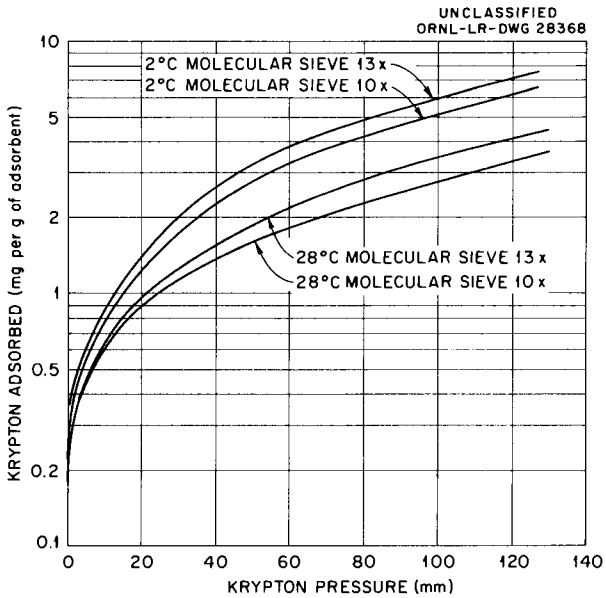

Fig. 17.4. Adsorption Isotherms for Krypton on Molecular Sieves.

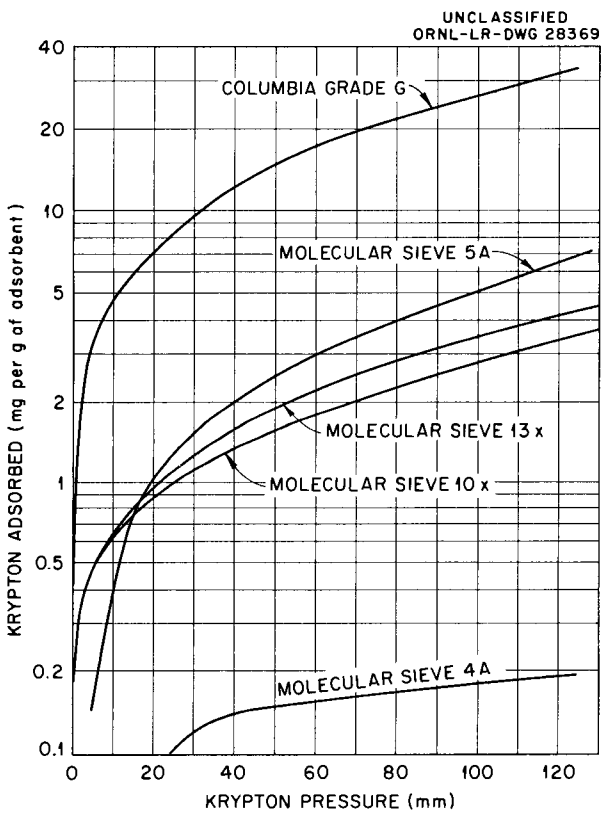

Fig. 17.5. Adsorption Isotherms for Krypton at 28°C.

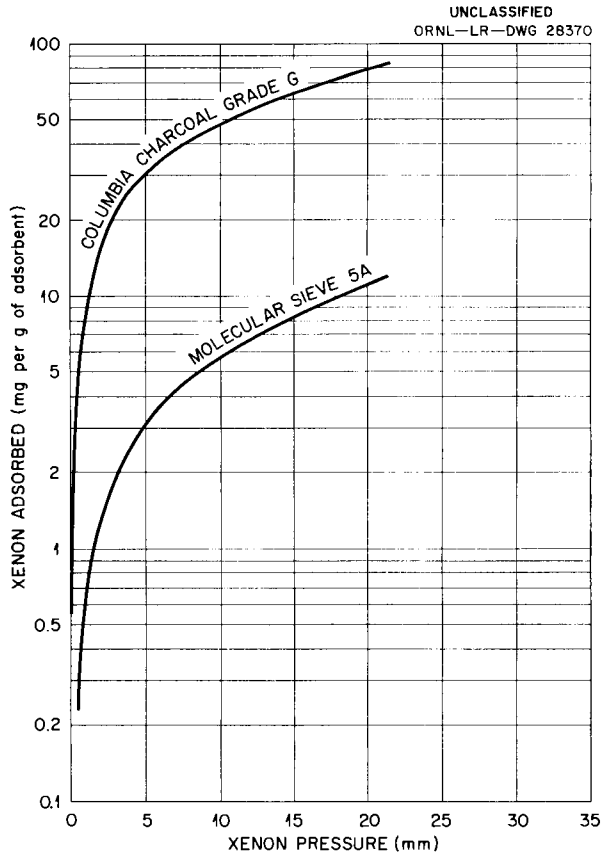

Fig. 17.6. Adsorption Isotherms for Xenon at 28°C.

18. URANYL SULFATE BLANKET PROCESSING

R. E. Leuze
J. M. Chilton
P. A. Haas
J. W. Snider

Experimental investigations during the quarter included studies of PuO_2 and PuO_2SO_4 behavior in 1.4 *m* UO_2SO_4 circulating in the P-1 loop and plutonium adsorption on metals from 1.4 *m* UO_2SO_4 in static bombs. Studies of the behavior of plutonium in 1.4 *m* UO_2SO_4 at 250°C were completed. Five equipment and procedure-check runs and five runs with plutonium present were made.

18.1 LOOP P-1 OPERATION

A heat balance based on the electrical input to the loop P-1 canned-rotor pump showed that 61.5% of the heat was removed by the cooling air on the loop walls and 36.5% by the pump cooling water. The losses through the container tank (evacuated to less than 0.5 psia) accounted for the remaining 2% and for heat introduced by the cooling-water circulating pump.

Corrosion rates, calculated from nickel concentrations and oxygen consumption, were much higher when soluble plutonium was present than when either no additive or zirconium was present (Table 18.1).

Plutonium contamination was essentially confined to the loop, loop container, and glove boxes throughout the tests. Dozens of samples were transferred between Buildings 4501 and 3508 without release of plutonium. This transfer was accomplished by sealing the samples inside plastic bags on a glove-box port; the bags could be removed without exposing the insides of the bags or of the glove boxes to the operating-area atmosphere.

Table 18.1. Loop P-1 Corrosion Rates

Conditions: 1.4 *m* UO_2SO_4 at 250°C

Material Added to Loop	Pu Concentration (mg/liter)	Generalized Corrosion Rate[a] (mpy)
None		1.5
$Zr(SO_4)_2$ or ZrO_2		1.4
$Pu(SO_4)_2$	1.7	18.1
PuO_2SO_4	13–70	23.2
PuO_2SO_4	70 to ppt[b]	22.8[c]
PuO_2	74[d]	11.3
PuO_2SO_4	10 to ppt[e]	9.9

[a]Values listed are from nickel concentrations; oxygen consumptions gave checks within ±25%.

[b]Sufficient plutonyl sulfate was added to increase the plutonium concentration to 342 mg/liter. Plutonium precipitated at concentrations >100 mg/liter.

[c]Based on oxygen consumptions; nickel anolyses were erratic.

[d]65 mg of plutonium per liter as PuO_2 plus 9 mg of plutonium per liter in solution.

[e]Sufficient plutonyl sulfate was added to increase the plutonium concentration to 580 mg/liter. Plutonium precipitated at concentrations >100 mg/liter.

18.2 PLUTONIUM BEHAVIOR IN THE P-1 LOOP

Results of four of the five runs with plutonium present in the P-1 loop are complete. The behavior of the plutonium was essentially the same as that of zirconium in previous runs.[1] Practically no plutonium was removed from the underflow pot of the hydroclone when soluble plutonium was hydrolyzed under these conditions, but about 20% of injected preformed PuO_2 was found in the underflow pot. Practically all the plutonium that did not remain in solution was found on the stainless steel walls.

18.2.1 Plutonium Distribution

When the soluble plutonium concentration was gradually increased from 2 to 75 mg per kg of H_2O, most of it remained in solution, a small amount was adsorbed on the walls, and practically none was removed by the hydroclone (Table 18.2). When the soluble plutonium concentration was increased to 342 mg per kg of H_2O, most of it was adsorbed on the walls, leaving about 100 mg per kg of H_2O in solution. Only a small amount was removed by the hydroclone. When a single injection of preformed PuO_2 was made, 20% was removed by the hydroclone, mostly in 2 hr. The 60% material balance in this run indicates that a large fraction of the oxide was held up somewhere in the loop and was not removed when the loop was drained. Some granular corrosion products were found in the horizontal pipe which held the sample coupons, adhering loosely to the metal. This scale was found to contain 2.6% plutonium by weight.

18.2.2 Solids Removal

Solids were removed from the loop in three ways: from the underflow pot of the hydroclone, in the solutions drained from the loop at the end of the runs, and as loose granular solids from the bottom of the sample coupon holder. The major constituent in the solids removed by the hydroclone was uranium (Table 18.3). The rate of loss of uranium from the 1.4 *m* UO_2SO_4, calculated from the average rate over approximately 300 hr of operation, was 3% of the total per year. A sample of the solids filtered from a drain solution was submitted for particle-size analysis and for x-ray diffraction analysis. Approximately 55 wt % of the particles were between 4 and 12 μ in diameter, and most of the remainder were between 12 and 17 μ. The only pattern identified positively by x-ray diffraction was that of α-Fe_2O_3. It appears that the hydroclone removes primarily very small particles, which are formed by hydrolysis of material in the solution. The preformed PuO_2 which was used was prepared in this way.

The rate of removal of preformed PuO_2 by the hydroclone was very rapid at first, but decreased to less than 1% of the original rate after about 12 hr (Fig. 18.1). The solid material removed from the underflow pot with circulating plutonyl sulfate (P-29) contained 188 mg of iron. The nickel

[1] R. E. Leuze *et al.*, *HRP Quar. Prog. Rep. Oct. 31, 1957*, ORNL-2432, p 149–150.

Table 18.2. Plutonium Distribution in the P-1 Loop

Plutonium injected into ~13 liters of 1.4 *m* UO_2SO_4 circulating at 250°C under 350–400 psi O_2

Run	Plutonium Added		Circulation Time (hr)	Plutonium Distribution (% of Pu added)			
	Compound	Amount (g)		Hydroclone	Solution	Adsorbed*	Sampler
P-27	$Pu(SO_4)_2$	0.0214	110	0.09	79	2.8	14
P-29	PuO_2SO_4	1.016	180	0.04	78	0.9	18
P-30	PuO_2SO_4	4.158	80	0.07	31	66	4.8
P-31	PuO_2	0.850	36	20		35	4.1

*Calculated by multiplying the average plutonium adsorption on coupons by the loop surface area.

Table 18.3. Chemical Analysis of Solids from P-1 Loop

Location	Amount in Solids (wt % of solid)			
	Uranium	Iron	Chromium	Plutonium
Underflow pot				
PuO_2SO_4 run	87	10	1.7	0.2
PuO_2 run	85	1.8	0.5	12.4
Drain precipitate	43	45	7.5	4.8
Loose scale	5.3	79	13	2.6

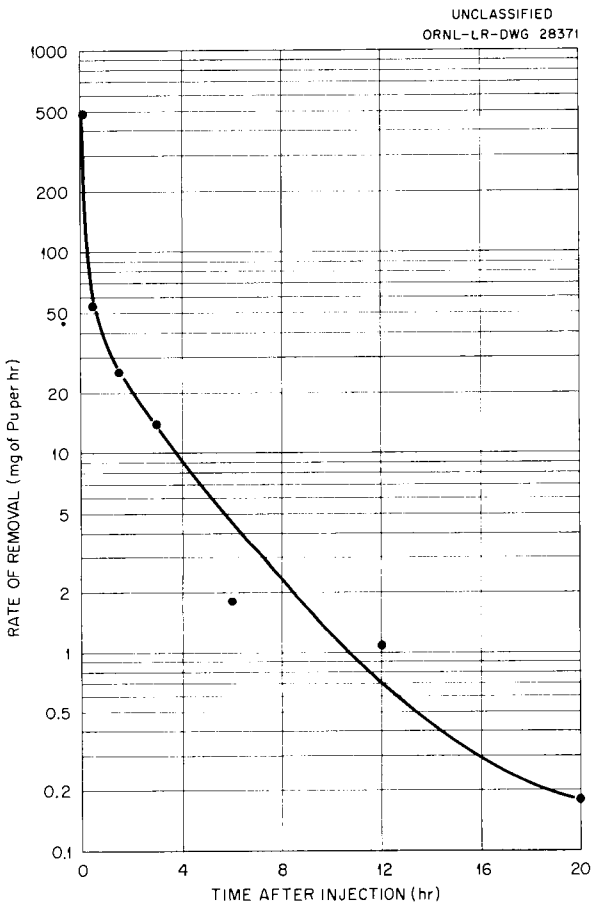

Fig. 18.1. Rate of Removal of PuO_2 by the Hydroclone in Run P-31. In this run, 850 mg of Pu as preformed PuO_2 was injected into 1.4 *m* UO_2SO_4 circulating at 250°C in the P-1 loop.

concentration in the solution had reached approximately 800 mg/liter (a total of 10.4 g), which would correspond to corrosion of approximately 73 g of iron. These results show that very little of the corrosion scale reached the hydroclone and was removed by the underflow pot.

The scale found lying in the bottom of the horizontal pipe containing the sample coupons was primarily corrosion products (Table 18.3). Its granular appearance, together with the fact that it was lying on the bottom of the pipe only, indicates that it had fallen out of the solution, probably because of the low velocity at this point. The flow velocity at the widest part of this line was calculated as slightly less than 1 fps.

18.2.3 Plutonium Solubility

In all these runs plutonium in solution was found to be in the Pu(VI) state. Chromium was 95–100% in the Cr(VI) state. This bears out previous laboratory tests, which indicate that the potential for the Cr(III)-Cr(VI) system is approximately the same as for the Pu(IV)-Pu(VI). One injection was made of Pu(IV) sulfate, and a sample taken only 5 min later showed complete conversion to Pu(VI).

Under the conditions of these runs no definite value for the solubility of Pu(VI) was obtained. Comparison of the analytical values for the plutonium solution with the theoretical amount that would have been in solution, assuming no adsorption or precipitation, indicates that the "solubility" varied with the length of time after plutonium injection (Figs. 18.2 and 18.3). In

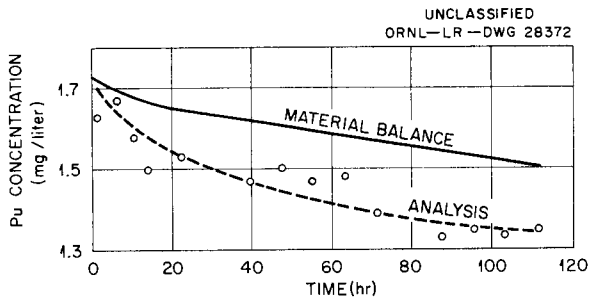

Fig. 18.2. Concentration of Plutonium in Circulating Uranyl Sulfate in Run P-27. About 13 liters of 1.2 *m* UO_2SO_4 was circulated at 250°C under oxygen pressure.

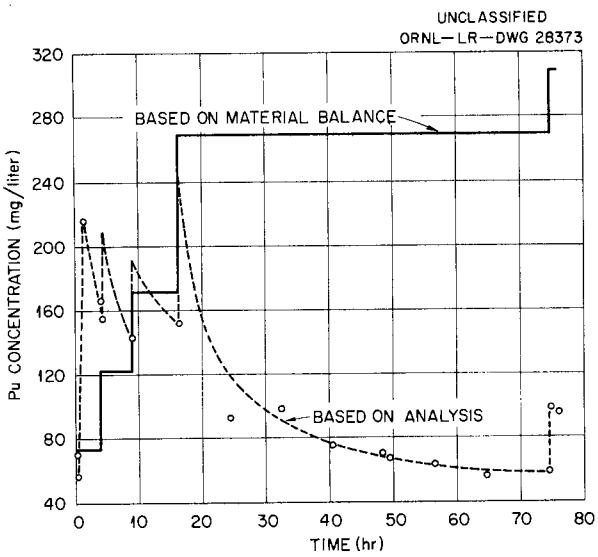

Fig. 18.3. Concentration of Plutonium in Circulating Uranyl Sulfate in Run P-30. About 13 liters of 1.4 *m* UO_2SO_4 was circulated at 250°C under oxygen pressure. Dissolved Pu(VI) was injected at intervals throughout the run.

run P-27 the starting concentration of 1.7 mg/liter was below the precipitation concentration at 250°C; yet, because of a small amount of adsorption, the analytical values for the amount in solution were consistently lower than those calculated from the material balance. The reason for the high concentration of plutonium circulating in solution early in run P-30 is not clear. This may have been the result of pickup of plutonium left in the loop from previous runs. The graph indicates that plutonium removal from solution is rapid but not instantaneous. The most likely figure for the equilibrium solubility of plutonium under these conditions is 75–100 mg per kg of H_2O. At higher concentrations, plutonium was rapidly removed from solution by adsorption on the stainless steel container.

18.2.4 Plutonium Adsorption on Metals

Throughout all these runs, as in the zirconium runs, sample coupons of type 347 stainless steel, titanium, and Zircaloy-2 were in a bypass stream off the main loop. At the end of each run the coupons were removed, and the plutonium adsorbed was determined by direct alpha counting. In some runs new coupons plus those removed from previous runs were used in order to determine the effect of the corrosion scale on the adsorption. All the old coupons adsorbed approximately the same amount of plutonium, regardless of the metal (Table 18.4). This is probably due to the fact that the titanium and the Zircaloy-2 were covered with a scale of corrosion products after they were exposed to the uranyl sulfate solution for a few days. The adsorption behavior was quite different in the three types of runs. In runs P-27 and P-29, no plutonium was precipitated and very little was adsorbed. The rate of adsorption was 4 to 7×10^{-4} $\mu g/cm^2/hr$ in run P-27 and 5×10^{-3} $\mu g/cm^2/hr$ in run P-29. In run P-30 plutonium was precipitated from solution, and the amount adsorbed was extremely high, averaging about 0.3 mg/cm^2; this amounts approximately to the total quantity of plutonium not remaining in solution. In run 31 the PuO_2 adsorption on metal surfaces previously exposed to the solution was approximately 10 times that on new surfaces. Adsorption of PuO_2 on the old coupons ranged from 12 to 31 $\mu g/cm^2$. The higher figure corresponds to an adsorption of 35% of the PuO_2 injected. Further runs with the coupons used in this run gave a total adsorption of 1.0–1.1 mg/cm^2, and it can be inferred that larger amounts would have been adsorbed if more plutonium had been precipitated. The plutonium, then, would be removed by the hydroclone only when the corrosion film leaves the wall surfaces and is collected in the underflow pot.

In the light of the results of these runs in loop P-1, some predictions can be made concerning the operation of the uranyl sulfate blanket on the HRT. There are several differences in conditions between the two, the most important of which are probably the presence of radiation in the blanket,

Table 18.4. Plutonium Adsorption on Metals in the P-1 Loop

Adsorption coupons exposed to 1.4 *m* UO_2SO_4 circulating at 250°C under 350–400 psi O_2

Run	Pu in Solution (mg/liter)	Exposure Time (hr)	Condition of Coupon[a]	Pu Adsorbed ($\mu g/cm^2$)		
				347 SS	Titanium	Zircaloy-2
P-27	2	110	New	0.071	0.019	0.039
			Old	0.042	0.040	0.048
P-29	2–70	180	Old	0.935	1.03	0.992
P-30	70 to ppt[b]	80	New	294	213	365
			Old	279	265	228
P-31	65[c]	36	New	2.84	3.54	5.07
			Old	20.6	20.5	30.7

[a]"Old" refers to coupons previously conditioned in 1.4 *m* UO_2SO_4 at 250°C.

[b]In run P-30 sufficient PuO_2SO_4 was added to increase the plutonium concentration to 342 mg/liter. Plutonium precipitated at concentrations >100 mg/liter.

[c]Preformed PuO_2 was added in run P-31.

the lower surface/volume ratio in the blanket, and the slower rate of increase of the plutonium concentration. The loop was operated under an oxygen overpressure in the absence of radiation. The radiation in the HRT may give a much stronger reducing condition and hold the plutonium in the tetravalent state, which is not soluble. The surface/volume ratio in the HRT blanket is approximately 25% of that in the loop, and the likelihood is greater that hydrolyzed PuO_2 would reach the hydroclone. However, based on the P-1 loop results, if the HRT blanket is operated for only 30 days, producing about 120 mg of Pu per kg of H_2O, a negligible amount of plutonium will be removed by the hydroclone and almost all the plutonium will be present in solution or adsorbed on the wall surfaces.

18.3 PLUTONIUM ADSORPTION ON METALS IN STATIC TESTS

Static bomb tests were carried out in the laboratory to determine the effect of various factors on plutonium adsorption on titanium and Zircaloy-2. The addition of 0.54 *m* H_2SO_4 to 1.4 *m* UO_2SO_4 decreased by a factor of 10 the adsorption from solutions containing 2.2 or 50 mg of plutonium per liter. Preconditioning of the sample specimens had no effect. Adding hydrogen to the gas overpressure generally increased the amount of plutonium adsorbed, probably by holding the plutonium in the tetravalent state (Table 18.5). The rate of adsorption from the acidified uranyl sulfate remained constant over a period of 242 hr but decreased with longer exposure. From a solution containing 50 mg of plutonium per liter, the adsorption apparently reached maximum values of 0.05 and 0.15 $\mu g/cm^2$ on the titanium and Zircaloy, respectively. The amount of plutonium adsorbed was determined by direct alpha counting of the metal samples.

Table 18.5. Plutonium Adsorption on Metals from 1.4 *m* UO_2SO_4 Containing 0.54 *m* H_2SO_4

Time of exposure: 16 hr at 250°C

Metal	Pu Adsorbed ($\mu g/cm^2$)			
	2.2 mg Pu/liter		50 mg Pu/liter	
	O_2	H_2 and O_2	O_2	H_2 and O_2
Titanium	0.0074	0.0045	0.039	0.059
Zircaloy-2	0.0077	0.0203	0.134	0.355

19. THORIUM OXIDE SLURRY DEVELOPMENT

J. P. McBride
C. V. Ellison
E. V. Jones
N. A. Krohn
C. C. Haws
P. A. Haas
K. O. Johnsson
W. J. Lee
K. H. McCorkle
L. E. Morse
E. M. Shank
C. E. Schilling
R. L. Pearson
W. M. Woods
E. L. Youngblood

19.1 SLURRY IRRADIATION STUDIES

19.1.1 Slurry Irradiations in the LITR

Short-term irradiation tests were carried out on a silicate-stabilized thoria sol submitted by Davison Chemical Company (LITR-36),[1] a slurry of 1600°C-fired pumped thoria in D_2O (LITR-37), a slurry of 1000°C-fired thorium-uranium oxide in D_2O (LITR-38), and a slurry of Dri-film–coated thoria in diphenyl (LITR-39).

The silicate-stabilized thoria sol containing 437 g of Th per kg of H_2O was stirred in-pile for 322 hr at 200°C. The pressure increased slightly on starting and leveled out at 500 psi above steam pressure. The autoclave was opened after three days' cooling, and the contents were recovered. The sol had broken to a slow-settling slurry which was badly discolored by stainless steel corrosion products. In an out-of-pile control run, stirred for 363 hr at 200°C, the slurry appearance was similar.

The 1600°C-fired pumped thoria, dried to constant weight at 120°C, was reslurried in D_2O (~750 g of Th per kg of D_2O) and irradiated at 300°C under an oxygen overpressure. After 212 hr of irradiation, the run was terminated by instrument failure. The autoclave was opened after 25 days' cooling, and the slurry, which had become slightly gray in color, was recovered. Recovery was excellent.

The 1000°C-fired mixed thorium-uranium oxide was prepared by firing the coprecipitated oxalates of thorium and natural uranium (U/Th = 0.005). It was slurried in D_2O (~750 g of Th per kg of D_2O) and irradiated for 332 hr at 300°C. The stirrer stopped after 62 hr, following a temperature excursion to 335°C caused by instrument failure, and could not be restarted.

[1] J. P. McBride *et al.*, *Chem. Tech. Monthly Prog. Rep. Oct. 1957*, ORNL-2417, p 72 (classified).

The slurry of Dri-film–coated thoria in diphenyl was irradiated at 300°C for 133 hr. The oxide was prepared by coating an 800°C-fired oxide with Dri-film, washing it free of chloride, and drying at 150°C. The stirrer stopped after approximately four days' irradiation, presumably because of a radiation-induced increase in viscosity. An out-of-pile control experiment was operated for more than 400 hr at 300°C without difficulty.

19.1.2 Postirradiation Examinations

Analyses of several recovered slurries showed essentially all the fission products associated with the solid phase, in agreement with previous results, except for the case of the Davison sol (Table 19.1). In this instance, the supernatant contained almost all the fission products as well as the protactinium. Apparently the large amounts of silicate used to stabilize the sol prevented adsorption on the thoria surface.

Table 19.1. Fission-Product Distribution in Irradiated Slurries

LITR-34: slurry of 1000°C-fired ThO_2
LITR-36: Davison sol
LITR-37: slurry of prepumped 1600°C-fired ThO_2

Radioactive Product	Amount in Supernatant (% of total)		
	LITR-37	LITR-34	LITR-36
Gross beta	0.03	0.001	81.1
Gross gamma	0.03	0.001	81.2
Total rare earths	0.11	0.04	81.3
Si	9.1	3.3	81.2
Ru	5.9	14.2	81.4
Cs	1.8	71.4	81.7
Nb	2.3	0.62	81.2
Zr	0.22	1.9	81.2
I		0.03	81.2
Pa	0.03	0.001	81.2

19.1.3 In-Pile Gas Production and Recombination

Further experiments were carried out in the ORNL Graphite Reactor with slurries prepared from the thorium-uranium oxide used in previous tests.[2] The oxide was refired at 900°C, and the slurries contained 250 and 500 g of Th per kg of H_2O. The refiring reduced the specific surface area from 21.7 m^2/g to 6.0 m^2/g. The gas production rates and equilibrium pressure showed no significant changes as a result of the refiring, but the data showed more scatter than those obtained with the lower fired material.

19.2 GAS RECOMBINATION STUDIES

Studies on the effect of MoO_3 concentration on the reaction of stoichiometric hydrogen-oxygen mixtures in aqueous slurries of thorium-uranium oxide (U/Th = 0.005) were continued. Slurries of simple mixtures of 1600°C-fired thorium oxide with $UO_3 \cdot H_2O$ and of the 1600°C-fired thorium-uranium oxide prepared from the coprecipitated oxalate containing MoO_3 at concentrations of 0.05 *m* and above both gave recombination rates far in excess of that required in a TBR blanket (>> 10 moles of H_2 per hour per liter).

19.2.1 Studies with Simple Mixtures

In previous studies[3] a concentration of 0.048 *m* MoO_3 in the mixed slurry at 291°C at a hydrogen partial pressure of 500 psi gave recombination rates (for a stoichiometric hydrogen-oxygen mixture) of 5 moles of H_2 per hour per liter for the slurry as prepared and 17.3 moles of H_2 per hour per liter after activation with hydrogen. Increasing the MoO_3 concentration to 0.06 *m* increased the rates in the slurry as prepared and after activation to 12.8 and 20.8 moles of H_2 per hour per liter under the same conditions. Increasing the MoO_3 concentration to 0.072 *m* gave very little increase in catalytic activity.

The simple oxide mixture for these experiments was prepared from a 1600°C-fired thorium oxide which had been circulated in a loop for 268 hr at 300°C (REED loop run B5-11) and $UO_3 \cdot H_2O$. After the addition of the $UO_3 \cdot H_2O$ and each increase of 0.012 *m* in the MoO_3 concentration, the slurry was heated to 280°C for 3 hr with a small oxygen overpressure. The slurry was activated by heating with hydrogen (250 psi at 250°C) for 2 hr at 270°C.

19.2.2 Mixed-Oxide Slurries

Study of the reaction rate of stoichiometric hydrogen-oxygen mixtures in aqueous slurries of 1600°C-fired thorium-uranium oxide prepared from the coprecipitated oxalates as a function of MoO_3 catalyst concentration from 0.012 to 0.06 *m* was completed. Reaction rates in excess of 10 moles of H_2 reacted per hour per liter of slurry at 280°C and a partial pressure of 500 psi of hydrogen were obtained in all the slurries as prepared and after hydrogen activation (Table 19.2).

In this series of experiments, the MoO_3 was added in successive aliquots, each increasing the concentration of MoO_3 in the slurry by 0.012 *m*. In an earlier experiment with a slurry prepared with the same thorium-uranium oxide which was made 0.05 molal in MoO_3 by a single addition, the reaction rate for the stoichiometric hydrogen-oxygen mixture was 11.2 moles of H_2 reacted per hour per liter of slurry at 250°C and a partial pressure of 500 psi of hydrogen for both the as-prepared slurry and the hydrogen-activated slurry. Comparison of these two experiments indicates that the manner of catalyst addition may influence the reaction rate.

The thorium-uranium oxide was prepared from 10°C-coprecipitated oxalates by final calcination at 1600°C for 24 hr. The slurry was formed by heating the oxide in water at 280°C for 3 hr under a small overpressure of oxygen. The MoO_3 was added as previously described, and the slurry was reheated at 280°C for 3 hr under a small oxygen overpressure after each addition.

19.3 THORIUM OXIDE PREPARATION DEVELOPMENT

19.3.1 Laboratory Studies

The effects of the chemical and physical variables of the batch oxalate precipitation step on the production of sized oxide are being evaluated. [The size and shape of thorium oxide particles produced by the thermal decomposition

[2] J. P. McBride and N. A. Krohm, *Chem. Tech. Monthly Prog. Rep. Aug. 1957*, ORNL-2400, p 59 (classified).

[3] J. P. McBride *et al.*, *HRP Quar. Prog. Rep. Oct. 31, 1957*, ORNL-2432, p 158.

Table 19.2. Reaction Rates of Stoichiometric Hydrogen-Oxygen Mixtures in 1600°C-Calcined Thorium-Uranium Oxide Aqueous Slurries as a Function of the Molybdenum Oxide Concentration

Oxalates coprecipitated at 10°C and calcined at 1600°C for 24 hr
Ratio of U to Th: 0.005
Slurry concentration: 500 g of Th per kg of H_2O
Reaction temperature: 250°C
Partial pressure of hydrogen: 500 psi

MoO_3 Concentration (m)	Moles of H_2 Reacted per Hour per Liter of Slurry	
	Slurry As Prepared	Hydrogen-Activated Slurry*
0.0	1	1
0.012	34.3	55.0
0.024	32.0	55.0
0.036	57.7	90.7
0.048	76.6	85.7
0.60	76.2	75.3

*Slurry heated with hydrogen (250 psi at 25°C) for 2 hr at 270°C.

of thorium oxalate are determined by the particulate properties of the oxalate.[4-6] Precipitation temperature (10 to 100°C) has been shown to markedly affect the average particle size and the particle shape, the smallest particles being produced at the lowest precipitation temperature (10°C).] Precipitation variables under investigation are:

1. direction of strike (direct strike: oxalic acid solution into thorium nitrate solution; reverse strike: thorium nitrate solution into oxalic acid solution),
2. stirring rate,
3. reagent addition rate,
4. temperature,
5. digestion time,
6. reagent concentration,
7. final nitric acid concentration.

The particulate properties of the oxide product of interest are:

1. average particle size,
2. uniformity (a limited size range for the bulk of the material),
3. fraction of oversize particles (>5 μ).

While the studies are not yet complete, preliminary data are listed in Tables 19.3, 19.4, and 19.5. For a direct strike, it appears that the average particle size of the oxide product decreases with decreasing precipitation temperature and increasing reagent concentration (Tables 19.4 and 19.5), that the more uniform oxide products are produced by lower precipitation temperatures (Table 19.4), and that the fraction of oversize particles decreases with increasing stirring rate and reagent addition rate (Table 19.3).

The reagents used in the laboratory studies were high-purity Lindsay code 103 thorium nitrate and cp oxalic acid solutions. The precipitations were made in a stainless steel beaker with a Brookfield counter-rotating mixer, model L-406, for a stirrer. The geometry of the equipment roughly approximated the large-scale pilot plant production equipment. Most of the precipitations were made with a direct strike, which appeared to give an oxide product of smaller average particle size and fewer oversize particles than the reverse strike (Table 19.3). The oxalic acid was introduced under pressure into the thorium nitrate

[4] R. Beckett and M. E. Winfield, *Australian J. of Sci. Research* **A4**, 644 (1951).

[5] V. D. Allred, S. R. Buxton, and J. P. McBride, *J. Phys. Chem.* **61**, 117 (1957).

[6] V. D. Allred and S. R. Buxton *HRP Quar. Prog. Rep. July 31, 1955*, ORNL-1943, p 181 (classified).

Table 19.3. Thorium Oxalate Precipitation: Effect of Reagent Addition Rate and Agitation

Conditions: Room temperature
1 *M* $H_2C_2O_4$; 1 *M* $Th(NO_3)_4$
Oxide product fired at 800°C

Total $H_2C_2O_4$ Addition Time (min)	Wt % Particles in Excess of 5 μ					
	For Direct Strike; Stirring Rate (arbitrary units)*			For Reverse Strike; Stirring Rate (arbitrary units)*		
	18	28	38	18	28	38
6	5	3	2.5	13	5	9.5
5	4.5	6	2.5	14	13	5.5
4	5	3	1	8	3.5	1

*Settings on Brookfield counter-rotating mixer, model L-406.

Table 19.4. Thorium Oxalate Precipitation: Effect of Precipitation Temperature

Conditions: Direct strike
1 *M* $H_2C_2O_4$; 1 *M* $Th(NO_3)_4$
Stirring rate: 38 (see Table 19.3)
$H_2C_2O_4$ addition time: 4 min
Oxide product fired at 800°C

Precipitation Temperature (°C)	Geometric Mean Particle Size, d_g (μ)	Geometric Standard Deviation, σ_g
10	0.88	1.36
20	1.02	1.39
30	1.20	1.45
40	1.25	1.62

solution through a capillary tube projecting beneath the surface of the nitrate solution, the tube exit being directly above the agitator blades. The thorium oxalate precipitates were filtered immediately after the addition of the oxalic acid (addition time 2 to 24 min) and washed with water four times on the filter. The recovered precipitate was dried at 150°C and decomposed to oxide by a multistage calcination ending at 800°C. Particle-size analyses were made by the improved neutron activation–sedimentation technique with sodium pyrophosphate dispersions in methyl alcohol, water, and glycerine-water mixtures. Particular attention was given to determining the fraction of oversize particles.

It is common practice to present the particle-size distribution in the form of a plot of the logarithm of the particle size versus the cumulative weight per cent undersize on a scale based on the probability integral. If the particle-size data follow a logarithmic probability distribution (as it usually does with the thorium oxide preparations), the resulting plot is a straight line, and the steeper the slope of the line, the less uniform the material. The 50% size in such a plot is the geometric mean particle diameter d_g. The geometric standard deviation σ_g is equal to the ratio of the 84.13% size to the 50% size (also the ratio of the 50% size to the 15.87% size).[7,8]

In the experiments on the effect of agitation (Table 19.3), it was found that the higher the rate of acid addition and rate of stirring the lower the percentage of oversize particles (> 5 μ). At a given temperature, the slope of the particle-distribution curve reached a minimum at a medium speed of agitation and was not changed by an increase in the stirring speed. The lower the precipitation temperature, the more uniform the particle size (low value of σ_g) and the smaller the average particle size d_g (Table 19.4). Decreasing the concentration of the two reagents

[7] J. M. Dalla Valle, *Micromeritics, the Technology of Fine Particles*, 2d ed., p 57, Pitman, New York, 1948.

[8] D. G. Thomas, *Comparison of Various Methods of ThO_2 Particle Size Determination*, ORNL CF-55-12-98 (Dec. 19, 1955).

increased the average particle size but did not affect the size distribution (Table 19.5), which appeared to be primarily temperature-dependent.

Current studies are emphasizing the effect of digestion time and temperature on the particulate properties and the effect of all the precipitation variables on localized sintering or clinker formation on firing at 1600°C. Preliminary results indicate that the well-digested, more-uniform materials form fewer clinkers and smaller oversize fractions after high firing.

19.3.2 Thorium Oxalate and Thorium Oxide Slurry Concentration

Tests with a Tolhurst laboratory centrifuge indicated that it effectively concentrates thorium oxalate and thorium oxide slurries (Table 19.6). Materials used were from pilot plant preparation LO-34, the thorium oxide being a 1600°C-fired small-particle material (<5 μ) separated by decantation. The machine is now being used in the pilot plant for interim thorium oxide production.

A continuous Sharples Super-D-Cantor centrifuge could not be used for concentrating thorium oxalate

Table 19.5. Thorium Oxalate Precipitation: Effect of Reagent Concentration

Conditions: Direct strike
Room temperature
Stirring rate: 38 (see Table 19.3)
$H_2C_2O_4$ addition time: 4 min
Oxide product fired at 800°C

$Th(NO_3)_4$ Concentration (M)	$H_2C_2O_4$ Concentration (M)	Geometric Mean Particle Size, d_g (μ)	Geometric Standard Deviation, σ_g
0.5	0.5	2.77	1.37
0.5	1.0	0.92	1.23
0.5	1.5	0.67	1.37
1.0	0.5	1.85	1.39
1.0	1.0	0.82	1.32
1.0	1.5	0.76	1.35
1.5	0.5	1.98	1.36
1.5	1.0	0.92	1.28

Table 19.6. Results of Batch Centrifugation Tests

Equipment: Tolhurst 12-in.-dia basket centrifuge at 2100 rpm to give 750 g

Feed Rate (ml/min)	Feed Material	Concentration of Feed (g Th/liter)	Concentration of Overflow (g Th/liter)	Per Cent Loss
330	Thorium oxide	4.12	0.042	1.01
500	Thorium oxide	2.26	0.013	0.57
680	Thorium oxide	2.36	0.043	1.8
1140	Thorium oxide	2.13	0.047	2.2
500	Thorium oxalate	16.2	0.085	0.53

precipitates. The cakes formed were too fluid for removal by the screw and built up until unclarified oxalate slurry came through the supernatant overflow.

19.3.3 Flame Preparation Methods

In experimental studies, the development of a flame calcination system starting with an organic slurry of thorium oxide has been emphasized. Presently developed procedures and apparatus should permit design and fabrication of a facility to produce 100-lb lots of flame-calcined oxide for evaluation tests. Testing of alternative feeding and firing methods is continuing.

A feed system with a centrifugal pump and an aspirating nozzle effectively handled a slurry of 10 g of ThO_2 per liter of methanol. There was some plugging of the capillary through which the slurry was injected into the flame; however, this problem was solved by providing a cleaning tip on the end of the nozzle metering rod. This tip can be forced through the length of the capillary when cleaning is needed. The circulating pump will have to be carefully selected to avoid erosion and shaft seal problems. The mechanical seal on the $\frac{1}{8}$-hp Eastern centrifugal pump used in these tests failed after 40 hr of operation.

A collection system consisting of a cooler and a commercial vacuum cleaner was installed and used in the deep bay of Building 4501. Water is contacted with the dust-bearing burner product gases in a vertical tube for the primary purpose of cooling these gases. Spray nozzles delivering a conical spray were selected for this cooler to minimize the collection of particulates in the water. The water entering the sprays is cooled externally and is recycled to limit the quantity of thoria-bearing water accumulated.

Material balances showed the over-all process efficiency (grams collected in vacuum cleaner/grams fed to flame) to be about 25%. Roughly equal amounts were found in the spray-cooler water, the spray-tower bottom, and the vacuum cleaner. The given process efficiency is probably a measure of the dispersing efficiency of the pump feeding system.

19.3.4 Thorium Oxide Classification

Two- and three-stage hydroclone systems for classifying thorium oxide were tested with oxide dispersed with oxalic acid in water and with oxide in methyl alcohol. Typical results of a two-stage system using a methyl alcohol suspension of thoria (10 g of ThO_2 per liter) are shown in Fig. 19.1. The underflow product had an average particle size of 0.9 μ as compared with 1.8 μ for the feed.

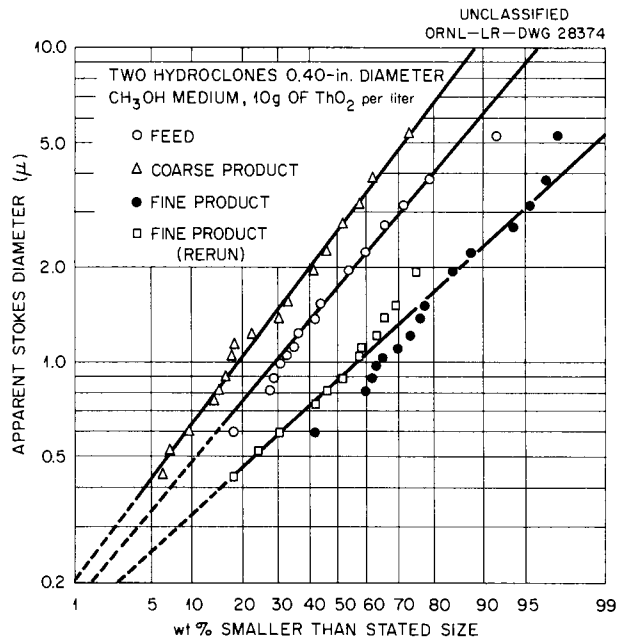

Fig. 19.1. Classification of ThO_2 by Hydroclones.

19.4 THORIUM OXIDE PRODUCTION

The thorium oxide production facility was modified to permit preparation of 750 lb/month of nominal 1-μ particles, calcined to 1600°C. Additional modifications are in progress to increase the capacity to 1500 lb/month.

The present procedure used for thorium oxide is:

1. precipitation of thorium oxalate at 10°C, followed by 8 hr of digestion at 25°C;
2. filtration of the thorium oxalate followed by three water washes to remove soluble impurities;
3. step-calcination to 650°C to convert the thorium oxalate to thorium oxide;
4. recalcination of the thorium oxide to 1600°C for 4 hr;
5. classification of the 1600°C-calcined thorium oxide by dispersion and sedimentation-decantation;
6. recalcination of the classified thorium oxide at 650°C.

Nine precipitations at 10°C (runs LO-34 through LO-42) were completed to produce about 2500 lb of 650°C-calcined thorium oxide; the yield through the initial calcination averaged about 96%. About 1300 lb of 1600°C-recalcined and 180 lb of 1400°C-recalcined thorium oxide were produced in two gas-fired furnaces; the yield through the recalcination step averaged 89%. About 550 lb of 1600°C-calcined and 130 lb of 1400°C-calcined thorium oxide, classified to less than 5 μ particle size, were produced. The yield from precipitation through the final classified product was about 50%.

19.5 HINDERED-SETTLING STUDIES

No effect of container diameter or height on the room-temperature settling rate of 800°C-fired thorium oxide in water at concentrations of 200, 400, and 700 g of Th per kg of H_2O was discernible in the ranges 0.5 to 3 in. in diameter and 3 to 12 in. in height. Thorium oxide fired to 1600°C and slurried in water at concentrations of 200 and 400 g of Th per kg of H_2O was not affected by column diameters from 0.25 to 3 in. and heights of 2.5 to 10 in. However, with a concentration of 700 g of Th per kg of H_2O the settling rate was higher with the smaller diameter tube (Table 19.7). The large range over which the data points scattered obscured any trends within ±30% of the average. The slurry interface fell in a noticeably stepwise manner in the 0.25-in.-dia tube.

The 95% confidence interval, assuming random variation of settling rates and based on the average rate at each geometric condition, was of the order of ±15% of the average settling rate. In addition to this variation at each geometric condition, the erratic variations in the average rates over the range of conditions studied were so great that a correlation was not possible except with the 1600°C-fired slurries containing 700 g of Th per kg of water. Attempts to reduce the scatter of the data by various refinements of experimental technique were unsuccessful. In general, the 1600°C-fired oxide gave more reproducible results than the 800°C-fired oxide.

19.6 SPECIAL PREPARATIONS

19.6.1 Cellulose Additions

The effect of the addition of cellulose in the precipitation of thorium oxalate or thorium nitrate on the characteristic properties of the oxide

Table 19.7. Effect of Container Diameter and Height on Room-Temperature Settling Rate of Thorium Oxide Slurries

Slurry Concentration (g Th/kg H_2O)	Column Diameter (in.)	Column Height (in.)	Settling Rate (cm/sec)
	800°C-Fired Oxide		
200	0.5, 3	3–12	0.19
400	0.5, 3	3–12	0.09
700	0.5, 3	3–12	0.05
	1600°C-Fired Oxide		
200	0.25, 3	2.5–10	0.065
400	0.25, 3	2.5–10	0.022
700	0.25	2.5	0.0045
700	0.25	5	0.012
700	0.25	10	0.025
700	3	2.5	0.0008
700	3	5	0.0027
700	3	10	0.0034

products (from thermal decompositions) was determined[9] for weight ratios of cellulose to thoria from 1.5 to 6. For the 650°C-fired oxide products, the surface areas were in general a factor of 2 or 3 lower than those of the oxide prepared in the usual way, but the x-ray crystallite size was unchanged. The average particle size was not markedly lowered by the addition of the cellulose. Striking decreases in the bulk densities of the oxide products were obtained at cellulose/thoria ratios of 4 or greater (bulk densities were 0.2 to 0.4 g/cc). Firing selected products at 1000 and 1200°C did not markedly change their bulk, but firing at 1600°C resulted in the formation of bricklike masses of oxide.

The thorium was precipitated by adding, with vigorous stirring, oxalic acid or ammonium hydroxide to a Thorex-product thorium nitrate solution in which the cellulose was suspended. Whatman cellulose pulp (ground) and 40- and 200-mesh Solka-flox cellulose powder were used.

19.6.2 Nitric Acid Addition to the Thorium Oxalate Precipitation Step

Using a rapid mixing technique, a series of thorium oxalate precipitations was made with 0.1 *M* Thorex thorium nitrate product and 0.22 *M* oxalic acid (15% excess) containing 1 to 8 *M* excess nitric acid. An induction period for oxalate precipitation was observed when the nitric acid was 5 *M* in excess. The length of the induction period increased with higher excess nitric acid concentrations. Despite the delay in the precipitation in the presence of concentrated acid, tests on the supernatant indicated nearly complete precipitation. Experiments with 0.6 *M* thorium nitrate and 0.5 *M* oxalic acid to which 6 *M* and 7 *M* excess nitric acid were added did not show an induction period.

19.6.3 Oxide from the Direct Calcination of Thorium Nitrate

Thorium nitrate solution by itself and with H_2SO_4, H_2SiO_3, $Al(NO_3)_3$, $Pb(NO_3)_2$, or $Na_4P_2O_7$ additive was evaporated under a heat lamp and then calcined at 600°C. Additive concentrations, expressed as the mole ratio of added oxide to the thorium oxide in the final product, ranged from 0.005 to 1. The final products were all of rather large average particle size (15 to 58 μ), and none appeared to be acceptable slurry products. The mixed-oxide products, except those containing the phosphate, had high specific surface areas as compared with the pure oxide. The products with P_2O_5/ThO_2 mole ratios of 0.02 and 0.05 had specific surface areas of 0.7 and 2 m^2/g, which are very low for a 650°C-fired product.

[9]In work carried out at KAPL bulky UO_2 and U_3O_8 products were obtained by this method (S. C. Firman, private communication).

19.7 SURFACE-CHEMISTRY STUDIES[10]

Gas adsorption studies with carbon dioxide on thoria were completed, and the results will soon be published. Adsorption isotherms indicated that the adsorption potential for carbon dioxide on thoria varies linearly with surface coverage. At temperatures below 200°C two kinds of surface sites are involved, both of which show a linear variation in adsorption potential with surface coverage, although the absolute adsorption potential of one site is much greater than that of the other. Since the adsorption process is exothermic, adsorption on one of these sites above 200°C drops to such a low value that only one site need be considered above 200°C. The shapes of the adsorption isotherms were evaluated theoretically, and the enthalpy of adsorption was determined under a variety of conditions.

Studies of the rates of desorption of carbon dioxide were also completed. The amount desorbed varied logarithmically with time. Such a desorption process indicates the systematic variation in either activation energy or adsorption potential with surface coverage and is consistent with the adsorption isotherms observed. The effect of surface coverage, however, is different in the desorption process than in the equilibrium adsorption, indicating that the activation energy also varies with surface coverage. A variation of surface potential or enthalpy of activation with surface coverage can be explained either by surface heterogeneities, repulsion, or surface strain. The work of other investigators in the field of catalysis indicates that the relief of strain on the surface is probably the factor which contributes predominantly to the variation in both enthalpy of activation and adsorption potential with surface coverage.

[10]Work done by M. E. Wadsworth, University of Utah, under subcontract.

In studies on the adsorption of sulfuric acid from aqueous solution, it appeared that for each surface site four hydrogen ions and two sulfate ions disappear from the solution per surface site. This was explained in terms of the adsorption of hydrosulfate ion on the surface displacing two hydroxyl groups or as an esterification reaction involving neutralization of sulfuric acid with surface hydroxyl groups. The adsorption studies are being extended to higher temperatures.

In continued differential infrared studies it was definitely shown that the amount of sulfate adsorbed can be measured directly by infrared spectroscopy. The relation between the adsorption determined by infrared spectroscopy and the amount of sulfate adsorbed determined chemically by solution depletion was linear. Tentative identification of sulfate adsorbed on the surface indicated it to be bisulfate.

Work on the adsorption of silicate from solution was initiated. Silicate absorbs strongly in the infrared region, and tentative results indicate that surface layers that have adsorbed silicates can be studied by infrared spectroscopy. This work will closely parallel the sulfuric acid adsorption studies, in that solution depletion will be determined both by infrared and by chemical techniques and the surface-adsorbed silicates will be determined by infrared absorption. It is hoped by this technique that adsorption isotherms under a variety of conditions of temperature, concentration, and pH can be obtained for silicate adsorption.

19.8 THORIA MICROSPHERE PREPARATION[11]

Approximately 50 kg of thoria microspheres classified into $<3\ \mu$, $3–30\ \mu$, and $30–50\ \mu$ fractions is being prepared for evaluation. This preparation is nearly complete. The 1000°C-fired beads are being classified, since no acceptable methods for classifying the wet beads have been developed.

[11] Work done by Houdry Process Corp.

20. IN-PILE SLURRY LOOP

W. E. Unger

T. A. Arehart L. J. King W. F. Schaffer

20.1 STATUS OF DESIGN

The design, development, and procurement of the various components necessary for the operation of the in-pile slurry loop project in the ORR progressed satisfactorily through the middle of December. This program is a cooperative effort of ORNL and the Pennsylvania Advanced Reactor Project (PAR). Difficulties in the program were first evidenced during inspection at ORNL of valves which failed to pass the leaktightness test normally required of valves for service on in-pile solution loops. Because the valves may leak after indeterminable usage, the loop design is being revised to permit maintenance or replacement of all valves essential to continuing operation.

A mockup (Fig. 20.1) of the PAR loop and the reactor-plug aperture has been constructed for use in testing the design of the loop support rollers and the jumper disconnects by which the loop is to be joined to the external auxiliary equipment. The loop faceplate with the jumper disconnects in place is shown in Fig. 20.2.

The design of the ORR installation is approximately 65% complete, based on the original project concept. The major items of design required for installation at the reactor are approximately 90%

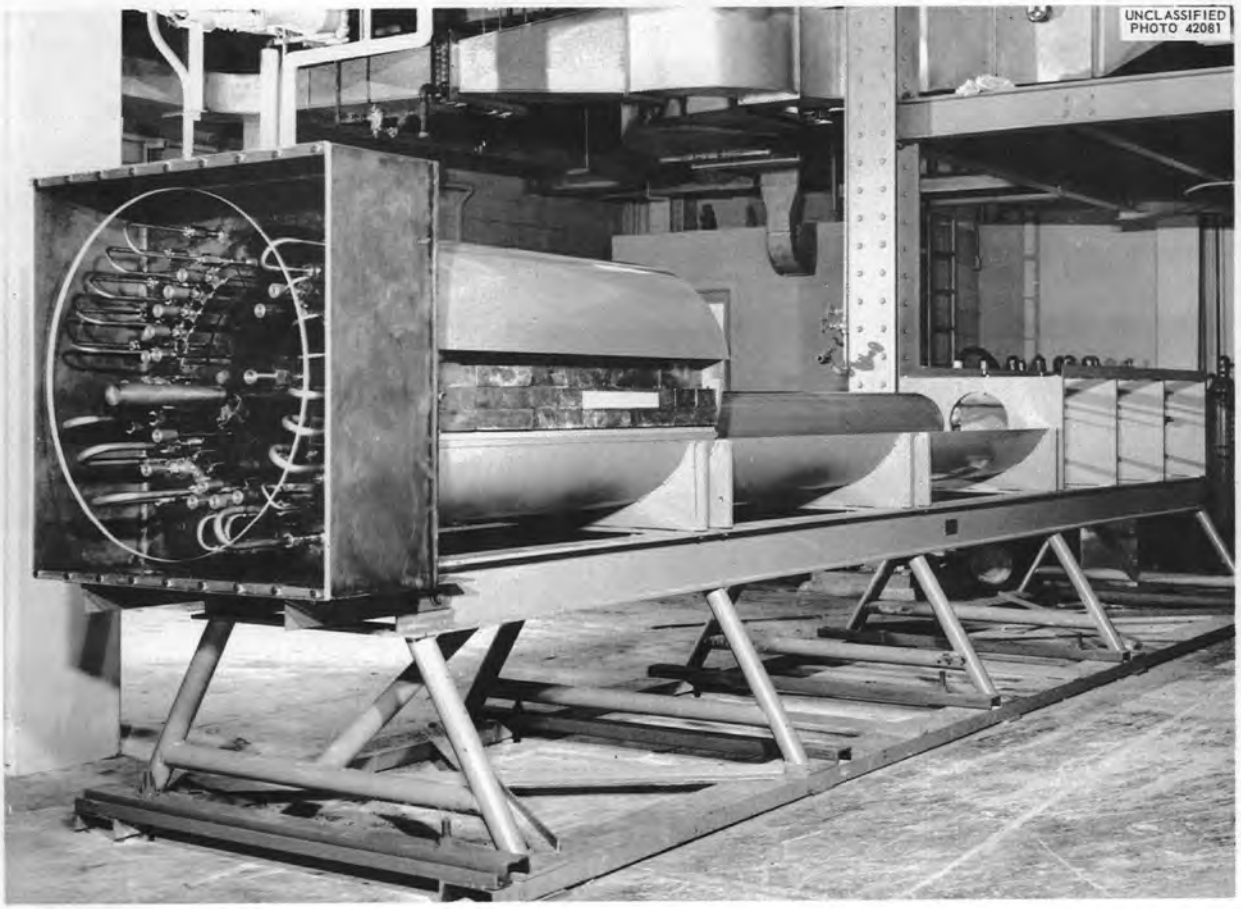

Fig. 20.1. PAR Loop Mockup Complete with Equipment Chamber A. Side view.

complete; these items include the five shielded equipment chambers, the special reactor plug, the shield door and shutter, and other miscellaneous equipment. The various shielded carriers and handling tools which do not require installation are approximately 50% complete.

20.1.1 Sampling

The early model of the sampler, the cavity-valve type, will be used for the first loop. The ultrasonic model requires further development; however, no additional work is planned in the immediate future.

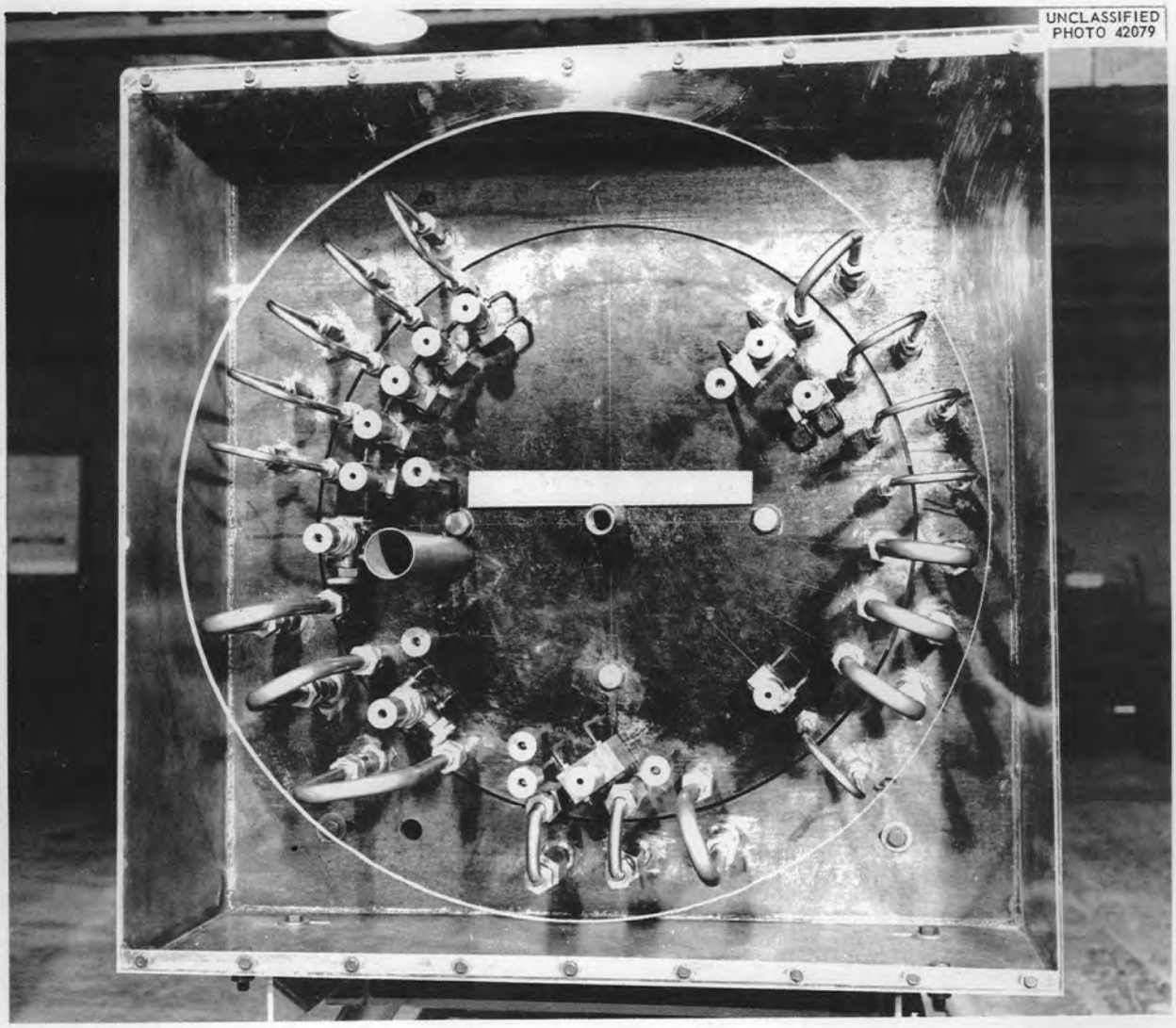

Fig. 20.2. PAR Loop Mockup Equipment Chamber A, Complete with Disconnect and Valve Handle Disconnect.

Part VI

SUPPORTING CHEMICAL RESEARCH

E. H. Taylor

21. AQUEOUS SYSTEMS AT ELEVATED TEMPERATURES

H. F. McDuffie H. H. Stone

21.1 HOMOGENEOUS CATALYSIS OF THE HYDROGEN-OXYGEN REACTION IN AQUEOUS SOLUTIONS

The reaction between dissolved hydrogen (or deuterium) and oxygen in aqueous solutions at elevated temperatures is catalyzed homogeneously by dissolved copper salts. Previous reports have indicated that deuterium reacts more slowly than hydrogen.[1-3] Since the HRT is being operated with heavy water as the fuel solvent, it was desirable to make recombination tests of the deuterium-oxygen reaction in simulated reactor fuel solution. Such tests make it possible to compare the ultimate performance of the reactor with its predicted behavior.

Four test solutions (chemical compositions given in Table 21.1) were prepared and studied. Solutions B, C, and D were prepared in the laboratory from heavy water, concentrated sulfuric acid, cupric sulfate pentahydrate, and uranyl sulfate trihydrate. Solution S was prepared by diluting with heavy water a concentrated enriched-uranium stock solution supplied by the HRT operations group; copper was added to this solution from a previously analyzed 0.98 *M* stock solution of cupric sulfate in light water. None of the test solutions contained more than 0.5% light water.

Tests were conducted at 250, 275, and 300°C; at least two concentrations of copper were tested at each temperature. For each combination of temperature and copper concentration a number of tests were made covering a range of gas-to-liquid volume ratios in the recombination apparatus. Figures 21.1 to 21.3 present the experimental data as plots of $1/k_{\pi}$ (the time constant for pressure decrease) vs the gas-to-liquid ratio. It has already been established that the slopes of the lines in these plots are equal to α/RTk_{sol} and measure the combined effects of solution activity and deuterium distribution between the gas and liquid phases.[1,2] Table 21.2 presents the observed values of these slopes, together with additional recombination parameters derived from the experimental data.

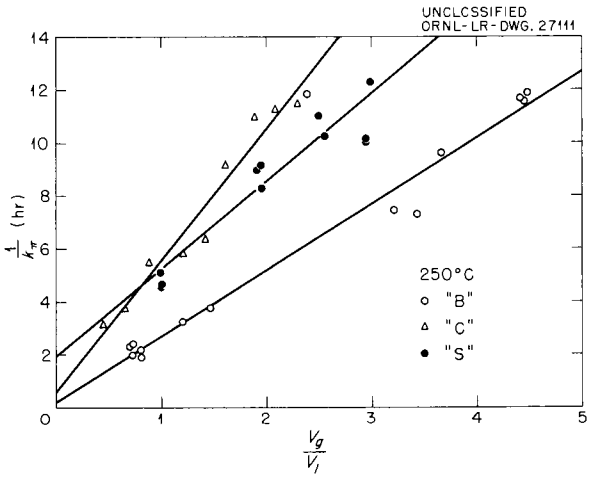

Fig. 21.1. Experimental Data at 250°C.

Table 21.1. Test-Solution Compositions

	Solution B	Solution C	Solution D	Solution S
Uranium, *M*	0.0461	0.0461	0.0461	0.0468
Sulfate, total, *M*	0.0657	0.065	0.065	0.0702
Sulfate, excess, *M*	0.018	0.018	0.018	0.0234
Copper, *M*	0.00144	0.00070	0.00035	0.0010

[1] H. F. McDuffie *et al.*, *The Radiation Chemistry of Homogeneous Reactor Systems. III. Homogeneous Catalysis of the Hydrogen-Oxygen Reaction*, ORNL CF-54-1-122 (Jan. 26, 1954).

[2] C. H. Secoy *et al.*, *HRP Quar. Prog. Rep. Jan. 31, 1957*, ORNL-2272, p 170–171.

[3] C. H. Secoy, in *HRP Civilian Power Reactor Conference Held at Oak Ridge National Laboratory, May 1–2, 1957*, TID-7540, p 170–171.

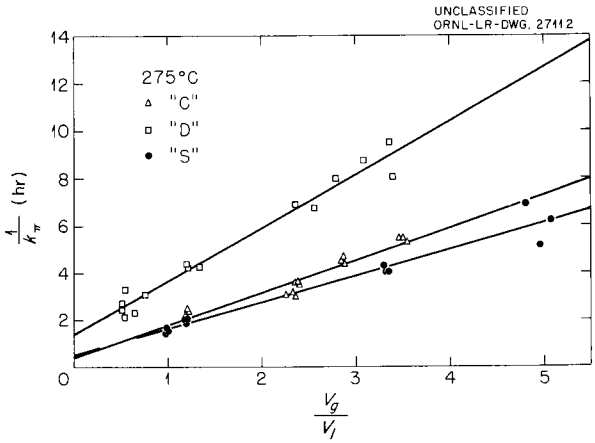

Fig. 21.2. Experimental Data at 275°C.

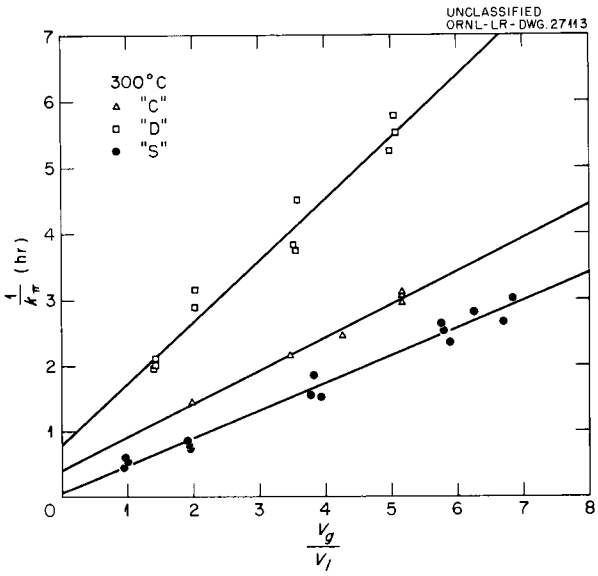

Fig. 21.3. Experimental Data at 300°C.

The effect of copper concentration upon the combined reaction parameter $10^4 k_{sol}/\alpha$ can be seen from Fig. 21.4. Extrapolation to higher copper concentrations of interest to reactor operation can be made from these data. The combined parameter appears to be very nearly proportional to the first power of the copper concentration.

The effect of temperature is shown in Fig. 21.5, a plot of the combined parameter, corrected for copper concentration, vs $10^4/T$. The temperature dependence of this combined parameter $k_{sol}/\alpha[Cu]$ is nearly the same as that previously observed for

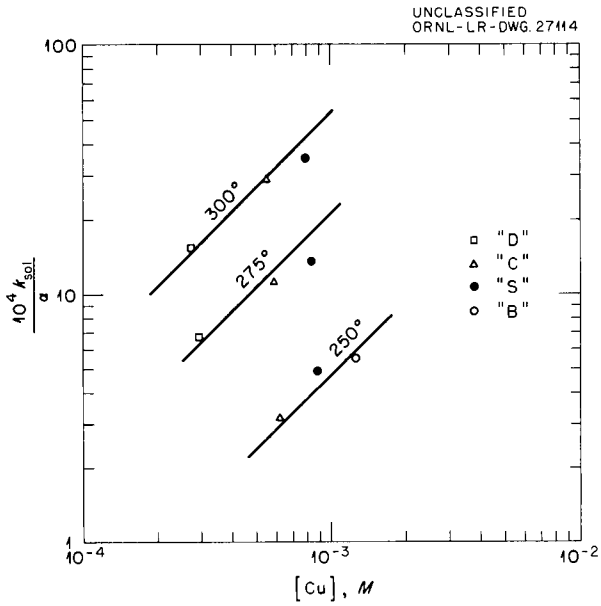

Fig. 21.4. Dependence of Combined Reaction Parameter upon Copper Concentration.

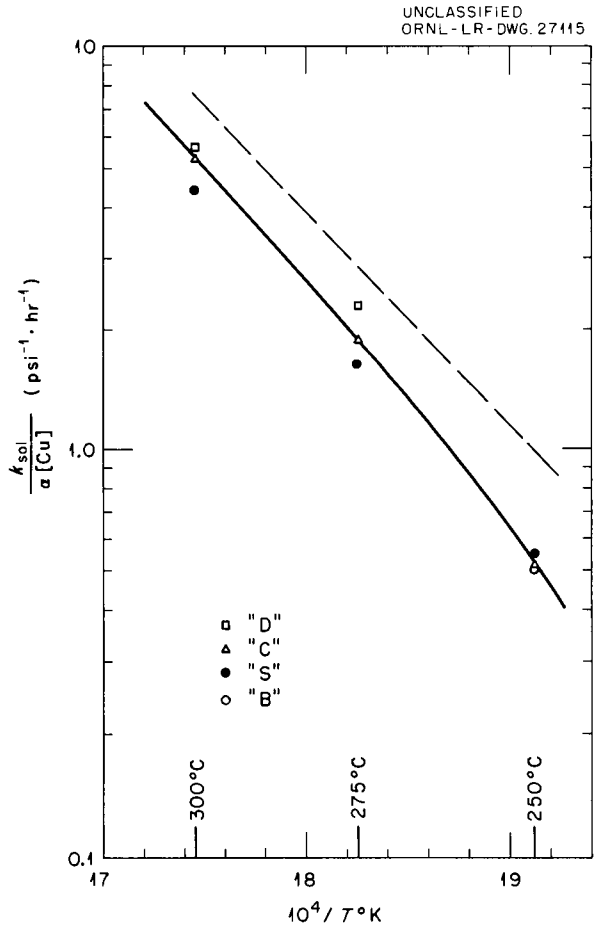

Fig. 21.5. Dependence of Combined Reaction Parameter upon Temperature.

light-water solutions (corresponding to an activation energy of 24 kcal). The present temperature dependence includes both that due to the solution activity and that due to changes in the deuterium distribution coefficient; the previously reported temperature dependence was the difference between that of the combined parameter and that reported for the solubility of hydrogen in water.

Table 21.2. Combined Reaction Parameters

Test Temperature (°C)	Test Solution	Copper Concentration* (M)	Experimental Slope,** α/RTk_{sol} (hr)	Combined Reaction Parameter, $10^4 k_{sol}/\alpha$ ($M \cdot psi^{-1} \cdot hr^{-1}$)	$\frac{k_{sol}}{\alpha[Cu]}$ ($psi^{-1} \cdot hr^{-1}$)
250	B	0.00127	2.492	6.37	0.502
	C	0.00062	4.968	3.19	0.514
	S	0.000882	3.281	4.83	0.548
275	C	0.00059	1.374	11.01	1.87
	D	0.000294	2.251	6.72	2.28
	S	0.000839	1.112	13.61	1.62
300	C	0.00055	0.504	28.71	5.22
	D	0.000275	0.934	15.49	5.63
	S	0.000787	0.418	34.62	4.40

*Corrected for change in density upon heating to test temperature.

**Slope of plot of $1/k_{\pi}$ vs ratio of gas volume to liquid volume.

Part VII

ANALYTICAL CHEMISTRY

M. T. Kelley

22. ANALYTICAL CHEMISTRY

O. Menis

R. G. Ball
C. M. Boyd
H. P. House
D. L. Manning
R. H. Powell
T. C. Rains
I. B. Rubin

22.1 ANALYSIS OF THORIUM OXIDE

22.1.1 Determination of Titanium

A sensitive method for the determination of titanium in slurries of thorium oxide was required in order to evaluate the corrosion-erosion rate of titanium components, such as pump impellers and wear rings, during a loop circulation test with this type of slurry in the REED slurry blanket test system. A spectrophotometric method, in which the chromogenic reagent is disodium-1,2-dihydroxybenzene-3,5-disulfonate (Tiron), was adapted for use in making this determination. The yellow-colored titanium-Tiron complex is formed at a pH of 5 in a 2 *M* acetate solution which contains 0.5 g of disodium ethylenediaminetetraacetate (EDTA). In this medium, major interferences are eliminated by complexation with EDTA. With the exception of chromium(VI) and molybdenum(VI), which can be removed by extraction with hexone, other minor components of thorium oxide slurries do not interfere. As much as 400 mg of thorium and at least 0.5 mg of iron(III) can be tolerated in making the absorbancy measurements with a Beckman DU spectrophotometer at a wavelength of 380 mμ. From 3 to 10 μg of titanium per gram of slurry was determined by this method, with a coefficient of variation of the order of 5%, on a series of samples from the slurry blanket test system. In a specific application, it was found that the titanium content, as established by this method, of a slurry after the circulation test agreed to within 10% with the actual weight loss of the titanium components which had been subjected to test in the loop.

22.1.2 Polarographic Determination of Uranium

A polarographic method was applied to the determination of microgram quantities of uranium in samples of thorium oxide slurry which had been withdrawn from the slurry blanket test system during a circulation test. Perchloric acid solutions of the slurries were analyzed polarographically, without prior separation of the uranium, since neither thorium nor those other impurities commonly found in slurries interfere with the reduction wave of uranium which occurs at a half-wave potential ($E_{1/2}$) of −0.15 v versus the saturated calomel electrode. Hydroxylamine sulfate was added to reduce any iron which may have been present. An ORNL model 1763 derivative polarograph was used in this work. From 200 to 500 ppm of uranium was determined in slurry samples which contained 300 to 400 mg of thorium oxide per gram, with a coefficient of variation of less than 3%.

22.1.3 Application of Gamma Counting to the Determination of Thorium Oxide

A study is being made of the applicability of a gamma-counting method for the determination of thorium oxide, particularly on fractions of slurry obtained by sedimentation methods for the measurement of particle-size distribution. The gamma emission of the daughter products of natural thorium, with energies of 0.085, 0.24, 0.58, and 2.6 Mev, is measured by means of a well-type scintillation counter with a thallium-activated sodium iodide crystal. Although the ratio of emissivity at different energy levels depends upon the extent to which the daughters are in equilibrium with the parent Th^{232}, this variable factor becomes unimportant if a portion of the same material which is contained in the samples under test is used for calibration purposes.

In sedimentation tests, two samples, the settled and the suspended fractions of oxide, must be analyzed for thorium. If the ratio of thorium oxide in these two fractions can be accurately determined, it is unimportant whether the absolute amounts are measured accurately. The gamma-counting method is adequate for this purpose; the ratio can be established by this means with an error of the order of 2%. It is, furthermore, fairly rapid, requiring no more than one-third the time of the conventional spectrophotometric method.

22.2 ANALYSIS OF URANYL SULFATE SOLUTIONS

22.2.1 Flame-Photometric Determination of Silver

A procedure was devised for the flame-photometric determination of microgram quantities of silver in uranyl sulfate solutions. No separation is required if the U/Ag weight ratio does not exceed 1000, in which case the interference of uranium can be corrected for by application of the Chow-Thompson standard addition technique.[1] For higher U/Ag ratios or if the sample contains sodium or nickel, which also interfere with the measurement of the emissivity of silver at 338 mμ, the silver must be separated from interfering substances. This separation is accomplished by internal electrolysis in which silver, plus copper if it is present, is deposited on a platinum cathode. Cadmium is used as the anode. The silver, with the copper, is then dissolved in nitric acid, and after volatilization of excess acid the silver is determined flame photometrically. Copper at a Cu/Ag ratio of 500 can be tolerated. Concentrations as low as 1 μg of silver per milliliter of solution can be estimated with a coefficient of variation of 10%.

[1] T. J. Chow and T. G. Thompson, *Anal. Chem.* **27**, 18 (1955).

22.2.2 Pyrolytic Separation of Ruthenium from Metals

The pyrolytic separation method previously reported[2] for the removal of ruthenium from materials containing salts of this element was applied successfully to the removal of milligram quantities of ruthenium metal from stainless steel parts. In this case, the addition of an oxidant, $NaBiO_3$, to the sample is necessary in order to effect complete volatilization of the ruthenium. The material can, furthermore, be pyrolyzed in a silica rather than a nickel boat. With these modifications, the procedure previously described[2] has been found to be useful for the pyrolysis of the sample and subsequent determination of the ruthenium, which is volatilized as the tetroxide and collected in a suitable absorbent.

[2] O. Menis *et al.*, *HRP Quar. Prog. Rep. Oct. 31, 1957*, ORNL-2432, p 181.

INTERNAL DISTRIBUTION

1. C. E. Center
2. Biology Library
3. Health Physics Library
4. Metallurgy Library
5-6. Reactor Experimental Engineering Library
7-9. Central Research Library
10-14. Laboratory Records Department
15. Laboratory Records, ORNL R.C.
16. G. M. Adamson
17. T. A. Arehart
18. A. L. Bacarella
19. J. E. Baker
20. R. G. Ball
21. S. J. Ball
22. R. D. Baybarz
23. S. E. Beall
24. L. L. Bennett
25. R. G. Berggren
26. G. B. Berry
27. R. E. Biggers
28. A. M. Billings
29. D. S. Billington
30. E. P. Blizard
31. R. Blumberg
32. E. G. Bohlmann
33. S. E. Bolt
34. C. J. Borkowski
35. B. F. Bottenfield
36. G. E. Boyd
37. J. C. Bresee
38. N. A. Brown
39. F. R. Bruce
40. J. R. Buchanan
41. W. D. Burch
42. C. A. Burchsted
43. S. R. Buxton
44. A. D. Callihan
45. T. A. Carlson
46. W. L. Carter
47. G. H. Cartledge
48. R. H. Chapman
49. R. A. Charpie
50. R. D. Cheverton
51. J. M. Chilton
52. C. J. Claffey
53. H. C. Claiborne
54. W. E. Clark
55. S. D. Clinton
56. T. E. Cole
57. C. W. Collins
58. E. L. Compere
59. R. S. Crouse
60. F. L. Culler
61. J. S. Culver
62. D. G. Davis
63. R. J. Davis
64. V. A. DeCarlo
65. B. D. Draper
66. J. S. Drury
67. W. K. Eister
68. L. B. Emlet (K-25)
69. J. L. English
70. D. E. Ferguson
71. J. D. Flynn
72. D. F. Frech
73. J. H. Frye, Jr.
74. C. H. Gabbard
75. J. L. Gabbard
76. W. R. Gall
77. R. B. Gallaher
78. C. H. Gibson
79. E. H. Gift
80. H. E. Goeller
81. R. S. Greeley
82. A. T. Gresky
83. J. C. Griess
84. E. Guth
85. R. H. Guymon
86. L. A. Haack
87. P. A. Haas
88. J. Halperin
89. B. A. Hannaford
90. P. H. Harley
91. R. J. Harvey
92. P. N. Haubenreich
93. D. N. Hess
94. J. W. Hill
95. E. C. Hise
96. A. Hollaender
97. P. P. Holz
98. H. P. House
99. A. S. Householder
100. S. Jaye
101. G. H. Jenks
102. D. T. Jones
103. E. V. Jones
104. K. O. Johnsson

105. W. H. Jordan
106. S. I. Kaplan
107. P. R. Kasten
108. C. P. Keim
109. M. T. Kelley
110. F. Kertesz
111. S. S. Kirslis
112. J. O. Kolb
113. R. B. Korsmeyer
114. U. Koskela
115. K. A. Kraus
116. N. A. Krohn
117. J. A. Lane
118. C. G. Lawson
119. R. E. Leuze
120. S. C. Lind
121. R. B. Lindauer
122. C. S. Lisser
123. R. S. Livingston
124. M. H. Lloyd
125. R. A. Lorenz
126. M. I. Lundin
127. R. N. Lyon
128. J. L. Marsh (C&CC, South Charleston)
129. W. L. Marshall
130. J. P. McBride
131. F. C. McCullough
132. H. F. McDuffie
133. H. A. McLain
134. R. A. McNees
135. J. R. McWherter
136. O. Menis
137. E. C. Miller
138. C. S. Morgan
139. K. Z. Morgan
140. L. E. Morse
141. J. P. Murray (Y-12)
142. I. K. Namba
143. M. L. Nelson
144. P. D. Neumann
145. R. H. Nimmo
146. A. R. Olsen
147. L. F. Parsly
148. R. L. Pearson
149. F. N. Peebles
150. Sigfred Peterson
151. H. O. Phillips
152. M. L. Picklesimer
153. R. M. Pierce
154. R. H. Powell
155. B. E. Prince
156. J. J. Prislinger
157. L. R. Quarles
158. W. D. Reel
159. P. M. Reyling
160. S. A. Reynolds
161. D. M. Richardson
162. A. E. Richt
163. G. W. Rivenbark
164. R. C. Robertson
165. W. Robinson
166. H. C. Roller
167. A. M. Rom
168. M. W. Rosenthal
169. H. C. Savage
170. W. F. Schaeffer
171. C. E. Schilling
172. H. E. Seagren
173. H. K. Search
174. C. L. Segaser
175. E. M. Shank
176. E. D. Shipley
177. M. D. Silverman
178. M. J. Skinner
179. A. N. Smith
180. A. H. Snell
181. J. W. Snider
182. D. L. Snyder
183. I. Spiewak
184. H. H. Stone
185. R. W. Stoughton
186. C. D. Susano
187. J. E. Sutherland
188. J. A. Swartout
189. E. H. Taylor
190. W. Terry
191. D. G. Thomas
192. P. F. Thomason
193. M. Tobias
194. D. S. Toomb
195. W. E. Unger
196. W. C. Ulrich
197. R. Van Winkle
198. D. W. Vroom
199. R. E. Wacker
200. F. J. Walter
201. K. S. Warren
202. B. Weaver
203. H. O. Weeren
204. A. M. Weinberg
205. S. H. Wheeler
206. J. K. White
207. E. P. Wigner (consultant)
208. H. D. Wills

209. G. C. Williams
210. J. C. Wilson
211. R. H. Winget
212. C. E. Winters
213. L. F. Woo
214. W. C. Yee
215. F. C. Zapp
216. ORNL – Y-12 Technical Library, Document Reference Section
217. HRP Director's Office, Y-12

EXTERNAL DISTRIBUTION

218. E. O. Christiansen, University of Utah
219. F. C. Moesel, AEC, Washington
220. Houdry Corporation (Attn: G. A. Mills)
221. Division of Research and Development, AEC, ORO
222-228. TISE for P.A.R.P.
229-805. Given distribution as shown in TID-4500 (13th ed., Rev.) under Reactors–Power category (75 copies – OTS)

Reports previously issued in this series are as follows:

ORNL-527	Date Issued, December 28, 1949
ORNL-630	Period Ending February 28, 1950
ORNL-730	Feasibility Report – Date Issued, July 6, 1950
ORNL-826	Period Ending August 31, 1950
ORNL-925	Period Ending November 30, 1950
ORNL-990	Period Ending February 28, 1951
ORNL-1057	Period Ending May 15, 1951
ORNL-1121	Period Ending August 15, 1951
ORNL-1221	Period Ending November 15, 1951
ORNL-1280	Period Ending March 15, 1952
ORNL-1318	Period Ending July 1, 1952
ORNL-1424	Period Ending October 1, 1952
ORNL-1478	Period Ending January 1, 1953
ORNL-1554	Period Ending March 31, 1953
ORNL-1605	Period Ending July 31, 1953
ORNL-1658	Period Ending October 31, 1953
ORNL-1678	Period Ending January 31, 1954
ORNL-1753	Period Ending April 30, 1954
ORNL-1772	Period Ending July 31, 1954
ORNL-1813	Period Ending October 31, 1954
ORNL-1853	Period Ending January 31, 1955
ORNL-1895	Period Ending April 30, 1955
ORNL-1943	Period Ending July 31, 1955
ORNL-2004	Period Ending October 31, 1955
ORNL-2057	Period Ending January 31, 1956
ORNL-2096	Period Ending April 30, 1956
ORNL-2148	Period Ending July 31, 1956
ORNL-2222	Period Ending October 31, 1956
ORNL-2272	Period Ending January 31, 1957
ORNL-2331	Period Ending April 30, 1957
ORNL-2379	Period Ending July 31, 1957
ORNL-2432	Period Ending October 31, 1957

OAK RIDGE NATIONAL LABORATORY
HOMOGENEOUS REACTOR PROJECT

FEBRUARY 3, 1958

PROJECT DIRECTOR
R. B. BRIGGS — D

ASSOCIATE PROJECT DIRECTOR
C. E. WINTERS** — D
A. L. GUINNELS, SEC. — REE

TECHNICAL ASSISTANT
F. KERTESZ — REE

PROJECT EDITOR
W. D. REEL — TI

DESIGN AND ENGINEERING
R. N. LYON, ASSISTANT DIRECTOR — REE
T. S. CARLSMITH,* SEC. — REE

DESIGN
W. R. GALL, SECTION CHIEF — REE
M. I. LUNDIN, ASSISTANT SECTION CHIEF — REE

MECHANICAL DESIGN
F. C. ZAPP, GROUP LEADER — REE
F. C. BOWEN — VITRO
C. A. BURCHSTEO — REE
E. M. GUGLIELMO — VITRO
W. L. WRIGHT — REE
C. W. COLLINS — REE

PROCESS DESIGN
R. C. ROBERTSON, GROUP LEADER — REE
E. H. GIFT — REE
H. A. MCLAIN — REE
L. A. HAACK — REE

HRE-3 MECHANICAL DESIGN
R. H. CHAPMAN, GROUP LEADER — REE
C. J. CLAFFEY — REE
R. E. SCHAPPEL — REE
D. W. VROOM — REE

HRE-3 SITE AND STRUCTURES
J. H. ROBINSON — REE

PLANT LAYOUT AND DRAFTING
C. L. SEGASER, GROUP LEADER — REE
W. ROBINSON — REE
H. H. BRADFORD — REE
R. L. CAUBLE — REE
C. W. DAY — REE
J. P. DILORENZO — REE
F. GUNNESS — REE
A. R. KERR — REE
W. B. KRICK — REE
A. S. LUDLOW — REE
C. A. ROBERTS — REE
R. D. SATTERFIELD — REE
R. H. SIGLER — REE
W. G. STERLING — REE

RESEARCH AND ANALYSIS
P. R. KASTEN, SECTION CHIEF — REE

HRE-3 REACTOR PHYSICS
M. W. ROSENTHAL, GROUP LEADER — REE
B. E. PRINCE — REE

FLOW VISUALIZATION AND SCALE-UP STUDIES
H. C. CLAIBORNE, GROUP LEADER — REE
W. P. MIXON — REE
H. MACCOLL — REE

TRANSPORT PROPERTIES OF SLURRIES
O. G. THOMAS, GROUP LEADER — REE
L. L. BENNETT — REE
R. H. NIMMO — REE
P. H. HAYES — REE
R. M. SUMMERS — REE

PHYSICIAL CHEMISTRY OF SLURRIES
C. S. MORGAN — REE
B. G. SUTTON — REE

STRESS ANALYSIS AND CLOSURE RESEARCH
R. D. CHEVERTON, GROUP LEADER — REE
T. H. MAUNEY — REE
E. VOLK — COMBUSTION

REACTOR ANALYSIS AND LONG RANGE PLANNING
T. B. FOWLER — REE
S. JAYE — REE
M. P. LIETZKE — REE
M. TOBIAS — REE

COMPONENT DEVELOPMENT
I. SPIEWAK, SECTION CHIEF — REE

HEAT EXCHANGERS, MECHANICAL ENGINEERING PROBLEMS
J. S. CULVER, GROUP LEADER — REE
B. D. DRAPER — TVA
P. P. HOLZ — REE
I. K. NAMBA — REE
H. C. ROLLER — REE
T. L. CASTILE — REE
T. M. CATE — REE
H. C. LeTELLIER — REE

CIRCULATING PUMPS
C. H. GABBARD, GROUP LEADER — REE
J. M. BAKER — REE
J. C. MOYERS — REE
H. R. PAYNE — REE
C. C. HURTT — REE
R. J. LOCKETT — REE

FEED PUMPS AND VALVES
E. C. HISE, GROUP LEADER — REE
R. BLUMBERG — REE
J. P. HURST — REE
G. A. WINDLE — REE

CORE AND BLANKET, CHEMICAL ENGINEERING PROBLEMS
C. G. LAWSON, GROUP LEADER — REE
B. A. HANNAFORD — REE
J. K. HAYES — COMBUSTION
J. E. MOYT — REE
D. L. SNYDER — REE
A. B. DAFFRON — REE
R. GOODMAN — REE
S. R. WEST — REE

SYSTEMS DEVELOPMENT
R. B. KORSMEYER, SECTION CHIEF — REE
F. N. PEEBLES, ASSISTANT SECTION CHIEF — REE

COMPONENT AND SLURRY TESTING
R. B. GALLAHER — REE
C. H. GIBSON — REE
C. M. FITZPATRICK — REE

HRT CORE MOCKUP
P. H. HARLEY, GROUP LEADER — REE
D. E. WILLIS — REE
W. M. PARKS — REE
L. E. PENTON — REE
T. R. WILSON — REE

SLURRY BLANKET DEVELOPMENT
L. F. PARSLY, GROUP LEADER — REE
V. L. KENYON* — REE
M. RICHARDSON — REE
R. E. CARNES — REE

OPERATIONS
A. N. SMITH, GROUP LEADER — REE
T. L. BOSWELL — REE
B. R. CHILCOAT — REE
J. T. DICKIE — REE
C. A. GIFFORD — REE
C. A. MCLAUGHLIN — REE
H. G. MOORE — REE
R. E. POTTER — REE
D. H. WALLACE — REE

INSTRUMENTATION AND CONTROLS
D. S. TOOMB, SECTION CHIEF — I&C

HRT-HRE-3 DESIGN
J. R. BROWN, GROUP LEADER — I&C
R. M. PIERCE* — TVA
J. A. RUSSELL — I&C
R. W. BORGERS — I&C

HRP SUPPORTING SERVICES
D. G. DAVIS, GROUP LEADER — I&C
S. J. BALL — I&C
G. W. GREENE — I&C
J. D. GRIMES — TVA
P. G. HERNDON — I&C
R. M. BURNETT — I&C
M. A. MEACHAM — I&C
P. E. SMITH — I&C

VALVES AND ACTUATORS
A. M. BILLINGS, GROUP LEADER — I&C
E. H. BELL — I&C
B. J. JONES — I&C
P. F. HURAY — I&C
A. J. SHARENBERGER* — I&C

INSTRUMENT DEVELOPMENT
R. L. MOORE, GROUP LEADER — I&C
H. D. WILLS — I&C

REACTOR MATERIALS RESEARCH
E. G. BOHLMANN, ASSISTANT DIRECTOR — REE
T. S. CARLSMITH,* SEC. — REE
B. H. BOLEN, STENO. — REE
R. E. WACKER, RECORDS — REE

SOLUTIONS
J. C. GRIESS, ASSISTANT SECTION CHIEF — REE

LOOPS
R. S. GREELEY, GROUP LEADER — REE
S. R. BUXTON — REE
J. E. JACKSON — REE
W. H. HINDS — REE

LABORATORY STUDIES
J. L. ENGLISH, GROUP LEADER — REE
D. N. HESS — REE
P. D. NEUMANN — C
L. L. FAIRCHILD — REE
H. L. BARKER — REE
P. B. DAVIS — REE
B. L. JOHNSON — REE
H. R. TINCH — REE
J. L. UNDERWOOD — REE

SLURRIES
E. L. COMPERE, ASSISTANT SECTION CHIEF — REE

LOOPS
S. A. REED,* GROUP LEADER — REE
F. E. McDANIEL — REE

TOROIDS
S. A. REED* — REE
R. F. BENSON — REE
B. H. PARKS — REE
G. G. WARNER — REE

IN-PILE BOMBS
L. F. WOO — REE

ENGINEERING
H. C. SAVAGE, ASSISTANT SECTION CHIEF — REE

SOLUTIONS
S. E. BOLT, GROUP LEADER — REE
W. C. ULRICH — REE

IN-PILE MOCKUPS
J. R. HART, LEADER — REE
C. H. BURBAGE — REE
H. F. HENDERSON — REE
R. W. RAY — REE
T. R. RAYBURN — REE
B. W. SCOTT — REE

100A LOOP OPERATIONS
J. F. WINESETTE* — REE
L. L. ALLEN — REE
C. M. BURCHELL — REE
C. L. FRANCIS — REE
J. B. FRENCH — REE
D. G. GATES — REE
J. W. GOOCH — REE
W. H. WAGNER — REE

SLURRIES
D. T. JONES, GROUP LEADER — REE
D. W. HUBBARD — REE
R. M. WARNER — REE

IN-PILE TOROIDS
J. D. BARNES — REE

100A LOOP OPERATIONS
J. F. WINESETTE* — REE
C. R. BENSON — REE
T. W. HODGE — REE
H. C. HOOVER — REE
G. A. MOORE — REE
D. G. PEACH — REE
L. G. PHELPS — REE
A. E. PUGH — REE

IN-PILE OPERATIONS
R. A. LORENZ, GROUP LEADER — REE
J. W. BROWN — REE
V. A. DeCARLO — REE
F. J. WALTER[2] — REE
V. R. BULLINGTON — REE
W. E. TEICHERT, A SHIFT LEADER — REE
J. W. MOSIER — REE
C. E. ROBERTS — REE
E. H. GUINN, B SHIFT LEADER — REE
J. P. GORDON — REE
A. L. SUTTON, C SHIFT LEADER — REE
R. A. JONES — REE
R. M. WALLER — REE
J. W. MYERS, D SHIFT LEADER — REE
R. G. ROSS — REE
D. M. SMITH — REE

RADIATION
G. H. JENKS, SECTION CHIEF — REE

IN-PILE LOOPS
J. R. McWHERTER, GROUP LEADER — REE
J. E. BAKER — REE
J. C. BANTER — REE
S. H. WHEELER — REE

IN-PILE BOMBS
R. J. DAVIS, GROUP LEADER — C
F. A. KNOX — REE
K. S. WARREN — C
J. L. RUTHERFORD — REE

SUPPORTING RESEARCH
A. L. BACARELLA — C
M. D. SILVERMAN — C
W. C. YEE[2] — C

REMOTE EVALUATION
A. R. OLSEN — REE
B. W. McCOLLUM, SHIFT LEADER — REE
W. J. SCHILL — REE
W. H. SMITH, JR. — REE
J. C. THOMPSON — REE

METALLURGY
G. M. ADAMSON, SECTION CHIEF — M

METALLURGICAL RESEARCH
M. L. PICKLESIMER, LEADER — M
P. L. RITTENHOUSE — M
R. L. STEPHENSON — M
P. J. JONES — M
G. C. NELSON — M
M. A. WHEELER — M

METALLURGICAL ENGINEERING
E. S. BOMAR, LEADER — M
F. W. COOKE — M
W. J. LEONARD — M
J. J. PRISLINGER — M
J. K. WHITE — M
C. H. WODTKE — M
C. M. SMITH — M
J. J. WOODHOUSE — M

METALLOGRAPHY
R. S. CROUSE,** LEADER — M
T. M. KEGLEY, JR. — M
E. R. BOYD — M
B. F. DAY** — M
R. L. FITZGERALD — M
T. J. HENSON** — M
L. G. SHRADER** — M
C. E. ZACHARY — M

RADIATION DAMAGE
R. C. BERGGREN — SS
J. C. WILSON — SS
F. M. GRIZZEL — SS

SUBCONTRACTS

AEROJET GENERAL CORPORATION
HOUDRY PROCESS CORPORATION
OHIO STATE UNIVERSITY
RICE INSTITUTE
STANFORD RESEARCH INSTITUTE
SYRACUSE UNIVERSITY
TULANE UNIVERSITY
UNIVERSITY OF UTAH
UNIVERSITY OF VIRGINIA

INDUSTRIAL PARTICIPATION

COMBUSTION ENGINEERING, INC.
PENNSYLVANIA POWER AND LIGHT COMPANY
PUERTO RICO WATER RESOURCES AUTHORITY
TENNESSEE VALLEY AUTHORITY

AC — ANALYTICAL CHEMISTRY
C — CHEMISTRY DIVISION
CT — CHEMICAL TECHNOLOGY DIVISION
D — DIRECTOR'S DIVISION
E&M — ENGINEERING AND MECHANICAL DIVISION
I&C — INSTRUMENTATION AND CONTROLS DIVISION
M — METALLURGY DIVISION
REE — REACTOR EXPERIMENTAL ENGINEERING DIVISION
SS — SOLID STATE DIVISION
TI — TECHNICAL INFORMATION DIVISION
* — DUAL CAPACITY
** — PART TIME ON PROJECT
- — ON LOAN FROM DUKE UNIVERSITY
1 — SPECIAL ASSIGNMENT

CHEMICAL TECHNOLOGY
D. E. FERGUSON,* PROGRAM LEADER — CT
J. LOOPE, SEC. — CT
Z. TROTTER, SEC. — CT

CHEMICAL DEVELOPMENT
D. E. FERGUSON,* SECTION CHIEF — CT

BLANKET PROCESSING
R. E. LEUZE, PROBLEM LEADER — CT
R. D. BAYBARZ — CT
J. M. CHILTON — CT
S. S. KIRSLIS — CT
J. H. GROOVER — CT
R. L. HICKEY — CT
O. K. TALLENT — CT

CORE PROCESSING
R. A. McNEES, PROBLEM LEADER — CT
M. H. LLOYD — CT
S. PETERSON — CT
H. H. CARMICHAEL — CO-OP, UNIV. OF TENN.
W. B. HOWERTON — CT

OXIDE PREPARATION
R. L. PEARSON — CT
K. H. McCORKLE — CT
C. E. SCHILLING — CT
C. W. GREENE — CT
W. L. PATTISON — CT

THORIUM BLANKET STUDIES
J. P. McBRIDE, PROBLEM LEADER — CT
E. V. JONES — CT
N. A. KROHN — CT
L. E. MORSE — CT
P. P. HAYDON — CT
H. F. SOARD — CT

DESIGN
W. E. UNGER, ASSISTANT SECTION CHIEF — CT

PROCESS DESIGN
J. C. SUDDATH — CT
H. O. WEEREN — CT

ThO_2 FACILITIES
B. F. BOTTENFIELD — CT
F. C. McCULLOUGH — CT
J. R. PHILLIPS — CO-OP, GEORGIA TECH.

LOOP FACILITIES
T. A. AREHART — CT
L. J. KING — CT
B. B. KLIMA — CT
W. F. SCHAFFER — CT

INSTRUMENTATION
C. S. LISSER — I&C

DRAFTING
G. B. BERRY** — E&M
E. E. BRIDGES** — E&M
J. D. CUPP** — E&M
J. W. DAY — E&M
H. W. FALLON** — E&M
L. C. HUBBARD — E&M
J. H. MANNEY** — E&M
F. L. PEISHEL** — E&M
J. D. PHILLIPS** — E&M
K. F. STOOKSBURY** — CT
J. H. THOMPSON — E&M
J. M. WHEELER** — E&M

PILOT PLANT
R. B. LINDAUER,** SECTION CHIEF — CT

SLURRY PREPARATION
E. M. SHANK, PROBLEM LEADER — CT
C. V. ELLISON — CT
W. T. McCARLEY — CT

UNIT OPERATIONS
P. A. HAAS, GROUP LEADER — CT

BLANKET PROCESSING
J. W. SNIDER — CT
R. C. EARLY — CT
F. N. McLAIN — CT
D. A. McWHIRTER — CT

THORIUM BLANKET STUDIES
C. C. HAWS — CT
J. M. HOLMES — CT
K. O. JOHNSSON — CT
W. M. WOODS — CT
E. L. YOUNGBLOOD — CT
R. D. ARTHUR — CT
V. L. FOWLER — CT
G. D. JUDY — CO-OP, AUBURN UNIV.

CHEMICAL RESEARCH
E. H. TAYLOR,** DIRECTOR — C
H. A. STEINKE, SEC. — C

FUEL SOLUTION CHEMISTRY
H. F. McDUFFIE, GROUP LEADER — C
W. L. MARSHALL, GROUP LEADER — C
J. S. GILL — C
L. O. GILPATRICK — C
G. M. HEBERT — C
R. SLUSHER — C
H. H. STONE — C
F. H. SWEETON — C

RADIATION CHEMISTRY
C. J. HOCHANADEL,** GROUP LEADER — C
J. W. BOYLE** — C
H. A. MAHLMAN** — C

HEAVY ELEMENT CHEMISTRY
R. W. STOUGHTON,** GROUP LEADER — C
J. HALPERIN** — C
M. H. LIETZKE** — C
W. C. WAGGENER** — C

INORGANIC SOLUTION CHEMISTRY
K. A. KRAUS,** GROUP LEADER — C
T. A. CARLSON** — C
H. O. PHILLIPS** — C

ANALYTICAL CHEMISTRY
MYRON T. KELLEY,** DIRECTOR
C. D. SUSANO,** ASSOCIATE DIRECTOR
K. A. ODOM, SEC. — AC

CORROSION ANALYTICAL LABORATORY
O. MENIS,* SECTION CHIEF — AC
H. P. HOUSE, ASSISTANT SECTION CHIEF — AC

RESEARCH
O. MENIS,* GROUP LEADER — AC
C. M. BOYD — AC
R. H. POWELL — AC
D. L. MANNING, GROUP LEADER — AC
R. G. BALL — AC
G. GOLDSTEIN — AC
T. C. RAINS, GROUP LEADER — AC
I. B. RUBIN — AC

SERVICES
C. K. TALBOTT, GROUP LEADER — AC
D. E. CARPENTER — AC
E. L. BLEVINS — AC
N. M. FERGUSON — AC
F. L. LAYTON — AC
T. P. BACON — AC
W. D. CLAPP, JR. — AC
C. A. CLARK — AC
P. S. GOODWIN — AC
B. D. HICKS — AC
A. H. MATTHEWS — AC
T. G. MILLER — AC
V. S. NORMAN — AC
E. ONKST — AC
C. M. WILSON — AC

HRT AND IN-PILE LOOP ANALYSES
U. KOSKELA, SUPERVISOR — AC
L. G. FARRAR, ASSISTANT SUPERVISOR — AC
J. E. ATTRILL — AC
C. P. BAKER — AC
R. E. CORCORAN — AC
S. R. DINSMORE — AC
J. L. MOTTERN — AC
G. M. CAMPBELL — AC
G. I. GAULT — AC
F. K. HEACKER — AC
M. H. McCORQUODALE — AC
J. L. SHARP — AC
J. SLESSINGER, JR. — AC
W. R. WARREN — AC
H. L. WEBB — AC
H. L. WHITTINGTON — AC

HRT DEVELOPMENT
P. F. THOMASON, GROUP LEADER — AC
R. E. BIGGERS — AC
F. J. MILLER — AC

S. A. REYNOLDS, GROUP LEADER — AC
J. S. ELDRIDGE — AC
T. H. HANDLEY — AC

HIGH RADIATION LABORATORY
J. E. MORTON — AC

HOMOGENEOUS REACTOR TEST
S. E. BEALL, PROJECT ENGINEER — REE
B. EUBANK, SEC. — REE
M. SWANK, SEC. — CT

REACTOR PLANNING
S. I. KAPLAN, GROUP LEADER — REE
J. R. BUCHANAN — CT

PLANT OPERATIONS
J. W. HILL, JR., CHIEF — REE
R. J. HUNTER — REE
D. W. LEIGH — REE
J. R. ENGEL, SUPERVISOR — CT
R. J. HARVEY — REE
H. K. SEARCH — PA. POWER AND LIGHT CO.
H. O. CURTIS — REE
D. T. GODWIN — REE
A. L. JOHNSON — REE
L. P. PUGH — REE
J. D. FLYNN, SUPERVISOR — REE
H. F. BAUMAN — CT
H. C. BRADLEY — CT
E. D. BOLLING — REE
W. T. BOSTIC — CT
E. W. BROWN — CT
T. G. HILL — REE
J. O. KOLB, SUPERVISOR — REE
N. A. BROWN — TVA
D. F. FRECH — REE
J. E. EVE — REE
R. J. SHANNON — CT
L. J. SHERSKY — CT
J. E. WOLFE — REE
G. W. RIVENBARK, SUPERVISOR — REE
D. F. BRULEY — CT
T. H. GLADNEY — TVA
R. H. GUYMON — CT
H. L. BROWN — REE
F. L. ROUSER — REE
R. SMITH, JR. — REE
J. L. STEPP — REE

REACTOR MATERIALS AND CHEMISTRY
D. M. RICHARDSON, GROUP LEADER — REE
J. E. SUTHERLAND — REE
J. D. JONES — REE

CHEMICAL PLANT
W. D. BURCH, GROUP LEADER — CT
R. H. WINGET — CT
O. O. YARBRO — CT
W. A. LINDSEY — CT

PERFORMANCE STUDIES
R. VAN WINKLE, GROUP LEADER — REE
J. A. WATTS — REE

REACTOR ANALYSIS
P. N. HAUBENREICH, GROUP LEADER — REE
J. HERNANDEZ — PUERTO RICO WATER RESOURCES AUTHORITY

MAINTENANCE PLANNING
W. TERRY, SUPERVISOR — REE
T. E. HAYNES — REE
G. H. JOHNSTONE — REE

INSTRUMENTATION
K. W. WEST, GROUP LEADER — I&C
R. M. PIERCE* — TVA
J. A. RUSSELL — I&C
A. J. SHARENBERGER* — I&C

PERSONNEL SUMMARY

	FULL TIME	PART TIME	INDUSTRIAL PARTICIPATION	TOTAL
ADMINISTRATION	7	4	0	11
ANALYTICAL CHEMISTRY	47	0	0	47
CHEMICAL RESEARCH	8	10	0	18
CHEMICAL TECHNOLOGY	50	10	0	60
DESIGN AND ENGINEERING	115	0	4	119
HOMOGENEOUS REACTOR TEST	47	0	5	52
REACTOR MATERIALS RESEARCH	104	4	0	108
TOTAL	378	28	9	415